ANNUAL REPORT 2011

INSTITUT LAUE-LANGEVIN

SYNTHESE ECA - Tél. 04 76 90 02 73

NEUTRONS FOR SCIENCE®

6, rue Jules Horowitz - BP 156 - 38042 Grenoble Cedex 9 - France - http: // www.ill.eu

This report has been printed using FSC certified paper (http://www.fsc.org/)

FSC

INSTITUT LAUE-LANGEVIN ANNUAL REPORT 2011

ANNUAL REPORT 2011

INSTITUT LAUE-LANGEVIN

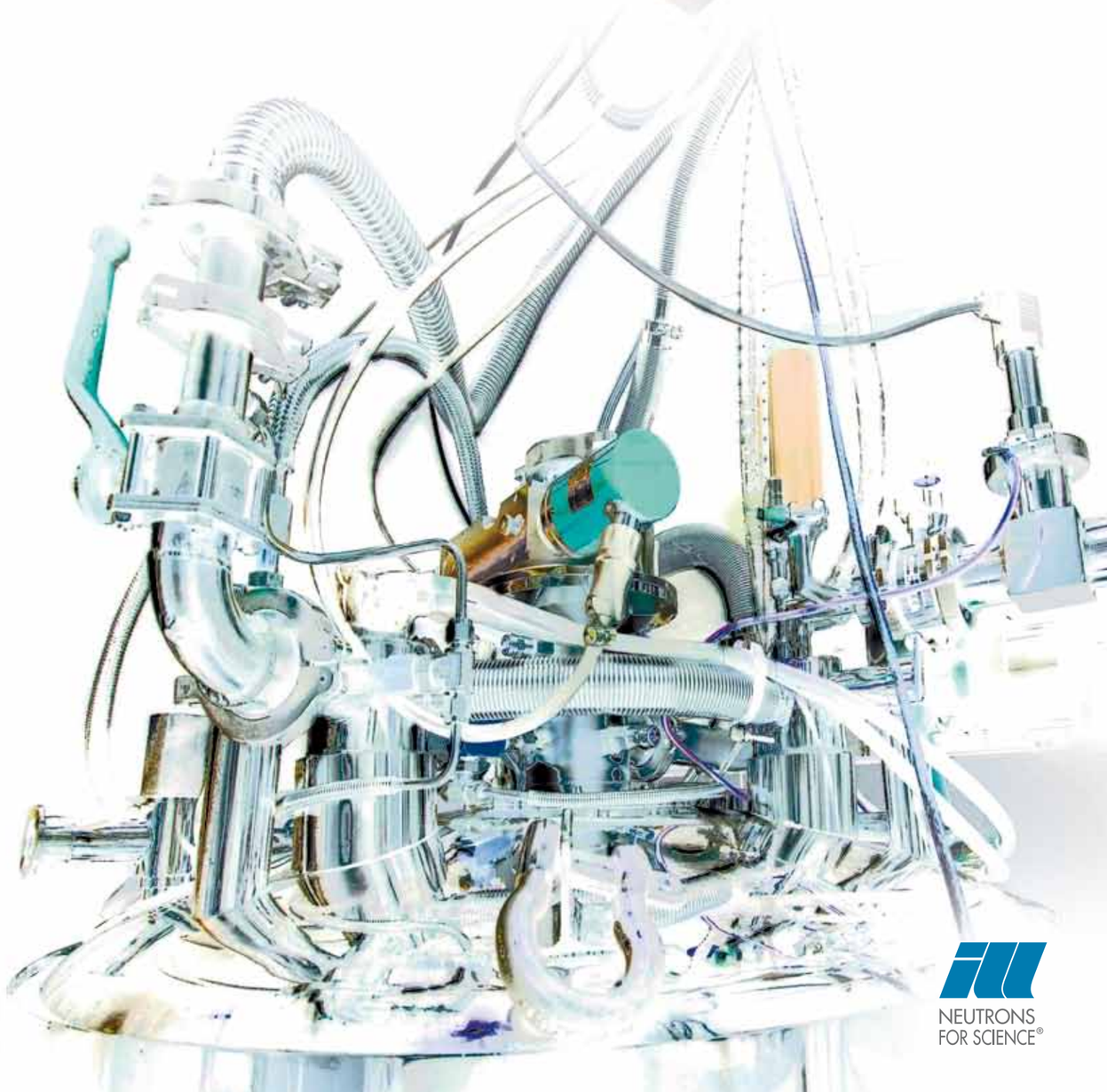

NEUTRONS FOR SCIENCE®

The world's leading facility in neutron science and technology

PUBLISHING INFORMATION
Editors: Giovanna Cicognani and Helmut Schober - **Production team:** Giovanna Cicognani, Alison Mader, Robert Corner and Susan Tinniswood
Design: www.synthese-eca.com - **Photos:** Serge Claisse (unless otherwise specified)

Further copies can be obtained from Institut Laue-Langevin - Scientific Coordination Office (SCO) - BP 156 - F-38042 Grenoble Cedex 9 (France) - Email: sco@ill.eu - web: www.ill.eu

CONTENTS

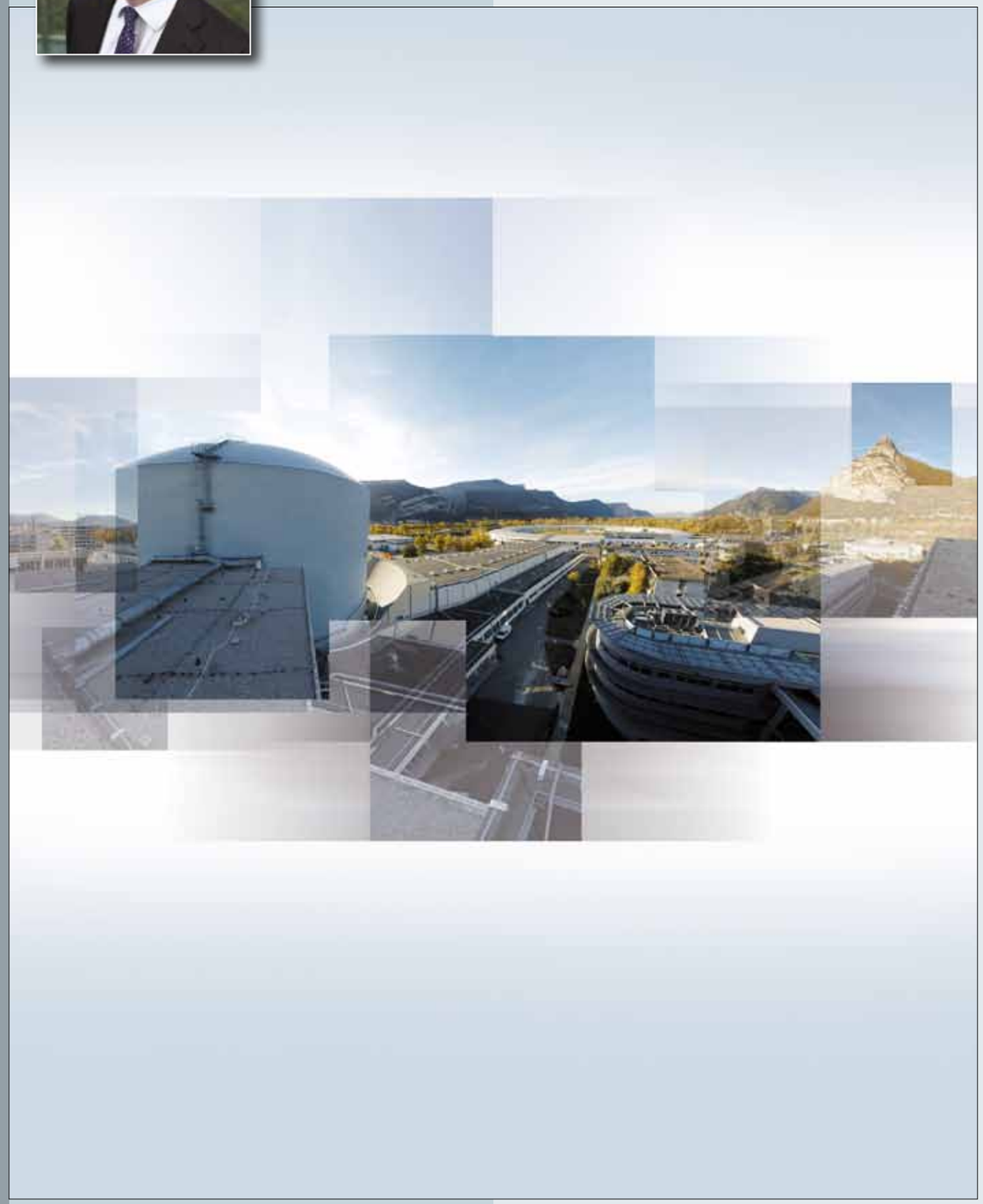

DIRECTOR'S FOREWORD

2011 has been a year of change and challenges for ILL and true to our past form, this has brought out the best in the Institute. The year began with the prospect of a progressive reduction in funding from our Associates to 2015 as national research budgets were hit by the global recession. Then in March the accident at the Fukushima nuclear power plant in Japan prompted the French Nuclear Safety Authorities – the ASN – to scrutinise yet more closely the ability of all nuclear installations in France to withstand natural disasters, however improbable. It is a testament to the skill and dedication of ILL engineers and support services that the ASN responded in glowing terms to our report, fully endorsing our plans to mitigate the consequences of such events, and envisaging continued operation of our reactor with a horizon of 2030. This result also reflects the foresight of those who originally conceived the reactor design, optimising not only brightness but also robustness with regard to safety: we celebrated their achievement on August 31st 2011, marking the 40th anniversary of the date the reactor first went critical.

Furthermore, neutron scattering continues to be a vital, multipurpose tool for science, equipping us to meet the grand technological challenges faced by our society, from clean, renewable sources of energy to new forms of therapy

ILL scientists also responded magnificently to the challenge of external review, presenting their instruments to an expert review panel that reported to our Scientific Council. Their verdict was that the overwhelming majority of our instrumental suite is world-leading, with recommendations of action to be taken to lift the rest to this level.

The evidence for such excellence in terms of scientific publications continues to be very impressive, with yet another record year for high-impact publications, and the strongest demand for beamtime in our history. We welcomed India as a new scientific member this year and have the prospect of further new members next year. News of our scientific achievements is also reaching a much wider audience after an initiative to communicate more effectively with media in our partner countries, with coverage in national newspapers and broadcasters such as the BBC.

Of course our instrument suite continues to be strengthened by our Millennium Programme which delivered first neutrons on the new small-angle instrument D33, as well as the IN1 upgrade LAGRANGE and increased flux on the cold-neutron Laue instrument LADI; we look forward to welcoming users to these instruments in 2012, as well as to an upgraded IN12 and IN16B.

Despite economic hardship, our upgrades will not end there. We will have to be clever, disciplined and determined to balance our budget over the next few years while keeping up scientific output. The remarkable improvements that the Millennium Programme has brought to date (an increase in the average detection rate across our suite by a factor of twenty over the past decade) will enable us to deliver a service at the limits of what is technically possible for several years without substantial new investment in instruments.

However, we have a longer term responsibility to the scientific community to continue to provide such a service; to this end we are already planning a future wave of developments of instruments and infrastructure to be funded when the economic environment is less harsh. This is very much in keeping with the recommendations this year* of the Neutron Working Group established by our Associates to review the longer term needs and provision of neutrons in Europe – a key point being that a future ESS will only be ready to take on a flagship role well into the next decade. We look forward to closer engagement with ESS in the future, building on a MOU for collaboration signed this year between Richard Wagner, as one of his last actions as Director, and his predecessor at ILL and leader of the ESS project, Colin Carlile.

Richard led ILL boldly and tirelessly through five remarkably successful years and has taken retirement after a lifetime of service to science. I feel particularly privileged to have been invited to take his place more than 30 years since first coming to ILL as a stagiaire with former Director John White. I leave behind the post of Director of Science which has been filled admirably by the new Associate German Director Helmut Schober, rising from the ranks through his most recent position as Head of the Time-of-Flight and High Resolution Instrument Group. There has been change too in the Division of Administration where Amin Saidoun has left for pastures new after 5 years with us, while Martin Walter has stepped up to the mark to lead this Division as we find a replacement. We are also very fortunate in being able to continue to enjoy the experience and expertise of both José Luis Martínez as French Associate Director and Head of the Division of Projects and Techniques, and Hervé Guyon, Head of the Reactor Division, completing the new management team.

The climate for funding will be cooler over the next few years, but we still have excellent prospects and we have the best combination of instruments and service in the world, and we are blessed with a remarkably skilled and dedicated workforce and a user community that is second to none. Furthermore, neutron scattering continues to be a vital, multipurpose tool for science, equipping us to meet the grand technological challenges faced by our society, from clean, renewable sources of energy to new forms of therapy. We look forward to the challenges – and the rewards – of the future with confidence and enthusiasm.

Director of the ILL

*http://tinyurl.com/d8mzd9t

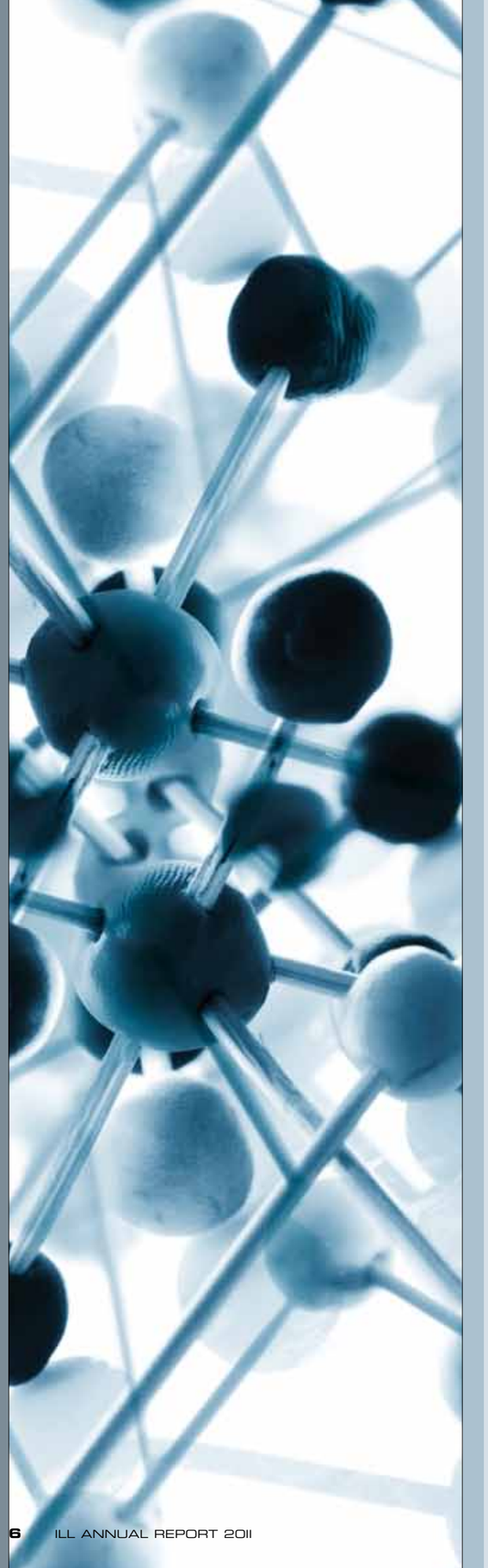

WHY NEUTRON SCATTERING IS USEFUL

When used as a probe for small samples of materials, neutron beams have the power to reveal what is invisible using other radiations. Neutrons can appear to behave either as particles or as waves or as microscopic magnetic dipoles, and it is these specific properties which enable them to uncover information which is often impossible to access using other techniques.

WAVELENGTHS OF TENTHS OF NANOMETERS

Neutrons have wavelengths varying from 0.01 to 100 nanometers, which makes them an ideal probe of atomic and molecular structures ranging from those consisting of single atomic species to complex biopolymers.

ENERGIES OF MILLIELECTRONVOLTS

The associated energies of millielectronvolts are of the same magnitude as the diffusive motions of atoms and molecules in solids and liquids, the coherent waves in single crystals (phonons and magnons) and the vibrational modes in molecules. An energy exchange between the incoming neutron and the sample of between 1 μeV (even 1 neV with spin-echo) and 1 eV can easily be detected.

MICROSCOPICALLY MAGNETIC

Neutrons possess a magnetic dipole moment which makes them sensitive to magnetic fields generated by unpaired electrons in materials. Precise details of the magnetic behaviour of materials at the atomic level can be investigated. In addition, the scattering power of a neutron by an atomic nucleus depends on the orientation of the spin of both the neutron and the atomic nuclei in a sample, thereby providing a powerful tool for detecting the nuclear spin order.

ELECTRICALLY NEUTRAL

Neutrons are electrically neutral and so can penetrate deep into matter, while remaining non-destructive. This makes them an ideal probe for studying, for example, biological samples or engineering components under extreme conditions of pressure, temperature or magnetic field, or within chemical-reaction vessels.

HIGH SENSITIVITY AND SELECTIVITY

The variation of scattering power from nucleus to nucleus in a sample varies in a quasi-random manner, even in different isotopes of the same atom. This means that light atoms are visible in the presence of heavy atoms and atoms that are close to one another in the periodic table may be distinguished from each other. This introduces the possibility of using isotopic substitution (for example deuterium for hydrogen or one nickel isotope for another) to allow contrast to be varied in certain samples thereby highlighting specific structural features.
In addition, neutrons are particularly sensitive to hydrogen atoms and therefore they are a powerful probe of hydrogen storage materials, organic molecular materials, and biomolecular samples or polymers.

ABOUT THE ILL

The Institut Laue-Langevin (ILL) is an international research centre at the leading edge of neutron science and technology, where neutrons are used to probe the microscopic structure and dynamics of a broad range of materials at molecular, atomic and nuclear level.

The ILL is owned by the three founding countries - France, Germany and the United Kingdom. The three Associate member countries contributed a total of about 58 M€ to the Institute in 2011, a sum enhanced by significant contributions from the ILL's Scientific Member countries, Austria, Belgium, the Czech Republic, Denmark, Hungary, Italy, Poland, Slovakia, Spain, Sweden and Switzerland. On 1 January 2011, India also joined the ILL, thus becoming the 12th Scientific Member country. ILL's overall budget in 2011 amounted to approximately 88 M€.

The Institute operates the most intense neutron source in the world, based on a single-element, 58.3 MW nuclear reactor designed for high brightness. The reactor normally functions round-the-clock during four 50-day cycles per year, feeding neutrons to a suite of 40 high-performance instruments that are constantly upgraded.

As a service institute, the ILL makes its facilities and expertise available to visiting scientists. Our user community is world-wide: every year, about 2000 researchers from more than 30 countries visit the ILL to perform over 800 experiments selected by a scientific review committee.
The ILL monitors the papers published as a result of the use of our facilities, of which there are more than 600 per year. We pay particular attention to papers published in high-impact journals. About 80 such papers are published per year from data taken on ILL instruments. This is a factor of two higher than the second most productive neutron source in the world.

The Institute has a Director and two Associate Directors who represent each of the Associate countries and are appointed on short-term contracts, normally for five years. A Scientific Council, comprising external scientists from the member countries, advises the Directors on scientific priorities for the Institute and how to develop the instrument suite and technical infrastructure in order to best meet the needs of the user research programme. It also assesses the scientific output of the Institute. Our governing body is the Steering Committee, which meets twice yearly and is made up of representatives of the Associates and the Scientific Members together with the Directors and Staff Representatives. Within the framework of the Intergovernmental Convention, the Steering Committee has the ultimate responsibility for determining operational and investment strategies for the Institute.

NEUTRONS AND SOCIETY

The scope of the research carried out at the ILL is very broad, embracing condensed matter physics, chemistry, biology, materials and earth sciences, engineering, and nuclear and particle physics. Much of it impacts on many of the challenges facing society today, from sustainable sources of energy, improved healthcare and a cleaner environment to new materials for information and computer technology.
For example, neutron scattering experiments have given us new insights into the structure and behaviour of biological and soft condensed matter, important in designing better drug delivery systems or improving polymer processing. They also provide a unique probe into the phenomena that underpin high-temperature superconductivity or the molecular magnetism that may provide the technology on which the computers of the future are based.

PREPARING FOR THE FUTURE

In 2000, the ILL launched an ambitious programme to modernise its instruments and infrastructure called the ILL Millennium Programme, whose aim was to optimise the ILL's instrument suite (Phase M-0: 2000-2007; Phase M-1: 2008-2014). We are now looking forward to and setting the scene – in the framework of our ILL2020 Vision - for developments still further into the future, in order to maintain the Institute's world-leading position for another 20 years.

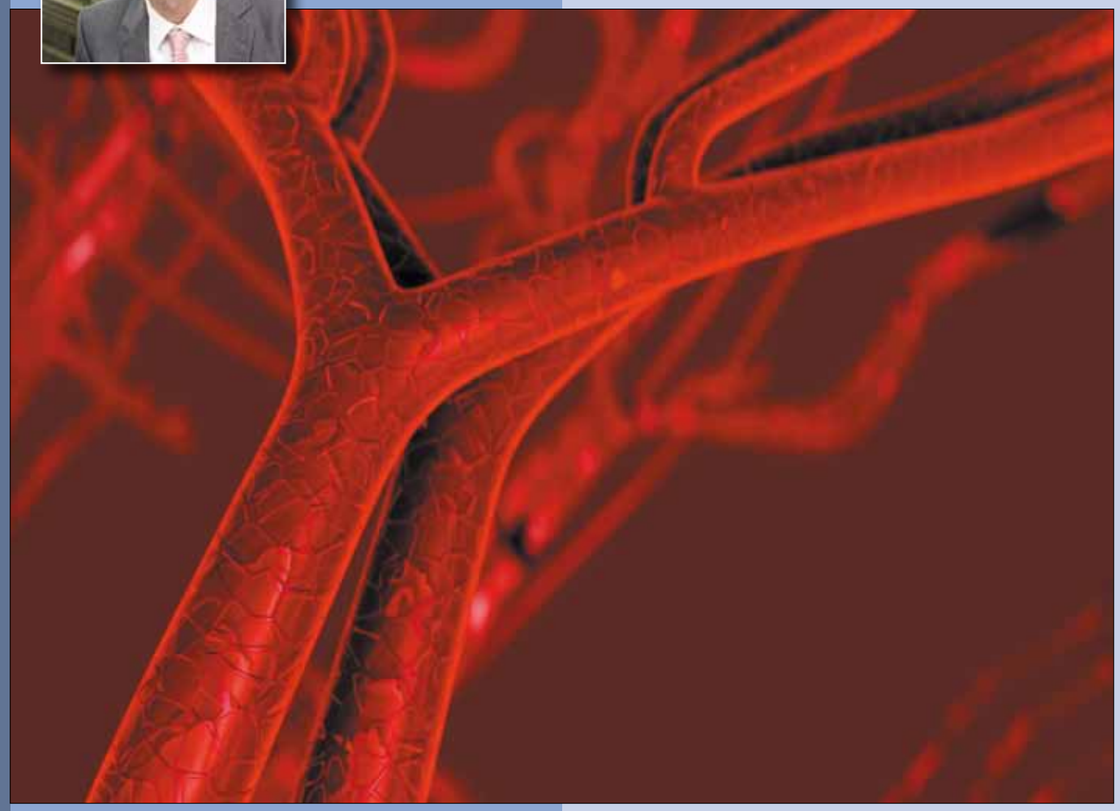

Adventure - and science is probably the greatest adventure of all - is driven by excitement. Despite the rigour they deploy in the conduct of their research, scientists will always hope, at the bottom of their hearts, for that big surprise at the end of the track. But scientific surprises are very rarely flashy. Students are taught very early on to be wary of sudden excitement, for unexpected results are generally due to faulty experimental set-ups or sample impurities. Real scientific surprises tend to come in disguise and, like hidden treasures, they are only accessible to those prepared to walk the extra mile.

Science is probably the greatest adventure of all

Systematic preparation for the unexpected may sound paradoxical. On reflection, however, it is not a vain philosophical exercise. It has real implications when it comes to developing rational processes for choosing directions of research or the development of scientific infrastructure. This is particularly true for service-oriented facilities like the ILL, where the anticipation of scientific trends and the selection of experiment proposals is part of daily life. It goes without saying that the ranking of proposals must be based on objective criteria - giving chance a chance is simply not an option. That said, to make the most of our portfolio of beamtime, we should be mixing safe assets with the more adventurous choices capable of delivering surprises. The highest potential for encountering the unexpected lies in those areas we know the least. But this leads to another difficulty - fields of ignorance are intrinsically ill-defined, and it is often only when you see the light that you realise you've been in the dark. It seems that we have little room for manoeuvre; we have to design our research in the full light of day, whilst hoping to glimpse unexplored shadowlands. It is only from the top of the mountain that you see all the possible paths.

The 2011 Nobel Prize in Chemistry provides an excellent example of how an unexpected result opened up a completely new area of research. At the beginning of the eighties Daniel Shechtman set out to study aluminium alloys for application in the aeronautical industry. To determine the atomic structure of his samples he used electron diffraction. The sharp signals he observed in the diffraction patterns indicated perfect ordering - nothing

spectacular in itself, as any crystal would show such behaviour. However, the five-fold symmetry of some of the reflections was completely at odds with accepted crystallographic knowledge. Any graduate student knows that translational periodicity is only compatible with two-, three-, four- and six-fold symmetries. There is simply no room for five-fold symmetry axes. Daniel Shechtman was naturally aware of this and initially suspected experimental artefacts or poor sample quality. But he could find no flaw in his experimental set-up, or problems with the sample. It takes courage and tenacity to counter coded knowledge. His colleagues rejected his claim, to the point of asking him to leave the research group, despite the fact that the ground had already been prepared by theorists in conceptual terms. Twenty years later, Shechtman's quasicrystals feature as common knowledge in any good text book on solid-state physics. It is still true of course that translational periodicity is incompatible with five-fold symmetry. We are now aware, however, that perfect long-range order leading to Bragg-like scattering can be achieved without translational periodicity, and that this kind of order admits a far broader range of symmetry operations. Neutrons played an important role in the quasicrystal saga that followed Shechtman's discovery and the ILL was always at the heart of it.

And the story is far from over. Micelles are very simple soft-matter systems showing like many other colloids self-assembly. Like atoms or molecules they can form ordered periodic structures. In 2009 a group of researchers from the University of Hamburg, now Bayreuth, received beamtime for studying twinning in soft fcc-crystals. On the last night of their experiment on instrument D11, they detected diffraction patterns with unusual symmetries. After discarding all possible artefacts and verifying their findings in a series of follow-up experiments, the verdict was clear: the micelles had arranged themselves to form quasicrystals (see scientific highlight by Exner *et al.*, p.34). Due to their distinctly different nature (micelles have no directional bonding for example), colloidal systems provide a completely new angle for the study of quasicrystals. By cross-correlating the properties of “soft” and “hard” quasicrystals we should now be able to focus on identifying the conditions that trigger quasicrystallinity.

Colloidal quasicrystals might well have gone unnoticed on D11, were it not for the bigger and faster detector with higher resolution which had just been installed as part of the ILL's Millennium Programme. What is the moral of the story? To prepare for the unexpected, don't forget to sharpen your tools.

Carrying out science is like preparing for a trip in the mountains. First make sure you have the equipment, and then decide on the route. And once you've started walking, stay tuned in, and ready for that breathtaking view that could be waiting at the turn of the bend. Well, I hope that's the feeling you get when you discover the scientific highlights collected in this report!

Helmut Schober

Helmut Schober
Associate Director

AUTHORS
H. Schober (ILL)
T. Pirling, M. Simson, P. Steffens, S. Capelli, G. Nenert, M. Brunelli,
M. Zbiri, M. Blakeley and R. Campbell (ILL College Secretaries)

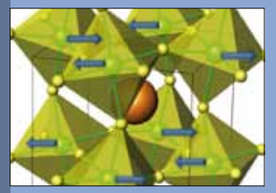

Magnetism:
cf. article "Magnetic structures on crossing the phase transition in perovskite $LaCrO_3$" p.20

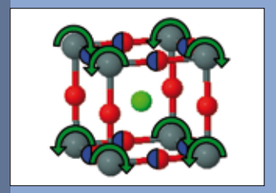

Chemistry and structure:
cf. article "Anion order in perovskite oxynitrides" p.24

Materials science and engineering:
cf. article "Evidencing hydride species in cerium nickel mixed oxides" p.32

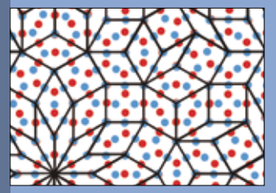

Soft matter:
cf. article "Discovery of colloidal quasicrystals" p.34

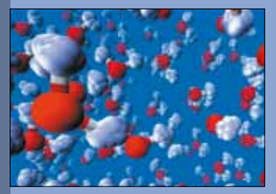

Liquids and glasses:
cf. article "Oxygen as a site specific probe of the structure of water and oxide materials" p.46

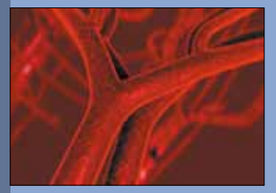

Biology: *cf. article "Softness of pro-atherogenic lipoproteins revealed by elastic incoherent neutron scattering " p.56*

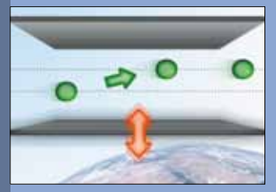

Nuclear and particle physics:
cf. article "Spectroscopy of gravity" p.60

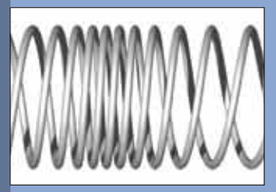

Modelling and spectroscopy:
cf. article "DNA as a safety belt" p.64

MAGNETISM

Neutrons are known to give unparalleled information in the field of magnetism. At the ILL the investigation of magnetism and magnetic materials amounts to one third of the attributed beamtime. The high number of proposals and breadth of the subjects attest to the good health of this field and pose a real challenge to the selection panels. There is a continuing high demand on pnictides. Improved sample quality helps to diversify the field with pioneering studies being teamed up with systematic investigations. High-Tc cuprates have a real revival following the discovery of magnetic excitations associated to the pseudogap phase. Heavy fermion systems are the focus of a high number of proposals, addressing a variety of topics from superconductivity to quantum critical points. Quantum magnetism, molecular magnets, and frustrated magnets are other significant trends in our users' activity. In particular when it comes to structural investigations multi-ferroic materials are the centre of attention. Finally, there are an increasing number of proposals on nano-sized materials, nano-particles, thin films or multilayers. For many of the studies ILL instrumentation offers unique possibilities. This holds in particular for polarisation analysis capabilities. With the fully upgraded IN12 coming back into user operation, the capacity for inelastic investigations with cold neutrons increased significantly. The selected highlights in this section further underline the diversity of the field. In particular, those on magnetic excitations focus on complex magnetic phases. For the first time in 45 years, we seem to understand the dynamics of uranium dioxide, where there is an intriguing interplay of lattice and magnetic excitations in conjunction with a quadrupolar order parameter (p.14). Also, in the manganites, there is an interplay of different order parameters, and neutrons prove to be an extremely efficient tool to understand these complex phases that are potentially of fundamental relevance for a wide class of materials (p.16).

CHEMISTRY AND STRUCTURE

The properties of a material are unquestionably related to its structure. ILL offers crystallographic capabilities over a very broad range of length scales, from wide-angle diffraction (D9, D19, D1B, D2B, D20) via diffuse scattering (IN1) and PDF analysis (D4) to small-angle scattering (D16, D11, D22). This allows for investigations in nearly all fields of natural science from geology to biophysics. Ferroelectric materials, oxides or oxide-ion conductors for energy applications and molecular hydrides for hydrogen storage are just a few examples of materials studied mainly by powder diffraction techniques. In the inorganic chemistry areas we see also an increase in dynamic studies under conditions of reactivity, temperature or pressure. The organic chemistry community is very active in single crystal diffraction via the study of phenomena related to hydrogen positions or bonding. Studies on molecules or molecular complexes used in pharmaceuticals or in agrochemicals, where polymorphism is often an issue, are also well represented and constitute an important point of contact with industry. The unavailability of VIVALDI in the second part of the year led automatically to the disappearance of proposals from the community that used Laue diffraction for small crystal crystallography. On the other hand, CYCLOPS, the new Laue diffractometer using the fast CCD imaging technique, has started showing great potential in some test experiments. We should give credit to the many years of good performances of the powder diffractometer D1A by mentioning that the last experiment before its final shutdown gave rise to a publication in *Science* [1]. In the year of her retirement, we would like to acknowledge Jane Brown for her outstanding contribution to the word-leading science done at the ILL and for the CCLS software package she developed for the analysis of diffraction data.

MATERIALS

Materials are at the heart of technological progress. In the two highlights chosen this year, the final technological use and not only the materials properties are the scope of the investigation. One example treats the conversion of biomass into hydrogen via an energy efficient catalytic process. The other studies the properties of light-emitting organic materials in the form of thin films. In the more classical sense materials science is often linked to engineering applications. ILL has an active community in this field and welds are still very much the centre of attention. Welding is a very complex process: the material is molten locally, then cooled down - often under conditions that are difficult to control - resulting in modified microstructure, changes in chemical composition and residual stresses. The stress diffractometer SALSA is very well suited to this type of investigation since it provides high lateral resolution for narrow welds such as laser- or electron beam welds (typically 1 mm large) and the penetration power for stress determination in thick welds (10-60 mm) as used in nuclear power plants, for example. A clear trend (~20 % of proposals in 2011) is on surface treatment. It is again the unique lateral resolution of 40 μm that makes the difference here allowing stress determination for protective coatings, surface peening (Laser-, water jet-...) and hardening (induction-, deep rolling...). More and more users equally take advantage of the capacity of SALSA to accommodate very large samples.

SOFT MATTER

Soft condensed matter is one of the identified growth areas at the ILL. The number of proposals submitted to college 9 reached almost 150 in each of the proposal rounds in 2011. This is one of the reasons why ILL deploys particular efforts in terms of instrumentation and broader scientific infrastructure. The scientific topics cover a broad range from fundamental to applied soft condensed matter, at the interface of physics, chemistry, and biology. The scientific themes are divided rather evenly among colloids / micelles / surfactants, polymers, and bio-related soft matter. The growth and continued use of the Partnership for Soft Condensed Matter (PSCM, p.108) equipment supports users of a broad range of experiments to prepare for their beamtime. Smart and responsive systems, including self-healing networks and model photovoltaics, continue to attract attention from the user community, demonstrating a clear commitment of soft matter science to the environment and energy harvesting. Also, a considerable number of proposals focus on nanocomposites, both model systems and industrially relevant, seeking to determine the polymer conformation and dynamics in the presence of nanofillers with well defined geometry. A particular highlight is the successful launch of FIGARO's publication record with 14 peer reviewed articles in 2011. The heavy overload on the college prompted lively discussions among the subcommittee and college members about the possibility of a hard or soft split for 9-13 proposals. A soft split was chosen, and a vice chairperson, vice expert and vice secretary have already been selected in preparation for the next proposal round.

BIOLOGY

The use of neutrons in biology has steadily increased at the ILL over recent years (now 11% of total request). The scientific themes of the submitted proposals were divided rather evenly among biological membranes, solution structure of biological membranes, and dynamics of biological macromolecules. The low availability of LADI in 2011 lead to fewer proposals submitted for macromolecular crystallography. LADI will be available again after the reactor restart with considerably increased performance. For macromolecular crystallography a highlight from this year (p.72) was a high-resolution diffraction study of xylose isomerase using D19 [2]. This resulted in the first identification of a hydronium ion (H_3O^+) in a crystallographic structure of a biological macromolecule. Another highlight was a high-resolution diffraction study of type-III antifreeze protein (found in the blood of arctic fish) using LADI [3]. This work indicated how this special protein recognises and binds to ice crystal nuclei as they form, inhibiting their further growth and allowing organisms to live in sub-zero environments. For SANS a particular highlight from this year (p.52) was the precise measurement of cholesterol transport rates using D22 [4]. This study indicated that cholesterol moves far slower within and between cells than previously thought. These findings reveal how different concentrations of cholesterol within cells are maintained and could impact the treatment of a range of diseases linked to cholesterol transport abnormalities, such as Alzheimer's. Finally for the majority of successful biological experiments performed at the ILL, the importance of D-Lab (p.108) for the production of deuterated samples cannot be understated. This is particularly the case for the crystallographic and SANS communities such that the lab is now reaching out to a wide and steadily increasing user community.

SCIENTIFIC HIGHLIGHTS

NUCLEAR AND PARTICLE PHYSICS

Activities in nuclear and particle physics are spanning a wide field of fundamental and applied physics. Especially in nuclear physics several new fields were explored in 2011. In addition to its applications for nuclear spectroscopy far from stability, the efficient germanium clover detectors at Lohengrin are now also used to derive previously inaccessible isotopic fission yields, making Lohengrin even more attractive for the fission community. In the framework of the EXILL partnership a workshop was held at the ILL where numerous possible measurements were discussed. The partnership will bring the EXOGAM germanium detector array to the ILL for an extended measurement campaign at PF1B. On the GAMS 5 spectrometer the new DIGRA set-up came into operation this year and is opening new possibilities to investigate the properties of crystals for applications in astrophysics. Of particular interest is the construction of a Laue lens for focusing high-energy gamma rays. Such a lens could enhance the performance of a space-based gamma ray telescope by several orders of magnitude. This is required for the study of Supernovae and other objects in nuclear astrophysics. The new source of ultra-cold neutrons (SUN2) produced its first ultra-cold neutrons (UCNs) in a test experiment on PF1B. A relatively new field in UCN physics is the investigation of gravitational quantum effects; the journal *Comptes Rendus Physique* devoted a special issue to experimental and theoretical approaches to neutron quantum states. A particular highlight in this field is the realisation of a gravity-resonance spectroscopy technique. Resonance spectroscopy is a well known technique but usually limited to electromagnetic interactions. For the first time, a gravitational resonance between quantum mechanical transitions was achieved using ultra-cold neutrons bouncing off a vibrating system consisting of a polished horizontal mirror and an absorber above it. An extension of this technique can probe the equivalence principle as well as Newton's gravity law.

MODELLING AND SPECTROSCOPY

The field of 'Spectroscopy in solid-state physics and chemistry' covers a broad scientific spectrum, which is increasingly extended towards topics of societal impact. A large part of the related work is ranked as highlight proposals offering a good mix between single crystal and polycrystalline samples and covering mainly condensed matter and materials physics, materials chemistry, and molecular systems. In this context some typical applications concern porous media and photosynthesis, thermoelectric materials and energy sustainability, ionic conductivity and sensor devices, water dynamics and hydrogen fuel cells, and last but not least, dynamics of DNA and life science. The importance of neutron spectroscopy and its versatility in different fields ranging from biology to materials for technological applications is exemplified by three highlights. The impact on life science is illustrated by two of them. The work on DNA (p.64) is of an innovative nature leading to deeper understanding of the mechanical properties of this building-block molecule of prime importance for the functioning of the cell. Interestingly, DNA is found to behave mechanically like a car safety belt! The second highlight (p.62) is dedicated to the apoferritin protein. Unique insight is gained into the dynamic landscape of this bio-macromolecule. Given the complexity and diversity of such biomaterials this work is of added value for the establishment of a detailed dynamical bio-database. We would like to stress the synergistic way in which modelling activities accompany spectroscopic data for accurate interpretation and efficient analysis. The third highlight (p.66) dealing with negative thermal expansion in a cyanide-based framework material reinforces this assertion. The mechanism leading to this remarkable and unusual phenomenon relevant to practical applications could be clearly identified.

REFERENCES

[1] A.D. Fortes *et al.*, *Science* (2011) 742-746
[2] A.Y. Kovalevsky *et al.*, *Angewandte Chemie* 50 (2011) 7520-7523
[3] E.I. Howard *et al.*, J. Mol. Recognit. 24 (4) (2011) 724-732
[4] S. Garg *et al.*, Biophysics Journal 101 (2) (2011) 370-377


NewScientist Life

search New Scientist Go »

Home News In-Depth Articles Blogs Opinion TV Galleries Topic Guides Last Word Subscribe Dating

SPACE TECH ENVIRONMENT HEALTH LIFE PHYSICS&MATH SCIENCE IN SOCIETY

Home | Life | Physics & Math | News

Water's quantum weirdness makes life possible

› 25 October 2011 by Lisa Grossman
› Magazine issue 2835. Subscribe and save
› For similar stories, visit the Quantum World Topic Guide

PRINT SEND SHARE

WATER'S life-giving properties exist on a knife-edge. It turns out that life as we know it relies on a fortuitous, but incredibly delicate, balance of quantum forces.

Water is one of the planet's weirdest liquids, and many of its most bizarre features make it life-giving. For example, its higher density as a liquid than as a solid means ice floats on water, allowing fish to survive under partially frozen rivers and lakes. And unlike many liquids, it takes a lot of heat to warm water up even a little, a quality that allows mammals to regulate their body temperature.

But computer simulations show that quantum mechanics nearly robbed water of these life-giving features. Most of them arise due to weak hydrogen bonds that hold H_2O molecules together in a networked structure. For example, it is hydrogen bonds that hold ice molecules in a more open structure than in liquid water, leading to a lower density. By contrast, without hydrogen bonds, liquid

Published in 'NewScientist' on 25 October 2011.


Thursday 26 January 2012

The Telegraph

HOME NEWS SPORT FINANCE COMMENT BLOGS CULTURE TRAVEL LIFESTYLE

UK World Politics Obituaries Education Earth Science Defence Health News

Science News Space Roger Highfield Dinosaurs Evolution Steve Jones

HOME » SCIENCE » ROGER HIGHFIELD

The physics of exotic soap bubbles

Developments in the study of neutrons - a building block of all matter - may help us understand the Big Bang, writes Roger Highfield.

Published in 'The Telegraph' on 20 September 2011.


SCIENTIFIC AMERICAN™

Winner of the 2011 National Magazine Award for General Excellence

Subscribe News & Features Blogs Multimedia Education Citizen Science Topics

Home » Nature »

Nature | Health

Cholesterol Moves Slowly Among Cells

A study tracking cholesterol movement within membranes suggests that it travels more slowly than expected.

July 19, 2011

Share Email Print

Published in 'Scientific American' on 19 July 2011.


WIRED.CO.UK

Search Wired.co.uk

HOME NEWS REVIEWS PHOTOS VIDEOS MAGAZINE PODCAST TOPICS

Technology Culture Science Business Gaming Autopia Geek Dad The Great

SCIENCE

Study: DNA is as stretchy as nylon

By Olivia Solon | 09 September 11

Researchers at the Institut Laue-Langevin have used neutron scattering to work out how stretchy DNA is, after many previous studies produced very different answers. The results can help to explain how DNA can bend and split in order to establish traits in living organisms and then pass these on from generation to

Published in 'Wired.co.uk' on 9 September 2011.


8 MedLabNews April 2011

Feature: **Imaging**

Giving resonance to miracle superconductors

The possibility of resistance-free electrical transfer at higher temperatures would reduce the cost of MRI scanners. Yet commercial deployment of these conductors has failed to materialise. We look at what went wrong and how new research is uncovering the mysteries behind high temperature superconductivity

It is 100 years since the discovery of superconductivity, the phenomenon that allows certain materials to conduct electricity without resistance at low temperature and therefore transport electrical energy without loss.

Usually, the 'critical' temperature required to induce superconductivity is so low – most superconductive magnets has driven the costs of MRI machines into millions of pounds, limiting their use in the financially-constrained health-care environment.

In response, manufacturers have developed less expensive, low-magnetic-field-strength (0.2 Tesla and below) MRI scanners. Most of the

The discovery was awarded with the Nobel Prize in physics and led US president Ronald Regan to declare a new age of technology. As well as MRI machines, many in industry envisaged application in a range of new areas including levitating high-speed trains, super-efficient power generators and ultra-powerful supercomputers.

Whilst considerable progress has been made in the last quarter of a century, an understanding of the mechanism driving high temperature superconductivity remains elusive and continues to hold back its commercial deployment.

In all superconductors, electrons form pairs below a critical temperature. At these temperatures, atoms or obstacles in the crystal do not posses the energy required to break the pair and therefore can no longer deflect electrons. As a result, electron pairs are able to fly around the material unimpeded, giving rise to superconductivity. In conventional superconductors, the pairing is a subtle consequence of the interaction of the electrons with vibrations of the atomic lattice. However this theory does not hold for

Published in 'LabNews' on 9 April 2011.


Berliner Zeitung

Berlin Politik Wirtschaft Kultur Sport Panorama Wissen

Übersicht | Fotogalerien | Videos | Blogs | Soziale Netzwerke | Umfragen

07.04.2011

VOR 100 JAHREN ENTDECKTE DER NIEDERLÄNDER HEIKE KAMERLINGH ONNES EINEN EFFEKT, DER PHYSIKERN BIS HEUTE RÄTSELHAFT IST

Die Supraleitung wartet noch auf ihren großen Auftritt

Von Christian Heier

Universität Leiden im April 1911: Der Physiker Heike Kamerlingh Onnes lässt seine drei Mitarbeiter mehrmals nachmessen, denn er ist überzeugt, dass es sich um einen Messfehler handeln muss. Aber es ist keiner. Alle elektrischen Kontakte sitzen richtig und die Apparatur gaukelt keine irrealen Messergebnisse vor. Schließlich, am 8. April, notiert er: "Quecksilber praktisch Null." Die Notiz markiert den Anfang eines der größten Rätsel der Physik. Vor hundert Jahren waren Kamerlingh Onnes und seine Kollegen weltweit die einzigen Menschen, die Helium so weit abkühlen konnten, dass es flüssig wurde. Das öffnete ihnen eine Spielwiese für damals einzigartige Experimente bei nur ein paar Grad über dem absoluten Temperaturnullpunkt (minus 273 Grad Celsius). Im April 1911 untersuchten sie das Sinken des elektrischen Widerstandes von hochreinem Quecksilber mit der Temperatur. Diese Frage, was mit dem Widerstand in der Nähe des absoluten Temperaturnullpunktes passiert, interessierte theoretische Physiker brennend. Einige dachten, der Widerstand falle bis zu einem bestimmten Wert und bleibe dann bis zum Temperaturnullpunkt konstant; andere dachten, er verschwinde bei dessen Erreichen ganz. Onnes Experiment zeigte, dass beide Parteien sich irrten. Schon etwa vier Grad über dem absoluten Nullpunkt fiel der Widerstand abrupt auf null. Sie hatten ein neues, mysteriöses Phänomen entdeckt: die Supraleitung. Die Konsequenzen für die Technik konnten enorm sein, wie Kamerlingh Onnes schnell erkannte. Denn ein Abkühlen auf ein paar Grad über dem absoluten Nullpunkt war technisch möglich, also ließen sich Stromkabel aus supraleitendem Material soweit kühlen, dass sie Strom verlustfrei leiten. In der Folgezeit entdeckten die Niederländer weitere Materialien,

Published in 'Berliner Zeitung' on 7 April 2011.


INSTITUT LAUE LANGEVIN Pour sa recherche de physique fondamentale, le Polygone scientifique possède un réacteur européen à haut flux

Un (petit) réacteur nucléaire à Grenoble

DÉCRYPTAGE

« Grenoble vibre comme une caisse de résonance »

Le réacteur de l'ILL peut résister à un séisme de magnitude 5,6 (!).

Pas d'habitation dans un rayon de 500 m

Published in the 'Dauphiné Libéré' on14 March 2011.

More articles on: http://www.ill.eu/news-events/press-room/ill-in-the-media/

AUTHORS
R. Caciuffo and **G.H. Lander** (Joint Research Centre, Institute for Transuranium Elements, Karlsruhe, Germany)
P. Santini, **S. Carretta**, and **G. Amoretti** (University of Parma, Italy) - **A. Hiess** (ILL and now ESS Lund, Sweden)
N. Magnani (Lawrence Berkeley National Laboratory, California, US) - **L.-P. Regnault** (CEA/UJF, Grenoble, France)

REFERENCES
[1] G. Dolling and R.A. Cowley, Phys. Rev. Lett. 16 (1966) 683; R.A. Cowley and G. Dolling, Phys. Rev. 167 (1968) 464
[2] S.J. Allen, Phys. Rev. 166 (1968) 530; ibid 167 (1968) 492
[3] R. Caciuffo *et al.*, Phys. Rev. B 59 (1999) 13892
[4] P. Santini *et al.*, Rev. Mod. Phys. 81 (2009) 807
[5] S. Carretta *et al.*, Phys. Rev. Lett. 105 (2010) 167201
[6] R. Caciuffo *et al.*, Phys. Rev. B 84 (2011) 104409

Three-axis spectrometers IN14, IN22 and IN3

The dynamics of ordered uranium dioxide: an understanding after 45 years

Simple spin-wave theory, based to a first approximation on Heisenberg exchange, often gives a qualitative description of the dynamics of many magnetic systems. However, as we examine more complex materials we find that higher-order interactions are often important, and can change dramatically the dynamics.

QUADRUPOLE EXCITATION

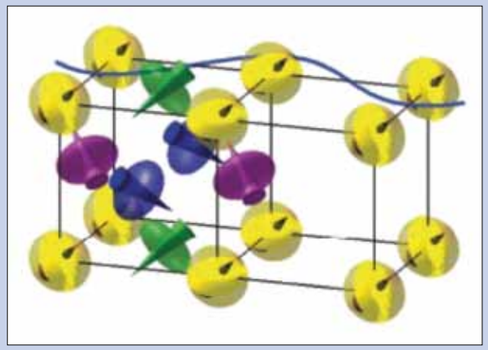

In solids with d- and f-electrons, under certain conditions the orbitals align to form an ordered pattern. Collective excitations breaking this arrangement can take the form of oscillations of electric quadrupoles, so-called quadrupolar waves.

Uranium dioxide (UO_2) has the cubic CaF_2 fcc structure and orders anti-ferromagnetically at 30 K (T_N). The first examination of the dynamics of UO_2 was reported in 1966 [1] and the strong magnon-phonon interactions, as well as the apparent complexity of the modes, have been investigated many times. Although quadrupolar interactions were already suggested as being important in the dynamics of UO_2 as early as 1968 [2], the lack of knowledge of the symmetry of UO_2 below T_N as well as the absence of any first-principles theory meant that progress was slow. Even by 1999, when the 3-k ordering and the Jahn-Teller distortion below T_N were well known, the appearance of *three* strong modes, instead of the two expected, was not understood [3].

The breakthroughs that allowed progress came through experiments with resonant X-rays and a deeper theoretical understanding of the role of higher-order interactions [4]. Unlike neutrons, resonant X-rays are *directly* sensitive to the ordering of the quadrupoles, and these were measured for both NpO_2 and UO_2 at the ESRF [4]. The development of the theory led to the prediction that in UO_2 it might be possible to observe the pure quadrupole waves through their interaction with normal spin waves [5].

The experiments at the ILL were made on two spectrometers: IN14, a cold-source triple-axis spectrometer with excellent resolution, and IN22, where we have used full polarisation analysis to separate the magnon and phonon modes [6].
Figure 1, using high-resolution data from IN14, shows the anti-crossing of the Transverse Acoustic (TA) phonon with the Spin-Acoustic (SA) mode of UO_2 around a reduced wave vector of $\xi \sim 0.45$ in the [001] direction. In the whole region $0.35 < \xi < 0.55$ both spectra have a magnetic and phonon-like character. A measurement of the repulsion between the components gives 1.71(5) meV. This magnon-phonon coupling is mediated by Q_{yz} and Q_{z^2} quadrupoles that have non-zero matrix elements between the $M = -1$ and 0 mean-field single-ion states.

Figure 2 shows the dynamics on the full spectral range up to 15 meV, where most of the data have been collected on IN22 with full polarisation analysis. At the zone center (Γ) both the pure Spin-Optic (SO) and Quadrupole-Optic (QO) modes may be observed. They strongly interact, with the intensity varying across the zone as it is transferred from one branch to the other and there is also mixing with the TA. The QO is the "3rd-mode" that has been one of the mysteries of the UO_2 magnetic spectra since 1966. The other point of interest is the presence of the Quadrupole-Acoustic (QA) modes, which are difficult to observe directly. In their pure form, as stated above, their neutron cross section is zero, but the intensity becomes non-zero if they are near in energy to a spin or a phonon mode [5], just as the QO mode picks up weight when it is near the SO mode. We have seen the weak QA mode with IN14 (see **figure 1**) at the position $\xi = 0.6$ at 6.5 meV.

In conclusion, for the dynamics of UO_2 in the ordered state the agreement between experiment and theory is excellent after 45 years! The key has been both new experiments and theory, especially a fundamental understanding of the complex role of higher-order multipoles on the dynamics. Pure quadrupole waves do not couple to the neutron cross section, but if the energy of these excitations is close to those of the pure magnons, then quadrupole modes acquire a magnon component, thus becoming observable by inelastic neutron scattering. It is as if we observe the uranium atomic moments surfing on the quadrupole waves, and the modification of their normal dynamical properties proves the existence of the underlying quadrupolar interactions. This work opens the way, both with theory and experiment, to examine systems more complex than UO_2, and understand in greater detail higher-order interactions and their effects on dynamic and other properties.

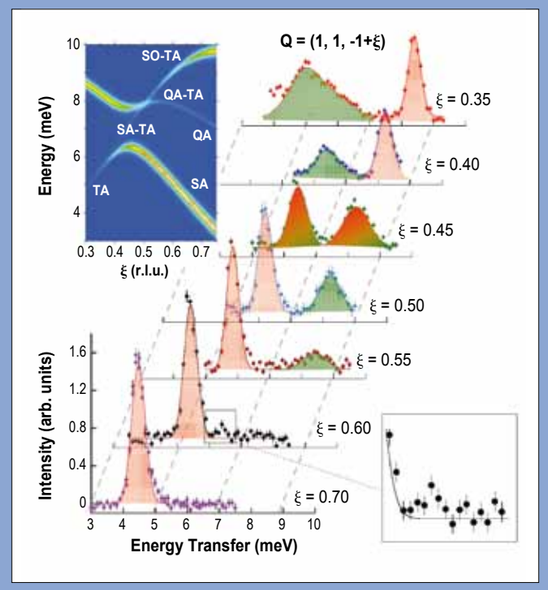

Figure 1:
Dispersion along the [00ξ] direction of the mixed magnon-phonon modes in UO_2 at 2 K, near the anti-crossing position at Q = [0,0,0.45] as measured on IN14. Red coloured peaks indicate spin-wave like; green are mostly phonon. However, there is mixing in the whole region $0.35 < \xi < 0.55$, and at $\xi \sim 0.45$ the excitations have 50% magnetic and 50% vibrational character. The upper inset shows calculated intensity maps in the energy-momentum transfer space. The lower inset shows an extra small peak at $\xi = 0.6$, which is identified as a quadrupolar acoustic mode.

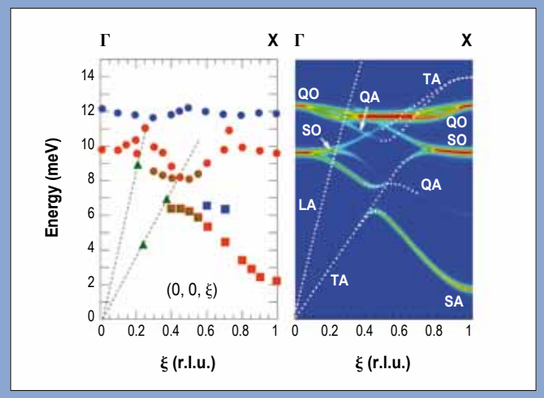

Figure 2:
Left panel: *Excitations in the low-temperature phase of UO_2 along ΓX. Red represents modes with predominant spin character. Green triangles are acoustic phonons. Blue represent modes with predominant quadrupolar character. Excitations around the magnon-phonon AC at $\xi = 0.45$ are shown by green-red (see **Figure 1**).*
Right panel*: Dipolar magnetic INS cross section along (1,1,1 – ξ), calculated by the present model.*

AUTHORS
H. Ulbrich and **M. Braden** (University of Cologne, Germany)
P. Steffens (ILL)
Y. Sidis (LLB, France)

REFERENCES
[1] J.M. Tranquada *et al.*, Nature (London) 375 (1995) 561; M. Cwik *et al.*, Phys. Rev. Lett. 102 (2009) 057201
[2] A.P. Ramirez *et al.*, Phys. Rev. Lett. 76 (1996) 3188
[3] B.J. Sternlieb *et al.*, Phys. Rev. Lett. 76 (1996) 2169
[4] J.B. Goodenough, Phys. Rev. 100 (1955) 564
[5] D. Senff *et al.*, Phys. Rev. Lett. 96 (2006) 257201
[6] H. Ulbrich *et al.*, Phys. Rev. Lett. 106 (2011) 157201

Three-axis spectrometer with polarisation analysis IN20

Evidence for charge orbital and spin stripe order in an overdoped manganite

Transition-metal oxides exhibit strong interplay between electronic and magnetic degrees of freedom which can give rise to complex novel phases. The cuprate stripe phases with antiferromagnetic regions separated by stripes of charges have attracted most interest due to the possible role of stripes in high-T_c superconductivity, but very similar stripe-type ordering was found in isostructural nickelates and cobaltates [1]. Also manganites exhibit coupled ordering of charge, orbital and spin degrees of freedom; these ordered phases compete with metallic ferromagnetic states giving rise to the colossal magnetoresistivity. Stripe phases have been proposed already long ago for highly doped manganites [2] but no consistent description of the different ordering patterns could be obtained so far.

We investigated a single-layered manganite of the $La_{1-x}Sr_{1+x}MnO_4$ series at and above half-doping. At half-doping (x = 0.5) first checkerboard-like ordering of Mn^{3+} and Mn^{4+} charges develops accompanied by an orbital ordering of e_g-electrons on the nominal Mn^{3+} sites. Below T = 110 K an antiferromagnetic (AFM) CE-type ordering sets in, which is described by the so called Goodenough model [3-5]. The excess of Mn^{4+} in overdoped $La_{0.42}Sr_{1.58}MnO_4$ perturbs such ordering. Several scenarios are possible to arrange the excess of Mn^{4+} into self-organised patterns. Our work aimed to develop a consistent model for the charge, orbital and spin order in $La_{0.42}Sr_{1.58}MnO_4$ which needs to be described by four order parameters. Although neutrons are not directly sensitive to charge or orbital distributions, the induced displacements of the oxygen atoms can be easily studied.

In contrast to previous studies, we determined the full neutron diffraction response in (hkl)-planes of reciprocal space with fixed l-component by using the Flatcone detector on IN20 [6]. A map of the scattering in the (hk0) plane is shown in **figure 2** for the half-doped (x = 0.5) and for the overdoped (x = 0.58) materials at T = 2 K. The fully ordered state of $La_{0.5}Sr_{1.5}MnO_4$ exhibits sharp superstructure reflections at exactly half and quarter-indexed positions. Different types of reflections can be easily attributed to the different ordering parameters, as illustrated in **figure 2a** [5]. The same region of reciprocal space is shown in **figure 2b** for the overdoped compound $La_{0.42}Sr_{1.58}MnO_4$. The data clearly exhibit diffuse signals which are broadened along the diagonals of the reciprocal lattice. The detailed analysis shows that the centres of scattering arising from the charge, orbital and magnetic ordering of Mn^{3+} become all incommensurate. The charge ordering satellites are displaced by an incommensurability of δ_{co} = 0.080(3) in comparison to the position seen for x = 0.5. The orbital and magnetic peaks are also displaced along the diagonals and by the same value: $\delta_{Mn3+} = \delta_{oo}$=0.037(2), which is half that of the charge order. Surprisingly, the magnetic scattering associated with the Mn^{4+} moments remains commensurate for x = 0.58. Magnetic and electronic order in $La_{0.42}Sr_{1.58}MnO_4$ corresponds thus to a coupling of three incommensurate and one commensurate order parameter. Upon increasing temperature, none of the incommensurate signals is found to shift in position but all intensities decrease.

The complete mapping of the diffraction signals allowed us to develop a consistent model for the four coupled ordering schemes in overdoped $La_{0.42}Sr_{1.58}MnO_4$ (**figure 1c**). Since all the incommensurate displacements are found along the diagonals of the cell, the excess Mn^{4+} must be arranged into stripes running along these diagonals. Due to the transverse modulation of the magnetic signal associated with the Mn^{3+} moments, these stripes must interrupt the zigzag chains, as it is illustrated in **figure 1c**. Different magnetic alignment and the orientation of the stripes result in total in four different domain orientations whose contributions need to be superposed to fully simulate the data. The amount of extra Mn^{4+} corresponding to x = 0.58 cannot be modelled by Mn^{4+} stripes with a unique distance. Instead, we have to mix blocks according to x = 0.6 (33%) and blocks with x = 0.57 (66%). Simple Fourier transforms of large supercells of the charge, orbital and magnetic order of the model shown in **figure 1c** give a perfect description of the positions of the scattering maxima as well as of the characteristic shape of the diffuse signals [6].

In summary, by using the Flatcone detector on IN20 full maps of elastic neutron scattering in an overdoped single-layered manganite $La_{0.42}Sr_{1.58}MnO_4$ are obtained. These patterns show the tight coupling between the electronic and magnetic ordering and allow to fully explain the complex order. Our observations point to a stripe-type arrangement very similar to such phases in layered cuprates, nickelates and cobaltates with the stripes of excess Mn^{4+} disrupting ferromagnetic zigzag chains.

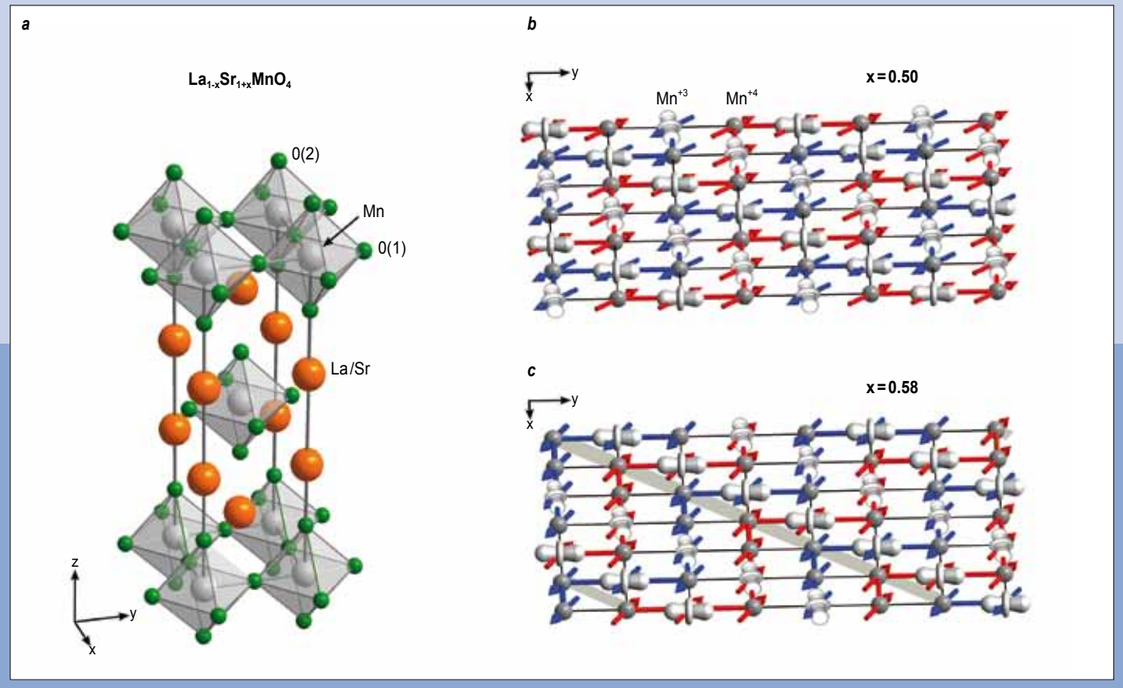

Figure 1: (a) *Tetragonal structure (I4/mmm) of the single-layered compound $La_{1-x}Sr_{1+x}MnO_4$.* ***(b)*** *The charge, orbital and spin ordering in the half-doped compound x = 0.5 inside the MnO-plane (the oxygen atoms are omitted) can be explained by the Goodenough model.* ***(c)*** *Sketch of charge, orbital and spin ordering in $La_{0.42}Sr_{1.58}MnO_4$.*

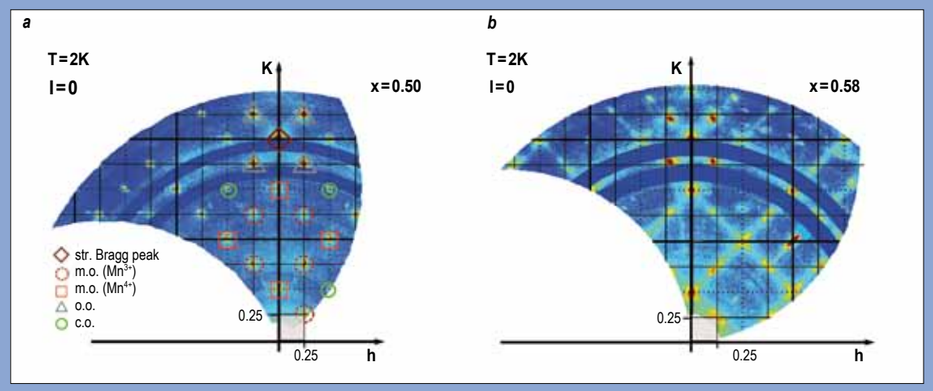

Figure 2: *Scattering map of the (hk0) plane in the half-doped compound* ***(a)*** *and in the overdoped material* ***(b)*** *at T=2 K. The different positions of the superstructure reflections reveal the different ordering parameters* ***(a)***.

AUTHORS
C. Opagiste, **R.-M. Galéra**, **M. Amara** and **C. Paulsen** (CNRS-UJF, Grenoble, France)
S. Rols and **B. Ouladdiaf** (ILL)

REFERENCES
[1] C. Opagiste, C. Paulsen, E. Lhotel, P. Rodière, R.-M. Galéra, P. Bordet, and P. Lejay, J. Magn. Magn. Mater., 321 (2009) 613
[2] K. Lea, M. Leask, and W. Wolf, J. Phys. Chem. Solids, 23 (1962) 1381
[3] M. Loewenhaupt, B.D. Rainford, and F. Steglich, Phys. Rev. Lett., 42 (1979) 1709
[4] P. Thalmeier and P. Fulde, Phys. Rev. Lett., 49 (1982) 1588
[5] P. Thalmeier, J. Phys. C: Solid State Phys., 17 (1984) 4153
[6] C. Opagiste, R.-M. Galéra, M. Amara, C. Paulsen, S. Rols and B. Ouladdiaf, Phys. Rev. B, 84 (2011) 134401

Four-circle diffractometer D10
Time-of-flight spectrometer IN4

$Ce_3Pt_{23}Si_{11}$ ferromagnet: unusual magnetic behavior brought to light by neutron studies

The ternary system R-Pt-Si (R = rare earth element) triggers a lot of interest, due to peculiar physical behaviours of some compounds, such as unconventional superconductivity, heavy-fermion properties, coexistence of superconductivity and magnetic ordering. $CePt_3Si$, for example, was reported as the first non-centro symmetric heavy fermion superconductor. Actually, several studies let suppose a sample dependence of the superconductivity and for instance, in Ce deficient samples, the coexistence of a new phase, $Ce_3Pt_{23}Si_{11}$, was suspected to interfere with superconducting properties. We have undertaken an extended investigation on this new phase.

$Ce_3Pt_{23}Si_{11}$ crystallises in a face-centered cubic structure (Fm-3m space group). Recently, we have synthesised very high quality single crystals. Magnetic measurements have shown that $Ce_3Pt_{23}Si_{11}$ orders ferromagnetically at T_c = 0.44 K with a spontaneous magnetic moment far smaller than the theoretical value of 2.14 μ_B/Ce expected for Ce^{3+} ion [1]. Such a reduction may arise from crystal electric field (CEF) effect and/or from magnetic arrangements more complex than the collinear ferromagnetic one.

Neutron diffraction experiments performed on a single crystal using the unique four-circle dilution cryostat available on the D10 diffractometer, confirmed the transition at T_C. Below T_C, as illustrated by the temperature dependence of the (220), (0-20) and (111) reflections (**figure 1**), the magnetic contribution is only observed on top of nuclear reflections with hkl all even. The non-observation of a magnetic contribution for odd reflections indices is a strong constraint. This leads to ferromagnetic couplings between pairs of Ce ions within the 6 Ce ions in the unit cell. Group theory analysis shows that the only non-zero basis vectors, consistent with a ferromagnetic arrangement on the Ce sites are those of the Γ_{10} irreducible representation. These vectors describe a ferromagnetic arrangement along [100], [010] and [001] axis respectively, while a combination of the three basis vectors leads to a ferromagnetic arrangement along the [111] direction. This is in very good agreement with the magnetisation process, shown in **figure 2a**. The refined value of the magnetic moment, 1.2(2) μ_B per Ce ion, is close to that deduced from the magnetisation measurements (**figure 2a**). Both determinations strongly indicate a doublet CEF ground state.

The CEF excitations were studied by inelastic neutron scattering on the IN4 time-of-flight spectrometer. For Ce^{3+} ions in cubic symmetry, only fourth degree terms are effective in the CEF Hamiltonian and thus only one parameter, W = ± $E_{CE}F/6$ has to be considered [2]. A positive (negative) W selects a doublet (quadruplet) as CEF ground state. Unexpectedly, two magnetic excitations are observed at E_1=12 meV and E_2=19.6 meV on the spectra (**figure 3**), while neutron diffraction experiments show that the structure remains cubic down to 800 mK. Observation of two CEF excitations in a cubic Ce compound was earlier reported in $CeAl_2$. It was interpreted in terms of an unusual magneto-elastic coupling that gives rise to a bounding state between the excited CEF quadruplet level and low-lying vibronic states [3-5].
Calculations of the magnetic susceptibility within the CEF formalism show that experimental data are in better agreement with a quadruplet CEF ground state (**figure 2b**).

In this case an interpretation similar to that of $CeAl_2$ should not apply, as the excited doublet cannot be split. The discrepancy between the different experimental observations in $Ce_3Pt_{23}Si_{11}$ together with an apparent crystal symmetry that remains cubic can be tentatively explained by the splitting of the quadruplet ground state via a dynamical Jahn-Teller effect [6]. This hypothesis will need further exploring.

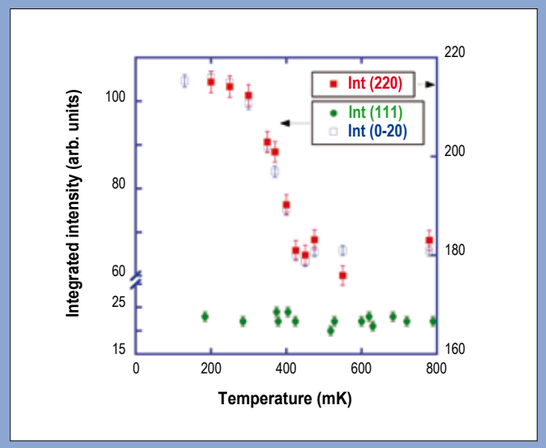

Figure 1: *Thermal variation of the integrated intensity of the (220), (0-20) and (111) reflexions (error bars are represented for each data point).*

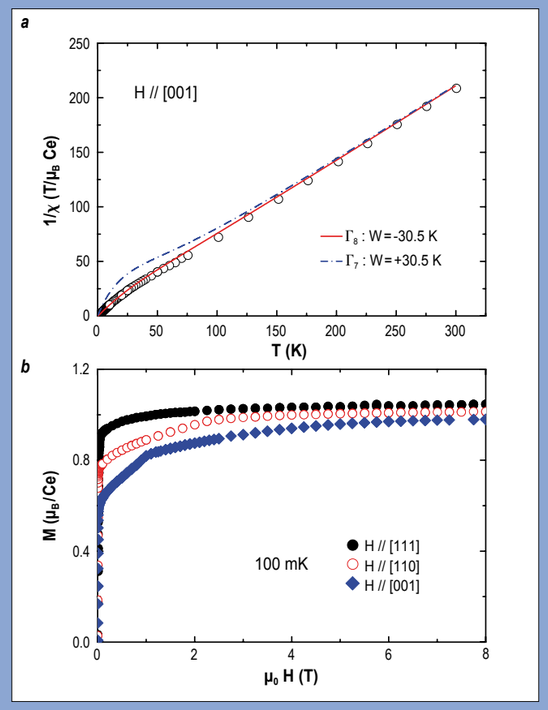

Figure 2:
(a) *Magnetisation curves along the three principle axes of the cube in the ferromagnetic phase at 100 mK.*
(b) *Thermal variation of the inverse of the magnetic susceptibility ($\mu_0 H$ // [001]). The lines represent the calculated curves using the values of the CEF parameter W reported in the figure.*

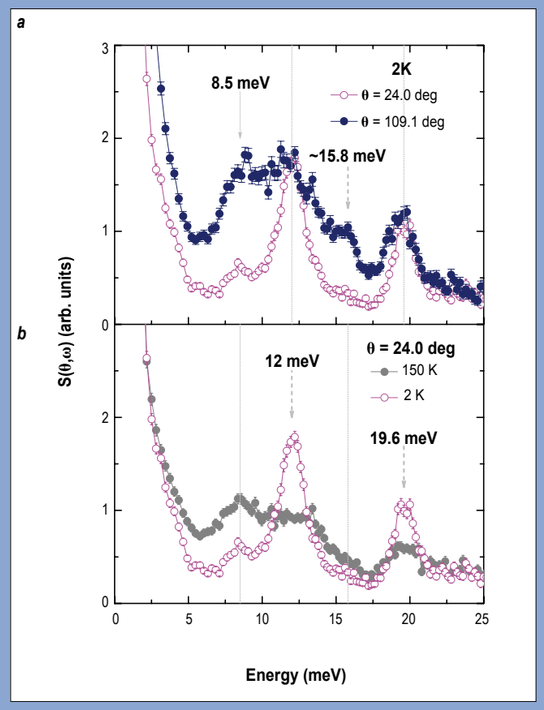

Figure 3:
(a) *Inelastic intensities for two scattering angles at 2 K.*
(b) *Inelastic intensities for T = 2 K and 150 K at low angle detector averaging.*

AUTHORS
J.-S. Zhou and **J.B. Goodenough** (University of Texas, Austin, US)
J.A. Alonso (CSIC, Cantoblanco, Spain)
A. Muñoz (University Carlo III, Avda and University Leganés-Madrid, Spain)
M.T. Fernández-Díaz (ILL)

REFERENCES
[1] Y. A. Izyumov, Sov. Phys. Usp. 23 (1980) 356
[2] E.F. Bertaut, in Magnetism edited by G.T. Rado and H. Suhl (AP, NY, 1963) Vol III, 149

High-intensity two-axis diffractometer D20

Magnetic structures on crossing the phase transition in perovskite $LaCrO_3$

The spin ordering in a magnetic crystal lowers the symmetry of the whole system, but it is normally within sub groups of the crystal symmetry of the paramagnetic phase [1]. Although the spin structures in perovskite oxides have been classified on the basis of some common crystal structures in the 1960s [2], it remains unknown whether and how spins are ordered in the rhombohedral phase. The pressure-induced phase transition from the orthorhombic phase to the rhombohedral phase in perovskite $LaCrO_3$ provides an excellent opportunity for us to study these problems and to explore whether the spin-spin interaction will be interrupted by the symmetry change.

Figure 1 displays crystal structures of orthorhombic and rhombohedral phases that are commonly seen in perovskite oxides. A first-order phase transition between these two phases can be triggered by either raising temperature or under high pressure. The transition temperature is expected to become lower under high pressure. On the other hand, the antiferromagnetic transition temperature T_N will increase under pressure based on the prediction from the Bloch rule. Therefore, the Néel temperature T_N will cross the structural phase transition temperature under a sufficiently high pressure. The orthorhombic phase accommodates type-G antiferromagnetic ordering with two possible spin directions.

On crossing the phase transition, however, the abrupt structural change, especially the symmetry change, leaves an open question: is the type-G antiferromagnetic ordering going to collapse in the rhombohedral phase? Resolving this fundamental issue is a challenge in the field of condensed matter science. First of all, neutron diffraction is required in order to reveal the detailed change in both crystal structure and magnetic structure. The sample also needs to be placed inside a high-pressure chamber with the capability of varying temperature on a neutron beamline. Developed in recent years at the ILL, a combination of a Paris-Edinburgh press mounted on a close-cycled refrigerator and high-flux neutron beam at D20 as well as the high-resolution detector is ideal to address this problem. This highly sophisticated experiment can only be made possible in collaboration with the instrument scientists at the ILL. Moreover, the software FULLPROF also developed at the ILL has been used to determine the atomic positions and spin structure from neutron diffraction.

Results of neutron diffraction on $LaCrO_3$ made at different temperatures and pressures are summarised in the phase diagram in **figure 2**.

The first-order orthorhombic/rhombohedral phase transition temperature is suppressed linearly as pressure increases. It is surprising that the antiferromagnetic ordering survives on crossing the first-order structural transition, which indicates that the symmetry change does not alter the spin-spin superexchange interaction. Although an antiferromagnetic spin arrangement remains on crossing the phase transition, the spin direction changes relative to the crystal structure of the nearest neighbour. Moreover, the canted spin structure, which is allowed in the orthorhombic phase, is prohibited in the rhombohedral phase. This study also reveals the structural change of perovskite $LaCrO_3$ under pressure. The T_N change as a function of pressure can be rationalised by the structural modification under pressure.

These new results indicate that the spin direction is always parallel to the rotation axis of the crystal structure with the highest symmetry in the space group. It is also a nice example to show the close correlation between canted spin structure and the crystal structure symmetry. Our new observations have a profound implication in designing new multiferroic materials for information technologies.

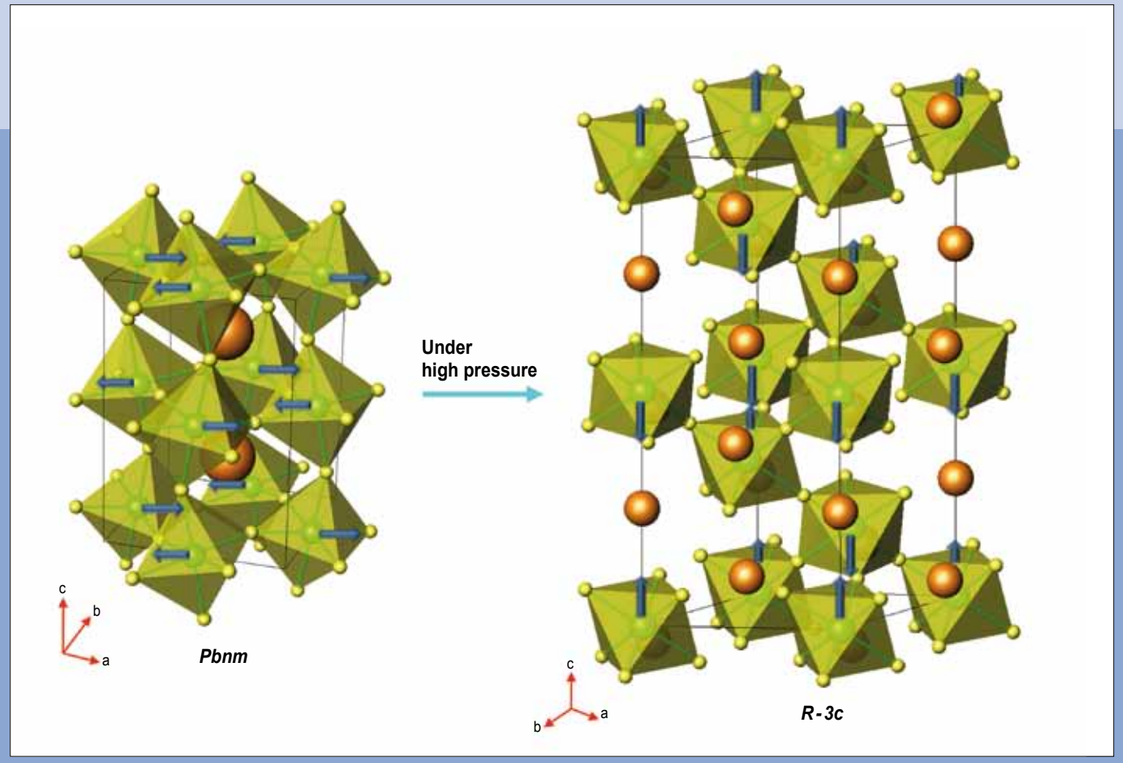

Figure 1: *Crystal structures of the orthorhombic phase (Pbnm) and the rhombohedral phase (R-3c). Arrows inside crystal structures represent arrangements of spin ordering.*

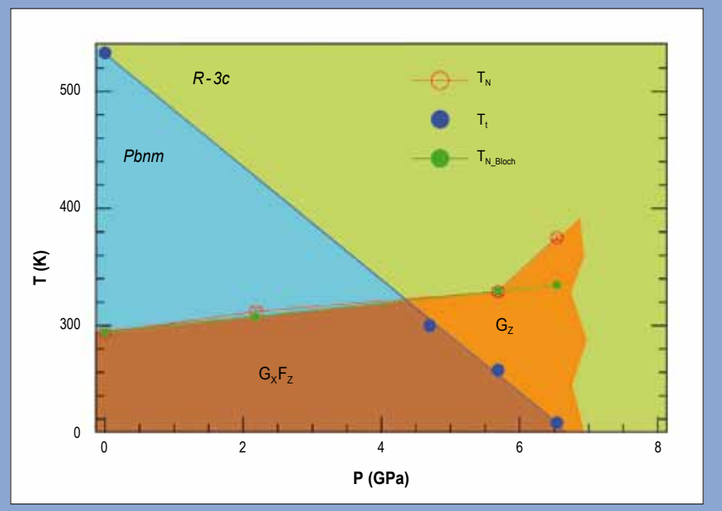

Figure 2: *The temperature-pressure phase diagram of perovskite $LaCrO_3$. Néel temperature T_N and the structure transition temperature T_t are determined by the experiment and T_{N_Bloch} is calculated based on the structural data determined in this experiment and the Bloch rule. G_xF_z stands for the type-G antiferromagnetic spin ordering with the easy axis on the x axis and the canted spin structure on the z axis; G_z is for the type-G antiferromagnetic spin ordering without any canted spin structure.*

AUTHORS
M.A. Uribe-Laverde, **D.K. Satapathy**, **I. Marozau**, **V.K. Malik**, **S. Das** and **C. Bernhard** (University of Fribourg, Switzerland)
A. Devishvili, **B.P. Toperverg** and **H. Zabel** (Institute of Solid State Physics, Ruhr University Bochum, Germany)
C. Marcelot and **J. Stahn** (Paul Scherrer Insitute, Villigen, Switzerland)
A. Rühm and **T. Keller** (Max-Planck-Institut, Stuttgart, Germany)

REFERENCES
[1] A.I. Buzdin, Rev. Mod. Phys. 77 (2005) 935
[2] F.S. Bergeret, A.F. Volkov and K.B. Efetov, Rev. Mod. Phys. 77 (2005) 1321
[3] M. Eschrig, Phys. Today 64 (2011) 43
[4] J. Stahn, J. Chakhalian, Ch. Niedermayer, J. Hoppler, T. Gutberlet, J. Voigt, F. Treubel, H-U. Habermeier, G. Cristiani, B. Keimer and C. Bernhard, Phys. Rev. B 71 (2005) 140509

Magnetic proximity effect in $YBa_2Cu_3O_{7-\delta}$ / $La_{2/3}Ca_{1/3}MnO_3$ superlattices

Atomically engineered multilayers combining materials with antagonistic orders such as superconductivity and ferromagnetism offer unique opportunities for realising novel quantum states and are also important from a technological point of view. Oxide-based superconducting/ferromagnetic multilayers in particular allow us to exploit the high superconducting transition temperature of cuprates and the versatile magnetic properties of the colossal-magnetoresistance manganites.

The interaction between superconducting (SC) and ferromagnetic (FM) orders has been studied widely and is still the subject of ongoing research. The initial theoretical predictions and later experimental proofs of proximity effects have opened the door for potential applications [1,2,3].
Nevertheless, most of this work has been focused on conventional low temperature superconductors, and little is known about the interaction between superconductivity and ferromagnetism in oxide-based materials.

These oxide based superconducting $YBa_2Cu_3O_{7-\delta}$ (YBCO) and ferromagnetic $La_{2/3}Ca_{1/3}MnO_3$ (LCMO) multilayers have obvious advantages, such as the high-T_C of cuprates or the versatile magnetic properties of manganites; these can be tailored by weak perturbations such as external magnetic fields and/or even by close proximity to SC layers. In this article, we show the results of a study of superlattices of superconducting YBCO and ferromagnetic LCMO using polarised neutron reflectometry (PNR). PNR enables us to probe magnetic depth profiles and track their evolution as a function of temperature. The superlattices consist of 10 repetitions of the bilayer structure with a nominal layer thickness of 10 nm. We found a strong magnetic proximity effect (MPE) in terms of a strong suppression of the ferromagnetic order on the LCMO side of the interfaces. We also observed anomalous superconductivity-induced changes in the thickness of these ferromagnetically depleted layers, suggesting that they should not be considered as magnetically dead, but may well host some kind of oscillatory magnetic state.

Figure 1a shows the reflectivity curves measured at different temperatures above and below the superconducting and ferromagnetic transition temperatures, T_{SC} = 88 K and T_C = 201 K respectively. Sharp and intense superlattice Bragg peaks, a product of the constructive interference between reflections coming from all the interfaces, can be observed, evidencing the high sample quality. At room temperature (green symbols), only the nuclear interaction of the neutrons is relevant and the even-order Bragg peaks are strongly suppressed, as is to be expected for a superlattice with equal layer thicknesses.

For the curves measured below the Curie temperature (red and blue symbols) intense even-order Bragg peaks are observed, the fingerprint of the reduced symmetry of the magnetic depth profile with respect to the nuclear one [4]. **Figure 1b** shows the nuclear and magnetic profiles for various temperatures, as obtained from fitting the data (solid lines in **figure 1a**).

Evidently, the ferromagnetic moment is strongly suppressed on the LCMO side of the interfaces.
Although the magnetic nature of these depleted ferromagnetic regions is not yet clear, their very large magnetic roughness and the anomalous evolution of their thickness with temperature suggest an inhomogeneous or oscillatory magnetic state.

Figure 2 shows the temperature dependence of the asymmetry of the third order superlattice Bragg peak. This asymmetry remains very small above 90 K; it exhibits a clear anomaly below TSC which reveals that the onset of superconductivity in the YBCO layers gives rise to marked changes in the depleted layers in LCMO. As shown in **figure 1b**, the thickness of the depleted layers reduces below T_{SC}.

Our PNR measurements have revealed a fascinating magnetic proximity effect, unambiguously confirming the presence of a layer on the LCMO side of the interface, where the FM order of the Mn moments is strongly suppressed. In addition, the superconducting-induced change in the thickness of the depleted FM layer is indicative of a sizeable coupling between superconducting and ferromagnetic orders across the interface.

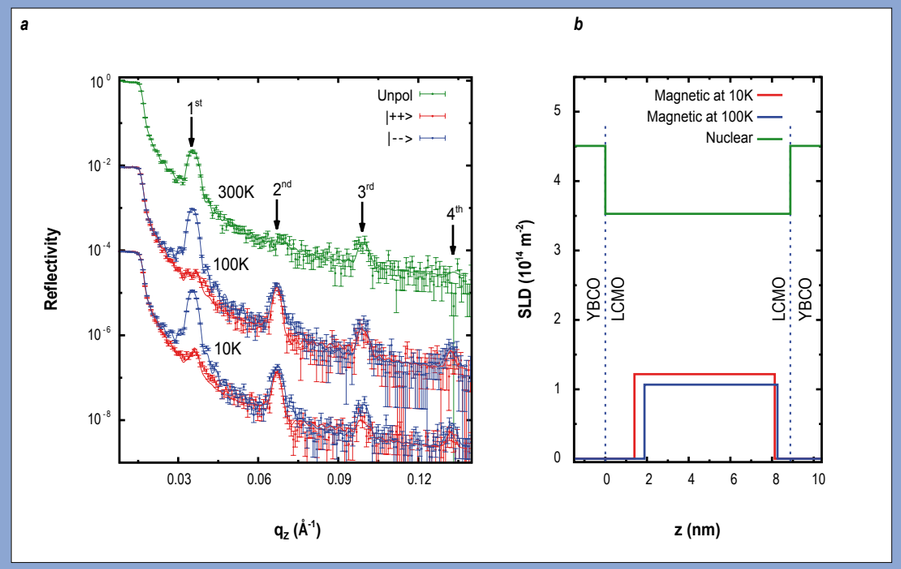

Figure 1:
(a) *Polarised neutron reflectivity curves as a function of the momentum transfer for a YBCO/LCMO superlattice at T = 300 K, T = 100 K and T = 10 K. The arrows indicate the position of the superlattice Bragg peaks. The solid lines are the results of the fits.*
(b) *Nuclear and magnetic scattering length density inside the LCMO layers as obtained from the fits.*

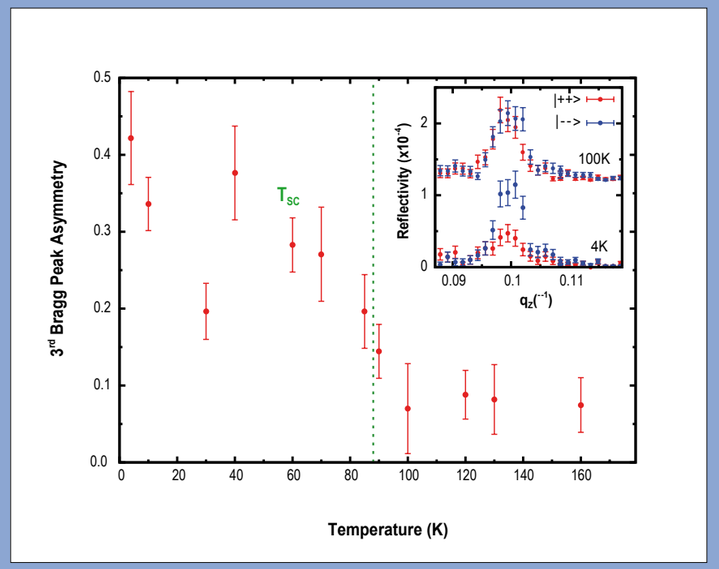

Figure 2:
Asymmetry of the third order Bragg peak, $[I^{--}\,I^{++}]/[I^{-+}\,I^{++}]$, as a function of temperature.
Inset: *Reflectivity in the vicinity of the third Bragg peak showing large splitting between the different spin channels below TSC.*

AUTHORS
M. Yang, **J.A. Rodgers** and **J.P. Attfield** (University of Edinburgh, UK)
J. Oró-Solé, **A. Belén Jorge** and **A. Fuertes** (ICMAB, Bellaterra, Spain)

REFERENCES
[1] S.G. Ebbinghaus, H.-P. Abicht, R. Dronskowski, T. Müller, A. Reller and A. Weidenkaff, Prog. Solid State Chem. 37 (2009) 173
[2] A. Fuertes, Dalton Trans. 39 (2010) 5942
[3] M. Yang, J. Oró-Solé, J.A. Rodgers, A.B. Jorge, A. Fuertes and J.P. Attfield, Nature Chem. 3 (2011) 47
[4] D. Logvinovich, S.G. Ebbinghaus, A. Reller, I. Marozau, D. Ferri and A. Weidenkaff, Z. Anorg. Allg. Chem. 636 (2010) 905

Anion order in perovskite oxynitrides

Transition metal oxynitrides with perovskite type structures are an emerging class of materials with important properties, for example, as photocatalysts that generate hydrogen from water for clean energy applications. Their properties are expected to be sensitive to any ordering of oxide and nitride anions, but the ordering principles in this class of materials were unclear. Our variable temperature neutron diffraction study of the representative compounds $SrNbO_2N$ and $SrTaO_2N$ has revealed a robust local anion order, in which disordered zig-zag metal nitride chains segregate into planes within the perovskite lattice.

Many transition metal oxynitrides adopt the AMX_3 perovskite type crystal structure [1,2]. The properties of perovskites are known to be sensitive to small structural distortions that may arise from tilting or rotations of the MX_6 octahedra. Oxide/nitride anion order is also expected to be important but consistent models have not been reported.

We have investigated anion order in the representative oxynitride perovskites $SrNbO_2N$ and $SrTaO_2N$ using powder neutron diffraction patterns collected on the high resolution instrument D2B at temperatures between 25 and 750°C [1]. At high temperatures (≥ 300°C for $SrNbO_2N$ or ≥ 200°C for $SrTaO_2N$) only the peaks expected from a cubic perovskite are observed. However, refinements of anion site occupancies in a tetragonal model gave a stable fit with the anion distribution shown in **figure 1**. This sensitivity to anion populations arises from the high neutron scattering contrast between oxygen and nitrogen. The anion order is observed up to the highest measured temperature of 750 °C for $SrTaO_2N$.

At 25°C, $SrNbO_2N$ and $SrTaO_2N$ both adopt a perovskite superstructure in which rotations of MX_6 octahedra are ordered, as evidenced by additional neutron diffraction peaks. Fits to the neutron data reveal that the rotational order axis is correlated with the anion ordering (**figure 1**). The rotational perovskite superstructure is usually described by the tetragonal space group I4/mcm, but the observed anion order is predicted to lower symmetry through loss of the c-glide operation.

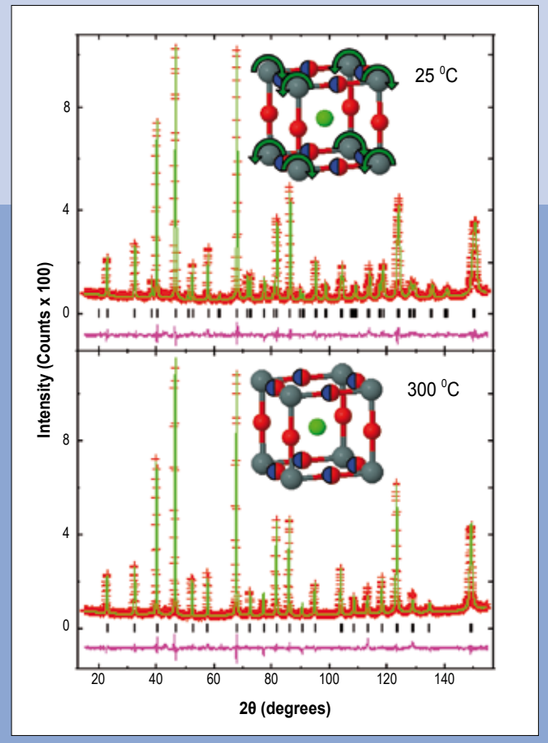

Figure 1:
Powder neutron diffraction patterns for $SrNbO_2N$ measured at a wavelength of ~1.6 Å. The atom distributions are shown in the insets (Sr/Nb/O/N = green/grey/red/blue spheres). Oxide anions occupy the cell edges in one direction, and statistical 50:50 averages of oxygen and nitrogen are observed in the other two. The 300°C neutron pattern appears cubic, with almost unresolvable broadenings arising from the anion order. Rotations (green arrows) order around one of the two 50:50 oxygen:nitrogen axes at 25°C, giving rise to additional superstructure diffraction peaks.

This is confirmed by electron diffraction studies of both materials, and of other perovskites $EuNbO_2N$, $EuTaO_2N$ and $EuWON_2$, which show that the coupling between rotational and anion orders is a common phenomenon in oxynitride perovskites.

The robust partial anion order observed in $SrMO_2N$ (M = Nb, Ta) by neutron diffraction is consistent with a well-defined short range order. This is driven by covalent effects which stabilise the cis- (90°) configuration of MN_2O_4 octahedra, as nitride is more strongly bonded to the d^0 transition metal M cations than oxide. The combination of cis-coordination of each M cation by two nitrides and the linear coordination of each nitride by two M cations results in the formation of zig-zag -M-N- chains within planes of the perovskite lattice as represented in **figure 2**. The chains are similar to those of organic polymers and are susceptible to disorder as there are two choices for the 90° turn at each M atom, resulting in randomised chains and rings within the planes (**figure 2a**) that average to the experimentally-observed anion distribution shown in **figure 1**.

The above principle of local anion order driven by differing M-N and M-O bond strengths predicts local structure across the range of $AMO_{3-x}N_x$ perovskites (**figure 2b**). The preference for the more strongly bonded nitride ligands to be mutually cis results in a symmetry between nitride order in $AMO_{3-x}N_x$, and oxide order in the corresponding AMO_xN_{3-x} composition. Hence, the representations of -M-N- chains in AMO_2N in **figure 2a** are equally applicable to -M-O- chains in $AMON_2$. This is corroborated by an independent powder neutron diffraction study of $LaNbON_2$, where an averaged oxide chain order is evident [4].

In conclusion, the oxygen/nitrogen distributions in the perovskites $SrNbO_2N$ and $SrTaO_2N$ determined by neutron diffraction evidence a well-defined local anion order, with disordered cis-metal-nitride chains confined to planes within the 3-dimensional perovskite framework. The anion order controls the axis around which the octahedra rotate to form a superstructure at room temperature. The anion order is robust but the resultant lattice distortions are very small so that high resolution neutron diffraction is needed to determine such structures. A wealth of similar local structures is expected across the range of $AMO_{3-x}N_x$ perovskites and further work will be needed to elaborate their influence on physical properties such as dielectric behaviour and photocatalysis.

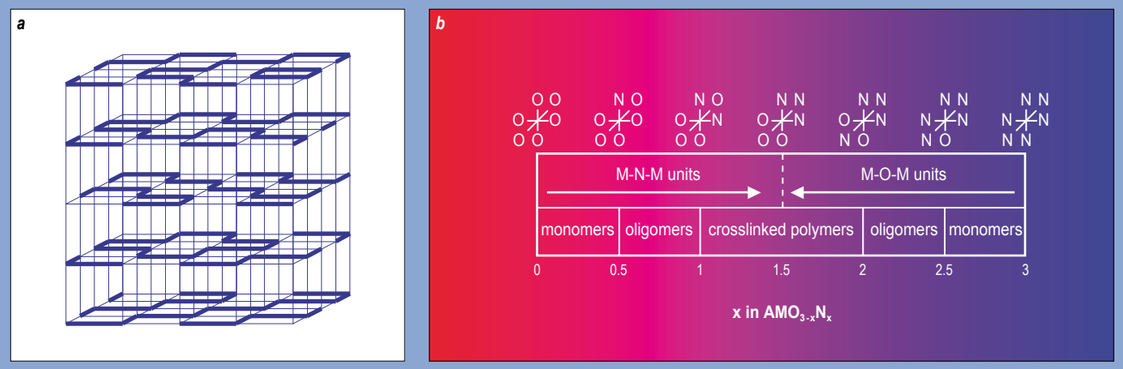

Figure 2: (a) *Planes of disordered cis-chains arising from local anion order in $SrMO_2N$ (M = Nb, Ta) perovskites. Heavy/light lines correspond to M-N-M/M-O-M units, which meet at 90° at each M cation, leading to the statistical anion distribution shown in **figure 1**.*
(b) *Predicted polymer-like anion orders across the range of $AMO_{3-x}N_x$ perovskites. M-N-M monomers are introduced into the perovskite oxide matrix as x increases from 0 to 0.5 and become connected into cis-oligomers and then infinite chains or rings at x = 1, with cis-crosslinking for 1 < x < 1.5. This is mirrored by the creation of M-O-M monomers within a perovskite nitride matrix and their polymerisation as x decreases from 3 to 1.5. Local MX_6 octahedral configurations are shown at the top.*

AUTHORS
T. Shima (RIKEN Advanced Science Institute, Saitama, Japan) - **Y. Luo** (Dalian University of Technology, China)
T. Stewart and **R. Bau** (University of Southern California, Los Angeles, US) - **G.J. McIntyre** (ANSTO, Kirrawee, Australia)
S.A. Mason (ILL) - **Z. Hou** (RIKEN Advanced Science Institute, Saitama, Japan and Dalian University of Technology, China)

REFERENCES
[1] L. Schlapbach and A. Züttel, Nature 414 (2001) 353
[2] T. Shima, Y. Luo, T. Stewart, R. Bau, G.J. McIntyre, S.A. Mason and Z. Hou, Nature Chemistry 3 (2011) 814

Diffractometer for single-crystal and fibre diffraction D19
Laue diffractometer VIVALDI

New metal-hydride clusters provide insights into hydrogen storage

Hydrogen, the most abundant element in the universe, holds great promise as a source of clean, renewable energy, producing nothing but water as a byproduct and thus avoiding the environmental dangers associated with existing mainstream energy sources. However, broad adoption of hydrogen has stalled because in its natural gaseous state the element simply takes up too much space to store and transport efficiently.

One way to solve this problem is to use metal hydrides, metallic compounds that incorporate hydrogen atoms, as a storage medium for hydrogen [1]. In this technique, the metal hydrides can bind additional hydrogen atoms to produce a solid at least one thousand times smaller than the original volume of hydrogen gas. The hydrogen can then later be released from the solid by heating it to a given temperature.

We have synthesised a new class of 'heterometallic' hydride clusters (**figure 1**) that may spur development of lighter and longer-lived fuel-cell devices [2]. The new heterometallic hydride clusters use rare-earth and *d* transition metals as building blocks and exploit the hydrogen-binding advantages of both. Even though rare-earth metal hydrides can accommodate several hydrogen atoms around each metal atom, on their own they do not undergo reversible hydrogen addition and release, the cornerstone of hydrogen storage. This becomes possible through the addition of a *d* transition metal, in this case tungsten or molybdenum.

While rare-earth/*d*-transition-metal hydride complexes have been studied in the past, our current research is the first to explore complexes of the form Ln_4MH_n with multiple rare-earth atoms and well-defined structures (Ln = a rare-earth metal such as yttrium, M = a *d* transition metal, either tungsten or molybdenum, and H = hydrogen). By incorporating multi-nuclear rare-earth metals into these compounds, we have produced the first high-density storage molecules whose hydrogen addition properties can be monitored directly using X-ray diffraction - a technique that provides crystal-clear insights into cluster structure and functionality (**figure 2**).

The location of the hydrogen atoms and the reaction mechanism were elucidated by extensive X-ray studies of the complexes before and after the addition of hydrogen, and were reinforced by a remarkable real-time study of the hydrogenation process in a single crystal and by DFT calculations.

Neutron diffraction studies on two of the hydrogen-loaded complexes using D19 and VIVALDI allowed more detailed discussion of the structure of the metal-hydride frameworks, thanks to the considerably greater sensitivity of neutrons to hydrogen in the neighborhood of heavy metal atoms. For the first yttrium-tungsten $Y_4W(PMe_3)H_{11}$ complex (**figure 1a**) accurate Y–H bond lengths and angles were obtained on the monochromatic D19 instrument, thanks to its new very large detector.

The small volume of the single crystal of the second yttrium-tungsten Y_4WH_{11} complex (**figure b**) dictated the use of neutron Laue diffraction. This complex is the first example of a well-defined hydride cluster that contains a trigonal bipyramidal five-coordinate hydrogen atom, and its unit cell is the largest that has been successfully studied on VIVALDI to date.

In summary, we have synthesised a new series of heterometallic polyhydride clusters composed of rare-earth and *d* transition metals. The structures have been determined precisely using the D19 and VIVALDI neutron diffractometers. The clusters reversibly add/eliminate hydrogen. Remarkably, the oxidative addition of hydrogen to the Y_4Mo cluster proceeds without loss of crystallinity and can be directly followed by X-ray crystallography. This study has shed first-ever light on a class of heterometallic molecular hydride structures whose unique features point the way to breakthroughs in the development of lightweight fuel-cell technology.

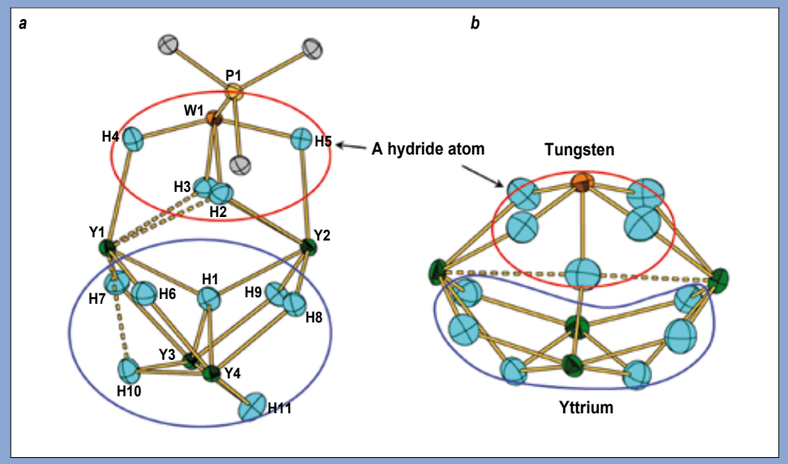

Figure 1: *Neutron structures of the core of heterometallic polyhydride complexes:* ***(a)*** *$Y_4W(PMe_3)H_{11}$ on D19,* ***(b)*** *Y_4WH_{11} on VIVALDI. Hydride ligands circled by red line (protonic) and blue line (electronic) do not exchange with each other.*

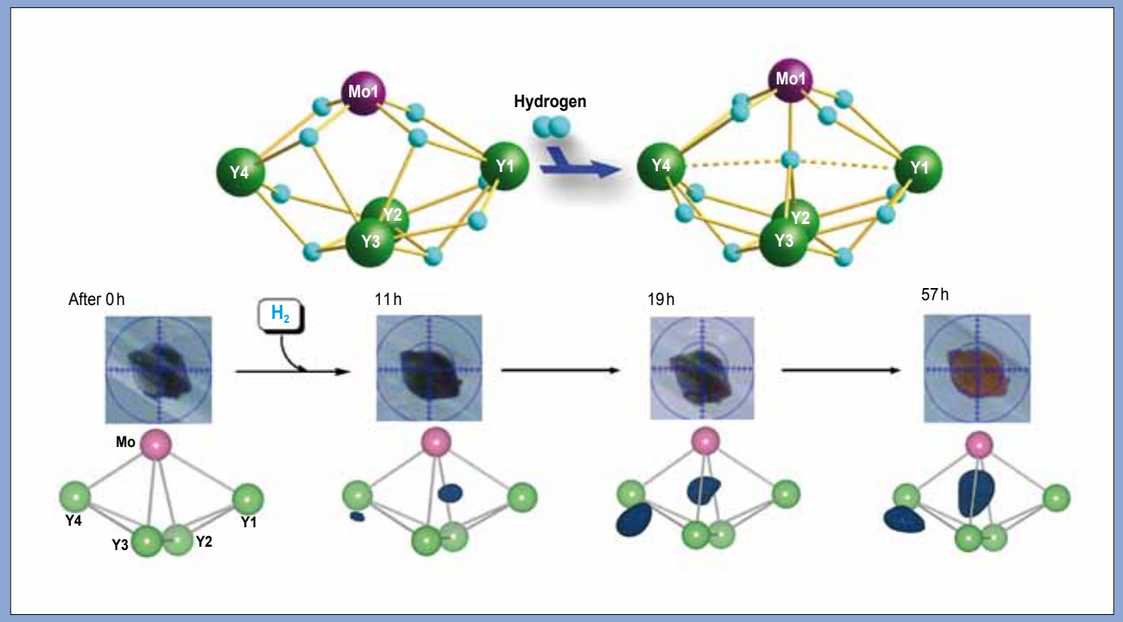

Figure 2: *Real-time monitoring of hydrogen addition reaction to the Y_4Mo cluster.*

AUTHORS
J. Meiners, **M.G. Scheibel**, and **S. Schneider** (Erlangen-Nürnberg University, Germany)
E. Herdtweck (TU München, Germany) - **M.-H. Lemée-Cailleau** and **S.A. Mason** (ILL)

REFERENCES
[1] a) M. Käß, A. Friedrich, M. Drees and S. Schneider, Angew. Chem. Int. Ed 48 (2009) 905;
b) A. Friedrich, M. Drees, M. Käß, E. Herdtweck and S. Schneider, Inorg. Chem. 49 (2010) 5482
[2] A. Friedrich, R. Ghosh, R. Kolb, E. Herdtweck and S. Schneider, Organometallics 28 (2009) 708
[3] a) P. Mura, J. Am. Chem. Soc. 108, (1986) 351; **b)** P. Mura, A. Segre, Angew. Chem. Int. Ed. Engl. 25 (1986) 460;
c) A. Albinati *et al.*, J. Am. Chem. Soc. 115 (1993) 7300; **d)** D. Capitani, P. Mura, Inorg. Chim. Acta 258 (1997) 169
[4] J. Meiners *et al.*, Angew. Chem. Int. Ed, 50 (2011) 905
[5] M.G. Scheibel *et al., submitted*

Laue diffractometer VIVALDI

A square-planar iridium(II) complex

Coordination compounds of the precious metals are of enormous importance as homogeneous catalysts for the transformation of organic substrates. Generally, their electronic structures favour closed-shell states, thus explaining the typical preference of two-electron (oxidative addition/reductive elimination) over one-electron elementary reactions. However, the importance of radical reactivity for platinum metal complexes has recently become more apparent, for example in radical H_2, C–H, and C–C activation reactions or catalytic oxidation. Nonetheless fully characterised metalloradical complexes of these metals remain comparatively scarce.

We earlier reported the dehydrogenative functionalisation of the amido pincer ligand $(PN=P^R)^-$ at the backbone of the enamido ligand $(PN=P^R)^-$ (**figures 1, 2**), allowing for fine-tuning of the ligand donor properties [1]. Here, we present the versatile functionalisation towards the novel dieneamido ligand $(P=N=P^{tBu})^-$ (**figures 1, 2**) which gives synthetic access to an iridium(II) with an open-shell electronic structure.

Single-crystal X-ray diffraction of the iridium(II) complex $[IrCl(P=N=P^{tBu})]$ **(*)** confirms a C_{2v} symmetric molecular structure (**figure 3**). The metal centre displays square-planar coordination geometry with an ideally linear N1–Ir1–Cl1 axis. The Ir1–N1 distance (1.985(2) Å) of **(*)** compares well with the iridium(I) amido complex $[Ir(C_2H_4)(PNP^{iPr})]$ (1.99(2) Å) and is slightly shorter than in $[Ir(CO)(PNP^{iPr})]$ (R=*i*Pr; 5; 2.035(4) Å) [3]. The short C2–C3 (1.348(4) Å) and N1–C2 distances (N1–C2 1.389(2) Å) are in agreement with the dehydrogenation of both pincer backbone ethylene bridges and formation of the novel $(P=N=P^{tBu})^-$ dieneamido ligand with considerable C=C and C=N double bonding contributions. However, the presence of further hydrido ligands could not be fully excluded on spectroscopic grounds, owing to the paramagnetism of **(*)** (S = ½). Interestingly, iridium(IV) dihydrido complexes $[Ir(H)_2(Cl)_2(PR_3)_2]$ (R=*iPr*, cyclohexyl) have been reported, but a reevaluation of these results could not confirm their existence [3]. Single crystal neutron diffraction was therefore used to explore this pending question. An experiment on the ILL's VIVALDI using a single crystal of **(*)** confirmed the absence of further hydride ligands and of significant Ir···H–C interactions at the vacant coordination sites. The structural features therefore fully support the formulation as a rare Ir(II) complex, stabilised by a novel, rigid 'pincer-type' ligand.

This compound provides an excellent platform for establishing isolable, electronically highly unsaturated complexes such as $[IrCl(P=N=P^{tBu})]PF_6$ [4]. In turn, these have served as starting materials for obtaining extremely rare species of precious metals with multiply bonded nitrogen, e.g. $[Ir(\equiv N)(P=N=P^{tBu})]PF_6$, or $[Ir(\equiv N)(P=N=P^{tBu})]$, which are currently being evaluated as catalysts for novel N–E (E = H, C, N) coupling reactions [5].

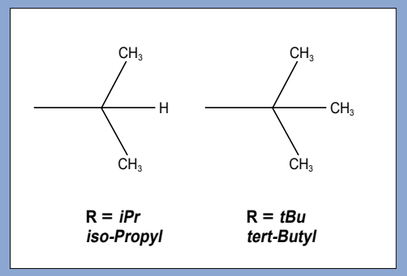

Figure 1

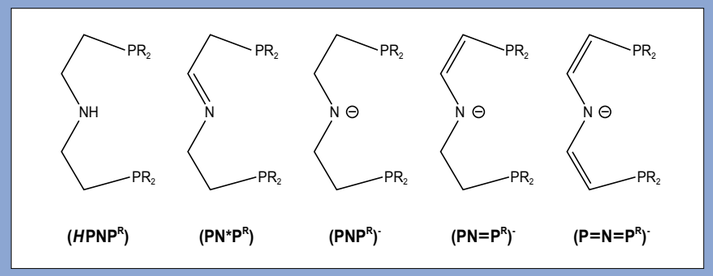

***Figure 2**: PNP chelating ligands used in our group derived from $HN(CH_2CH_2PR_2)_2$.*

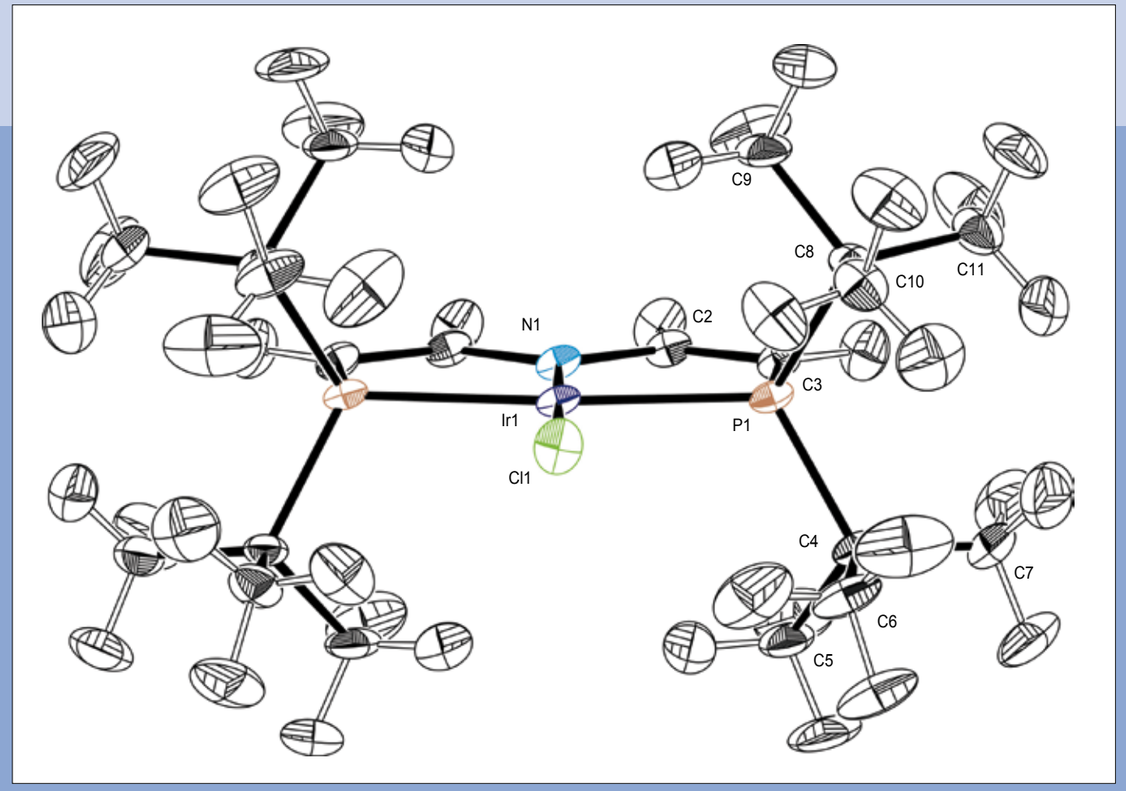

***Figure 3:** Ortep-style plot of the molecular structure of $[IrCl(P=N=P^{tBu})]$ in the solid state from single crystal neutron diffraction (ellipsoids set at 20% probability). Selected bond lengths [Å] and angles [°]: Ir1–Cl1 2.340(2), Ir1–N1 1.975(2), Ir1–P1 2.320(3), N1–C2 1.389(2), C2–C3 1.348(4); N1-Ir1-Cl1 180.0, P1-Ir1-P1i 166.45(12).*

AUTHORS

S.V. Vickers and **R.K. Thomas** [Department of Chemistry, University of Oxford, UK]
P.L. Burn [Centre for Organic Photonics & Electronics, The University of Queensland, Australia]
G. Fragneto [ILL]

REFERENCES

[1] P.L. Burn, S.-C. Lo and I.D.W. Samuel, Adv. Mater. 19 (2007) 1675
[2] G.R. Webster, W.J. Mitchell, P.L. Burn, R.K. Thomas, G. Fragneto, J.P.J. Markham and I.D.W. Samuel, J. Appl. Phys. 91 (2002) 9066
[3] W.J. Mitchell, P.L. Burn, R.K. Thomas and G. Fragneto, Appl. Phys. Lett. 82 (2003) 2724
[4] W.J. Mitchell, P.L. Burn, R.K. Thomas, G. Fragneto, J.P.J. Markham and I.D.W. Samuel, J. Appl. Phys. 95 (2004) 2391
[5] A.M. Higgins, P.C. Jukes, S.J. Martin, M. Geoghegan, R.A.L. Jones, and R. Cubitt, Appl. Phys. Lett. 81 (2002) 4949
[6] P.C. Jukes, S.J. Martin, A.M. Higgins, M. Geoghegan, R.A.L. Jones, S. Langridge, A. Wehrum and S. Kirchmeyer, Adv. Mater. (Weinheim, Ger.) 16 (2004) 807
[7] A.M. Higgins, A. Cadby, D.C. Lidzey, R.M. Dalgliesh, M. Geoghegan, R.A.L. Jones, S.J. Martin and S.Y. Heriot, Adv. Funct. Mater. 19 (2009) 157
[8] S.V. Vickers, H. Barcena, K.A. Knights, R.K. Thomas, J.-C. Ribierre, S. Gambino, I.D.W. Samuel, P.L. Burn and G. Fragneto, Appl. Phys. Lett. 96 (2010) 263302

Light-emitting dendrimer film morphology: a neutron reflectivity study

Organic semiconductors are being extensively studied in a range of applications including organic light-emitting diodes for displays and lighting, solar cells, transistors, and sensors. There are three classes or organic semiconductor materials: small molecules, conjugated polymers and most recently dendrimers. Phosphorescent light-emitting dendrimers have attracted significant attention as they have given rise to some of the most efficient solution processed OLEDs [1]. Light-emitting dendrimers are branched macromolecules that have a modular architecture and consist of a core, dendrons (branching units), and surface groups. The core and dendrons are responsible for the optoelectronic properties of the dendrimers while the surface groups provide solubility and processability. The modularity of the dendrimer structure enables independent tuning of the electrical, optical, and processing properties. For all light-emitting organic materials the morphology of the film can play a critical role in device performance as it governs the intermolecular interactions that control charge transport and the photophysical properties. With phosphorescent dendrimers it has been found that the OLED performance is dependent on dendrimer generation and/or the number of dendrons attached to the core complex.

Neutron reflectivity (NR) has been used to study the morphology of conjugated polymer films and the interface with the commonly used anode indium tin oxide (ITO) [2-7]. In this work, we applied NR measurements to study the morphology of phosphorescent dendrimer films [8]. The dendrimers are comprised of *fac*-tris (2-phenylpyridyl)iridium(III) cores (green), biphenyl-based dendrons (blue), and 2-ethylhexyloxy surface groups (red) (**figure 1**-**1**). **1** and **2** are first and second generation "singly dendronised" (one dendron per ligand) dendrimers, and because of the *facial* arrangement of the ligands are somewhat "cone" shaped. Dendrimer **3** differs from **1** and **2** in that it has two first generation dendrons attached per ligand, which we call "doubly dendronised," and is consequently more spherical in shape. The NR results provide useful information on the crucial structure-semiconducting property relationships in conjugated light-emitting dendrimer films. The dendrimers were synthesised with perdeuterated 2-ethylhexyloxy surface groups to provide contrast for the NR experiments. Importantly the perdeuterated surface groups did not change the photoluminescence properties of the dendrimers.

For the NR experiments, neat films of **1**, **2**, and **3** were spin-coated from solutions of concentrations of 20 mg/mL in chloroform onto ITO substrates. The NR measurements were carried out in the time-of-flight mode with a wavelength range of 2–20 Å at an incidence angle of 0.7° on the D17 reflectometer with the samples held under vacuum. NR measurements of the ITO on glass showed it was comprised of three layers excluding the bulk glass: the first layer immediately on the bulk glass had a thickness of 280 Å and SLD of 3.3×10^{-6} Å^{-2}; the second layer was 84 Å thick and had a SLD of 4.3×10^{-6} Å^{-2}; and the bulk layer of ITO was 1490 Å thick and had a SLD of 3.9×10^{-6} Å^{-2}. These parameters for the ITO were fixed during the analysis of the dendrimer films.

The room temperature reflectivity profiles for films of the first-generation, second-generation, and doubly dendronised dendrimers (**1**, **2**, and **3**, respectively) are shown in **figure 2**. In each case the solid markers represent the data points and the solid lines represent the fits achieved from modeling the film; the fitting parameters are summarized in **Table 1**, and the SLD *versus* position in the film is shown pictorially in **figure 3**. Our results show that NR can give direct information about the physical structure of phosphorescent dendrimer films that explains their optoelectronic properties.

For example, the NR measurements show that the shape and not just the volume of the dendrimer are important for the film morphology. The second-generation dendrimer **2** has a larger solution hydrodynamic diameter (DH in **Table 1**) than the doubly dendronised first-generation dendrimer **3**, but the cone-shaped nature of dendrimer **2** enables it to pack more efficiently in the film when compared to the more spherical dendrimer **3**. The effect of the dendrimer packing and core (the light-emitting component) dilution in the second generation and doubly dendronised dendrimers compared to the singly dendronised first generation material is consistent with the solid-state photoluminescence quantum yields increasing in the order **1** < **2** < **3**. These results confirm that NR measurements are a powerful technique for the study of organic semiconductor thin films.

Table 1

Dendrimer	SLD of bulk material (10^{-6} Å^{-2})	MW of deuterated dendrimer (g/mol)	SLdend (Å)	Density of bulk material (g/cm^3)	Volume per molecule (Å^3)	DH of protonated dendrimer (Å)
1	5.0±0.1	2211	0.0145	1.26±0.03	2900±100	20.4
2	4.5±0.1	3997	0.0280	1.07±0.02	6200±100	28.4
3	4.5±0.1	3768	0.0273	1.03±0.02	6100±100	25.6

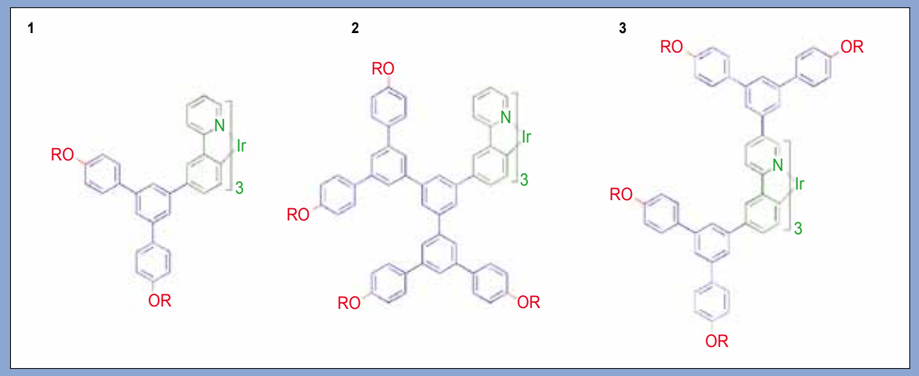

Figure 1: *Structures of the singly first **1** and second generation **2**, and doubly dendronised **3**, dendrimers where R= d_{17}-2-ethylhexyl.*

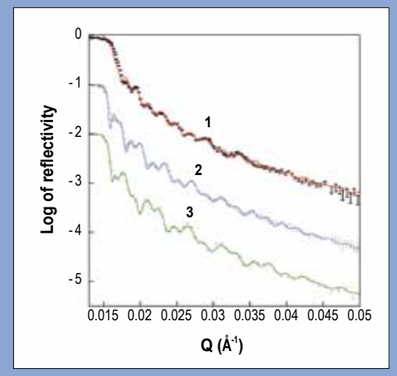

Figure 2: *Room temperature reflectivity profiles of dendrimers **1**, **2**, and **3**. The solid lines are the fits from the model. The profiles are offset for clarity.*

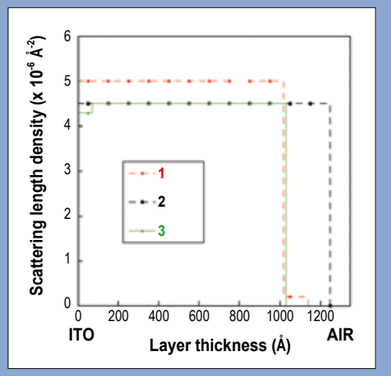

Figure 3: *SLD versus position in the film for films of the three dendrimers from the ITO surface to the air interface.*

AUTHORS
C. Pirez, **M. Capron** and **L. Jalowiecki-Duhamel** (Lille University and UCCS CNRS Villeneuve d'Ascq, France)
H. Jobic (IRCELYON, France)
F. Dumeignil (Lille University, UCCS CNRS Villeneuve d'Ascq and Institut Universitaire de France, Paris, France)

REFERENCES
[1] V.A. Goltsov, T.N. Veziroglu, L.F. Goltsova, Int. J. Hydrogen Energy 31 (2006) 153
[2] G. Zhou, L. Barrio, S. Agnoli, S.D. Senanayake, J. Evans, A. Kubacka, M. Estrella, J.C. Hanson, A. Martínez-Arias, M. Fernández-García and J.A. Rodriguez, Angew. Chem. 122 (2010) 1
[3] A. Kowal, M. Li, M. Shao, K. Sasaki, M.B. Vukmirovic, J. Zhang, N.S. Marinkovic, P. Liu, A.I. Frenkel and R.R. Adzic, Nature Materials 8 (2009) 325
[4] C. Pirez, M. Capron, H. Jobic, F. Dumeignil and L. Jalowiecki-Duhamel, Angew. Chem. Int. Ed. 50 (2011) 10193

IN1 BeF spectrometer

Evidencing hydride species in cerium nickel mixed oxides

Hydrogen and fuel cells are crucial to any clean energy policy [1]. Hydrogen can be used in almost any application in which fossil fuels are being used today. It can be used as a fuel in furnaces, internal combustion engines, turbines and jet engines, even more efficiently than fossil fuels (coal, petroleum and natural gas). Hydrogen can also be converted directly to electricity by fuel cells, leading to a variety of applications for transportation and stationary power generation. The combustion of hydrogen with oxygen results in pure steam; this has a number of applications in industrial processes and space heating. Moreover, hydrogen is an important industrial gas and raw material in industry. Hydrogen, however, has to be produced, as it is only found in nature in its compound form. In this article we describe our work at the ILL on the production of hydrogen from alternative sources.

About 90% of the hydrogen produced today comes from high temperature steam reforming processes, in large central plants at high temperatures (700°C–1000°C), in the presence of a catalyst. The hydrogen produced is used predominantly for petroleum refining and the production of ammonia for fertilisers.

To meet the growing demand for hydrogen, we need to find alternative sources and develop energy-efficient production techniques.

A number of different ways of producing hydrogen from alternative sources have recently been investigated. The production of hydrogen from biomass seems now to hold the greatest promise, given the abundance of biomass in the world.

Bio-ethanol can be obtained from biomass and has been proposed as a major renewable source of hydrogen, in so far as this approach also addresses the issue of greenhouse gases. The challenge therefore today is to provide low-cost catalysts capable of efficiently breaking the bio-ethanol C-C bond [2]. There is now a high demand for materials such as catalysts or electrocatalysts capable of activating fuels like H_2 and alcohols for the development of these new technologies [3].

At the UCCS we have successfully developed the oxyhydride compound $CeNiH_2O_y$, an exceptional catalyst that totally converts ethanol at room temperature and produces H_2 in the presence of water and oxygen (**figure 1**). H_2 is produced from ethanol in a sustainable way using the chemical energy provided by the reaction between hydride species of the nano-oxyhydride catalyst and O_2 [4].

Part of the hydride species formed from the ethanol reacts with O_2, providing the chemical energy which maintains the catalytic reaction. The reaction is sustainable because the hydride species are being continuously replaced and provided by the ethanol.

The oxyhydride compound is formed by the *in situ* activation of the $CeNiO_y$ compound with H_2 at 250 °C. The presence of hydride species in the cerium- and nickel-based mixed-oxide catalyst has been confirmed by the inelastic neutron scattering experiments performed using the IN1 BeF spectrometer at the ILL (**figure 2**).

The hydrogen species of the hydride nature related to the peak at about 460 cm^{-1} appear clearly after treatment in H_2 at 250 °C [4].

Neutron spectroscopy is the only technique able to demonstrate the coexistence of different hydrogen species stored in the solids under study; it provides important information about the nature of the hydrogen species stored in the compounds. By demonstrating the presence of hydride species in the mixed-oxide catalyst, we were able to develop a new way of producing hydrogen with lower energy costs. We are confident that this will encourage additional theoretical and experimental studies, which will expand our understanding of the fundamentals and eventually lead to exciting new developments.

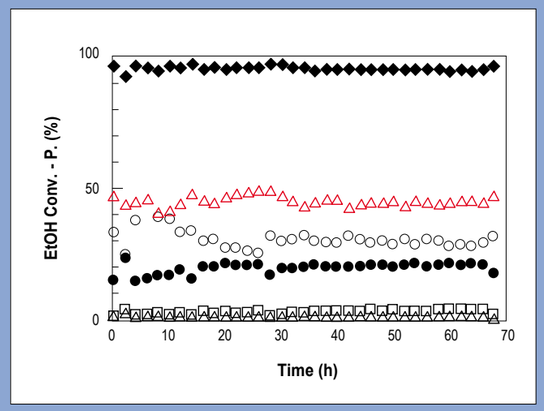

Figure 1: *Ethanol conversion [◆] and gas phase products distribution [H_2 [△], CO_2 [○], CO [●], CH_4 [△] and CH_3CHO [□] in mol. %] obtained versus time over $CeNiH_2O_y$ oxyhydride catalyst [0.03 g] with oven temperature at 60° C. The reaction mixture is $EtOH/H_2O/O_2/N_2$= 1/3/1.6/1.3.*

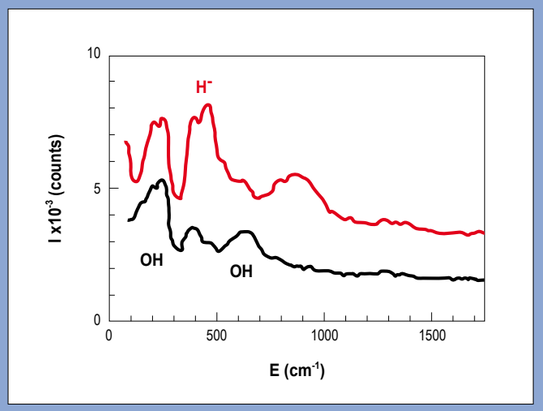

Figure 2: *Inelastic neutron spectra of $CeNiO_y$ treated in a vacuum at 200 °C (black) and in H_2 at 250 °C (red).*

AUTHORS
A. Exner, **S. Rosenfeldt** and **S. Förster** (University of Bayreuth, Germany)
P. Lindner (ILL)

REFERENCES
[1] D. Shechtman, I. Blech, D. Gratias and J.W. Cahn, Phys. Rev. Lett. 53 (1984) 1951
[2] A.R. Denton, H. Löwen, PRL 81 (1998) 469-472
[3] M.E. Zoorob, M.D.B. Charlton, G.J. Parker, J.J. Baumberg and M.C. Netti, Nature 404 (2000) 740-742
[4] S. Fischer, A. Exner, K. Zielske, J. Perlich, S. Deloudi, W. Steurer, P. Lindner and S. Förster, Proc. Natl. Acad. Sci. 108 (2011) 1810-1814

Original contribution **[4]** featured in S.C. Glotzer, M. Engel, Nature 471 (2011) 309-310 and in "Scientific Background of the Nobel Prize in Chemistry 2011" *http://www.nobelprize.org/nobel_prizes/chemistry/laureates/2011/sciback_2011.pdf*

Small-angle neutron scattering diffractometer D11

Discovery of colloidal quasicrystals

Micelles are the simplest example of self-assembly found in nature. Like many other colloids, they can self-assemble in aqueous solution to form ordered periodic structures. Until now these structures all exhibited conventional crystallographic symmetries. Using small-angle neutron scattering (SANS), quasi-crystalline micellar phases exhibiting 12-fold diffraction symmetry were observed for the first time. Colloidal water-based quasicrystals are physically and chemically very simple systems. This discovery is of particular importance, as it opens a versatile new route to the fabrication of quasicrystalline photonic band gap materials using water-based colloidal self-assembly techniques.

The formation of micelles by the association of amphiphilic molecules in aqueous solutions is one of the simplest examples of self-assembly found in nature. Micelles are ubiquitous colloids; they are used in washing detergents, for the solubilisation of pharmaceuticals, as well as in the preparation of advanced materials. Above concentrations of about 10% there is an order-disorder transition, where micelles self-assemble into liquid crystalline structures. In the case of spherical micelles, the most common structure types are of cubic symmetry with space groups $Fm\bar{3}m$ (face-centred cubic, FCC) or $Im\bar{3}m$ (body-centred cubic, BCC).

With the SANS instrument D11, we investigated the liquid crystalline phase behaviour of polymeric micelles in this concentration range in greater detail. For this investigation, we used block copolymer micelles with a well-defined micellar core containing the hydrophobic polymer blocks, surrounded by a relatively large shell consisting of the hydrophilic polymer blocks. The block copolymers were poly(isoprene-*b*-ethylene oxides) with different degrees of polymerisation of the respective polymer blocks. By shear-orientation using a Searle-type rheometer, it was possible to prepare large monodomain centimetre-dimension samples, allowing a very detailed analysis of the liquid crystalline structure.

When investigating the phase behaviour of the micelles near the order-disorder transition with SANS, we discovered a phase with a diffraction pattern of unusual 12-fold rotational symmetry (**figure 1**). This diffraction symmetry is forbidden for all of the 230 known periodic lattice space groups. In later experiments, we even discovered a further micellar phase with 18-fold diffraction symmetry. Such symmetries are typical for quasicrystals. The structure of quasicrystals resembles that of decorated tilings.

The sample showing the 12-fold rotational symmetry was investigated in planes parallel and normal to the rotation axis. The encircled reflections are typical for quasicrystals and are indexed based on generalised Miller indices (**figure 2**).

Quasicrystals were first discovered in 1984 by D. Shechtman on Al-Mn alloys [1]. They are most commonly found in binary and ternary metallic alloys, and recently also in binary nanoparticle mixtures. We have found quasicrystals that are spontaneously formed by micellar self-assembly in colloidal solutions. As they are water-based one-component quasicrystals, they are physically and chemically very simple systems. Quasicrystals with 18-fold diffraction symmetry have never been reported before for any material.
The existence of colloidal quasicrystals has been theoretically predicted for colloids with soft interaction potentials [2]. They were predicted to be stable at low temperatures in a range of concentrations between the disordered state and close-packed crystals of FCC or HCP type, which is in agreement with our experimental observations. The stability can be traced to a competition between two factors, namely packing efficiency, favouring the FCC or HCP crystal, and nearest neighbour coordination, favouring quasicrystalline order.

The unusual symmetry of quasicrystals has been exploited in recent years for the fabrication of photonic band gap arrays [3]. Owing to their high symmetry, two-dimensional quasiperiodic structures induce and widen the photonic band gap, preventing light within a range of wavelengths from propagating in any direction. To produce photonic quasicrystals elaborate electron-beam lithographic techniques are currently used. As colloidal quasicrystals are water-based, this opens the way to use established colloidal self-assembly wet chemistry routes to generate photonic quasicrystals.

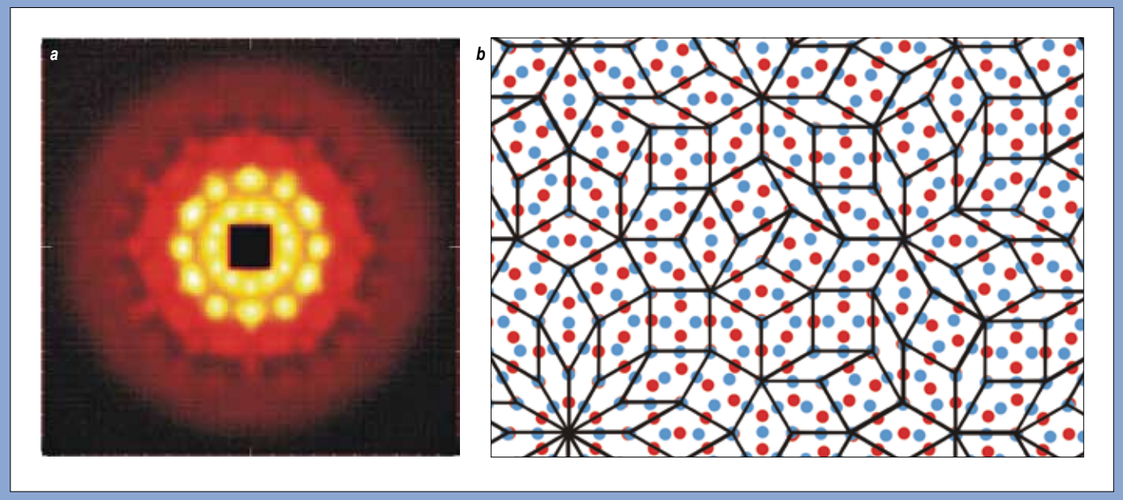

Figure 1: (a) *SANS pattern as measured at D11 showing the 12-fold diffraction symmetry of a quasi-crystalline micellar phase.* ***(b)*** *Description of the diffraction image with the 12-fold symmetry by the corresponding decorated tiling pattern. The positions of the micelles in the different layers are represented by the colour code.*

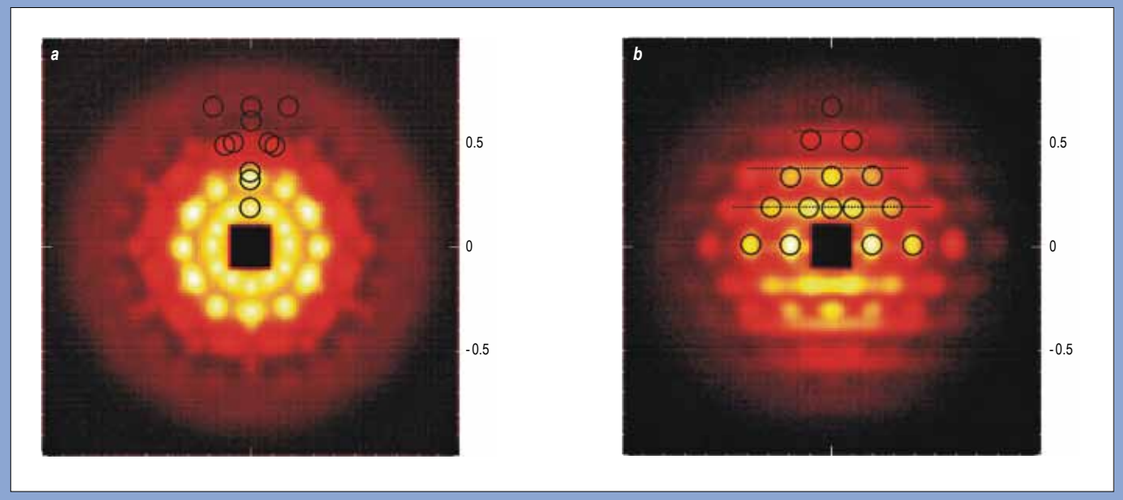

Figure 2: *SANS patterns have been recorded in planes parallel* ***(a)*** *and normal* ***(b)*** *to the 12-fold rotation axis. The circles and lines indicate the position of the reflections that are predicted for a quasicrystalline phase.*

AUTHORS
B. Lonetti, **J. Stellbrink**, **L. Willner** and **D. Richter** (JCNS-1 and ICS-1, Forschungszentrum Jülich, Germany)
M. Camargo (Heinrich-Heine University Düsseldorf, Germany, University Antonio Nariño, Bogotá, Colombia and University of Vienna, Austria)
C.N. Likos (University of Vienna, Austria) - **E. Zaccarelli** (CNR-ISC and University La Sapienza, Roma, Italy) - **P. Lindner** (ILL)

REFERENCES
[1] K.N. Pham *et al.*, Science 296 (2002) 104
[2] J. Mattson *et al.*, Nature 462 (2009) 83
[3] B. Lonetti *et al.*, Phys. Rev. Lett.106 (2011) 228301

Small-angle scattering diffractometer D11

Ultrasoft colloid/polymer mixtures: making complex fluids look simple

Hard spheres or hard spheres with added linear polymer chains have been established in the past as model systems for investigating at a fundamental level the effective interactions and phase behaviour of soft matter. Building on these simple models, great advances have been made in the study of colloidal systems in general [1]. Mixtures of soft particles offer much greater versatility compared with their hard counterparts, both in terms of structural and rheological properties and of effective interactions [2]. However, an accurate comparison between theoretical predictions and experimental results for structural correlations in soft mixtures has taken much longer to emerge [3].

A microscopic understanding that allows us to tailor macroscopic material properties is one of the great challenges for complex soft matter systems. Ideally, such an understanding must be based on both experiment and theory, quantitatively calibrated against each other. We have performed such a benchmark by investigating mixtures of ultrasoft colloids and polymer chains using rheology, small-angle neutron scattering (SANS) and liquid state theory. In this work, we show that experimental data can be described by employing recently developed effective interactions in which both components are modelled by a coarse-grained approach.

Our new theoretical approach systematically eliminates the rapidly moving degrees of freedom and focuses on the relevant slow degrees of freedom, a time-consuming and challenging task. Each complex macromolecule is replaced with a sphere of the appropriate size as schematically shown in **figure 1**. The challenge involves integrating the degrees of freedom that have been eliminated in the simplified systems as averages, so that the characteristics of the substances are retained.

As experimental model system, we studied mixtures of star-like micelles (ultrasoft colloids) and linear polymer chains, and provided a systematic and quantitative characterisation of the structure factors and phase behaviour in terms of effective interactions. By combining SANS experiments and liquid state theory, we measured and modelled the correlations between star-like micelles and linear chains. SANS measurements in core contrast allow a direct determination of experimental structure factors S(Q), providing the basis for a comparison with the recently developed theory in which both components are modelled as point particles in a coarse-grained approach that traces out the monomeric degrees of freedom. A direct comparison without any adjustable parameters, i.e. using the quantities given directly by experiment, produces very good agreement between experiment and theory for structure factors, phase behaviour and concentration dependence of the interaction length. The comparison is performed for a broad range of concentrations and highlights the influence of the added chains on the larger star polymers.

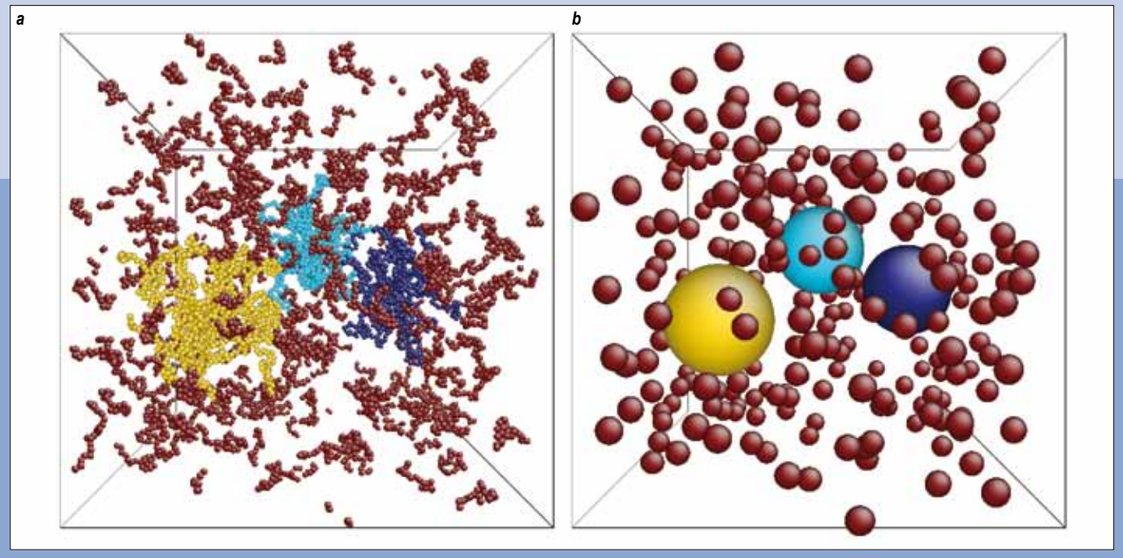

Figure 1: *Theory uses "coarse-grained spheres" on the right* ***(b)*** *to replace the complex macromolecules of the mixture of star polymers (yellow and blue) and linear polymers (red) shown on the left* ***(a)****. Using SANS on D11, we quantitatively validated that the simplified system retains all the characteristics of the original substances.*

Figure 2 shows SANS intensities I(Q) (measured on D11) for selected concentrations below and around the overlap concentration c*= 3%. To compare with theory, we set the interaction range to be given by the typical star size at low concentrations, and above c* we varied it according to well-established scaling laws; thus, the theory contained no free adjustable parameters. Agreement between experiment and theory for all other concentrations is very convincing. The position, height and width of first and second order peaks of liquid-like experimental structure factors are indeed nicely described by theory. For direct comparison, theoretical S(Q) were multiplied by P(Q) and convoluted with the instrumental resolution function. The inset in **figure 1** demonstrates the strong weakening of the peak of the star-like micelle scattering intensity upon increasing the chain density at fixed star density.

To strengthen our quantitative comparison between experiment and theory, we also considered the phase behaviour of the system. Indeed, while S(Q) is only slightly affected by varying the size ratio $\xi = R_g^c / R_g^s$, the phase behaviour may be significantly altered by a small change in the same. The agreement in phase behaviour therefore provides an additional consistency check to narrow down the values of σ_s, σ_c and ξ and to establish the correctness of the effective interactions that we adopted. Experimentally, no phase separation was observed for any of the samples under investigation. Hence they all lie in the one-phase region, in agreement with the theoretical results for $\xi = 0.30$. In addition, we investigated the rheological properties of all the samples by means of both steady and oscillatory shear measurements and found a transition to a solid (glassy) state around 29%. Indeed, the rheological properties of all the investigated samples are in accordance with the theoretical phase diagram.

In summary, we have described the structural and phase behaviour of binary mixtures of ultrasoft colloids and linear polymers. By combining rheology, small-angle neutron scattering and liquid state theory, we offer robust experimental evidence to the accuracy of the theoretical coarse-graining procedure. Without any adjustable parameters, we find quantitative agreement between experiment and theory in a wide range of concentrations. Our work provides a comprehensive characterisation of soft binary mixtures in terms of effective potentials and is therefore a successful benchmark in the study of complex soft matter systems [3].

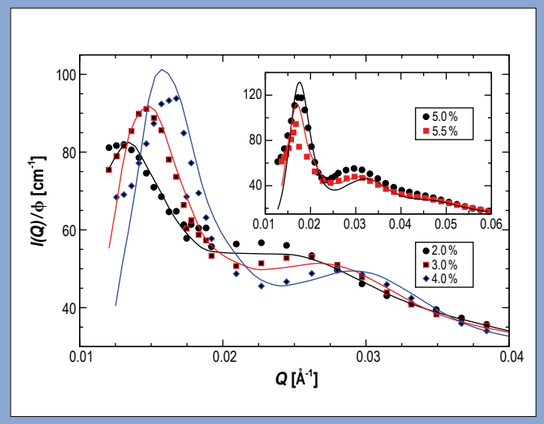

Figure 2:
Normalised SANS intensity for intermediate polymer volume fractions.
Inset: *Effect of adding chains on I(Q) at $\rho_s\sigma_s^3 = 0.37$ for $\rho_c\sigma_s^3 = 0$ (circles) and $\rho_c\sigma_s^3 = 8.6$ (squares). Symbols: experiment; lines: theory.*

AUTHORS
R.A. Campbell (ILL)
K.J. Edler (University of Bath, UK)

Growth-collapse mechanism of polyethyleneimine with cetyltrimethyl-ammonium bromide (PEI-CTAB) films at the air-water interface

Polymer-surfactant mixtures are used in countless formulations encountered in our everyday lives such as detergents, conditioners, cosmetics, paints and foods [1]. There has been sustained interest in understanding molecular interactions in such systems, and also in developing new methods to prepare ordered materials at surfaces for applications in responsive coatings, encapsulation/release and sensors [2]. Over the last decade there has also been a drive to prepare self-assembled nanostructured films at the air-solution interface [3]. The present work provides new insight into the interfacial mechanism of an intriguing system which has high potential for use in a range of applications.

Initial work on the self-assembly of thick nanostructured polymer-surfactant films focussed on the system polyethyleneimine (PEI) with cetyltrimethylammonium bromide (CTAB). Membranes involving the high molecular weight, (long) polymer (LPEI) were shown to be sufficiently robust to be recovered onto a mesh [4]. The structure of the LPEI-CTAB films at the air-solution interface involves a 2D hexagonal phase of close-packed cylindrical micelles surrounded by a polymer-water matrix. Previous work has indicated that thick film formation is driven by an evaporative steady state [5]. It was also noted that films do not form under acidic conditions, yet questions remained about the nature of the film growth process.

In the present work we have used three complementary reflectometry techniques to gain an elevated understanding of the PEI–CTAB system for which we have revealed a remarkable growth-collapse mechanism [6]. First we employed a novel approach to track quantitatively the film thickness on the micron scale using an optical technique in the Partnership for Soft Condensed Matter (PSCM) laboratory called ellipsometry. This work represented – to our knowledge – the first quantification of the thickness of films on the micron scale at the air-water interface.

Figure 1A-D shows the changing film thickness for four solutions with a range of polymer concentrations, each with 1 mM CTAB above its critical micelle concentration (cmc). A growth-collapse mechanism is observed in each case: after initial growth, the thickness reaches a plateau (up to 4 µm) before undergoing a period of instability, followed by total collapse. **Figure 1E–F** shows measurements with CTAB below its cmc and with LPEI swapped for a low molecular weight, (short) polymer (SPEI): both films are 2–3 orders of magnitude thinner. The growth of the thick PEI-CTAB films is clearly enhanced by the interaction of long hyperbranched polymer chains with surfactant micelles.

With such an insightful pre-characterisation of the system we then carried out structural measurements using neutron reflectometry on FIGARO. Data were recorded of the film state shown in **figure 1B** to track a Bragg diffraction peak at about 0.1 Å^{-1} during the growth-collapse mechanism (**figure 2**). The Bragg peak changes sharpness with its highest intensity coming just after the thick film is fully formed. The subsequent broadening of the peak suggests that the micellar ordering in the films becomes less well-defined during the period of instability after the film growth is complete. During this time the spacing between micelles in the film also varies, with the smallest d-spacing (57.1 Å) observed at the same surface age as the narrowest diffraction peak (about 1 h), suggesting that large domains of tightly packed micelles are present at this time. As the film ages, the peak position moves to smaller momentum transfer, indicating an expansion of the mesostructure due to increasing distance between micelles in the domains of the ordered phase. The Bragg peak disappears completely after 3 h which coincides well with the total collapse of the film from ellipsometry.

We also recorded optical images of films to track changes in lateral film morphology on the micron scale using another technique in the ILL laboratories, Brewster angle microscopy (**figure 3**). In the thin film regime at the start (2 min) and end (160 min) of the process the film is evenly textured and mobile. The lateral morphology of the films is similar when it is thickest (60 min) except that it is now solid and stationary. In contrast, during growth (15 min) there are linear ripples indicating the presence of long range correlations of > 300 µm, and during collapse (140 min) circular defects are evident. These observations suggest that film collapse may occur by the opening up of point defects or perhaps by spinodal decomposition.

In conclusion, as a result of the use of three complementary reflectometry techniques on the PEI-CTAB system, we are now in a position to propose an interfacial mechanism. The generation of macroscopic films is due to the interaction between trimethyl-ammonium groups on the surface of surfactant micelles with lone pairs of electrons on the primary amine groups of long polymer chains, which adsorb to the surface under an evaporative steady state. The arrest in the growth is consistent with the adsorption of CO_2 into the solution which increases the cationic polyelectrolyte charge density. Collapse is caused by the film breaking up as it dries combined with thinning as the solution acidifies. This insight can be useful for potential applications, e.g., the harvesting of solid polymer-surfactant membranes at the optimal time for defined film thickness and nanoscale structure.

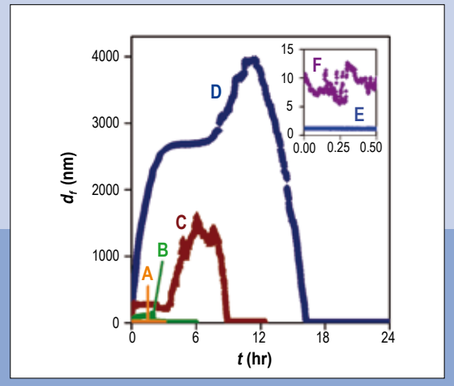

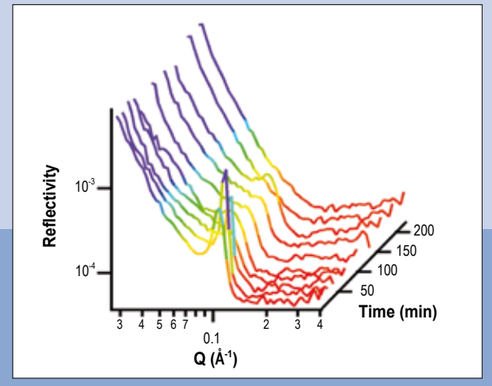

Figure 1: *Time-resolved layer thickness, d_f, with respect to the surface age, t, from ellipsometry measurements of LPEI-CTAB films where c_{PEI} is **(A)** 0.025 wt%, **(B)** 0.05 wt%, **(C)** 0.1 wt% and **(D)** 0.2 wt% and c_{CTAB} = 1 mM; **(E)** an SPEI-CTAB film where c_{PEI} = 1wt% and c_{CTAB} = 1 mM; **(F)** an LPEI-CTAB film where c_{PEI} = 0.2wt% and c_{CTAB} = 0.1 mM.*

Figure 2: *Specular neutron reflectivity profiles of an LPEI-CTAB film at the air-water interface where c_{PEI} = 0.05 % and c_{CTAB} = 1 mM.*

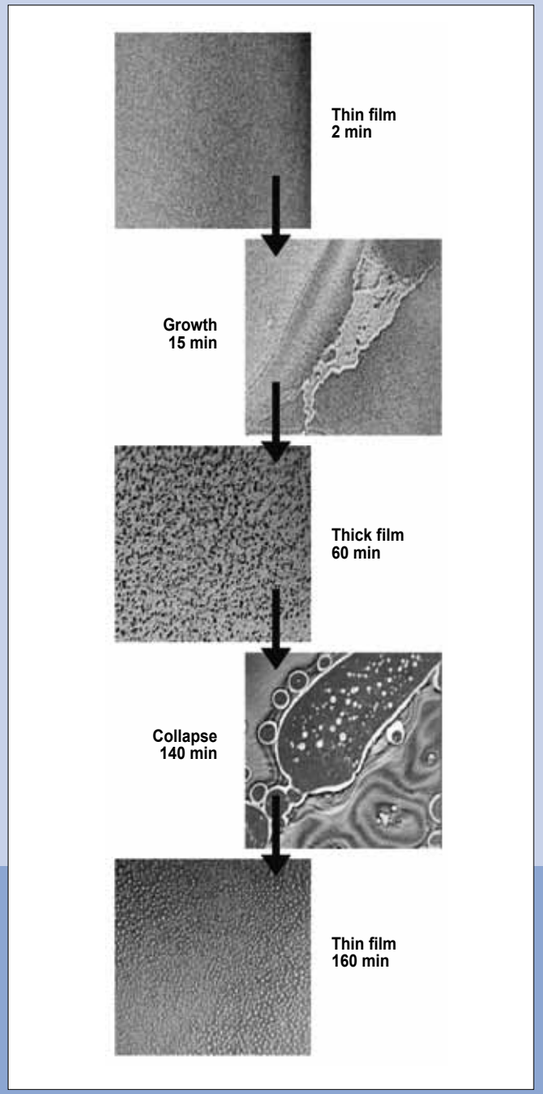

Figure 3: *Brewster angle microscopy images showing the lateral morphology on the micron scale of an LPEI-CTAB film at the air-water interface where c_{PEI} = 0.05 % and c_{CTAB} = 1 mM. Each image has a width of 340 µm.*

REFERENCES
[1] J.C.T. Kwak, Ed. Polymer-Surfactant Systems, Marcel Dekker, New York (1998) Vol. 77
[2] L. Piculell, A. Svensson, J. Norrman, J.S. Bernardes, L. Karlsson and W. Loh, Pure Appl. Chem. 79 (2007) 1419
[3] K.J. Edler, A. Goldar, T. Brennan and S.J. Roser, Chem. Commun. 14 (2003) 1724
[4] B.M.D. O'Driscoll, C. Fernandez-Martin, R.D. Wilson, S.J. Roser and K.J. Edler, Langmuir 23 (2007) 4589
[5] C. Åberg, E. Sparr, K.J. Edler and H. Wennerström, Langmuir 25 (2009) 12177
[6] R.A. Campbell and K.J. Edler, Soft Matter 7 (2011) 11125

AUTHORS
J. Valle-Orero (ILL and Ecole Normale Supérieure de Lyon, France) - **N. Theodorakopoulos** (National Hellenic Research Foundation, Greece, and Konstanz University, Germany)
M. Peyrard (Ecole Normale Supérieure de Lyon, France) - **S. Cuesta-López** (Ecole Normale Supérieure de Lyon, France, and University of Burgos, Spain)
J.-L. Garden (CNRS Grenoble, France) - **A. Wildes** (ILL)

REFERENCES
[1] R.E. Franklin and R.G. Gosling, Nature 171 (1953) 740; J.D. Watson and F.H.C. Crick, Nature 171 (1953) 737
[2] M. Peyrard and A.R. Bishop, Phys. Rev. Lett. 62 (1989) 2755; T. Dauxois, M. Peyrard and A.R. Bishop, Phys. Rev. E 47 (1993) R44
[3] N. Theodorakopoulos, Phys. Rev. E 82 (2010) 021905
[4] R. Lavery, M. Moakher, J.H. Maddocks, D. Petkeviciute and K. Zakrzewska, Nucl. Acids Res. 37 (2009) 5917
[5] A.R. Wildes, N. Theodorakopoulos, J. Valle-Orero, S. Cuesta-López, J.-L. Garden and M. Peyrard, Phys. Rev. Lett. 106 (2011) 048101; A.R. Wildes, N. Theodorakopoulos, J. Valle-Orero, S. Cuesta-López, J.-L. Garden and M. Peyrard, Phys. Rev. E. 83 (2011) 061923

Watching DNA 'melt'

DNA is a highly dynamic molecule in which the base pairs, which carry the genetic information, can have large fluctuations. This can lead to a temporary breaking of a closed pair and to a local separation of the two strands. Heat can be used to activate local openings, or "bubbles", whose size and longevity increase with the temperature until complete separation, or "melting" occurs at a sufficiently high temperature. Many studies have been made of the melting transition, however they could not provide spatial information about the size and distribution of the bubbles. This information is invaluable for comparison with statistical dynamics theory developed to describe this structural phase transition.

Neutron scattering can give this information through measurements of the thermal behaviour of Bragg peaks from an ordered material. Indeed, in the case of DNA it is perhaps the only method that can reliably give quantitative spatial information that is necessary to develop and improve the theory. The integrated intensity of a Bragg peak is proportional to the number of objects that scatter in phase, while the width of the peak is inversely proportional to the correlation length. As bubbles grow, the intensities decrease and the widths increase. These quantities can be directly calculated and compared with a theory that describes the statistical fluctuations through a phase transition.
Ordered DNA can be made in the form of oriented fibre samples. As shown by the pioneering work of Rosalind Franklin and Maurice Wilkins, these samples give Bragg peaks. X-ray diffraction images from fibre DNA allowed James Watson and Francis Crick to determine the double helix structure of the molecule [1]. DNA in fibre form can also take numerous configurational structures, dictated by the method of fabrication and by the water content of the samples.

We measured fibre DNA in the so-called B-form, which is the most commonly studied as it is the configuration found in solution. We used IN8 to measure a Bragg peak as a function of temperature. The Bragg peak was the strongest along the fibre axis and its d-spacing corresponds to the distance between the base pairs in DNA. **Figure 1** shows reciprocal space maps of the Bragg peak at two temperatures. The Bragg peak is clearly strong at room temperature, and to follow its evolution we made two scans parallel to the fibre axis. At elevated temperatures the Bragg peak vanishes.

The data were analysed to determine the integrated intensity and the width, which are plotted in **figure 2**. The intensities of the two scans differed only by a scale factor and hence they have been normalised. The widths are qualitatively different and both sets of data are in the figure. The data vary smoothly, with a gradual amplitude decrease associated with the beginning of the melting above about 345 K until a sudden change at about 350 K. The change is due to the collapse of the DNA fibre structure at this temperature, which was verified using optical microscopy. The subsequent loss of orientation of the molecules causes the sharp peaks to disappear. We do not believe that the DNA has fully melted at this temperature, however, and as a result our comparisons with theory can only be made for the initial stages of the transition.

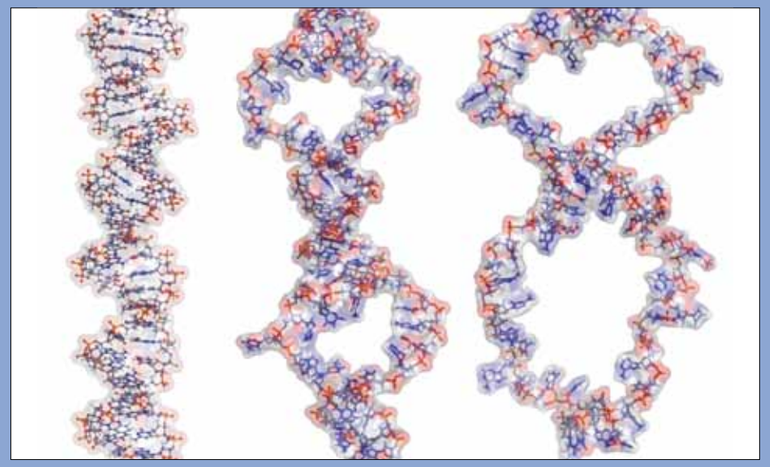

The results were analysed with the Peyrard-Bishop-Dauxois (PBD) model of DNA melting [2]. Statistical physics of its nonlinear Hamiltonian gives the probability that a base pair is open or closed along the sequence and the distribution of sizes of closed regions, which determines the expected structure factor for a neutron scattering experiment. The model parameters had been independently optimised [3], requiring only an "effective ionicity" to be estimated from calorimetric measurements of our sample. The structure factor calculation also required the knowledge of the local DNA structure, which could be obtained from conformational analysis [4].

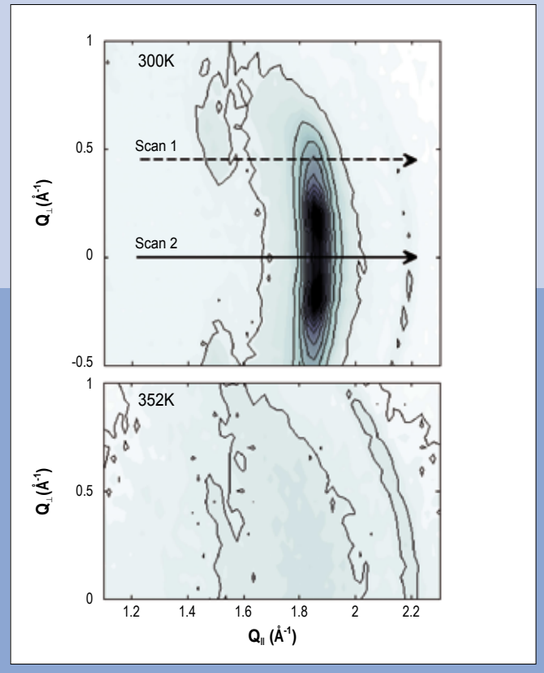

Figure 1: *Reciprocal space maps of the base-pair Bragg peak in B-form fibre DNA, measured at low and high temperatures. The trajectories for the temperature-dependent scans used for the experiment are also shown.*

The results are shown in **figure 2**. The agreement between calculation and experiment is extremely good until the collapse of the fibre structure, at which point we estimate that 50% of the molecule has melted. No free parameters have been used in the calculations for the behaviour of Scans 1, and the intensities and widths agree quantitatively. Scan 2 has a component of Q that is perpendicular to the molecule axis, and a correlation parameter linking thermal fluctuations parallel to and perpendicular to the axis is required to calculate the expected Bragg width. This parameter needed to be greater than zero for the best agreement. It has not yet been determined using conformal analysis, and represents the only free parameter in the comparison.

This result is a great success, being the first effort to measure and successfully model DNA bubble correlations and their behaviour in the melting transition of genomic DNA. Models like PBD are already used in biotechnology, for example the design of PCR (Polymerase Chain Reaction) probes, and our experiments provide important information to help improve them. We have continued our experiments with A-form fibre DNA, in which the collapse of the fibre structure does not appear to occur, and hope to have a similar degree of agreement between theory and experiment over the full range of the melting transition.

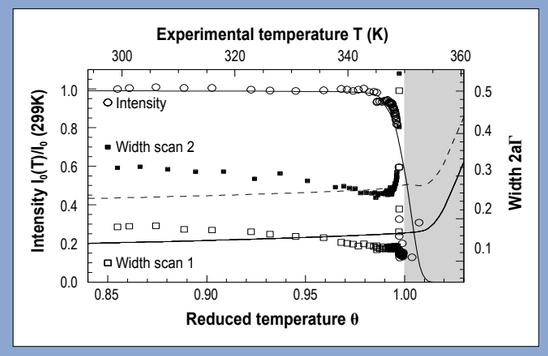

Figure 2: *The widths of the two scans and the (combined) integrated intensities as a function of temperature. The fibre structure collapses at around 350 K, and this temperature has been used to define a reduced temperature. The intensities and widths have been calculated using the Peyrard-Dauxois-Bishop model, and are shown with lines.*

AUTHORS
C.L. Armstrong (McMaster University, Canada) - **M. Trapp** (Heidelberg University and HZB Berlin, Germany)
J. Peters (ILL, IBS and UJF, Grenoble, France) - **T. Seydel** (ILL)
M.C. Rheinstädter (McMaster University and Canadian Neutron Beam Centre, Canada)

REFERENCES
[1] M.C. Rheinstädter, J. Das, E.J. Flenner, B. Brüning, T. Seydel and I. Kosztin, Phys. Rev. Lett. 101 (2008) 248106
[2] E. Falck, T. Rög, M. Karttunen and I. Vattulainen, J. Am. Chem. Soc. 130 (2008) 44–45
[3] S. Busch, C. Smuda, L. Pardo and T. Unruh, J. Am. Chem. Soc. 132 (2010) 3232–3233
[4] E. Flenner, J. Das, M.C. Rheinstädter and I. Kosztin, Phys. Rev. E: Stat., Nonlinear, Soft Matter Phys. 79 (2009) 011907
[5] G.R. Kneller, K. Baczynski, M. Pasenkiewicz-Gierula, J. Chem. Phys. 135 (2011) 141105
[6] C.L. Armstrong, M. Trapp, J. Peters, T. Seydel and M.C. Rheinstädter, Soft Matter 7 (2011) 8358-8362

Short range ballistic motion in fluid lipid bilayers studied by quasi-elastic neutron scattering

Despite intense efforts, there is still no coherent model which describes the motions of lipid molecules from less than lipid-lipid to macroscopic distances. The aim of our experiment was to prove the validity of the Brownian diffusion model down to very small length scales. During our investigation, we observed, for the first time, the transition from Brownian to ballistic motion of lipids in a fluid lipid membrane and demonstrated that the early stage of lipid motion is the result of a flow-like ballistic motion rather than the previously accepted “rattling-in-the-cage”.

Diffusion is the primary mechanism for the movement of lipids and proteins in a biological membrane. It is important in the formation of various macromolecular structures, such as lipid rafts. The commonly accepted theory for diffusion in membranes suggests that the molecules undergo continuous Brownian diffusion at long length scales, with a "rattling-in-the-cage" motion at short length scales, as shown in **figure 1**. However, this model has recently been challenged by experimental and simulation results. It has been observed that lipids move in loosely bound clusters rather than as individual molecules [1,2], and that there is a flow-like component to long range lipid diffusion [3]. Ballistic and sub-diffusive regimes have been observed in molecular dynamics simulations [4,5].

Diffusion is mainly studied by two experimental methods: fluorescence techniques and incoherent quasi-elastic neutron scattering. The two techniques access distinctly different length scales, resulting in a “blind spot” at mesoscopic distances. We note that the diffusion coefficients measured by these two techniques often differ by as much as orders of magnitude. The mechanism for diffusion, therefore, seems to depend on the length scale at which it is observed. The blind spot in the mesoscopic range will hopefully be closed in the future using high energy resolution lamor precession techniques performed with spin-echo spectrometers.

To extend the window of length scales and investigate the motion of lipid molecules at very short distances, we used the unique capabilities of the IN13 thermal backscattering spectrometer. IN13 provides access to an exceptionally large Q range, covering length scales from 1.3 to 31 Å ($0.2\,Å^{-1} < Q < 5\,Å^{-1}$). We used IN13 to study lipid diffusion at length scales smaller than a typical lipid-lipid distance in fluid bilayers. The aim of the experiment was to prove the validity of the Brownian diffusion model down to very small length scales. We chose a stacked model membrane system (DMPC) for this study and analysed the quasi-elastic neutron scattering response of the lipid molecules. Membranes were prepared as solid-supported, multi-lamellar membrane stacks on silicon wafers. Protonated lipids were hydrated by heavy water, so that the experiments were sensitive to the incoherent signal of the lipids. To increase the scattering signal, several wafers with thousands of highly oriented membranes were stacked. The membranes were studied in their physiologically relevant fluid state, at high temperature (T=30 °C) and full hydration.

The width of the quasi-elastic energy response (full width at half maximum, FWHM) is shown in **figure 2**. If a particle diffuses via random Brownian motion, the time evolution of its displacement can be written as $\sigma = \sqrt{2Dt}$, and the quasi-elastic energy broadening has a Lorentzian shape, which demonstrates the well-known quadratic behaviour $FWHM_L = 2\hbar DQ^2$. If a particle moves ballistically, $\sigma_b = vt$, the broadening has a Gaussian peak shape and the width follows $FWHM_B = 2\sqrt{2\ln 2}\,\hbar vQ$ (please refer to the original article [6] for more details). We found that at longer length scales the lipid motion can be characterised by continuous diffusion with a diffusion constant of $64 \times 10^{-12}\,m^2/s$, in excellent agreement with published values. We note that the linear fit of the Brownian diffusion in **figure 2** is not a line through the origin, as is often observed in the literature. This may point to a general shortcoming in our models for microscopic and mesoscopic diffusion in membranes. At very short length scales, however, there is a distinct change in the character of the motion. The energy broadening is no longer well described by a Lorentzian peak shape is better fit using Gaussian profiles. We therefore observe a transition from Brownian to ballistic lipid diffusion at a length scale of about 2.5 Å. From the fit, the velocity of the lipid molecule is determined to be about 1.2 m/s. This is about two orders of magnitude slower than the thermal velocity at 30 °C of about 90 m/s, which can be calculated from the equipartition theorem $k_BT = \frac{1}{2}mv^2$.

Rather than observing a thermally driven "rattling-in-the-cage" motion, we see evidence of a flow-like motion, as pictured in **figure 3**. The flow velocity was found to be significantly smaller than the thermal velocity. Viscosity and friction are essentially macroscopic properties based microscopically on short-time diffusion. However, ballistic diffusion happens before hydrodynamic interactions set in. This type of motion may therefore be impacted by mechanisms such as nano-friction and nano-viscosity.

This is the first observation of a transition from Brownian to ballistic motion in a biological material. The transition occurs at a length scale of about 2.5 Å, 1/3 of the lipid-lipid distance. Future experiments will address the question as to whether the transition is abrupt, as it appears in the data in **figure 3**, or whether the two regimes are separated by a sub-diffusive regime.

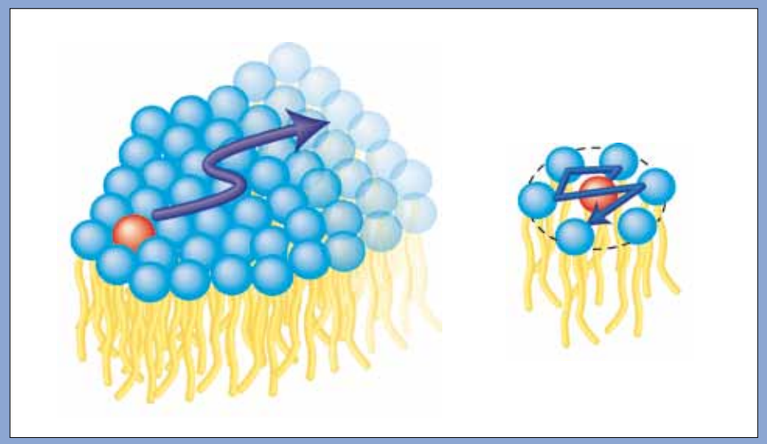

Figure 1: *Continuous Brownian diffusion at long length scales. The early stage of this motion is often modeled as a "rattling-in-the-cage" motion.*

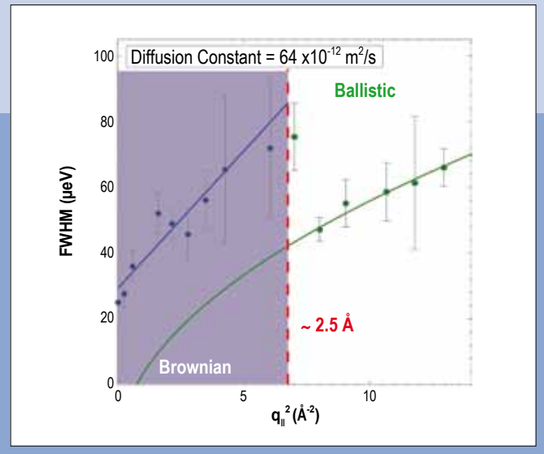

Figure 2: *FWHM of the quasi-elastic broadening plotted as function of Q^2. The linear Q^2 relationship at low Q (blue) is indicative of continuous diffusion. The high Q data (green) show a quasi-elastic broadening described by a Gaussian peak shape, with a corresponding FWHM that scales linearly with Q.*
The fit of the high Q data (green) displays as a square root when plotted against Q^2. The transition between continuous and ballistic diffusion is observed at $Q=2.5\,Å^{-1}$, marked by the red dashed line.

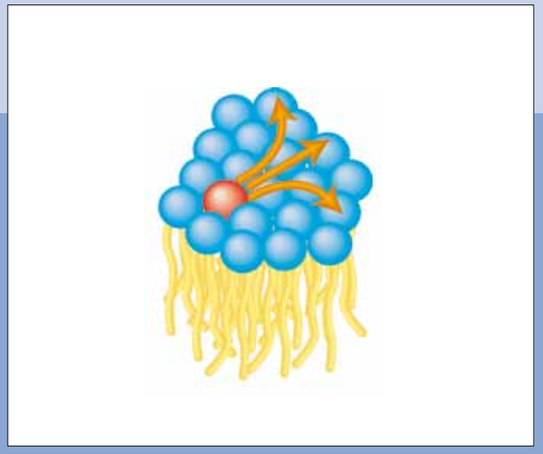

Figure 3: *Flow-like motion of lipid molecules at short length scales.*

AUTHORS
F. Roosen-Runge, **F. Zhang**, **F. Schreiber** (University of Tübingen, Germany) - **M. Hennig** (University of Tübingen, Germany, ILL and ANSTO, Australia)
R.M.J. Jacobs (University of Oxford, UK), **M. Sztucki** (ESRF), **H. Schober** and **T. Seydel** (ILL)

REFERENCES
[1] T. Ando and J. Skolnick, Proc. Nat. Acad. Sci. USA 107 (2010) 18457
[2] A.J. Banchio and G. Nägele, J. Chem. Phys. 128 (2008) 104903
[3] F. Roosen-Runge, M. Hennig, F. Zhang, R.M.J. Jacobs, M. Sztucki, H. Schober, T. Seydel and F. Schreiber, Proc. Nat. Acad. Sci. USA 108 (2011) 11815
[4] M. Hennig, F. Roosen-Runge, F. Zhang, S. Zorn, M.W.A. Skoda, R.M.J. Jacobs, T. Seydel and F. Schreiber, Soft Matter 8 (2012) 1628

Backscattering spectrometers IN10 and IN16
ESRF beamline ID02

Protein self-diffusion in crowded solutions

Reaction kinetics, information exchange, and transport processes in biological systems are based on molecular motion. The interior of biological cells contains macromolecules at a high volume fraction typically in the range of 30 to 40% in the aqueous intracellular fluid. This macromolecular crowding influences the macromolecular motion, which governs intracellular transport processes and information exchange. Applying neutron backscattering, we study concentrated aqueous solutions of a globular protein as a model system. The resulting protein short-time self-diffusion as a function of the protein volume fraction on nanosecond time scales and nanometer length scales agrees quantitatively with predictions from colloid theory. This opens up a new path to a fundamental understanding of protein diffusion.

The motion of macromolecules inside a biological cell is strongly influenced by the presence of other macromolecules in the intracellular fluid. Therefore, a quantitative understanding of macromolecular motion driven by diffusion on a molecular scale contributes to fundamental biological insights. Biological macromolecules and in particular proteins are soft and in general inhomogeneous in shape and surface charge pattern. Nevertheless, recent simulation results on the protein diffusion in a hypothetical cellular environment have found reasonable agreement with predictions from colloid theory [1, 2]. In our study [3], we experimentally investigate the protein self-diffusion under the conditions of macromolecular crowding and compare the results with the existing colloid theories. In our model system, the protein Bovine Serum Albumin (BSA) in an aqueous (D_2O) solution serves as both crowding agent and tracer particle at the same time.

The nanosecond time window of neutron backscattering allowed for the first time to access the short-time limit of protein self-diffusion. In this limit, the diffusion is solely affected by hydrodynamic interactions, since the displacement is too small to considerably change interparticle interaction potentials. A large number of backscattering spectra have been recorded to obtain the diffusion constant $D(\varphi)$ as a function of the protein volume fraction φ. The model used for the fits accounts for intramolecular dynamics, the instrumental resolution and, importantly, diffusion of the entire protein (an example data set with fit components is depicted in the inset of **figure 1**) [3]. The quadratic behavior of the linewidths γ of the narrow Lorentzian (green line), representing the diffusion of the entire protein, versus the scattering vector Q indicates simple diffusive behavior on the experimental time and length scales even in crowded solutions (main part of **figure 1**).

However, due to the experimental scales, the extracted diffusion coefficient $D(\varphi)$ consists of both translational and rotational diffusion. In order to isolate the experimental translational diffusion coefficient $D_t(\varphi)$, we developed a new framework for the full volume fraction range based on predictions [2] for diffusion of charged and uncharged hard spheres. To this end, the protein molecule was mapped to an effective sphere using Perrin factors and an approximate ellipsoid shape using data from small-angle X-ray scattering. By this means we can compare the theoretical predictions from colloid theory for effective hard spheres to the experimental system of non-spherical soft proteins.

Figure 2 displays the resulting experimental translational diffusion constants $D_t(\varphi)/D_0$ for two temperatures (symbols) in comparison with theoretical predictions for short-time self-diffusion of charged and uncharged hard spheres (blue dashed and blue solid line, respectively). D_0 is the diffusion constant in the dilute limit of the protein concentration obtained from dynamic light scattering. Within the experimental accuracy, the agreement is quantitative, suggesting that the slowing down of the self-diffusion is caused solely by hydrodynamic interactions. This agreement despite the rather simplistic spherical protein model is promising for future studies also on intramolecular dynamics of freely diffusing proteins is aqueous solution [4].

The experimental data (**figure 2**) show that $D_t(\varphi)/D_0$ decreases by more than a factor of 5 at biologically relevant volume fractions around 30% compared to the dilute limit. This considerable slowing down of the self-diffusion already on nanosecond time scales and nanometer length scales indicates a non-negligible role of hydrodynamic interactions also for longer time scales.

In conclusion, hydrodynamic interactions are an important ingredient for a full understanding of cellular processes and macromolecular crowding. Interestingly, diffusion can be understood at least to some level in terms of colloid theory also for the case of complex biomolecules. Future studies will address charge effects through a systematic charge tuning. This fundamental research can be assumed to be of interest in biomedical applications.

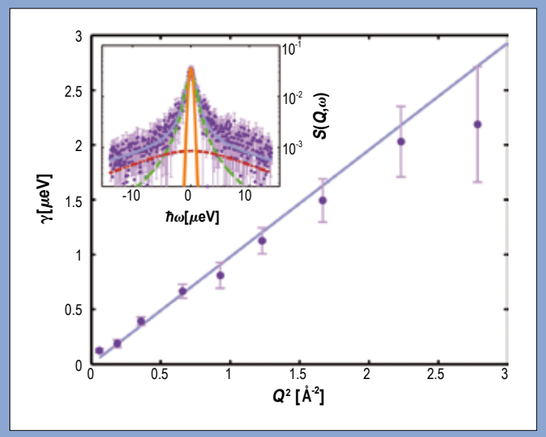

Figure 1:
Inset: *Example of a backscattering spectrum (symbols) recorded at IN16 for BSA in D_2O (concentration 500 mg/mL, φ = 28.5%, T = 300 K, individual detector at Q= 0.81 Å^{-1}). The model (magenta solid line) accounts for diffusion (green dashed line), intramolecular dynamics (red dash-dotted line) and the resolution function (orange solid line). Main figure: Fitted linewidth γ (symbols) of the narrow Lorentzian vs. Q^2.*

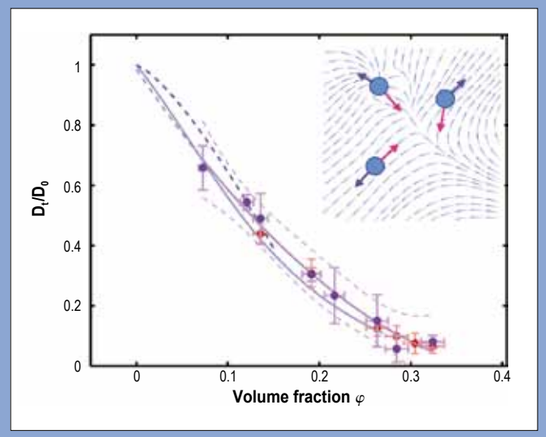

Figure 2:
Normalised translational self-diffusion coefficients $D_t(\varphi)/D_0$ (circles) vs protein volume fraction φ in aqueous solution for two temperatures (red: 280 K, purple: 300 K) indicating a temperature-independent master-curve (purple line as guide to the eye).
The data agree with predictions from colloid theory for short-time self-diffusion of hard spheres (light blue solid line) and charged spheres (dark blue dashed line).

AUTHORS
A. Zeidler and **P.S. Salmon** (University of Bath, UK) - **H. E. Fischer** (ILL) - **J.C. Neuefeind** (SNS, Oak Ridge, US)
J. Mike Simonson (Center for Nanophase Materials Science, Oak Ridge, US)
H. Lemmel and **H. Rauch** (ILL and University of Technology, Vienna)
T.E. Markland (Stanford University, US)

REFERENCES
[1] N. Lane, Oxygen: The Molecule that made the World, Oxford University Press, Oxford (2002)
[2] F. Franks, Water: A Matrix of Life, 2nd edn, Royal Society of Chemistry, Cambridge (2000)
[3] F. Paesani and G.A. Voth, J. Phys. Chem. B 113 (2009) 5702
[4] A. Zeidler, P.S. Salmon, H.E. Fischer, J.C. Neuefeind, J.M. Simonson, H. Lemmel, H. Rauch and T.E. Markland, Phys. Rev. Lett. 107 (2011) 145501

Neutron interferometer S18
Liquids and amorphous diffractometer D4

Oxygen as a site specific probe of the structure of water and oxide materials

Oxygen is a ubiquitous element, playing an essential role in many scientific and technological disciplines. Establishing the structure of a liquid or glassy oxide and thereby its relation to the functional properties of a material is not, however, a trivial task. Here we introduce the method of neutron diffraction with oxygen isotope substitution to study the structure of water. The results give insight into the role played by quantum mechanics in water's properties.

Structurally disordered oxides are important materials where examples include molten silicates in planetary science, glasses used for lasers and optical communications, the insulating oxide layers in silicon-based electronic devices, and water in biological processes [1-3]. The method of isotope substitution in neutron diffraction has provided a pivotal role in unraveling the structure of liquids and glasses. It has not, however, found application in the case of oxygen owing to the small contrast reported in the literature between the bound coherent neutron scattering lengths *b* of its isotopes. In view of the importance of oxide materials and in the absence of a suitable theory to calculate the cross section for interaction of thermal neutrons with a specific nucleus, we have used the neutron interferometer S18 at the ILL to measure the *b* values of the isotopes ^{17}O and ^{18}O relative to oxygen of natural isotopic abundance ^{nat}O [4]. The results reveal a scattering length contrast between the ^{18}O and ^{nat}O isotopes of 0.204(3) fm, giving a factor of about 6 increase by comparison with standard tabulations, and suggest that it is feasible to apply the method of oxygen isotope substitution in neutron diffraction to study the coordination environment of this element in disordered materials.

Water provides an important test bed to exploit this approach since there are several elements of its structure and dynamics that remain hotly debated [3]. One aspect of the controversy is the role played by nuclear quantum effects, such as zero point energy and tunneling, on water's hydrogen bonded network. This is manifested by differences between the structure and dynamics of heavy versus light water which lead to changes in properties such as their melting and boiling points, their temperature of maximum density, and their interaction with biological systems.

Neutron diffraction experiments were made with the instrument D4 at the ILL using either heavy water samples of $D_2{}^{nat}O$ and $D_2{}^{18}O$ or light water samples of $H_2{}^{nat}O$ and $H_2{}^{18}O$ [4]. These experiments took advantage of the count rate stability for D4 of ±0.01% over 3 days. The measured diffraction patterns for either heavy or light water were subtracted to eliminate either the D-D or H-H correlations along with the main contributions arising from inelastic scattering. The resultant first difference functions in reciprocal and real space are shown in **figures 1** and **2**. The results show that the O-H bond is about 0.5% longer than the O-D bond.

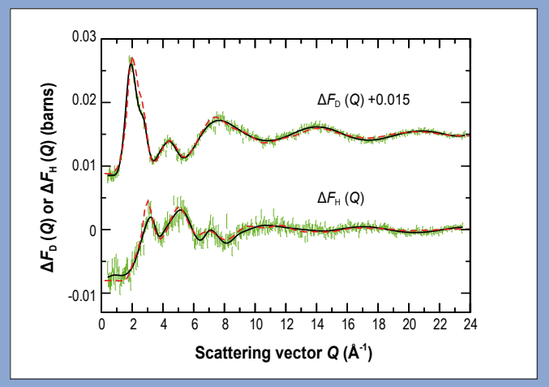

Figure 1: *The first difference functions $\Delta F_D(Q)$/barns = 0.0059(2) $[S_{OD}(Q)-1]$ + 0.00262(8)$[S_{OO}(Q)-1]$ and $\Delta F_H(Q)$/barns = −0.0033(1) $[S_{OH}(Q)-1]$ + 0.00263(8)$[S_{OO}(Q)-1]$ where $S_{\alpha\beta}(Q)$ denotes a partial structure factor. The vertical bars give the statistical errors on the data points measured by using neutron diffraction and the solid curves were used to generate the corresponding real space functions shown in* ***figure 2****. The broken curves show the path integral molecular dynamics results.*

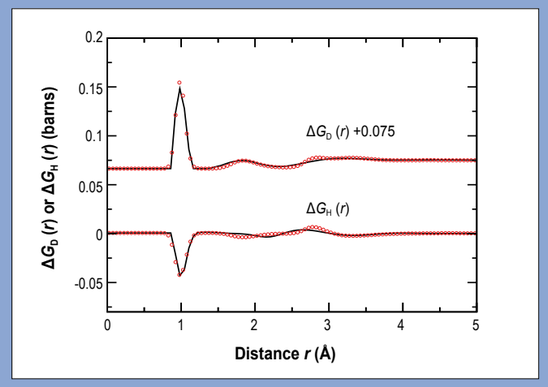

Figure 2: *The first difference functions $\Delta G_D(r)$/barns = 0.0059(2) $[g_{OD}(r)-1]$ + 0.00262(8)$[g_{OO}(r)-1]$ and $\Delta G_H(r)$/barns = −0.0033(1) $[g_{OH}(r)-1]$ + 0.00263(8)$[g_{OO}(r)-1]$ where $g_{\alpha\beta}(r)$ denotes a partial pair distribution function. The O-H correlations in $\Delta G_H(r)$ have a negative weighting factor because the coherent neutron scattering length of light hydrogen $b_H < 0$. The first peak or trough arises from the O-D or O-H intra-molecular bonds. The neutron diffraction results are shown by solid curves and the path integral molecular dynamics results are shown by circles.*

To provide a comparison for our diffraction data we made path integral molecular dynamics simulations of light and heavy water, shown in **figure 3** [4]. These calculations, in which a system of quantum mechanical particles is mapped onto a simulation of classical ring polymers, provide an exact treatment of nuclear quantum fluctuations in the structure of a given potential energy model for water. The polarisable flexible TTM3-F model was found to agree best with the experimental data and this model reproduces accurately the O-H stretching region of the infra-red (IR) absorption spectrum of liquid water as well as its diffusion coefficient.

The quantitative agreement between the measured and calculated first difference functions (**figures 1** and **2**) supports the proposal of "competing quantum effects" where inter-molecular zero point energy and tunneling weaken the hydrogen bond network but where quantum fluctuations in the anharmonic intra-molecular O-H bond increase its length and hence the dipole moment of each water molecule. This higher dipole acts, in turn, to increase the binding between molecules, and hence the net effect of quantum fluctuations is smaller than originally suggested from rigid water simulations. Our results indicate that these competing quantum effects more-or-less cancel which is fortuitous for experimental methods that exploit H/D isotope substitution, such as 2-D IR spectroscopy, NMR spectroscopy and neutron diffraction. This is because when these methods are used to study either light or heavy water at room temperature the structural environments probed, as well as the quantum contribution to the dynamics, are likely to be similar.

Our experimental results show that there is great potential for applying the method of neutron diffraction with oxygen isotope substitution as a site-specific structural probe of oxide materials. Current neutron diffraction instrumentation will allow for this approach to be applied to materials where the oxygen content ≥ 1/3. With the advent of the higher count rate instrumentation that is coming online at the next generation of neutron sources, materials with even lower oxygen contents should be accessible.

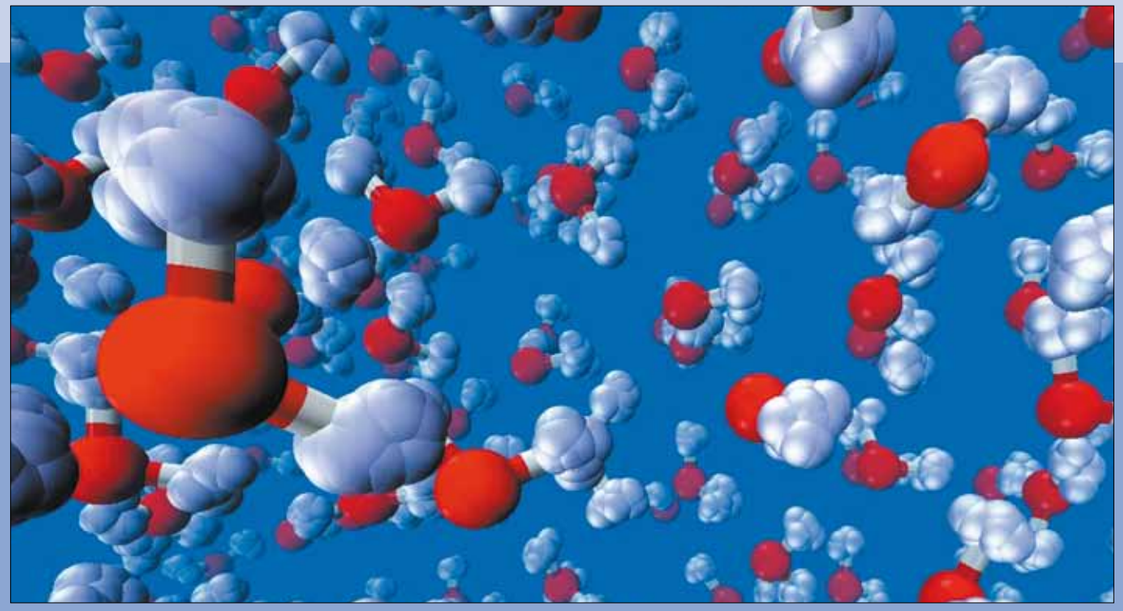

Figure 3: *A snapshot taken from a path integral molecular dynamics simulation of liquid water. The oxygen atoms are shown by red spheres and the hydrogen atoms are shown by multiple white spheres (bubbles) which represent their positional uncertainty in the quantum simulation.*

AUTHORS
M. Celli, **U. Bafile**, **D. Colognesi** and **M. Zoppi** (ISC-CNR, Florence, Italy)
E. Guarini (University of Florence, Italy)
M. Neumann (University of Vienna, Austria)
A. De Francesco and **F. Formisano** (IOM-CNR c/o ILL)

REFERENCES
[1] J.P. Boon and S. Yip, Molecular Hydrodynamics, McGraw-Hill, New York, 1980
[2] A. Rahman, K.S. Singwi, and A. Sjölander, Phys. Rev. 126 (1962) 986
[3] D. Colognesi, M. Celli, M. Neumann, and M. Zoppi, Phys. Rev. E 70 (2004) 061202
[4] K. Sköld, J. M. Rowe, G. Ostrowski, and P.D. Randolph, Phys. Rev. A 6 (1972) 1107
[5] M. Celli *et al.*, Phys. Rev. B 84 (2011) 140510(R)

Brillouin spectrometer BRISP
Time-of-flight spectrometer IN4

Dynamics of liquid hydrogen: the realm of neutron scattering

A still open problem in the diffusive dynamics of fluids is the validity of the Gaussian approximation to the self dynamic structure factor. In particular, this issue is of high impact in the case of liquid hydrogen, for its importance in fundamental physics, its technological applications, and its role in the development of quantum simulation methods. A neutron investigation carried out on BRISP and IN4 sheds new light on this long-standing problem.

Hydrogen is the most abundant substance in the universe, made of the simplest nuclei bound together in pairs to form the simplest molecules. It was one of the first chemical elements to be recognised and produced, and the explanation of its atomic properties was one of the first major successes of the new-born quantum ideas about one hundred years ago. The role played by hydrogen in the progress of science has been immense.
In addition hydrogen, particularly in its liquid state, is nowadays becoming increasingly important on the technological side, particularly as an energy carrier and storing medium.

Exploiting hydrogen potentialities requires a deep knowledge of its properties at the molecular level. Yet, the understanding of the dynamics of hydrogen molecules is still incomplete.
In this study we are concerned with the diffusive motions in the liquid, the so-called *self* dynamics [1], usually studied by combining experiments and computer simulations. From the experimental point of view, diffusion dynamics is the field of incoherent neutron scattering *par excellence*, and hydrogen is the ideal sample for this spectroscopic technique.

Nevertheless, experimental studies on liquid hydrogen are rare. On the other hand, the light mass and the very low temperature of liquid hydrogen make its study a problem in quantum physics, but quantum simulation is a still immature technique, which does not yet produce reliable spectra.

Self dynamics is traditionally described using the *Gaussian approximation* (GA), where all the relevant information is contained in a function of time expressing the amount of correlation between the velocities of a molecule at different instants [2].
Such a function cannot be measured and needs to be determined by simulation.

Fortunately, quantum simulation methods are able to calculate the velocity correlation function and, if the GA is *assumed* to be valid, can be used to compute the spectra that can also be measured in a neutron scattering experiment.
Thus, the comparison of calculations and neutron data makes it now possible to test the validity of the GA in a quantum fluid.

In order to carry out such a programme, we used two ILL spectrometers (BRISP and IN4) to measure the *self* part of the dynamic structure factor S(Q,E) of liquid hydrogen as a function of energy E, in a wide range of values of the wave vector Q.
The GA is known to be valid at small and large Q, but preliminary neutron results had revealed its breakdown in some Q range not yet identified [3]. Our work has confirmed this failure, but also allowed us to precisely locate it in Q space.

Figure 1 shows a comparison between the spectra measured with neutrons and calculated within the GA. The agreement is nearly perfect at the lowest and highest Q, while a discrepancy can be seen in the intermediate case. The analysis of the full set of experimental data showed that the GA does not correctly describe the diffusion dynamics in liquid hydrogen in the Q interval which starts above 10 nm^{-1} and extends up to about 40 nm^{-1}.

We have also been able to obtain the first semi-quantitative determination of the strength of non-Gaussian effects. Interestingly, this appears to be quite larger than in a classical liquid like argon [4], as shown in **figure 2**.

In conclusion, we have deepened our knowledge of hydrogen molecular dynamics beyond the usual Gaussian approximation limits.
This result can greatly help in testing quantum algorithms for the simulation of all dynamical properties of a fundamental system such as hydrogen, including those relevant for the advance of its present technological applications.

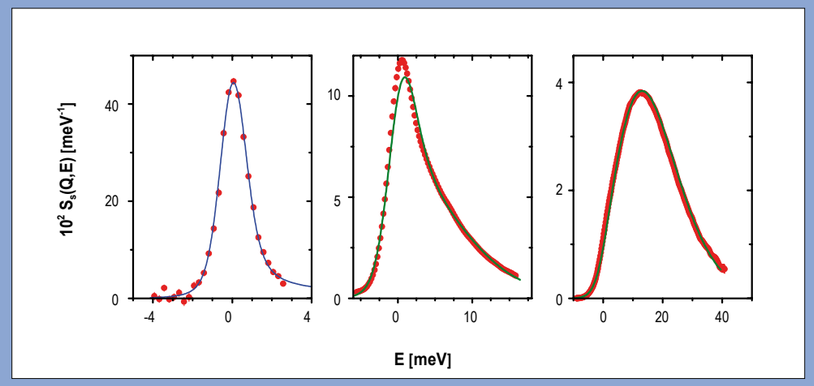

Figure 1:
The self dynamic structure factor of liquid hydrogen at Q = 10, 21, and 41 nm^{-1}, from left to right. The red dots are the neutron data taken on BRISP (first frame) and IN4 (second and third frames). The solid line is the calculation of Gaussian approximation using the quantum simulation of the velocity correlation function.

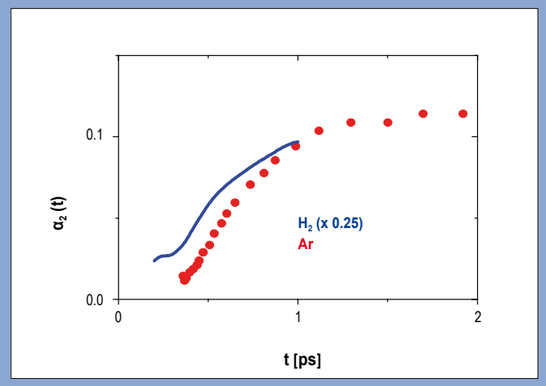

Figure 2:
The non-Gaussianity parameter $\alpha_2(t)$ [1] of liquid H_2 (blue line) and liquid Ar (red dots). The hydrogen data are divided by 4. The argon data are from [4].

AUTHORS
G. Vitiello, **G. D'Errico** and **L. Paduano** (University of Naples, Italy)
G. Fragneto (ILL)

REFERENCES
[1] M. Lorizate, N. Huarte, A. Saez-Cirion and J.L. Nieva, Biochim. Biophys. Acta 1778 (2008) 1624
[2] A. Merlino, G. Vitiello, M. Grimaldi, F. Sica, E. Busi, R. Basosi, A.M. D'Ursi, G. Fragneto, L. Paduano and G. D'Errico, J. Phys. Chem. B, 116 (2012) 401-412
[3] P.M. Peter, E. Lindhal, V.S. Pande, J. Am. Chem. Soc. 133 (2011) 3812

Reflectometer D17
Horizontal reflectometer FIGARO

Destabilisation of lipid membranes by a peptide derived from the feline immunodeficiency virus glycoprotein gp36

Viral entry is the first step in the infection process and is accomplished by the fusion of the viral envelope with the target cell membrane. Viruses exhibit a marked tendency to reside stably at the membrane interfaces; this leads, via mechanisms as yet unknown, to a destabilisation of the membrane structure. Neutron reflectivity (NR) experiments have provided details on the variations in the lipid structure induced by peptide binding, and this has highlighted its role in the membrane fusion process.

Viral fusion is controlled by one or more viral surface glycoproteins that undergo conformational changes driving membrane fusion. Viral fusion glycoproteins present a membrane-proximal external region (MPER) which is usually rich in aromatic residues and exhibits a marked tendency to reside stably at the membrane interfaces; this leads, via mechanisms as yet unknown, to a destabilisation of the bilayer structure. This step is fundamental for the fusion process between target membrane and viral envelope.

Even though the exact mechanism by which fusion proteins favour the fusion process is still unknown, recent studies suggest the MPER domain to be crucial in the infection pathway [1, 2].
We have investigated the effect on the structure of palmitoyl-oleoyl phosphatidylcholine (POPC) membranes of a tryptophan-rich octapeptide named C8 (Ac-Trp-Glu-Asp-Trp-Val-Gly-Trp-Ile-NH_2), derived from the MPER domain of FIV gp36. We performed NR measurements on the D17 reflectometer at the ILL in time-of-flight mode using a spread of wavelengths between 2 and 20 Å with two incoming angles of 0.8 and 3.2°. We also used the contrast variation technique (using water of different scattering-length densities by mixing H_2O and D_2O) in order to enhance certain components of the system.

We analysed the NR profiles by box-model fitting, using the AFIT and MOTOFIT programmes. A five-box model was found to best fit the data relative to POPC membranes. The first two boxes correspond to the silicon block and to the thin solvent layer interposed between the silicon surface and the adsorbed bilayer. The three other boxes describe the lipid bilayer, which is subdivided in the inner headgroups, the hydrophobic chains, and the outer headgroups layers.

We first characterised the pure POPC bilayer using D_2O, SMW (silicon-matched water) and H_2O as isotopic contrast solvents (**figure 1**), which presents a thickness of 44 ± 1 Å and a slow content of water solvent (about 30%) in the hydrophilic layer. We then investigated the effect of the C8 peptide by measuring the NR curves of the fully hydrogenated POPC to which the peptide with deuterated Trp residues was added (**figure 2**). Four contrast solvents, D_2O, 4MW, SMW and H_2O, were used. Data from the peptide-interacting bilayer were fitted by an additional layer with respect to the pure POPC model. This layer evidently consists of the peptides interacting with the outer bilayer surface, indicating that the presence of the peptide effectively perturbs the outer hydrophilic layer of the POPC membrane and that this perturbation propagates in the chain region. In particular, the thickness values of the two layers corresponding to the polar headgroups decrease slightly, while the thickness of the chains region increases. The clearest variations are observed for the solvent content values of both inner and outer headgroup layers; these increase dramatically, although to different extents. Whilst this increase is directly related to the peptide binding in the case of the outer hydrophilic headgroups layer, the changes in the inner headgroups layer indicate that the peptide effectively perturbs the whole bilayer structure. The fact that the inner leaflet is less perturbed can be put down to an asymmetry in the bilayer structure (**figure 3**).

These results are in agreement with those obtained with other spectroscopic and computational experiments. Electron spin resonance techniques and circular dichrosim and fluorescence measurements, combined with molecular dynamics simulations have also shown revealed membrane surface-peptide binding, confirming the hypothesis suggested by the NR model [2]. Altogether, the experimental and computation results indicate that lipid bilayer destabilisation could be a consequence of the asymmetric perturbation of the bilayer, which starts with an increase in the hydration of the lipid headgroups coupled with an increase in lipid ordering in the leaflet exposed to the approaching viral glycoprotein. In particular, since water organisation at the membrane interface has been proposed to control the fusion dynamics [3], the rise in bilayer hydration could be fundamental in the role played by the MPER fusion protein domain during the process.

In conclusion, our neutron reflectivity study gave us a detailed picture of the membrane-peptide interaction. It furnished a clear indication of C8 positioning relative to the lipid bilayer, as well as changes in the bilayer thickness on peptide binding. The results indicate that C8 interacts directly with the hydrophilic region of the membrane's external leaflet, but it causes a structural perturbation which involves the whole bilayer.
These results suggest a mechanism in the MPER domain inducing the membrane fusion process.

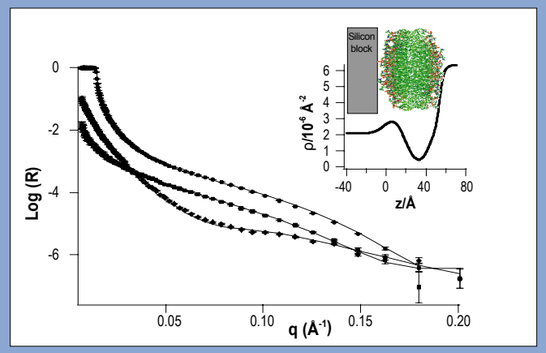

Figure 1: *Neutron Reflectivity profiles (points) and best fits (continuous lines) corresponding to pure POPC bilayer in (●) D_2O, (■) SMW and (♦) H_2O solvents. The* ***inset*** *shows the ρ profile for the POPC bilayer in D_2O.*

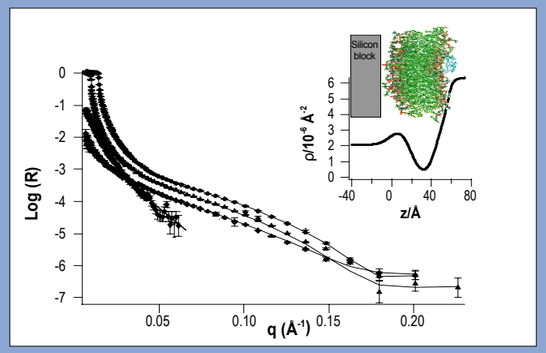

Figure 2: *Neutron reflectivity profiles (points) and best fits (continuous lines) corresponding to POPC bilayer with C8 peptide in (●) D_2O, (▲) 4MW, (■) SMW and (♦) H_2O solvents. In the last set, data at high q fall quickly into the background due to the roughness of the layer and incoherent scattering of the solvent. The* ***inset*** *shows the ρ profile for the bilayer in D_2O after peptide addition.*

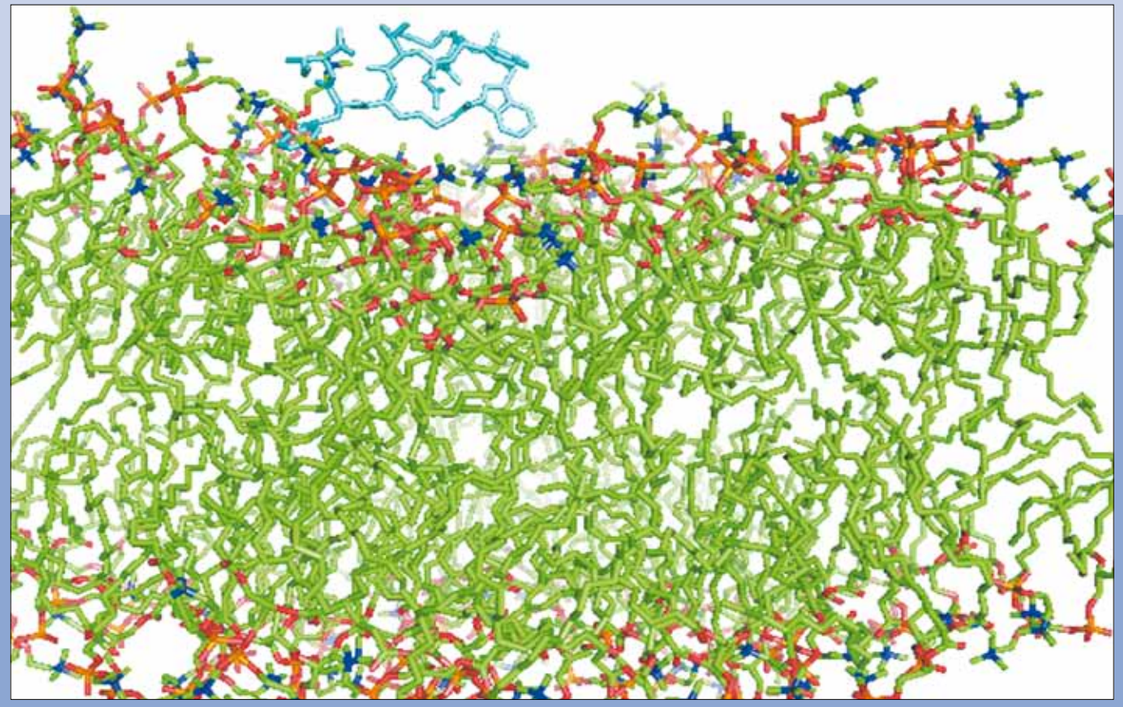

Figure 3: *Schematic representation of the destabilising effect induced by C8 peptide on the POPC bilayer.*

AUTHORS
L. Porcar (ILL and University of Delaware, USA)
S. Garg (ANL, Chicago, USA)
A. Woodka and **P. D. Butler** (NIST Center for Neutron Research, Gaithersburg, USA)
U. Perez-Salas (ANL, and UIC, Chicago, USA)

Small-angle scattering diffractometer D22

Cholesterol transport in model lipid membrane system

Cholesterol is an important structural component of most cell membranes that controls the functions of membrane proteins crucial for several trans-membrane signaling processes. Transfer of cholesterol in cells is vital to maintain appropriate levels of cholesterol in membranes. Cardiovascular disorders, some dementias, such as Alzheimer's, and other fatal diseases like Niemann Pick TYPE-C are associated with cholesterol transport deficiencies. We used *in situ* time-resolved SANS to determine and quantify the key parameters controlling cholesterol trafficking in model membranes.

To track the redistribution of cholesterol between lipid vesicles, the total scattered intensity resulting from mixing lipid vesicles with and without cholesterol was measured as a function of time. Only the contribution from cholesterol was detected as the lipids in the vesicles were rendered completely invisible by the solvent (**figure 1**). The resulting intensity decay is then directly related to cholesterol transfer and was fitted using a kinetic model that allowed cholesterol to flip within the same membrane as well as to exchange to a different membrane. The activation energies for flipping and exchange obtained from measurements at three different temperatures, were, surprisingly, similar. Replacing cholesterol with DHE, a self-fluorescent cholesterol analog, demonstrated an exquisite sensitivity to minute structure differences since both flipping and exchange rates were faster than for cholesterol.

The widely held belief that cholesterol, being mostly hydrophobic, flips easily within the hydrophobic core of the membrane while exchanges slowly between membranes due to its extremely low solubility in an aqueous medium is at odds with our data. Our results with POPC vesicles suggest that the mechanism for cholesterol flipping is not dominated by hydrophobic/hydrophilic interactions between lipids and cholesterol. Other forces, including steric interactions: cholesterol-lipid interactions and lipid tail packing, and Van der Waals interactions are important.

Time-resolved SANS offers the versatility to measure tagged and untagged molecules alike, and therefore, it is possible to begin addressing questions concerning possible artifacts in reported flipping and exchange kinetics using other experimental techniques. Our data, using non-invasive *in situ* measurements, clearly challenge the assumptions made in previous studies and more generally highlight the difficulty in using chemical tags or additives to understand the transport properties and energetics of self-assembled systems.
Further, this work establishes time-resolved SANS as a powerful tool for elucidating the myriad of contributions to the kinetics of these complex and interacting systems.

The cell membrane is a rich and complex environment and it is easy to see, given the exquisite sensitivity of cholesterol transport to the details of this environment, how organisms might be able to very finely tune the cholesterol balance within their cellular structures. Further, the slower cholesterol flipping rates detailed in this work provide a better explanation as to how cells can sustain an asymmetric distribution of cholesterol between the extracellular and cytoplasmic leaflets of the plasma membrane: because membrane cholesterol asymmetry is regulated by transporter proteins (as any active pumping mechanism) only if cholesterol flipping rates are relatively slow can this mechanism be realistically possible.

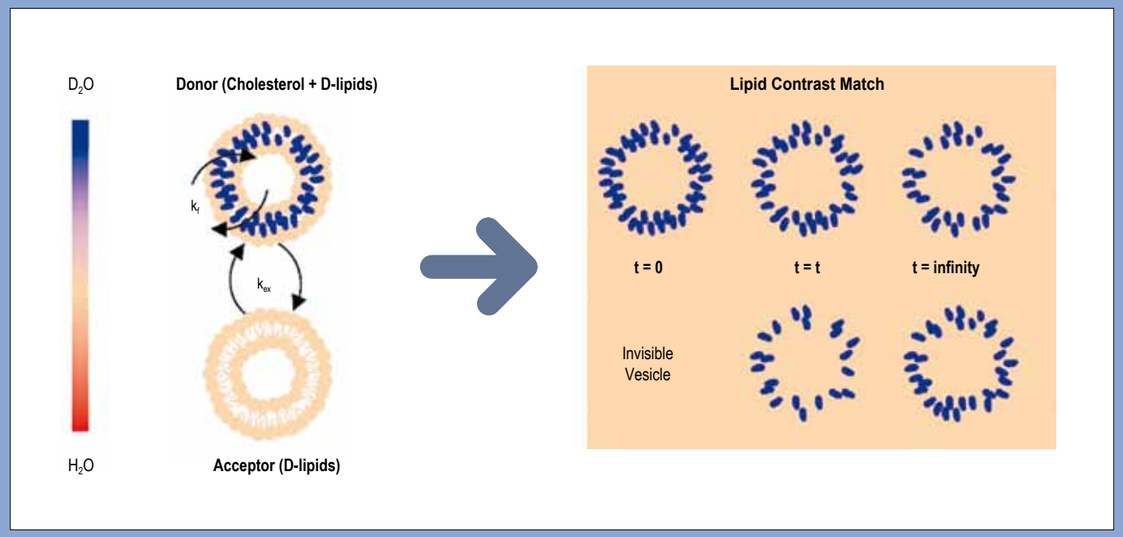

Figure 1: *Schematic of the experimental protocol: donor and acceptor vesicles made of dPOPC (deuterated palmitoyl-oleoyl-phosphocholine) in a solvent which completely matches the lipids rendering them invisible to neutrons. At t = 0, only the donor vesicles are visible as they contain cholesterol, the only highlighted component in the mixture. As cholesterol moves from donor to acceptor vesicle, the acceptor vesicles gradually begin to appear.*

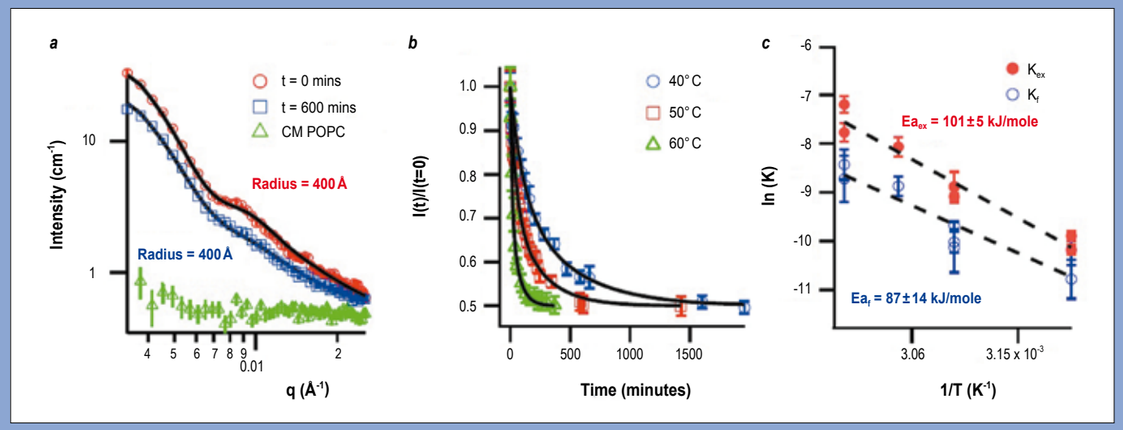

Figure 2: ***(a)*** *Scattering curves for a sample with donor (cholesterol + dPOPC) and acceptor (dPOPC) 100 nm vesicles mixed together at t = 0 (open circles) and t = 600 min (open squares) showing that the vesicle size and shape remain unchanged during the experiment. The solid lines are form factor fits to the data. The open triangle data are for pure dPOPC vesicles and shows that a complete contrast matching condition is achieved.* ***(b)*** *Temperature dependence of the normalised intensity as function of time with corresponding fits.* ***(c)*** *Arrhenius fits for flipping and exchange rates using data for four temperatures (from 40 °C to 60 °C), three of which are shown in* ***(b)***.

AUTHORS
O.J. Burrows, **A. Paul**, **J. W. Regini** and **P.C. Griffiths** (Cardiff University, Wales, UK)
M. Haertlein, **P. Callow** (ILL)

REFERENCES
[1] T.M. Treweek, A.M. Morris, and J.A. Carver, Australian Journal of Chemistry 56(5) (2003) 357-367
[2] H. Ecroyd and J.A. Carver, Cell Mol Life Sci 66(1) (2009) 62-81
[3] D. Boyle, and L. Takemoto, Exp Eye Res 58(1) (1994) 9-15
[4] J.M. van Noort, J.J. Bajramovic, M. Ouagmiri, C.H. Polman, H. Lassmann and R. Ravid. Nature 375(6534) (1995) 798-801

Towards a detailed mechanistic study of small heat-shock chaperone protein action

The ageing population is recognised as a world-wide problem and represents a significant financial burden for all economies. In terms of vision alone, age-related cataract is responsible for nearly 50% of world blindness, affecting some 18 million people (World Health Organisation, WHO). The reasons for cataract development are many and varied – age, long-term exposure to ultraviolet light, exposure to radiation, disease (diabetes, hypertension) or trauma – all usually arise as a result of unfolding, mis-folding and aggregation of lens proteins. Small-angle neutron scattering (SANS) has been used to examine the interactions between proteins that lead to such physiological manifestations.

α-Crystallin is a member of the small heat shock proteins (sHsps) family, a varied group of intracellular molecular chaperones found in all organisms [1]. In humans, they are present in many tissues at varying concentrations depending on the stage of development and the level of physiological stress. The function of sHsps is versatile but their common role is to interact with and stabilise the partially folded states of other ("target") proteins to prevent their aggregation and possible precipitation, for example under conditions of environmental stress such as elevated temperature, low pH and oxidation.

The principal eye lens protein, α-crystallin, is a sHsp that is comprised of two closely related subtypes, αA and αB-crystallin, both approximately 20 kDa in mass. In the human lens, these two subtypes are co-expressed in the ratio of 3:1 αA: αB, and form a heterogeneous globular protein with a molecular mass of between 300 kDa to 1.5 MDa and an average size about 150 Å in diameter. Protein concentrations in the lens are high (up to 450 mg/ml in the nucleus or centre of the lens). α-Crystallin is the primary protein component and can approach 50% of the total dry weight of the lens.

In a structural role, α-Crystallin assists in the maintenance of short-range order in the lens cytoplasm, ensuring the correct amount of refraction of light on to the retina, and maintenance of lens transparency.

Secondly, it acts as a molecular chaperone to maintain the stability and solubility of the other classes of crystallin proteins, β and γ [2]. However, α-crystallin does not refold denatured proteins, nor does it hydrolyse ATP, and thus, since protein is not continually being replaced in the centre of the lens, α-crystallin is involved in limiting lens protein precipitation over many years to prevent lens opacification and cataract formation [3].

αβ-crystallin is also expressed at significant levels outside of the lens where it plays a key role as a molecular chaperone protein, and is implicated in other protein misfolding diseases such as Alzheimer's disease, multiple sclerosis, Parkinson's disease and in the ischaemic heart [4].

The small-angle diffractometer D22 was used to quantify the size and shape of a series of crystallin proteins, in simple solutions under non-stressed (20 °C) and stressed (65 °C) conditions, and in binary mixtures.

In the non-stressed conditions, there was no change in the scattering intensity and thus the calculated radii of gyration R_g remained constant, indicating no aggregation.

In the binary mixtures, however, there was an increase in scattered intensity over a period of several hours, and a concomitant perturbation in the radii of gyration, **figure 1**.
It was found that:

(i) $R_g(\alpha H{:}\gamma ED/D_2O) > R_g(\alpha H{:}\gamma EH/D_2O) > R_g(\alpha H/D_2O)$, and
(ii) $R_g(\alpha H{:}\gamma EH/D_2O) \approx R_g(\alpha H/D_2O)$.

Contrast variation with isotopic substitution was subsequently employed to investigate the internal structure of the complex formed from between the target lens protein (γE-crystallin) and α-crystallin (αH), and to follow the evolution of the radius of gyration (R_g) of the binary protein complexes in solution under thermal stress.

The relative sizes observed for the complexes weighted by the respective scattering powers of the various components imply that γE-crystallin binds in a central cavity of the α-crystallin oligomer, during chaperone action.

Contrast variation SANS experiments using deuterated proteins have provided a level of resolution on crystallin aggregate structure that was not obtainable from any other technique.

These structural insights are providing a deeper understanding of the mechanism of chaperone action of α-crystallin, and could have long-reaching implications in the prevention and treatment of cataracts and other degenerative diseases.

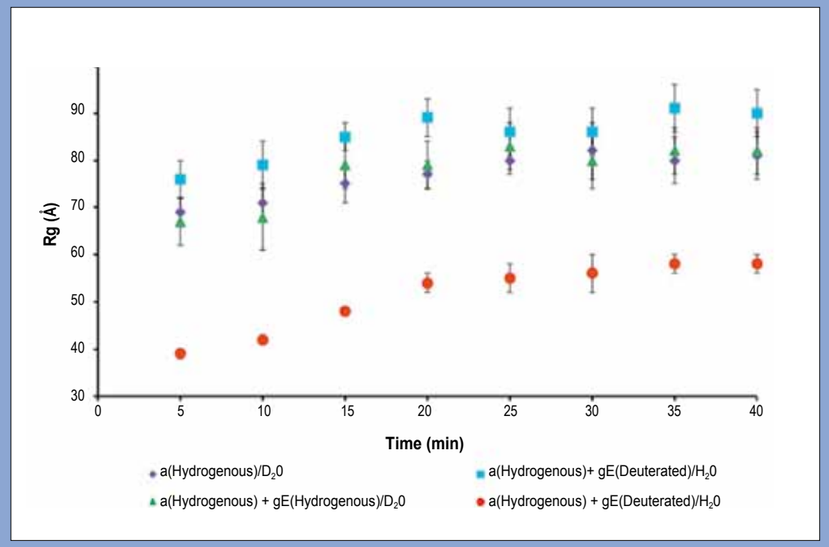

Figure 1:
R_g obtained from an analysis of the SANS data for hydrogenous α-crystallin in D_2O, hydrogenous α-crystallin complexed with deuterated γE-crystallin in D_2O, hydrogenous α-crystallin plus hydrogenous γE-crystallin in D_2O, and hydrogenous α- crystallin plus deuterated γE-crystallin in H_2O. (All mixtures had a total concentration 4 mg ml^{-1}).

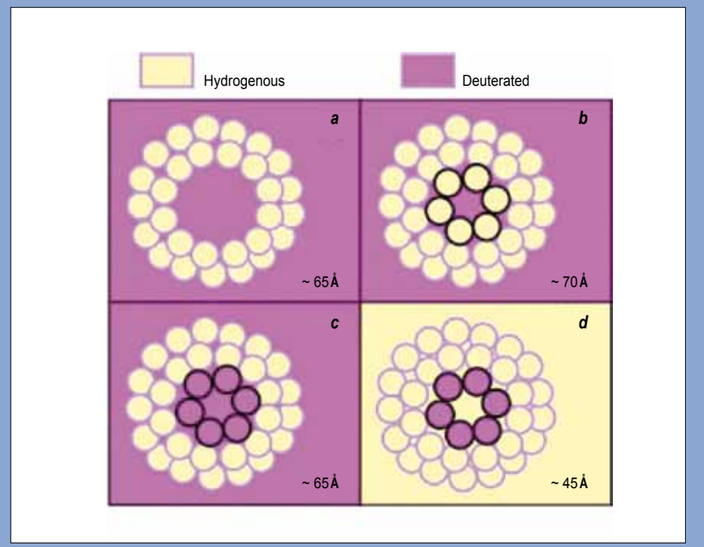

Figure 2:
Schematic representation of contrast experiments performed and key results obtained.
(a) *h-α ;*
(b) *h-α + h-γ ;*
(c) *and* ***(d)*** *h-α + d-γ.*
Numbers denote approximate radii of gyration R_g at 30 minutes.

AUTHORS
C. Mikl, **K. Kornmueller** and **R. Prassl** (Institute of Biophysics and Nanosystems Research, Graz, Austria)
W.J. Schneider (Medical University, Max F. Perutz Laboratories, Vienna, Austria)
M. Trapp (University of Heidelberg and HZB Berlin, Germany) - **J. Peters** (IBS, Université Joseph Fourier and ILL, Grenoble, France)

REFERENCES
[1] A. J. Lusis, Nature 407 (2000) 233
[2] G. Zaccai, Science 288 (2000) 1604
[3] C. Mikl, J. Peters, M. Trapp, K. Kornmueller, W.J. Schneider and R Prassl, J. Am. Chem. Soc. 133 (2011) 13213

Backscattering spectrometer IN13

Softness of pro-atherogenic lipoproteins revealed by elastic incoherent neutron scattering

Lipoproteins are naturally occurring globular nanoparticles circulating in the blood which function to supply tissues and cells with cholesterol and other lipids. These substances are essential for membrane synthesis and fuel storage in cells and are precursors for signaling molecules. However, lipoproteins are also associated with cardiovascular diseases such as atherosclerosis or stroke, which are among the most prevalent causes of death in developed countries [1]. Elastic neutron scattering was used to study thermal motions, dynamical transitions, and molecular fluctuations of lipoproteins to shed light on the key determinants of the functionality of lipoproteins in both health and disease.

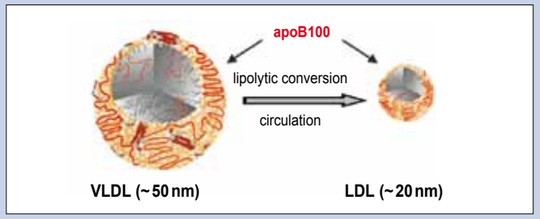

Figure 1: *Scheme of the lipolytic conversion of VLDL to LDL during lipoprotein metabolism.*

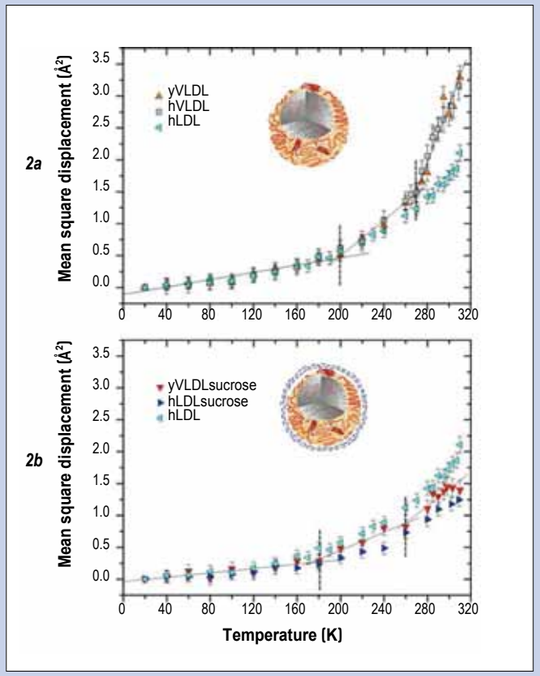

Figure 2: *Comparison of mean square displacements describing* ***(a)*** *the dynamics of pro-atherogenic lipoproteins and* ***(b)*** *the effects of sucrose surrounding the surface of lipoproteins [mimicked by blue wavy lines] on molecular motions [h, human; y, yolk].*

Apolipoprotein B100 (apoB100)-containing plasma lipoproteins, i.e. very low density lipoprotein (VLDL) and low density lipoprotein (LDL), are the principal transporters for cholesterol and energy-rich fat in the circulation. During metabolism the triglyceride content of VLDL becomes gradually lower while the particle size decreases from about 50 to 20 nm diameter. Eventually, VLDL is converted to LDL that is rich in cholesteryl ester. In the course of shrinking apoB100 remains bound to its carrier stabilising the whole particle (**figure 1**). The molecular physical parameters which control lipoprotein remodeling, enable particle stabilisation by apoB100, and control receptor-mediated uptake of the lipoproteins are largely unknown.

To study the molecular dynamics of apoB100-containing lipoproteins in terms of thermal molecular fluctuations, which can be assessed by mean square displacements, we have performed a comparative study using elastic incoherent neutron scattering (EINS). The experiments were performed on the thermal neutron backscattering spectrometer IN13 at the ILL. We have used hydrated lipoprotein powders, which were measured in a temperature range of 20K to 310K. EINS experiments shed light on global thermal motions and molecular fluctuations of lipoproteins that reflect the temperature-dependent motional coupling between lipid and protein.

In the low temperature regime, motions are reduced to harmonic vibrations around equilibrium positions. In this range we did not find noticeable differences between the two lipoprotein classes, but still, lipoproteins were softer compared to well-studied model proteins. This behaviour can be correlated to the contribution of lipids to the global dynamics of lipoproteins [2]. A first onset of anharmonicity was seen at about 180 - 200K, and a second dynamical transition was observed in the range of 260 to 270K. Above this second transition, distinctions in the dynamics between LDL and VLDL became clearly visible. Most important, at physiological temperature, less structural resilience and higher mean molecular displacements are observed for VLDL samples (**figure 2**).

It is likely that the pronounced softness of VLDL is dominated by its larger lipid content. To address this question, we have performed EINS measurements in the presence of sucrose, which was added to the aqueous lipoprotein solutions before lyophilisation. With this approach we expected to obtain more information about the individual contributions from the outer shell and the inner core components, respectively, to global lipoprotein dynamics.

As expected, with sucrose both lipoproteins were more rigid over the entire temperature range (**figure 2b**). The most striking feature, however, was that the dynamics of VLDL became dramatically restricted and nearly equaled that of LDL, in particular at higher temperatures. We supposed that sucrose molecules surrounding the lipoprotein particle most likely interact with other hydrophilic groups or domains on the surface of the particle in addition to water. This led us to the assumption that the rigidifying effects of sucrose, especially on VLDL samples, are limited to surface-exposed apolipoprotein domains and in part to phospholipid headgroups and cholesterol. Since the striking changes in VLDL cannot only be explained by the higher amount of surface-located molecules, it appears likely that apoB100 displays distinctly different mobilities in VLDL and LDL, controlled by its direct molecular environment.

Our data support the notion that the lipolytic conversion of VLDL to LDL forces apoB100 into a more condensed and therefore rigid state, entirely compatible with the observed inhibition of relaxation caused by the presence of sugar.

Taken together, EINS measurements of LDL and VLDL revealed the pronounced softness of pro-atherogenic lipoproteins. We found substantial differences in the molecular resiliences of lipoproteins, especially at higher temperatures, with VLDL being more flexible than LDL. These discrepancies cannot only be explained in terms of lipid composition and mobility, but suggest that apoB100 displays different dynamics dependent on the lipoprotein it is bound to.

Hence, we propose that the inherent conformational flexibility of apoB100 permits particle stabilisation upon lipid exchange, whereas the dynamic coupling between protein and lipids might be a key determinant for lipoprotein conversion and atherogenicity.

Our results revealed that lipoproteins are extremely soft and flexible, with VLDL being more fluid than LDL [3]. We propose that the intrinsic flexibility and the dynamic coupling between lipids and the apolipoprotein moiety are the key determinants of the functionality of lipoproteins in both health and disease. A deeper understanding of the relationship between structure, dynamics, stability, and biological function of apoB100 in lipoprotein species may well help to prevent the progression of cardiovascular diseases.

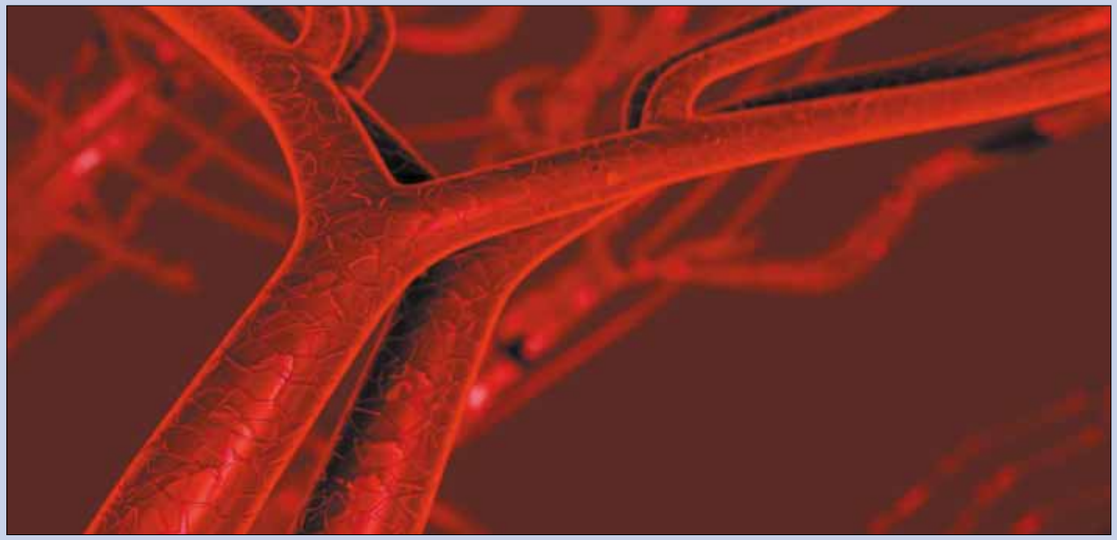

AUTHORS
A. Bail, **O. Serot**, **L. Mathieu** and **O. Litaize** (CEA, DEN-Cadarache, France)
T. Materna, **U. Köster** and **H. Faust** (ILL)
A. Letourneau and **S. Panebianco** (CEA, DSM-Saclay, France)

REFERENCES
[1] A. Bail *et al.*, Phys. Rev. C 84 (2011) 034605
[2] M. Kellett *et al.*, JEFF Report 20, NEA N° 6287 (OECD, 2009)
[3] D. Boyle, and L. Takemoto, Exp Eye Res, (1994) 58(1) 9-15
[4] T. Materna *et al.*, in AIP Conf. Proceedings 1175, 4th Int. Workshop on Nuclear Fission and Fission Product Spectroscopy, Cadarache, May 13–16, 2009, edited by A. Chatillon *et al.*, p. 367

Isotopic yield measurement in the heavy mass region

Since fission yield data are of importance in various nuclear energy applications (reactivity or decay heat in nuclear power, post-irradiation experiments, neutron flux determination, etc.), a large number of experiments were carried out in this field during the last decades. Nevertheless, in particular because of enhanced radiation protection security requirements and to cope with extended reactor lifetimes, strong efforts are needed to reduce fission yield uncertainties.

Up to now, thanks to the ILL's Lohengrin mass spectrometer, various fissioning nuclei have been investigated. Combining the mass spectrometer with a high resolution ionisation chamber allows good nuclear charge discrimination within a mass line, yielding an accurate isotopic yield determination. Nevertheless, this procedure can only be applied for fission products with a nuclear charge Z less than about 42, i.e. in the light mass region. In order to study also fission product characteristics in the heavy mass region, a new experimental set-up based on gamma spectrometry (for the fission product identification) has been installed.

The Lohengrin recoil-mass spectrometer is a nuclear physics instrument which uses low-energy fission reactions for fission fragment production. For the present work, a highly enriched ^{239}Pu target was placed close to the core of the ILL's high-flux reactor in a thermal-neutron flux of about 5×10^{14} n/cm^2/s. Fission products with mass A emerge from the target with an ionic charge state q and a kinetic energy E. The selection of these fission products is performed by a combination of a magnetic and an electric sector field. At the exit slit, the combined action of the two fields separates ions according to their A/q and E/q ratios.

In order to investigate the heavy mass region by taking profit of the very high mass and energy resolutions, a new experimental set-up has been developed. It is based on gamma spectrometry, which is for the first time combined with the Lohengrin spectrometer. The γ-rays are used to identify the fission products and to determine their yields.

For this purpose, the measurement is performed in several steps:
- The electric and magnetic fields of the mass spectrometer are set to select fission products with a given mass (A), ionic charge (q) and kinetic energy (E).
- These fission products are implanted during the measuring time in a tape located inside a vacuum chamber which is placed at the focal point of the spectrometer.
- During this measuring time, γ-rays are registered with two high efficiency germanium clover detectors placed close to the vacuum chamber.
- Then, the tape is moved to remove the residual activity. In this way, a new measurement can start.

Isotopic yield values for the 65 measured fission products (19 in the light mass region and 46 in the heavy mass region) are plotted in **figure 1**. For the large majority of fission products, a very good agreement between the Lohengrin data and the European library JEFF-3.1.1 [2] values is achieved, but with a significant reduction of the uncertainties. The average yield uncertainty reaches 11.9% (our measurements) and 23.3% (JEFF-3.1.1), respectively, which corresponds to a reduction of a factor of nearly 2.

In addition, we have observed for some fission products an asymmetric ionic charge distribution. In particular, an important tail for high ionic charge states can be highlighted. This effect results from nanosecond isomers that decay by a highly converted internal transition. Owing to the short half-life of these isomeric states (of the order of some nanoseconds), conversion and Auger electrons, which are emitted between the target and the first dipole of the spectrometer, increase the ionic charge of the fission product. This new ionic charge state is maintained during the flight through Lohengrin and can therefore be detected. An example of such an isomeric state is given in **figure 2**, where the ionic charge distributions were measured by γ spectrometry for both ^{140}Xe and ^{140}Cs. A "normal" Gaussian shape was found for ^{140}Xe (no nanosecond isomer), while for the ^{140}Cs nucleus, a strongly deformed distribution was observed, showing the presence of nanosecond isomers. By this method, new nanosecond isomers were identified as reported by Materna *et al.* [3].

Lastly, isobaric charge distributions were investigated for all masses where at least three fission product yields were measured. Assuming a Gaussian shape distribution, the most probable charge (Z_P) and the variance (σ_Z) were determined. In low-energy fission, fission products present an average charge density different from the fissioning nucleus charge density. Compared to the unchanged nuclear charge (Z_{UCD}), light fragments are found to have a smaller nuclear charge while heavy fragments show the opposite tendency. This difference ($\Delta Z = Z_P - Z_{UCD}$) confirms the existence of a charge polarization of nuclear matter.

In conclusion, Lohengrin is still the most accurate instrument for measuring thermal neutron fission yields, and with the present work, its range of application is practically doubled, now allowing the study of isotopic yields of heavy fragments. Results are very encouraging considering how uncertainties have been decreased compared to other experiments and evaluated data respectively.

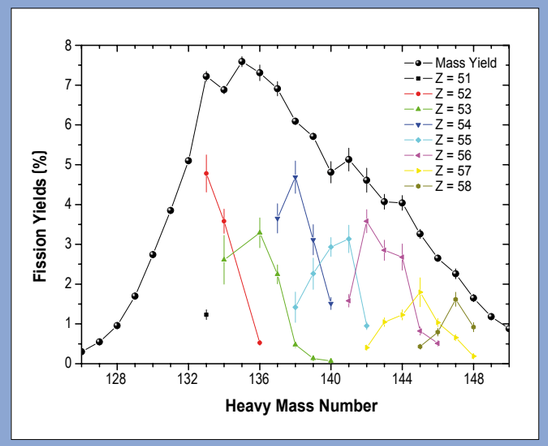

Figure 1:
Isotopic yields measured in the heavy mass region for the ^{239}Pu[n,f] reaction [1].

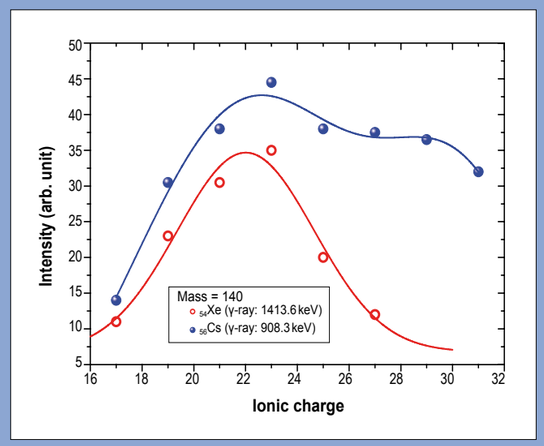

Figure 2:
Ionic charge distributions measured for ^{140}Xe and ^{140}Cs.

AUTHORS
H. Abele and **T. Jenke** (Atominstitut TU Wien, Vienna, Austria)
P. Geltenbort (ILL) on behalf of **the qBounce collaboration**

REFERENCES
[1] T. Jenke *et al.*, Nature Physics 7 (2011) 468-472
[2] V. Nesvizhevsky *et al.*, Nature 415 (2002) 297-299
[3] J. Felber *et al.*, Phys. Rev. A53 (1996).319-328
[4] H. Abele *et al.*, Phys. Rev. D81 (2010) 065019

Spectroscopy of gravity

Patients undergoing nuclear magnetic resonance (NMR) diagnosis won't necessarily think about spectroscopy. And people setting their clock don't even reason about the functioning of atomic clocks either. But both the spectacular images from smooth tissues obtained by NMR and the ultimate precision of atomic clocks are based on a quantum technology called resonance spectroscopy. It turns out that resonance techniques have been restricted to electromagnetic interaction so far. The qBounce-collaboration presents here a new spectroscopy technique for gravity investigation realized with ultra-cold neutrons at the instrument PF2.

The new method allows precise measurement of quantum states of ultra-cold neutrons in the gravitational potential of the Earth with a Schrödinger wave packet bouncing off a hard horizontal surface [1]. Two features of quantum physics put up together are responsible for the precision, which can be achieved. First of all most quantum systems only allow for discrete energy levels. As atomic clocks are concerned it is the energy splitting of Caesium atoms in their own magnetic field and with NMR techniques an outer magnetic field - usually provided by superconducting magnets - defines the energy levels of the magnetic moments of the nuclei. This also works for an ultra-cold neutron bouncing off a hard horizontal surface.
In 2002, the first demonstration of discrete energy levels of quantum states in the gravitational potential of the Earth has been performed with ultra-cold neutrons [2] at ILL on PF2 and started as a collaboration between the ILL, PNPI (Gatchina), JINR (Dubna) and the authors (at that time at the Physics Institute at Heidelberg University). In that experiment neutrons were allowed to populate the lower states of **figure 1**. Higher, unwanted states were removed.

The other feature of quantum physics, which provides high precision, is the possibility to drive transitions between these quantum-mechanical energy levels. An external oscillating force causes a coupling between these levels. The transition occurs on resonance, when the frequency is adjusted to the energy difference. All resonance techniques so far use electromagnetic fields one way or the other. A novelty of this work is the fact that the quantum-mechanical transition is driven by an oscillating field, which is not a direct coupling of an electromagnetic charge or moment to an electromagnetic field. Instead, we observe transitions between gravitational quantum states by mechanically oscillating the boundary conditions of our quantum states. The physics behind these transitions is related to earlier studies of energy transfer when matter waves bounce off a vibrating mirror [3].

For this purpose, ultra-cold neutrons are taken from PF2 as in previous experiments. Their horizontal velocity component is restricted to 5.7 m/s < v < 7 m/s.

For an energy difference measurement between two gravitational quantum states |p> and |q>, ultra-cold neutrons are prepared into state |p>. An oscillator drives transitions between |p> and |q>, if the oscillation frequency matches their energy difference. An analyser only transmits neutrons in state |p>. A detector behind this system counts the neutrons transmitted. In our experiments, this has been realized with only one bottom mirror coupled to a mechanical oscillator, a scatterer on top and a neutron detector behind (see **figure 2**). The scatterer only allows the ground state to pass and prepares the state |p>. The vibrating mirror induces transitions to |q> which are again filtered out by the scatterer. Therefore, by tuning the oscillating frequency of the neutron mirror, characteristic drops of intensity are found, if the resonance condition $\Delta E = Eq - Ep = \hbar (\omega_q - \omega_p)$ is fulfilled (see **figure 3**).

In conclusion, spectroscopy of gravity has been seen for the first time. This is interesting, because it addresses some of the unsolved questions of modern science: the nature of the fundamental forces and underlying symmetries and the nature of gravitation at small distances. The method can usefully be employed in measurements of fundamental constants or in a search for non-Newtonian gravity [4].

The experiment combines quantum theory with gravitation, two fundamental pillars, which have not been described in a common language, yet. What is more, only 4 % of the Universe's content has been identified as quantum particles. The rest are dark matter particles and dark energy, which again is linked to the modification of gravity at small distances.
The new method profits from small systematic effects in such systems, mainly due to the fact that, in contrast to atoms, the electrical polarisability of neutrons is extremely low. Neutrons are not disturbed by short range electric forces such as van der Waals or Casimir forces. Together with its neutrality, this provides the key to a sensitivity of several orders of magnitude below the strength of electromagnetism.

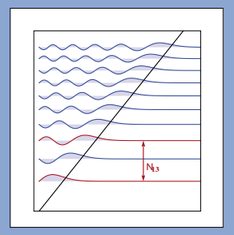

Figure 1: *High precision measurements of energy differences between discrete quantum states of atoms have been performed with resonance spectroscopy techniques for a long time. This is since now also possible with neutrons. At production, these neutrons are very hot; the energy is about 2 MeV corresponding to 10^{10} degrees Centigrade. On the other side of the scale, the gravity experiment uses neutrons having 10^{18} times less energy in the pico-eV range. Energy differences between gravitationally bound quantum states of a neutron are therefore ten thousand billion times smaller compared to an electron bound in the hydrogen atom.*

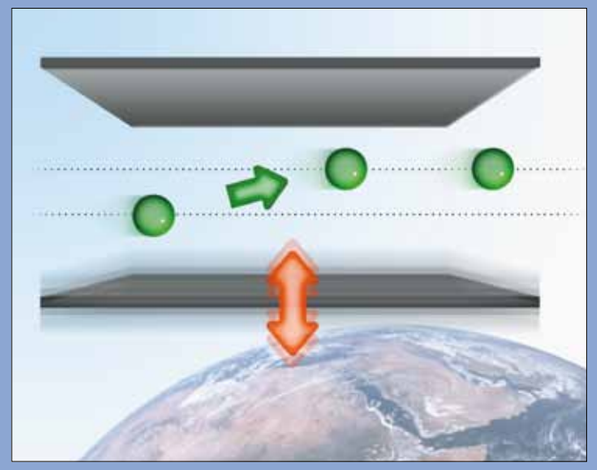

Figure 2: *Ultra-cold neutrons in between two plates form bound quantum states in the Earth's gravitational field. By vibrating these plates, transitions between the states have been induced and observed in the experiments.*

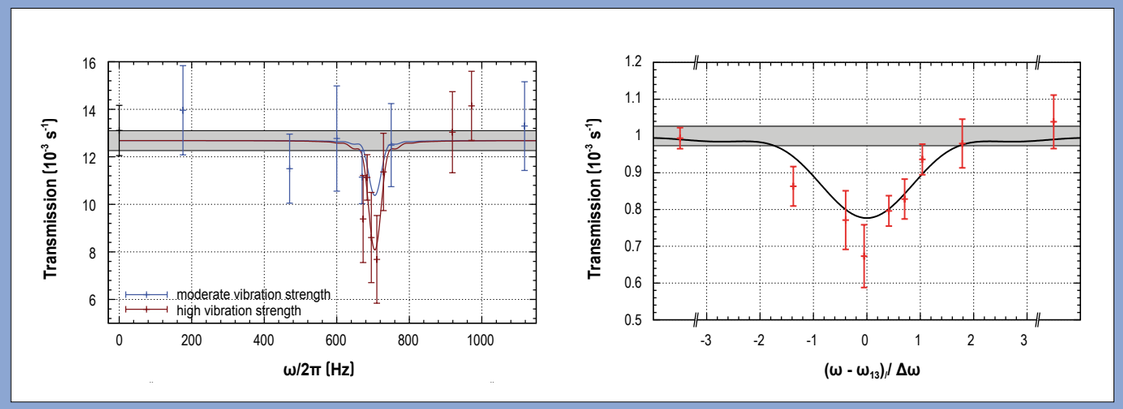

Figure 3: *The transmission as a function of the oscillation frequency of the neutron mirrors shows a fast decrease on resonance. The grey bands indicate the out of resonance transmission (taken from [1]).*

Backscattering spectrometer IN16
Backscattering instrument IRIS (ISIS, UK)

Thermal motion in the multi-subunit protein, apoferritin, as studied by high energy resolution neutron spectroscopy

Protein dynamics play a pivotal role in biological functions such as enzyme catalysis, ligand binding and protein folding and mis-folding. As a result, detailed appreciation of the relationships between dynamics and biological function requires analysis based on models that realise the full complexity of macromolecular material. Neutron spectroscopy is an ideal tool with which to gain insight into the dynamics of bio-molecules [1] since it is not only a non-destructive and selective technique but also provides simultaneously spatial and temporal information; parameters extracted from experimental neutron studies being akin to those calculated in molecular dynamic (MD) simulations. The range of bio-macromolecular problems addressed using neutron spectroscopy is considerable. However, it is clear that there is a need for further complete dynamical data given the complexity and diversity of bio-macromolecules.

AUTHORS
M.T.F. Telling (ISIS Facility and University of Oxford, UK)
C. Neylon, **L. Clifton**, **S. Howells** and **V. García Sakai** (ISIS Facility, UK) - **L. van Eijck** (TU Delft, The Netherlands)

The high resolution backscattering spectrometer IN16, has allowed us unique insight into the dynamic landscape of apoferritin (**figure 1**), the multi-subunit intracellular iron storage protein found in almost all living organisms and a model system for colloidal bio-systems due to its mono-disperse spherical form factor. Using elastic neutron scattering methods, we have shown without ambiguity that in its lyophilised form, apoferritin, above 100 K, over the length scale 3.5 Å to 9 Å and in the ps-ns time regime, exhibits a *single* dynamic response driven by methyl (CH_3) groups *alone*; the data have been successfully modelled (**figure 2**) using theory originally developed to describe motion in glassy polymers [2]. We observe a distribution of CH_3 activation energies consistent with the environmental heterogeneity that exists around the methyl species in this protein. A mean activation energy of $E_{a,ave} = 17\,kJ\,mol^{-1}$ with a width of the distribution of activation energies of $4\,kJ\,mol^{-1}$ is observed.

Detailed analysis of complementary quasi-elastic neutron scattering data collected using the IRIS backscattering instrument (ISIS, UK) has allowed us to validate the theoretical assumptions required by the CH_3 activation model used to model the IN16 data. Here, we confirm that the methyl species undergo 3-fold jump rotations and that the characteristic relaxation time of the jump process follows the Arrhenius form with activation energy in agreement with our IN16 result.

Our results show that over the temporal and spatial range studied the main apoferritin peptide chain and other side groups remain rigid. Interestingly, yet seemingly counter-intuitively, similar results are reported for other smaller, more flexible lyophilised bio-materials. Nonetheless, these results are supported by findings from NMR. Our results will allow us to develop accurate MD force fields for the apoferritin molecule as well as further advance, via collaboration, complex molecular dynamic model simulations of other proteins. We believe this work, and analysis approach, could act as a benchmark for the investigation of methyl group dynamics in other proteinacious materials using neutron scattering. Furthermore, it is clear that there is a need for detailed dynamical data given the complexity and diversity of bio-macromolecules and we believe our work will add to this knowledge database [3].

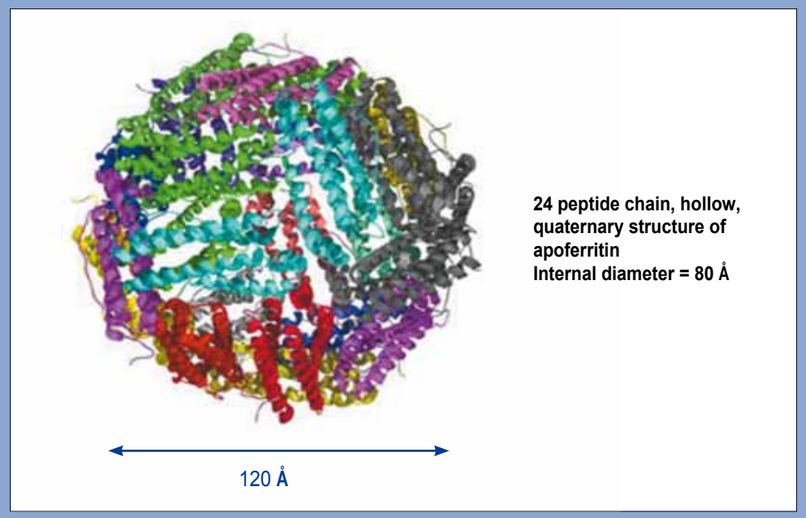

Figure 1:
The quaternary structure of apoferritin.

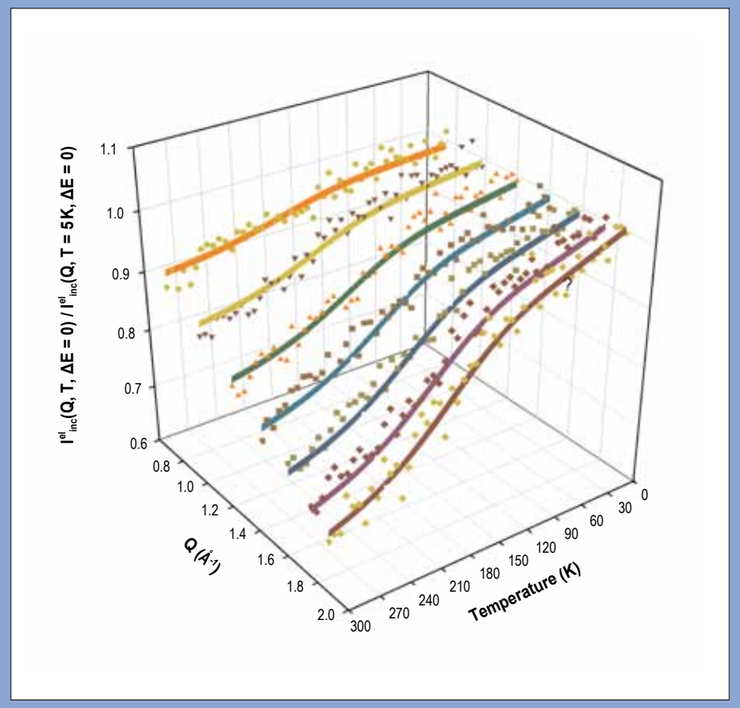

Figure 2:
Data collected from lyophilised apoferritin taken on IN16 at Q = 0.78, 1.01, 1.24, 1.44, 1.61, 1.76 and 1.87 Å^{-1}. The solid lines are the result of simultaneously fitting the CH_3 jump rotation model of Grapengeter et al [2] to the data.

REFERENCES
[1] Dynamics of Biological Molecules by Neutron Scattering, eds. S. Magazu and F. Migliardo, pp. 4-21 (18), Bentham Science (2011), DOI: 10.2174/978160805219611010l
[2] H.H. Grapengeter, B. Alefeld and R. Kosfeld, Colloid Polym. Sci. 265 (1987) 226–233
[3] G. Zaccai, Acta Crystallogr., Sect. D: Biol. Crystallogr., 66 (2010) 1224–1228

AUTHORS
L. van Eijck (Delft University of Technology, The Netherlands) - **F. Merzel** (National Institute of Chemistry, Ljubljana, Slovenia)
S. Rols, **J. Ollivier** and **M.R. Johnson** (ILL)
V.T. Forsyth (ILL and EPSAM/ISTM, Keele University, UK)

REFERENCES
[1] M. Peyrard, Nature Phys. 2 (2006) 13
[2] R. S. Mathew-Fenn, R. Das and P.A.B. Harbury, Science 322 (2008) 446

Time-of-flight spectrometer IN5

DNA as a safety belt

The DNA molecule inside a living cell undergoes many mechanical manipulations, both to pack it in the cell and to fulfill its biological functions. Understanding DNA functions therefore requires its mechanical properties, expressed as elastic or force constants, to be known [1]. The improved inelastic neutron scattering spectrometer IN5 and samples of aligned DNA fibers, combined with atomistic phonon and MD calculations, now make the very soft collective dynamics in DNA measurable. From these measurements the base-pair, stretching force constant is derived.

Most experimental techniques apply forces to the DNA molecule or require some molecular sculpturing (optical or magnetic tweezer, attaching nano-particles to DNA, etc) in order to obtain the values for the corresponding force constants. However, the reported values in literature for this force constant vary by nearly three orders of magnitude, with a clear tendency for structure-based measurements to give softer force constants.

We have determined the stretching force constant, free from such external manipulations, by measuring with inelastic neutron scattering (INS) the dispersion of harmonic vibrations along aligned, wet-spun fibers on the new IN5 spectrometer. The observed dynamics are confirmed by phonon calculations, using the standard CHARMM force field, on a fully atomistic model of DNA surrounded by water molecules and counter ions.
This is the first observation of the acoustic phonon branch along the DNA fiber, enabled by the very high resolution in both energy and momentum transfer, as well as the excellent signal-to-noise ratio, available on IN5. The width of the helix Brillouin zone is 0.18ÅÅ^{-1} and the acoustic branch peaks below 2 meV. These collective dynamics, measured up to 335 K i.e. far above physiological temperatures, are remarkable considering the common understanding of DNA existing of randomly distributed soft and stiff regions along the helix.

Phonon calculations reconcile these data with inelastic X-ray scattering (IXS) data. The apparent liquid-like damping of the phonon dynamics in the IXS data, in the much (10x) bigger Brillouin zone defined by the distance between base-pairs, is simply a manifestation of the random sequence of base-pairs and the one-dimensional character of the excitations. The apparent acoustic phonon branch as measured by IXS, extending up to about 10 meV, is actually the average of many optic modes polarised along the helix axis.
The atomistic model that is used to describe both the INS and IXS data can be used to mimic the stress-strain experiments performed on single DNA molecules. Molecular dynamics simulations probe the stretching stiffness of DNA on a longer time scale up to 100 ns, compared to the pico- to femto-second vibrational timescale. The elongation and compression of the simulation cell in the direction of the helix axis results in a force constant that is an order of magnitude or more lower than the 83 N/m obtained from the inelastic scattering data and lattice dynamics calculations. At longer time scales the reorganisation of the surrounding water molecules and counter ions effectively softens the DNA. Force-based methods to determine the force constant and techniques based on molecular sculpturing (like [2]) include such relaxation in their determination of force constant.

In this way, DNA is like a car safety belt that resists when pulled suddenly (on a short picosecond time scale) but extends more easily when pulled gently.
The next step will be to determine the sensitivity of the DNA force constant to variations of its direct environment like water molecules and counter ions.

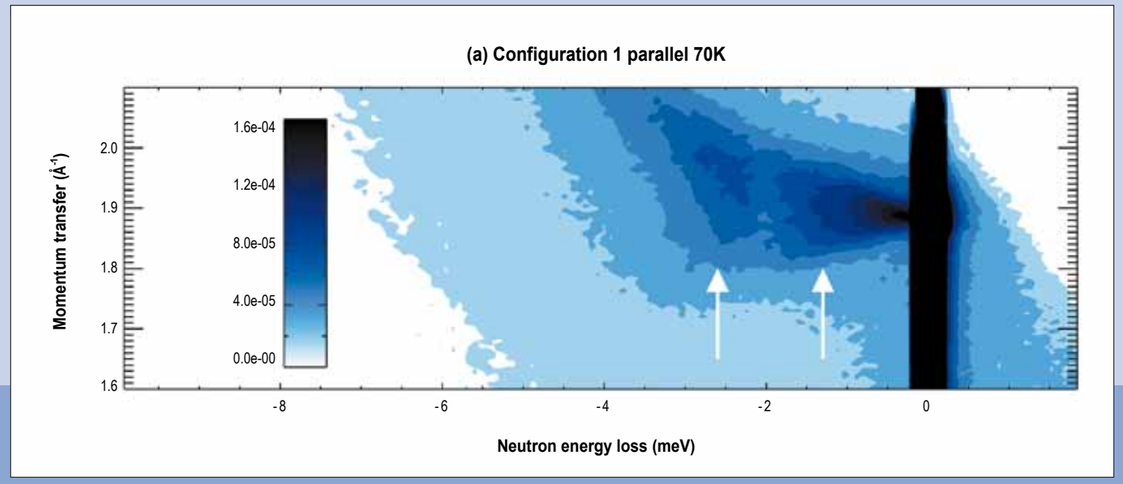

Figure 1: *S(Q,E) map of DNA fibers aligned parallel to the instrumental scattering plane. The Bragg peak at 1.9 ÅÅ^{-1} and the acoustic branch are clearly visible. At higher energy the first optic dispersion is seen.*

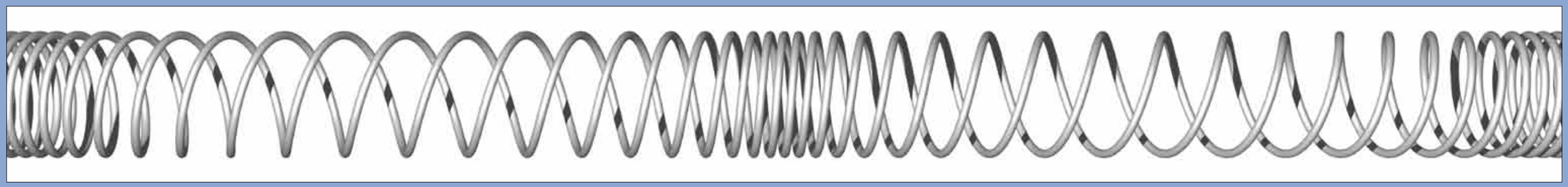

AUTHORS
M. Zbiri and **H. Schober** (ILL)
R. Mittal and **S.L. Chaplot** (Bhabha Atomic Research Centre, India)
S.J. Hibble, **A.M. Chippindale** and **E. Marelli** (University of Reading, UK)

REFERENCES
[1] R. Mittal, M. Zbiri, H. Schober, E. Marelli, S.J. Hibble, A.M. Chippindale, and S.L. Chaplot, Phys. Rev. B 83 (2011) 024301
[2] R. Mittal, S.L. Chaplot, and H. Schober, Appl. Phys. Lett. 95 (2009) 201901
[3] M. Zbiri, H. Schober, R. Mittal and S.L. Chaplot - *in preparation*

Insights into the unusual phenomenon of negative thermal expansion: Relevancy to dynamics

Interest in the phenomenon of negative thermal expansion (NTE) and its fascinating effects is fully justified both in the engineering industry and in the field of biomedicine in view of its many potential practical applications for the development of advanced materials and biomaterials. For instance, by mixing a negative thermal expansion material with a "normal" material (i.e. one which expands on heating), it would be possible to produce a zero-expansion composite material which could be embedded in the fabrication process of materials used in civil engineering (bridges), high-speed public transport (railway tracks), biomedical engineering (prostheses, implants) and the aerospace industry (protection of aircraft against large temperature swings, telescope mirrors).

NTE is a macroscopic property that needs to be understood at the fundamental level as it involves a number of different microscopic physicochemical aspects. Dynamics plays a major role in this context and is intimately related to thermal properties through phonons (quantum of vibrations). The latter reflect the dynamical character of the material and build up its thermodynamical picture.

There is keen interest in the quest for NTE materials. As well as in oxide-based materials, anomalous thermal expansion behaviour has been observed in molecular framework systems containing linear diatomic bridges, such as cyanide anions. In this article, we focus on $Zn(CN)_2$, which is reported to have a large isotropic NTE coefficient over a wide temperature range. **Figure 1** shows the ordered structure of $Zn(CN)_2$, which is a cubic network where the Zn ions are linked by CN molecules. It consists of a ZnC_4 tetrahedron (at the centre of the cell) linked to four neighbouring ZnN_4 tetrahedron (at the corners of the cell) with CN groups along four of the body diagonals.

To explore and elucidate the connection between phonon dynamics and NTE, we employed inelastic neutron spectroscopy using the time-of-flight instrument IN6 to measure the temperature and pressure dependencies of the phonon spectra [1,2]. We also carried out density functional theory (DFT) calculations to analyse and interpret the observations [1,3]. The measured Bose-factor corrected dynamical structure function $S(Q,E)$ for $Zn(CN)_2$ is shown in **figure 2**. There is clearly a low-energy flat acoustic mode at about 2.5 meV. This is well reproduced by the *ab initio* DFT-based lattice dynamical simulations in **figure 3**, where the observed feature is well predicted and highlighted [3]. Having established a reliable and appropriate model calculation, we went further by analysing the pressure-dependent data and extracting the details that were relevant to NTE. **Figure 4** compares the measured and calculated contribution of the various phonons to the volume thermal expansion coefficients (α_V) as a function of phonon energy. The mode Grüneisen parameters Γ_i/B (measured and calculated) were used to evaluate these coefficients. Γ_i/B were experimentally extracted from pressure-dependent phonon measurements [2]. The maximum negative contribution to α_V stems from the low-energy modes at about 2.5 meV. In order to determine the character of these phonon modes, we calculated the mean squared displacements of the various atoms, $\langle u^2 \rangle$, arising from all phonons of energy E in the Brillouin zone (**figure 5**). There are significant and equal amplitudes for all the atoms up to 5 meV. The contribution from Zn vanishes above this energy. Moreover, analysis of the normal modes allowed us to identify the motions responsible for NTE. We found that they are mainly of a translational and bending nature and are within the zone boundary along [100] and [110], exhibiting very large negative Γ values of -48.4 and -85.8, respectively [1]. The CN molecules (**figure 1**) can be assimilated to rigid rods at the energies of interest for NTE. As the rods exhibit a strong lateral motion, the bond between the Zn ions has to contract if averaged over time. As the amplitude of the lateral motions increases with temperature, the lattice contracts with temperature in all directions.

In conclusion, by combining inelastic neutron spectroscopy and DFT simulations, we have shown unambiguously that low-energy phonon modes at about 2.5 meV are responsible for the large isotropic NTE in the non-oxide molecular cyanide-based framework material $Zn(CN)_2$. We have succeeded in identifying the modes which are the cause of this unusual phenomenon. This finding provides new and deeper understanding of the role of dynamics in this fascinating thermal property that is relevant to both fundamental and applied sciences.

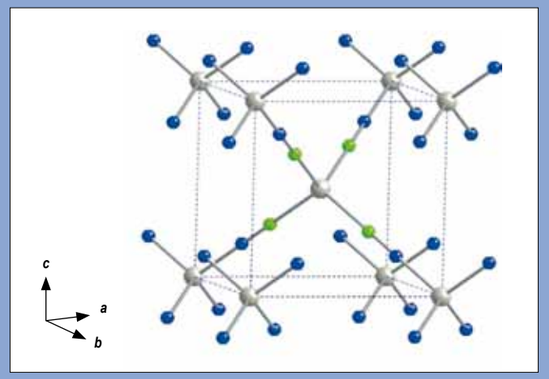

Figure 1: *The structure of $Zn(CN)_2$. Key: Zn, gray spheres; C, green spheres; N, blue spheres.*

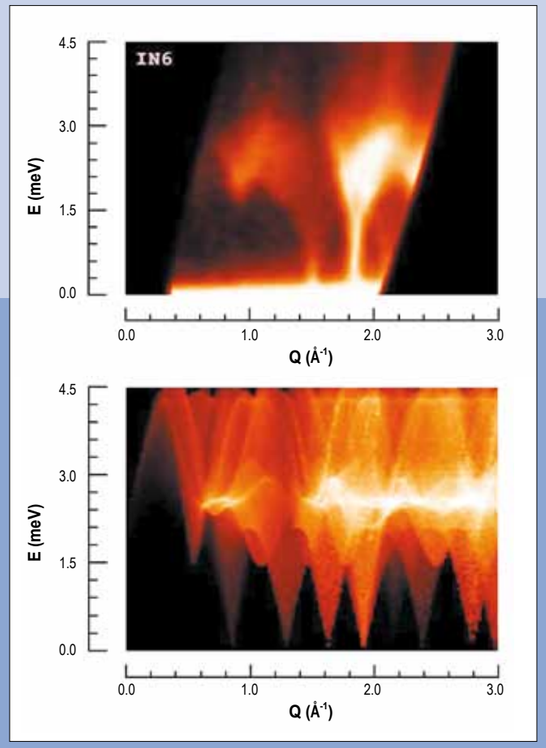

Figure 2 (top): *The experimental Bose-factor corrected dynamical structure function S(Q,E) measured on IN6 with an incident neutron wavelength of 5.12 Å at 180 K.*

Figure 3 (bottom): *The ab-initio simulated S(Q,E) map calculated for the Stokes process at 0 K (one-phonon annihilation) [3].*

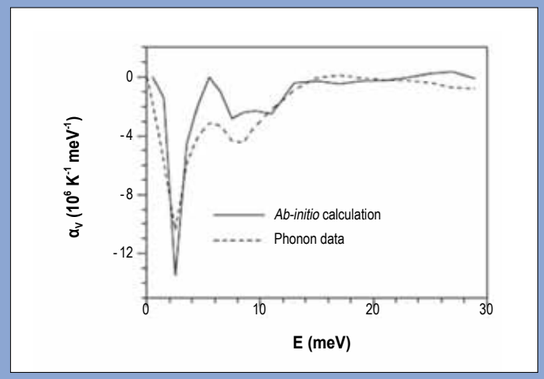

Figure 4: *The experimental (IN6 at 165 K) vs. calculated (DFT) contribution of phonons of energy E to the volume thermal expansion coefficients α_V, involving the measured and estimated mode Grüneisen parameters Γ_i/B, respectively.*

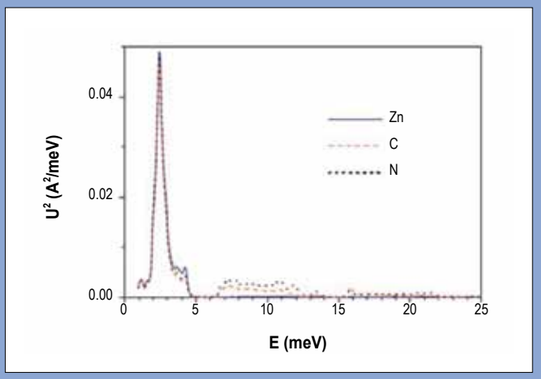

Figure 5: *The calculated contribution to the mean squared amplitude of the various atoms arising from phonons of energy E at 300 K.*

AUTHORS
D.J. Bicout (ILL, UJF and VetAgro Sup, France)
E. Kats (ILL and Landau Institute for Theoretical Physics, Russia)
A.K. Petukhov (ILL)
R.S. Whitney (ILL and LPMMC, UJF and CNRS, Grenoble, France)

REFERENCES
[1] R.E. Jacob, S.W Morgan, and B. Saam, Phys. Rev. Lett. 87 (2001) 143004

Depolarisation of ^{3}He due to wall collisions

Hyperpolarised ^{3}He gas is slowly depolarised by collisions between the ^{3}He atoms and the walls of the container it is in. This depolarisation is thereby related to the statistics of a random-walk's collisions with walls. We find that the statistical fluctuations in the number of wall collisions show *universality* in the long time limit, being *independent* of the distance between walls. Remarkably, this means that wall-scattering can induce depolarisation processes which are independent of the container size.

Hyperpolarised ^{3}He is used extensively in neutron facilities for neutron-spin filtering, and in a variety of other contexts from engineering to medicine. However its use is impeded by the fact it loses its polarisation with time. In good containers, ^{3}He remains polarised for hundreds of hours. In other containers made in the same manner, it may lose its polarisation after a few hours. Currently, good and bad containers are identified by trial and error. To improve the proportion of good containers, we need to identify the depolarisation process which leads to such huge variations.

We believe that they are due to variations in the density of unwanted magnetic impurities on the container walls. For a typical cell (a few centimetres across) of ^{3}He gas (at room temperature and pressure), the depolarisation takes tens or hundreds of hours, while the time to diffuse across the cell is about a second; so each atom undergoes a huge number of wall collisions before it is depolarised. Thus the depolarisation could originate from the fact that when a ^{3}He atom collides with the wall, its spin is very slightly rotated by the tiny short-range magnetic field generated by such an impurity (see **figure 1**).

We model the motion of each ^{3}He atom as a random-walk, so it is crucial to analyse the number of times the random walk hits the container walls in a time t (see **figure 2**).

This number will be different for different random walks, and so we must think in terms of the probability distribution of the number of boundary collisions. This distribution is characterised by two quantities; (i) the average number of wall collisions, $N(t)$, in the time t, and (ii) the variance in the number of wall collisions, var$[N(t)]$, in the time t.

For a one-dimensional random walk enclosed between two walls a distance X apart, we find that for times t much bigger than the time to diffuse across the container:

$$N(t) = vt/X \quad (1)$$
$$\mathrm{var}[N(t)] = t/(3\,\tau_{mfp}) \quad (2)$$

where v and τ_{mfp} are the velocity and mean-free-path of the walker (the ^{3}He atom). The result for the average is not unexpected, it goes like $1/X$. However the result for the variance is quite remarkable, despite being an effect of the walls it is completely *independent* of the inter-wall distance, X. We can then approximate an atom's motion in a cubic container by three independent random-walks in the x,y,z-directions.

Typically, $\tau_{mfp} \sim 10^{-10}$s and $X/v \sim 10^{-5}$s, thus the variance in Equation (2) is 10^5 times larger than the average in Equation (1). This vast difference is due to strong correlations between subsequent wall collisions, see **figure 2**. If correlation had been weak, one would have found the average and variance to have been of similar magnitude, so fluctuations about the average (square-root of variance) would have been of order the square-root of the average. This type of argument was used by Smoluchowski in his model of Brownian motion. For our problem, in contrast, neglecting correlations would under-estimate the variance by a factor of 10^5.

The fluctuations in the number of boundary collisions are so much larger than one would naively expect, we argue that they should not be neglected when calculating the depolarization rate of the gas.

In particular, we show that they are a strong source of depolarization in those cases where the spin-rotation at each wall collision has a preferred direction (e.g. a rotation by angle $+\theta$ is more probable than by angle $-\theta$). This will be the case whenever the magnetic impurities in the container walls have been partially aligned, for example by exposure to a magnetic field before the container was filled with ^{3}He. Similar effects were observed during an experiment in [1], which we are now trying to reproduce and study systematically.

Remarkably, the depolarisation rate associated with this process is *independent* of the container-size. This is despite the fact that it is induced by wall-collisions, and the typical number of such collisions decays with increasing container-size.

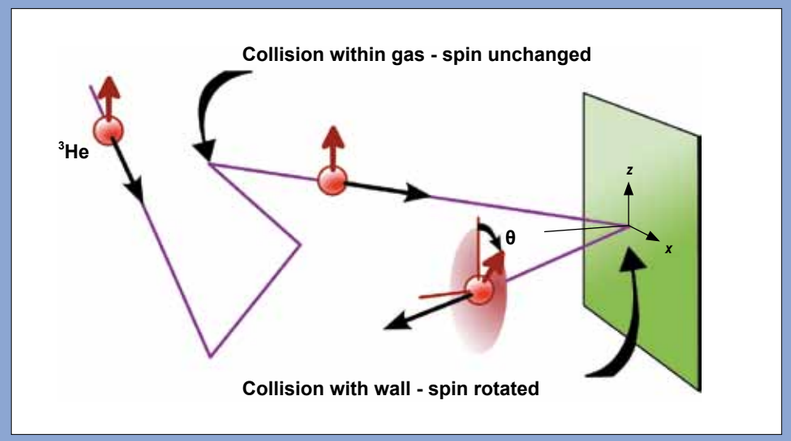

Figure 1:
At each wall collision, the spin of the ^{3}He atom is rotated by a very small random angle, θ. We neglect spin rotations at collisions within the gas, since wall collisions dominate the depolarisation in all but the very best containers.

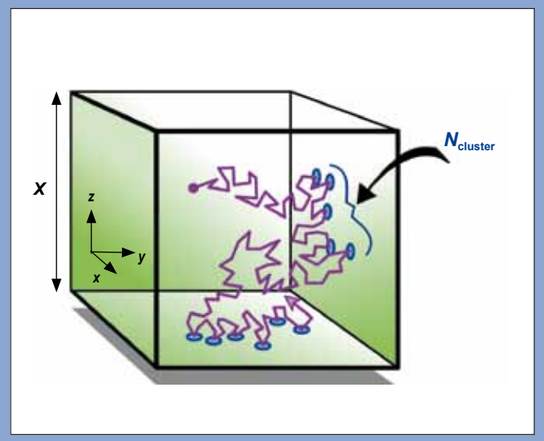

Figure 2:
The random-walk of a ^{3}He atom as it diffuses in the gas in a cubic container. Wall collisions (marked with blue circles) occur in clusters, which means that there are strong positive correlations between subsequent collisions. An atom far from the wall has no wall-collisions until it diffuses there, then it will typically undergo $N_{cluster}$ collisions before diffusing a way from the wall again. Approximating this motion by three independent random-walks in the x,y,z-directions, we find that $N_{cluster} \propto 1/X$, which leads to the X-independence of var[N(t)].

AUTHORS
R.S. Whitney and **T. Ziman** (ILL and LPMMC, UJF and CNRS, Grenoble, France)
M. Clusel (ILL and Laboratoire Charles Coulomb, CNRS and University Montpellier II, France)

Noise enhancing coherent oscillations at a Landau-Zener transition

Quantum systems can be in a superposition of two different states at once. Such superpositions can be detected by looking for coherent oscillations of observables. Usually noise decoheres superpositions and thereby suppresses coherent oscillations. However we showed that noise may enhance the coherent oscillations of a system driven through a Landau-Zener transition, via an effect we call "Lamb-assisted coherent oscillations". We propose verifying this with polarised ^{3}He, before using it as a probe of the sources of quantum noise which affects molecular magnets.

Quantum systems can be in a coherent superposition of two different states. These "Schrödinger cats" are characteristic of the quantum world and cannot exist in classical mechanics. Coherent superpositions are identified by the coherent oscillations of observables. However noise (of a quantum or classical origin) is a huge impediment to observing or using such coherent superpositions. Even a small amount of noise causes the decoherence of quantum superpositions into classical mixtures: the noise makes the quantum system lose this essential quantum property, stopping the cat being in a superposition of "dead" and "alive".

Quantum noise originates from the system's coupling to other quantum degrees of freedom in its environment, while classical noise is due to random fluctuations in classical (macroscopic) fields coupled to the quantum system. Macroscopic systems typically couple strongly to many degrees of freedom, and thus decohere too fast for superpositions to be observable. Even small systems, such as molecular magnets or nanoscale superconducting circuits, decohere sufficiently fast that it is impracticable to use their superpositions for applications such as quantum computing. As a result, there is currently research on superpositions in many different quantum systems, with the objective of understanding the origin of the noise which causes the decoherence in each of them. However, in a recent work we show that under certain conditions the noise can also *enhance* the coherent oscillations that appear when a quantum system is driven through an avoided level crossing.

Such an enhancement can occur because noise does not only cause decoherence, it also *modifies* the system's Hamiltonian. Such a modification was first proposed by Hans Bethe as an explanation of the Lamb shift of energy levels in the hydrogen atom. There the noise source is the vacuum fluctuations of the photon field. This noise certainly has a decoherence effect, however the crucial point was that it modified the Hamiltonian of the atom sufficiently to create a shift of certain energy levels.

In 1932, Landau, Zener, Stueckelberg and Majorana independently addressed the problem of a quantum system being driven through an avoided level-crossing, see **figure 1b**, a problem now known as the Landau-Zener transition. They showed that the transition amplitude from the ground state to the excited state has an exponential dependence on the gap at the avoided crossing, Δ. We therefore argue that this amplitude will be exponentially sensitive to any noise-induced Lamb shift of this gap. The sign of the Lamb shift is a function of the noise-spectrum (noise at higher frequencies than Δ reduces the gap, while noise at lower frequencies enhances it). If the Lamb shift reduces the gap slightly, then the small transition amplitude will be exponentially enhanced, exponentially magnifying the coherent oscillations. We show that this effect, which we call "Lamb-assisted coherent oscillations", often dominates over the decohering effect of the noise.

Highly polarised ^{3}He is an ideal testing ground for our theory. Each ^{3}He atom has a spin-half which can be flipped by electromagnetically driving the system at radio-frequencies. In the rotating frame, the spin-flip can be seen as a Landau-Zener transition. Since all atoms in the gas behave in the same manner, the time-dependence of a ^{3}He atom's spin-state is observed by measuring the magnetisation of the whole gas as a function of time. The intrinsic noise in the system has been made extremely small (decoherence times are relatively long) thanks to recent work within the Nuclear and Particle Physics group at the ILL. However it is very easy to add man-made noise in a controlled manner. In addition to testing our theory (which assumes the noise to be a weak perturbation), a ^{3}He experiment can be used to study the effect of strong noise on Landau-Zener transitions.

These "Lamb-assisted coherent oscillations" could be used as a probe of the source of noise in various quantum systems, since its temperature dependence is a function of the noise-spectrum. One should thus distinguish high-frequency noise (which enhances the coherent oscillations) from white-noise or low-frequency noise (which both suppress the oscillations). For example, this could help resolve the current debate about whether the principle source of decoherence in molecular magnets is a low-frequency bath of nuclear spins, or a high-frequency bath of phonons.

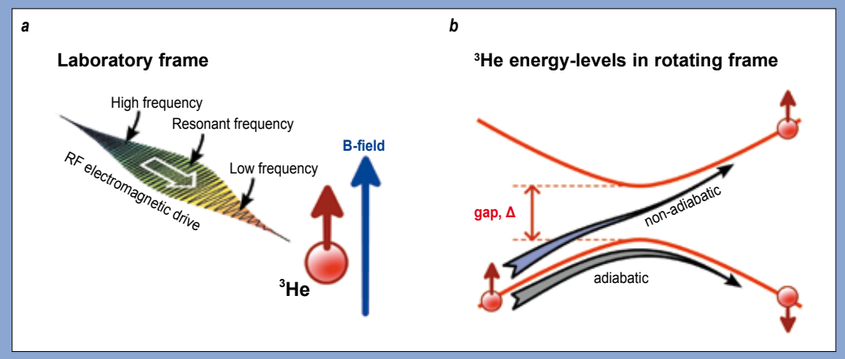

Figure 1:
A ^{3}He atom whose spin is driven by a radio-frequency electromagnetic (EM) field whose frequency changes with time. In the rotating frame this has the effect of sweeping the system through an avoided crossing. For a large gap, the Landau-Zener transition is adiabatic. For smaller gaps, the system passes into a superposition of the two states (ground and excited state). A Lamb-shift of the gap modifies this superposition.

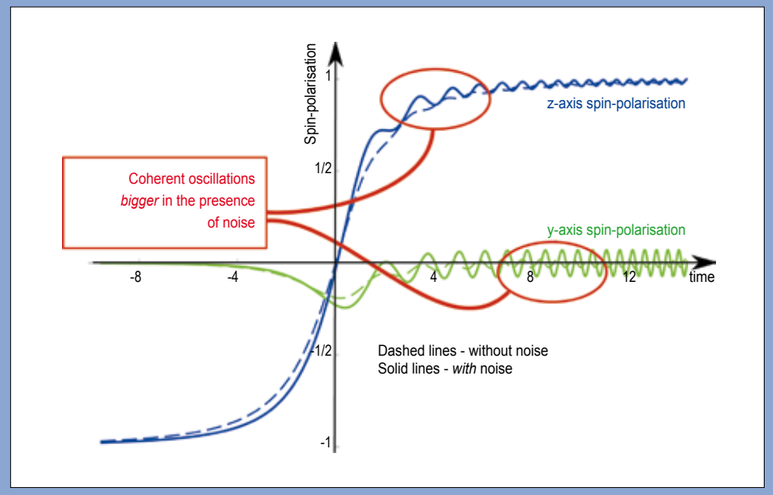

Figure 2:
The spin-polarisation of the ^{3}He atom measured along the y and z axis, as a function of time. Noise clearly enhances the coherent oscillations.

AUTHORS
J.R. Allibon, J. Archer, S.C. Capelli, J.F. Clergeau, V.T. Forsyth and S.A. Mason (ILL)

D19: a Millennium Programme success story

ILL's D19 diffractometer is a multifunctional instrument that tackles challenging problems in Chemistry, Physics, and the Biosciences. Its capabilities were vastly enhanced by a major UK EPSRC award to Durham, Keele and Bath Universities* as part of the initial phase of the ILL's Millennium Programme. The new instrument features a large solid-angle area detector, a flexible monochromator assembly matching a wide range of length scales, and an effective gain factor of about 25. The new D19 is now yielding remarkable results in structural/materials chemistry, protein crystallography, and a wide range of partially ordered systems.

The new D19 detector (top), built by the ILL detector group, subtends an angular range of 120 x 30 degrees, and is the centrepiece of the refurbished instrument. Also shown is a diffraction pattern from a protein recorded using this detector.

[1] A.Y. Kovalevsky, B.L. Hanson, S.A. Mason, T. Yoshida, S.Z. Fisher, M. Mustyakimov, V.T. Forsyth, M.P. Blakeley, D.A. Keen, and P. Langan, *Angewandte Chemie* 50 (2011) 7520-7523
[2] A.Y. Kovalevsky, B.L. Hanson, S.Z. Fisher, M. Mustyakimov, S.A. Mason, V.T. Forsyth, M.P. Blakeley, D.A. Keen, T. Wagner, H.L. Carrell, A.K. Katz, J.P. Glusker and P. Langan, *Structure* 18 (2010) 688-699
[3] V.L. Davidson, *Nature Chemistry* 3 (2011) 662
[4] M. Wada, Y. Nishiyama, G. Bellisia, V.T. Forsyth, S. Gnanakaran, and P. Langan, *Cellulose* 18 (2011) 191-206
[5] P. Langan, S. Gnanakaran, K.D. Rector, N. Pawley, D.T. Fox, D.W. Cho, and K.E. Hammel, *Energy & Environmental Science* 4 (2011) 3820-3830
[6] S. Rizzato, J. Berges, S.A. Mason, A. Albinati, and J. Kozelka, *Angewandte Chemie* 49 (2010) 7440-7443
[7] L.R. Falvello, *Angewandte Chemie* 49 (2010) 10045-10047
[8] D. Chateigner, B. Ouladdiaf, and F. Leon, *Solid State Phenomena* 160 (2010) 75-82
[9] G.D. Gatta, G.J. McIntyre, R. Sassi, N. Rotiroti, and A. Pavese, *American Mineralogist* 96 (2011) 34-41
[10] A. Albinati, E. Cesarotti, S.A. Mason, I. Remoldi, S. Rizzato, and D. Zerla, *Tetrahedron Asymmetry* 21 (2010) 1162-1165
[11] G. Cioci, A. Srivastava, D. Loganathan, S.A. Mason, S. Perez, and A. Imberty, *J. Am. Chem. Soc. USA* 133 (2011) 10042-10045
[12] K. Fucke, K.M. Anderson, M.H. Filby, M. Henry, J. Wright, S.A. Mason, M.J. Gutmann, L.J. Barbour, C. Oliver, A.W. Coleman, J.L. Atwood, J.A.K. Howard, and J.W. Steed, *Chem. Eur. J.* 17 (2011) 10259-10271
[13] K.M. Anderson, A.E. Goeta, J.E. Martin, S.A. Mason, G.J. McIntyre, B.C.R. Sansam, C. Wilkinson, and J.W. Steed, *Cryst. Growth Des.* 11 (2011) 4904-4919

** P.Is: J.A.K. Howard, M. Davidson, W. Fuller, V.T. Forsyth and S.A. Mason.*

BIOLOGICAL CRYSTALLOGRAPHY

Below part of a density map from a combined neutron and X-ray crystallographic study of xylose isomerase – the enzyme that is responsible for the conversion of glucose to fructose. Following the initial work on this system, published as a cover article in *Structure* [2], further studies published in *Angewandte Chemie* [1] described the presence of hydronium ions in the structure. This article was highlighted in *Nature Chemistry* [3] where the importance of hydronium ions and associated protonation shifts in aqueous environments were emphasised. Such information is not accessible to X-rays crystallography where clearly H_3O^+, H_2O and OH^- groups (or even O atoms) are almost indistinguishable.

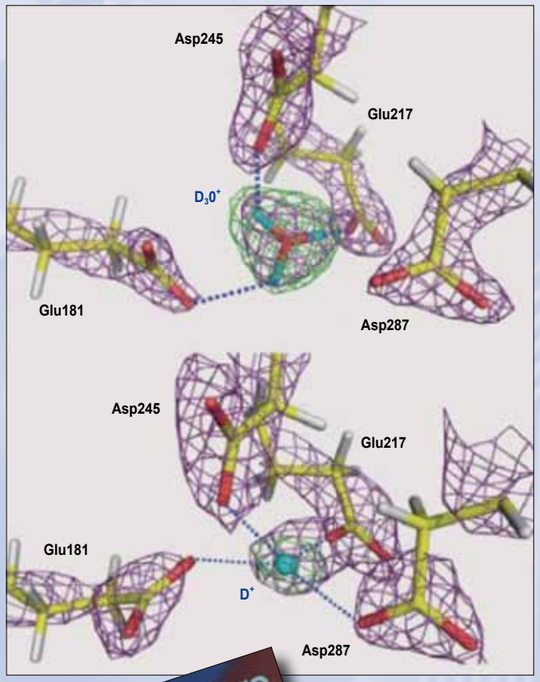

A hydronium ion in xylose isomerase [1].

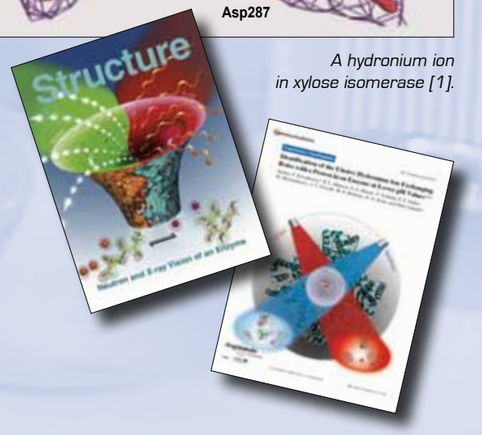

FIBRES AND PARTIALLY ORDERED SYSTEMS

D19 has a long history of elegant experiments involving the study of fibrous systems including synthetic polymers, DNA, filamentous viruses, and polysaccharides such as chitin and cellulose. The rebuilt instrument has provided a quantum leap for the study of these partially ordered systems. For example, during 2011, Wada and co-workers [4] published a novel study providing high-resolution information associated with the mercerisation of cellulose. Mercerisation is an important preparative step in the processing of raw cellulosic material [5]. D19 data, used in conjunction with molecular modelling, have provided new information on the hydrogen bonding patterns involved and also on the associated movement of ammonia molecules.

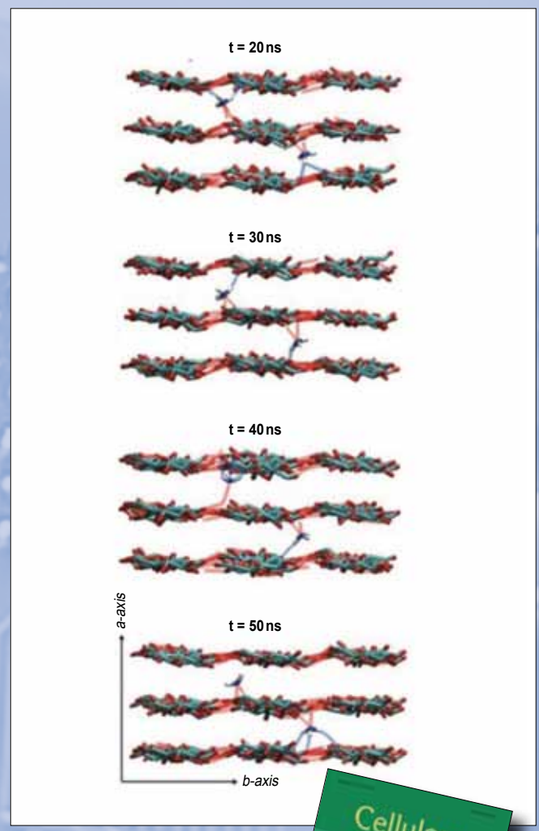

Movement of ammonia in the mercerisation of cellulose [4].

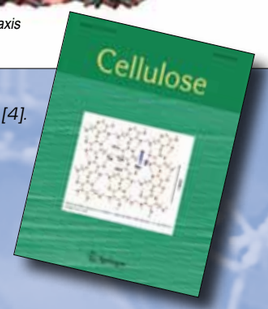

STRUCTURAL AND MATERIALS CHEMISTRY

In structural chemistry and materials chemistry, recent studies include magnetic texture analysis [8], analysis of the presence of hydrogen bond and cation partitioning in minerals [9], determination of absolute stereochemistry [10], as well as very accurate structural studies of glycoprotein analogues [11], the importance of charge - assisted H bonds in symmetry breaking [12], and the probing of O-H...π H bonds in water structure in the hydrophobic cavity in calixarenes [13]. The common factor in such studies is often the ability of D19 to provide unique information at high resolution on the location of hydrogen atoms and hydrogen bonding geometry.

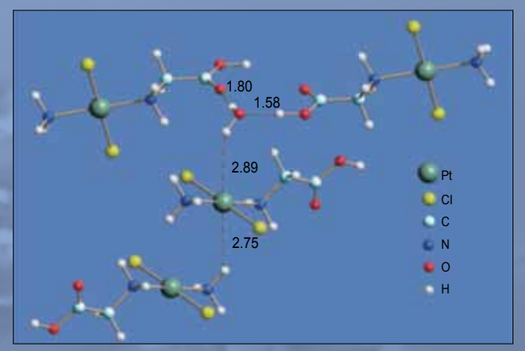

Crystal structure of non-classical hydrogen bond involving a central platinum atom [6,7].

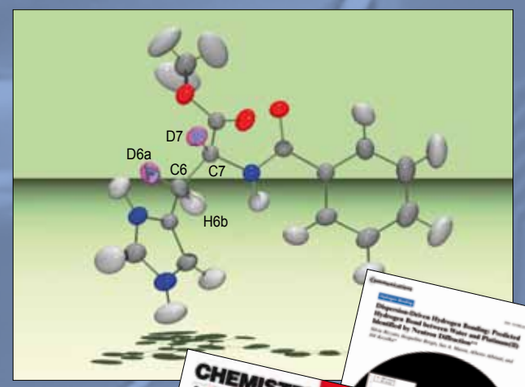

Absolute stereochemistry of cation moiety of deuterium-labelled substituted histidine [10].

© Alexis Cheziere

MILLENNIUM PROGRAMME AND TECHNICAL DEVELOPMENTS

MILLENNIUM PROGRAMME
NEW EXPERIMENTAL TECHNIQUES
TECHNICAL DEVELOPMENTS

It has to be said that 2011 brought its share of uncertainties, leaving a bittersweet taste behind. 2012 and even 2013 will doubtless be intense, as the economic crisis waxes and wanes and further challenges and opportunities arrive at our door. The decisions we make during this crucial period will certainly mark the years to come, but we have been charting our course carefully. We are confident that our users will maintain their demand for our beamtime, given the quality of the results and support they receive at the ILL. It is an ILL rule never to compromise on user support and always to ensure that instrument performance pays dividends.

The progress made this year with the Millennium Programme has been very rewarding, of course. We have commissioned two of the main neutron guides (H112 and H14) as well as the instrument LAGRANGE, with very promising results in terms of improved performance. We have also started commissioning D33. The final components of IN16B started arriving at the end of the year, in time to allow commissioning during the first reactor cycle of 2012. Eight M€ were invested in the different instrumentation projects. By the end of 2011, therefore, the total investment in the 2007-2014 phase of the Millennium Programme (the "M-1 phase") has amounted to 31.4 M€. This is 68% of the total 45.9 M€ budget allocated for the period.

Given the quality of the results achieved in 2011, I have no doubt that the concerns and uncertainties for 2012 will fade as the year progresses

For the rest of the M-1 phase we will be concentrating on the projects associated with the ILL22 neutron guide hall. We will start with the extension of the guide hall itself. This will create space for new instruments and also, temporarily, for the thousand tons of radiological shielding that needs to be set aside to allow work on the horizontal cold neutron source and H5 guide. The ILL22 instrument projects, WASP and ThALES, are progressing very well in terms of design and manufacture (the latter in collaboration with Charles University of Prague).

The Projects and Techniques Division (DPT) services are committed to delivering the very best to our users and instrument responsibles. Our Neutron Detector Service achieved a major success this year with the development of a large-area detector based on boron-10 thin layers (as an alternative to the now scarce helium-3). A first prototype of 2m in length has been tested successfully. These encouraging results confirm the leading position of the ILL's detector service; we are collaborating with different neutron facilities, keen to share our knowledge for the benefit of the neutron community as a whole. In the same spirit, in 2011 we completed the construction of two helium-3 filling stations for polarising neutrons, one for ISIS and the other for ANSTO. This was a long and complex project, which was of benefit also to the ILL, as we managed to improve the device with more robust new technology. We also continued our efforts to ensure that these sophisticated filling stations remain as simple and automatic to use as possible.

Given the quality of the results achieved in 2011, I have no doubt that the concerns and uncertainties for 2012 will fade as the year progresses. The confidence, capacity and determination of everyone at ILL will ensure the launch of new projects for the instruments and reactor and facilitate the demanding decisions to be taken for the long-term future of the ILL. I have always believed that adversity brings out the best in us all; it has revealed the reserves we need to continue our advances in both knowledge and technology.

José Luis Martínez
Associate Director

AUTHOR
J.L. Martínez (ILL)

Millennium programme 2011

The 2011 Millennium harvest was an excellent one, to be remembered for years to come. In a complicated and demanding programme our teams successfully installed and commissioned two important neutron guides (H112 and H14), which will feed neutrons to five instruments (IN16B, D33, IN12, IN11 and LADI) and provide an inclined end position on H112 for future instruments. Early measurements of total flux within both guides indicate that the choices on the distribution of the guides were well made, that the quality of the guide elements is high and that alignment is excellent. Two new instruments will be soon ready for our user community: IN1-LAGRANGE and D33. In parallel, work continued on ThALES and WASP, with the necessary re-design of the H5 neutron guide. Other successes are therefore in the pipeline! Finally, but also very importantly, the design of the new shielding is proving to be very effective, significantly reducing the background from the new high-m coating guides and also making realignment operations far easier in the future.

The IN1-LAGRANGE secondary spectrometer was commissioned in 2011 (see article on p.82). Once extra shielding had been installed against local background, the improvement over the former Be-filter spectrometer was obvious. The increase in signal and the reduction of background are providing a final gain factor of between 10 and 20. It's a great pleasure to deliver a new instrument, on time, on budget, and performing as promised!

The new **D33** small-angle spectrometer is now almost ready to fly (see article on p.78). Close to the end of 2011, the first neutrons started lighting up the optical casemate. The commissioning of D33 will continue during the first cycle of 2012. All the components have been delivered, except for four panels for the mobile front detector. We started component commissioning with the optical casemate (see **figure 1**). The initial results are very satisfactory. The next step, to be taken in the first cycle of 2012, is to commission the collimation system and the main high-resolution rear detector and trolley which slides inside the main 14-metre vacuum tube. Full instrument commissioning will take place in the first cycle of 2012. All the options (monochromatic pin-hole, TOF, polarisation,..) are due to be optimised. The second cycle of 2012 could see our first “friendly users” on the instrument.

The high flux/high resolution backscattering spectrometer **IN16B** is a complex instrument, almost complete. By the end of 2011 only the first few meters of the focussing guide remained pending (see article on p.80). The main vacuum chamber and shielding have been installed, as has the new phase-space transformer and background chopper system. The Doppler system and analysers will be brought in from the old IN16, although we have also started a new project to design and construct a set of 6 full-size analysers, optimised for its new and enlarged vacuum chamber. The new analyser system will be available by the end of 2012; it will almost double the effective surface available. The first two cycles of 2012 will be devoted to commissioning, with the aim of launching the instrument's scientific programme with external users in the last quarter of 2012.

The **neutron guides** are a very important element in the overall design of new high-performance neutron instruments. Ideally, the guide and its instruments should really be designed together, as the system delivering the neutrons has a major influence on instrument performance. This was clearly the case for IN16B harnessed to the cold neutron guide H112. H112 has a total length of around 122 metres, with an initial 20-metre "double-barrel" section; its upper section (H112 b) will be available for a future instrument in ILL7. Preliminary total flux measurements at different points along the guide show a perfect match between the early flux simulations and the final results. Congratulations to the H112 team!

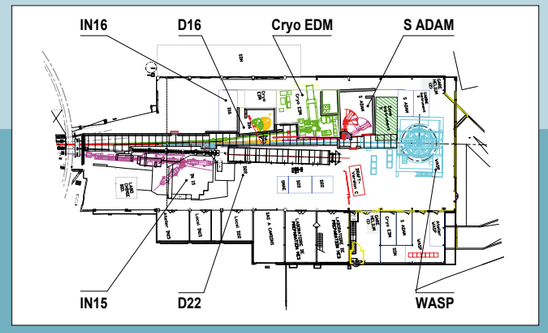

Figure 2: *New design of the ILL22 neutron guide hall, with the re-sited instruments (top left) and the experimental area for **WASP** at the end of the hall (right).*

Figure 1: *View of the optical casemate for **D33**, with its 4-chopper system, velocity selector, and polarising options, inside the stainless steel bunker (roof not yet in position).*

We also brought the **H14 guide** project to a very successful conclusion in 2011. This is a complex cold neutron guide, which starts out as a large single guide equipped with a number of sophisticated optical elements, before splitting into four separate guides. Four different instruments are being built (D33 and IN12) or re-sited (LADI and IN11) on H14. We have been able to compare the final performance of the guide at a particular instrument position with the same position on the previous H14. Initial flux measurements have been very encouraging. They differ from one point on the guide to another, but the gain factor is always between 1.5 and 2.5. This can essentially be put down to the better design, better manufacture, and improved alignment. We are very proud of the H14 team, who have run this project with brio!

In 2011 the DPT teams also worked hard on the final projects of the Millennium Programme's (M1-phase): the **ILL22** guide hall projects, and the horizontal cold source inside the **H5 beamtube**. The first step in this process is to make more space available in the ILL22 guide hall, to host an optimised H5 guide and new instruments (**figure 2**). A call for tenders was launched for the extension of the hall, with construction work planned to start in the first quarter of 2012. The extended hall should be ready for service in May 2013. As soon as the redesign of the H5 guide was completed in 2011 we started on the manufacture of its various parts. We were also able to make the final decisions on the distribution of guide space amongst the different instruments. Starting from the reactor, the instruments on the right (D22 and IN15) will not be affected by the new design; ThALES and the instruments on the left however (D16, CryoEDM and superADAM) will be re-sited and will benefit from the new guide specifications. H5 will be installed during the very long reactor shutdown lasting from June 2013 to June 2014.

The first instrument to be built on the H5 guide is **ThALES**, an upgrade of IN14, which will be dismantled and rebuilt as ThALES on ILL5's Level C. The ThALES project is managed by Charles University in Prague (Czech Republic) in collaboration with ILL. The design of the instrument (**figure 3**) was finalised during the year and the main construction contracts awarded. Construction started on the new non-magnetic sample table, the main primary casemate with non-magnetic mobile shielding, and a sophisticated monochromator. The secondary spectrometer will be reinstalled and IN14's current analyser upgraded.

The new Wide-Angle Spin-Echo instrument **WASP** will be located in the extended ILL22 hall (see **figure 4**). We finalised its design in 2011 and prepared specifications for the call for tenders for manufacturing the sophisticated coil system. Supermirror production has continued smoothly and we plan to be able to furnish at least half of the full 180 degrees of the wide-angle analyser by the end of 2014. Efforts then focused on the design and construction of the complex primary cooling facility for the coil system, a project conducted in parallel to the guide hall extension in order to improve synergies and cost.

Figure 3: *Overall final design of the **ThALES** cold neutron triple-axis spectrometer.*

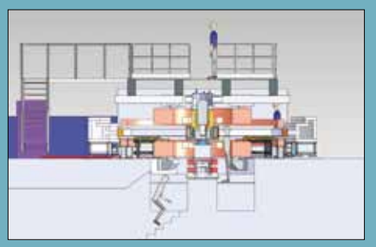

Figure 4: *3D model of **WASP**, showing the different accesses to the instrument's experimental areas.*

AUTHORS
C. Dewhurst, **A. Perillo-Marcone** and **M. Bonnaud** (ILL, on behalf of the project team)

New small-angle scattering instrument D33

Massive dynamic Q-range with a time-of-flight small-angle scattering instrument: D33

In 2004, the ILL management raised the possibility of constructing a third small-angle neutron scattering (SANS) instrument. It has been a long, and sometimes turbulent, ride but the winter shutdown 2011/2012 saw the build completion of D33, the so-called 'Massive dynamic Q-range time-of-flight SANS instrument'. D33 will be a relatively smaller 'younger brother' and operate in a different manner to the existing SANS instruments, D11 and D22. D33 forms part of a larger suite of projects including the extension of the ILL7 guide hall, the ambitious renewal of the H14 neutron guides and installation of new (D33, IN16), upgraded (IN12) or relocated (LADI, IN11) instruments. In this article, we describe the principal features of D33, and put them in context with its siblings.

TIME-OF-FLIGHT

'White' pulses of neutrons are shaped by a cascade of four choppers in the D33 casemate and wavelength discrimination is made by their arrival time (time-of-flight, TOF) at the detector. The advantage of using the TOF method is that a wide band of neutron wavelengths illuminate the sample and hence simultaneously sample a massive dynamic Q-range – or range of length scales - that characterises the material. D33 will use the 'optically blind' double-chopper system already employed at the ILL on the D17 and FIGARO reflectometers along with a velocity selector for D33's monochromatic mode. TOF techniques on a reactor source offer a significant advantage in efficiency and flexibility over spallation neutron sources as the chopper systems are able to tailor neutron pulses exactly to specification, thus optimising both resolution and frequency which ultimately translates to an optimised neutron flux on the sample and better data quality.

MULTIPLE DETECTORS

On D11 and D22 a single large area and position sensitive multi-detector sits in the evacuated detector tank at a variable distance from the sample depending on the Q-range, or length scale, of interest and typically covers a dynamic Q-range of about 10 for a single measurement, i.e. we can 'see' material structures from, for example, 10 Å to 100 Å, or 100 Å to 1000 Å (0.1µm), or 1000 Å (0.1µm) to 10000 Å (1µm) in a single measurement. Thus, in order to cover a sufficiently wide range of material length scales often two, three or even four individual measurements must be made and their data 'knitted together' in order to fully characterise a sample. D33 has two large multi-detectors consisting of a 'rear' square detector of 64 cm x 64 cm (128 x 128 pixels) and a 'front' detector made out of four individual panels of 16 cm x 64 cm (32 x 128 pixels) arranged horizontally and vertically to form a central aperture. D33's detectors are based on the new Monoblock technology developed by the ILL's detector group with much of the mechanics being machined in-house. Both front and rear detectors can move independently of each other within the detector tank to achieve various distances from the sample. The central aperture of the front detector can be adjusted either to match the solid angle of the rear detector or can be extended to extremes to maximise Q-range in D33's TOF mode.

LITTLE BROTHER

Optimisation of the 'pin-hole' resolution conditions for a SANS instrument requires careful consideration of the maximum sample size, neutron guide size and distances for a given instrumental resolution. In other words, SANS instruments are essentially infinitely scalable as long as the sample size can also be scaled. The overall size of D33 has been down-scaled based upon these principles where everything from guide size, collimation length, detector and tank size have all been down-sized to about 2/3 relative to an instrument such as D22. This gives resolution advantages when working in TOF mode as well as saving the cost and space involved in building much larger instruments. D33 is in fact better optimised for smaller samples up to 15 mm in dimension and is consistent with the scientific trend of, for example, forever faster kinetic measurements with smaller and smaller samples.

PERFORMANCE AND APPLICATION

There have been few compromises in the design and expected performance of D33. The newly re-built H14(2) guide which will provide neutrons to D33, should achieve similar neutron flux for a given resolution (brightness) as the existing D11 or D22 instruments. D33's monochromatic and TOF modes, in combination with the large and flexibly configured detector arrays, will achieve dynamic Q-ranges from about 30 in monochromatic mode to a *massive* 1000 in TOF mode and should have positive implications for studying kinetic processes where a large Q-range is required quickly and in a single measurement. The above features of D33 lend themselves usefully to the usual wide range of scientific problems studied using SANS from biology, soft matter, materials science, physics and magnetism. The latter will benefit from the day-1 implementation of polarisation and analysis techniques for additional neutron contrast in magnetic materials. Furthermore, the location of D33 is such as to permit the use of high magnetic fields, such as provided by the 17T horizontal solenoid magnet belonging to the University of Birmingham.

GET READY

The construction of D33 was completed during the winter shutdown 2011/2012. The first reactor cycle of 2012 will see the hardware commissioning of the instrument while the second cycle will be devoted to a scientific commissioning with 'friendly users' from all science domains. Are you a friendly user? Don't be scared to try something new. With D33 we aim to extend our possibilities in SANS with a particular emphasis on studies requiring a large simultaneous Q-range, polarisation and analysis, and extreme sample conditions. D33 is coming soon!

Figure 1: *The D33's detector tank (left), lying next to D11 in the newly extended ILL7 guide hall.*

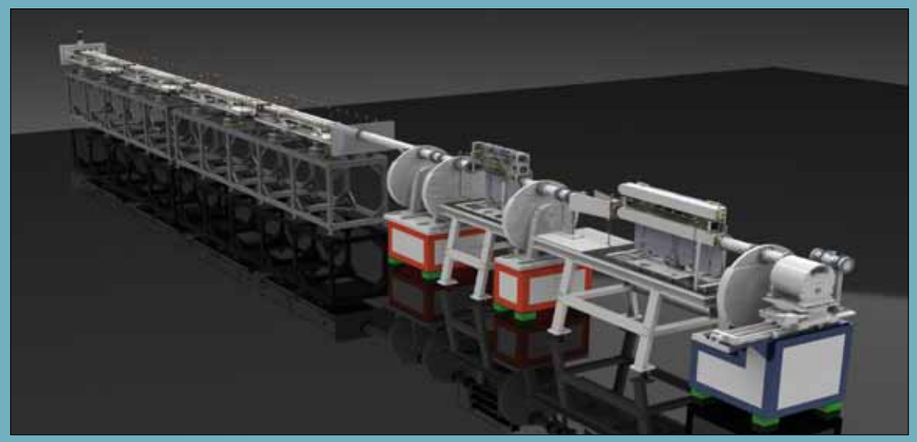

Figure 2: *Solidworks impression of the D33 casemate components and collimation housing showing optical components such as the velocity selector, choppers, polarisation components and wavelength filters.*

AUTHORS
B. Frick, **D. Bazzoli**, **T. Seydel** and **J. Combet** (on behalf of the IN16B team)

REFERENCES
[1] J. Schelten and B. Alefeld, Proc. Workshop on Neutron Scattering Instrumentation for SNQ, ed.: R. Scherm & H. Stiller, Jül-1954 (1984) 378
[2] M. Hennig, B. Frick and T. Seydel, J. Appl. Cryst. 44 (2011) 467

A big step forward for neutron backscattering: IN16B

New possibilities are about to open up for high energy resolution neutron spectroscopy at the ILL. Major visible steps were taken this year towards completing the new backscattering spectrometer IN16B. Built as part of the ILL Millennium Programme (phase M-1) and located at the end of the new ILL7 guide hall, IN16B will soon help scientists to better understand the dynamics of materials thanks to the very high energy resolution and count rate it is expected to achieve.

The study of very small energy exchanges between neutron and sample requires a well-defined incident neutron wavelength and an equally precise analysis of the scattered beam. In backscattering spectroscopy, neutrons are selected at the monochromator and analyser using perfect crystals (e.g. silicon wafers) under a Bragg angle of 90°, thus achieving a high energy resolution (better than 1 μeV). This means that the incident wavelength for spectroscopy can no longer be tuned by rocking the Bragg angle; the incident wave vector is scanned instead with a Doppler monochromator, which oscillates as fast as possible parallel to the neutron trajectory (on IN16B up to 4.7 m/s with an amplitude of ±25 or ±75 mm). The price to pay for such high energy resolution is a low count rate, a penalty which in backscattering can be partially compensated by an increased incident beam divergence.

New on IN16B is a Phase Space Transformation (PST) chopper [1], which promises an intensity gain of about 4 [2]. Neutrons are reflected from mosaic crystals moving at a speed of about 243 m/s, which transform the neutron energy to the range of interest, at the expense of an increased divergence. This divergent beam is then collected with the large spherical backscattering monochromator and is focused back towards the sample. The PST must be fed with neutrons of a wide wavelength band and of reasonably large divergence. This is ensured by a velocity selector and by ILL's longest neutron guide (source-sample distance about 130 m) focusing ballistically onto the PST.
The PST is the 'heart' of the instrument (**figure 1**) and technologically the most demanding and innovative component. A series of packages with fragile, tilted graphite crystals and neutron absorbers, arranged as two segments on the circumference of a chopper disc, have to withstand the high centrifugal forces. With its 43 cm radius, this will also be the world's most compact PST with the highest centrifugal force.

Figure 1: *Phase Space Transformation (PST) disc with dummy cassettes on the test drive.*

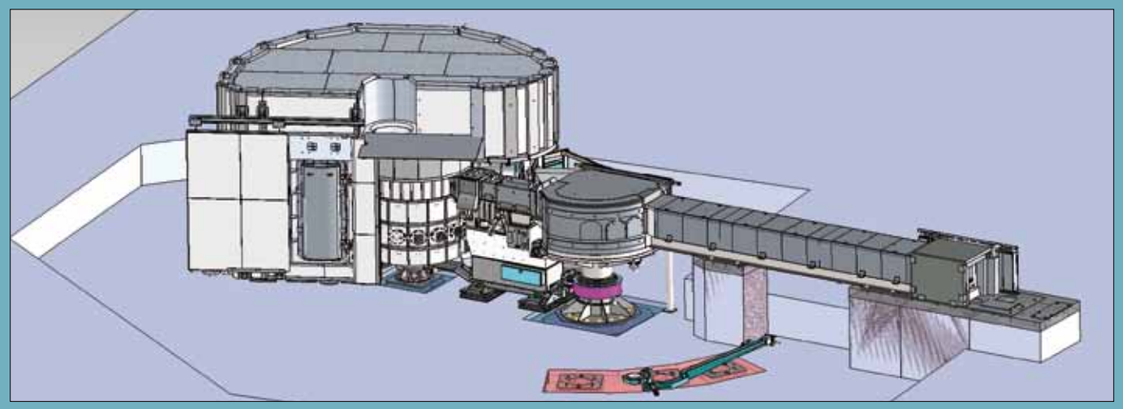

Figure 2: *CAD presentation of the new IN16B backscattering spectrometer.*

The high flux entering the instrument close to the detector needs efficient shielding and vacuum wherever possible to maintain a low background level. Furthermore the energy transfer range, limited today on IN16 by the narrow bandwidth of the graphite deflector, will be doubled by the combination of the PST and a linear motor Doppler drive. The huge vacuum vessel of the secondary spectrometer contains the PST and analysers, which are planned to be twice as high as the current IN16. A prototype of such an analyser is under construction. This also requires a new vertical position sensitive multi-detector and adapting the cryostat and furnace tails to the vertical space angle. Taken together, all these improvements promise to increase the count rate by a factor of 10 compared to the present IN16. Finally, flexibility has been built into the design to allow for a number of different instrument configurations: a low background side position configuration, possible operation with Si (311) crystals extending the Q-range to $Q_{max} \sim 3.7 Å^{-1}$, a GaAs test configuration with a possible 8-fold improvement in energy resolution, and an inverted time-of-flight option. This explains the large instrument site needed to rotate the whole vacuum chamber (4 m high, 35 tons), including the Doppler drive, around the PST position or to move it, together with part of the focusing guide, to the side position, where, as on IN16, the incident wavelength band is further limited by a deflector crystal.

At the time of writing, the radiological shielding (HDPE/B4C and cadmium) are being mounted and we have received delivery of the background chopper and selector together with their control electronics and those of the PST. Testing of the PST with a dummy disc is under way.

And when can we expect the first neutrons? This exciting event should take place after the winter shutdown in May 2012. In view of the complexity of the instrument, the commissioning, neutron tests and improvements will take some time. We hope to be able to accept a few 'friendly user experiments' in the second half of 2012 and then regularly schedule the Si (111) configuration as of the reactor restart in 2013.

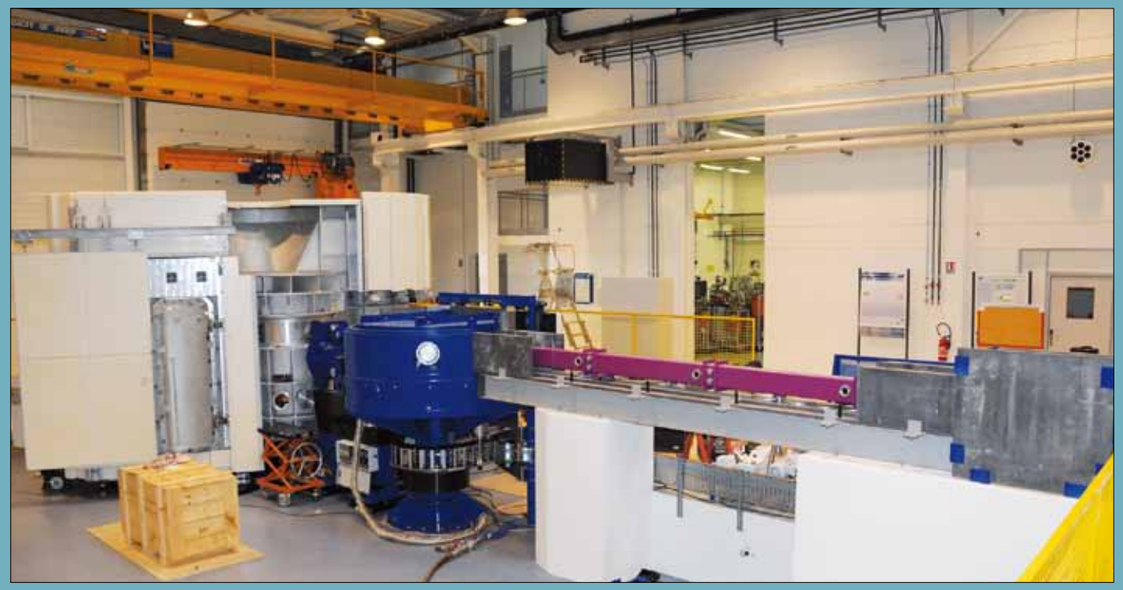

Figure 3: *Photo of the state of progress on the new IN16B spectrometer in March 2012.*

AUTHORS
A. Ivanov, S. Fuard and J. Kulda (ILL)

New spectrometer IN1-LAGRANGE

A powerful tool for exploring vibration dynamics in complex materials: IN1-LAGRANGE

The IN1-LAGRANGE spectrometer has been designed and built within the framework of the M-1 phase of the ILL Millennium Programme. The new instrument replaces the IN1 beryllium-filter (BeF) secondary spectrometer in order to offer ILL users increased possibilities for investigating atomic dynamics in complex molecular compounds.

The IN1-LAGRANGE project was launched at the ILL a few years ago with the aim of creating a new spectrometer for the study of lattice and molecular excitations in the extended energy range up to several hundred meV typical for materials containing light chemical elements, in particular hydrogen. The new instrument provides much higher sensitivity to small and low scattering samples through a substantially increased detector count rate combined with considerably improved energy resolution in comparison to the beryllium filter-analyser used in the past on IN1.

It is important to note that the new instrument takes advantage of the recently upgraded double-focussing monochromator, which - thanks to a set of several different reflecting planes - currently enables a more than two-fold increase in monochromatic flux in the high neutron energy range available from the ILL reactor's hot neutron source.

The IN1-LAGRANGE (**LA**rge **GR**aphite **AN**alyser for **G**enuine **E**xcitations) secondary spectrometer set-up (**figure 1**) is based on the space focussing of neutrons scattered by the sample in a very large solid angle and then registered with a relatively small single counter (a ^{3}He gas detector). The focussing reflecting surface of about 1 m^2 is built around the vertical sample-detector axis from pyrolytic graphite crystals set to reflect neutrons with the fixed average energy of 4.5 meV. The appropriately shaped cooled beryllium filter is installed right after the sample in order to remove higher-order harmonics in the analyser reflections. It is important to note that the accepted solid angle of about 2.5 steradian is among the highest solid angles of the most ambitious instrument projects today. At the same time, it is achieved in a relatively small spectrometer volume. The instrument background, contaminated with the high neutron energy components, is reduced thanks to massive polyethylene shielding built around the whole analyser. There are no mutually moving parts within the secondary spectrometer, which moves around the monochromator in a step-by-step fashion in order to change the incident energy, in a similar way to a typical experiment on a three-axis spectrometer.

The instrument was designed at the ILL thanks to in-house scientific and technical input. The detailed design and fabrication of the main mechanical components were performed by the Spanish company Tekniker. The work was financed in approximately equal shares by the ILL Millennium budget and a dedicated Spanish contribution to the ILL. Part of the project budget was also provided in the form of an "in kind" contribution from the Spanish partners.

An example of the inelastic scattering spectrum measured with IN1-LAGRANGE is presented in **figure 2**. We used a sample of 2.5-diiodothiophene, $(CH)_2(CI)_2S$, to characterise the instrument performance. This material is known to exhibit very sharp vibration lines at low temperatures and can therefore be used as a standard for spectrometer resolution measurements. The sharp peaks in the energy spectrum visible in **figure 2** are due to vibrations involving hydrogen atoms, present in the sample in a relatively small quantity: 6 mg of the partial hydrogen weight. It should be noted that the statistics collected in the energy interval below 200 meV, left panel of **figure 2**, correspond to some 12-30 seconds of the measurement time per point (the difference is due to the energy variation of the incident monochromatic neutron flux). As a result, this informative energy interval could be scanned in less than 2 hours whereas the scan time for the whole of the spectrum shown, up to 600 meV, is about 4 hours.
In comparison with the IN1-BeF configuration, we note a considerable improvement in energy resolution and approximately one order of magnitude increase in the inelastic signal with respect to the beryllium filter-analyser, as shown in **figure 3**. In the energy range below 150 meV, the energy resolution of IN1-LAGRANGE is noticeably better than that of IN1-BeF, allowing it to reveal fine details of the spectrum, for instance the observed energy splitting of the lowest vibration line.
The energy resolution of IN1-LAGRANGE can be further improved in the broad energy range by using the available Cu(331) reflecting plane of the IN1 monochromator. Many more fine details of the vibration density of states are revealed in the higher resolution run at the expense of merely an approximate 2-fold decrease in the statistics for the same counting time. The measured energy resolution is presented in **figure 4**, together with the calculated curves for several analyser and monochromator configurations. It should be emphasised that the changeover from one resolution setting to another can be done on IN1-LAGRANGE in about half an hour, giving users extremely flexible conditions for optimising their measurements with respect to the choice of resolution vs intensity.

The IN1-LAGRANGE spectrometer opens up outstanding possibilities for spectroscopic studies of complex materials. The new instrument makes it possible to investigate much smaller samples, inherent in novel materials studies, to record well-resolved vibration spectra, and to probe in greater detail external parameters, such as temperature, pressure, and chemical composition. As a result, this spectrometer is highly competitive compared with the instruments for high-energy neutron spectroscopy found elsewhere.

Figure 1: *Cross-section view of the LAGRANGE set-up* ***(a)****, positioning of graphite crystals on the analyser frame* ***(b)****, and completed spectrometer* ***(c)*** *ready for first neutron tests.*

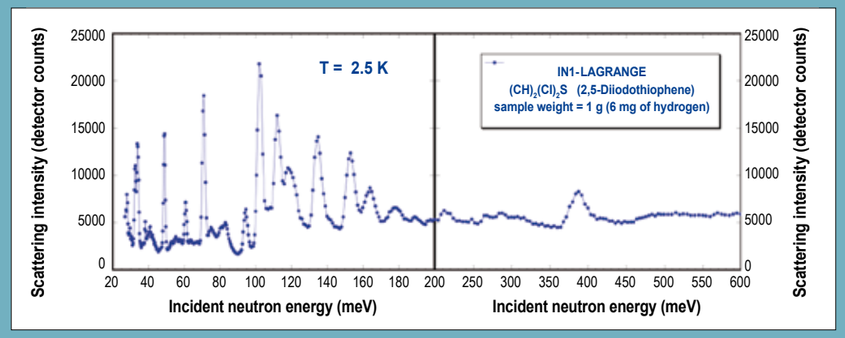

Figure 2: *Inelastic scattering spectrum recorded with the LAGRANGE analyser (note the different energy scale on the two panels) from a 2.5-diiodotiophene sample at 2.5K. The measurements were performed in a "fixed-monitor" regime with the 2D-focussing Cu(220) monochromator face. The intensity is as-measured, without any further treatment; no background (cryostat and sample holder) is subtracted.*

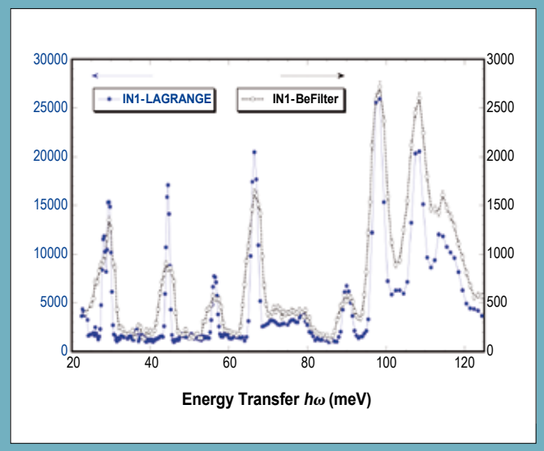

Figure 3: *Low-energy fragment of the energy dependence of the inelastic scattering intensity from the same sample as in figure 2, measured with the IN1-LAGRANGE and IN1-BeF analysers. The measurement time per point is the same for both spectra. The cryostat background is subtracted. Note the 10-fold difference in the intensity scale. This intensity gain factor for IN1-LAGRANGE is also observed in the high-energy part of the spectrum not presented here.*

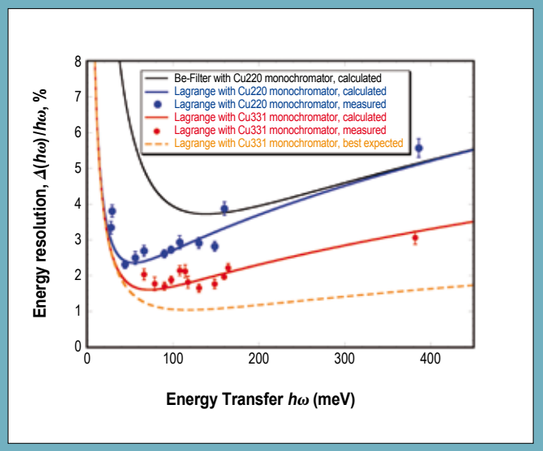

Figure 4: *Calculated (lines) and measured (points) relative energy resolution of IN1-LAGRANGE with different primary spectrometer settings. The points are the peak widths divided by the peak energies, as measured in the corresponding conditions with the 2.5-diiodothiophene sample. The lowest broken line represents the anticipated resolution of IN1-LAGRANGE once the future collimator changer has been installed in front of the monochromator.*

AUTHORS
R. Cubitt, **R. Schweins** and **P. Lindner** (ILL)

REFERENCES
[1] D.W. Schaefer and M.A. Agamalian, Current Opinion in Solid State and Materials Science 8 (2004) 39–47
[2] E.M. Forgan and R. Cubitt, Neutron News, V9 N4 (1998) 25-31
[3] R. Cubitt, R Schweins and P. Lindner, Nuclear Instruments and Methods in Physics Research A 665 (2011) 7–10

Countering the effects of gravity

Small-angle neutron scattering (SANS) is a powerful technique for determining chemical, biological and hard matter structures of materials over a wide range of length-scales. There is a wide range of research using neutron scattering to probe structures in the micron range. This varies from the fractal nature of rocks to self organised polymer structures [1]. The larger the structure the smaller the scattering angles and the longer the collimation and detector distances need to be. In addition, in order to determine the structure of materials in the micron range long neutron wavelengths are required. The combination of the slow speed of long wavelength neutrons coupled with the large distances of the instrument result in a significant displacement of the beam with gravity. This can affect the neutron flux available, the resolution, the completeness of the signal on the detector and hence the largest length-scales that can be measured. We tested a new method for countering the effects of gravity.

Previous ideas of cancelling the effects of gravity have used prisms [2] but this approach has problems working over the full height associated with typical sample sizes. Here we describe a different method, recently published [3], using simple mirrors that can be exploited using existing components of SANS instruments and results in reducing the minimum momentum transfer by a factor of 5.

The problem can be thought of as trying to throw a ball through two holes some distance apart and then hitting a target even further away as shown in **figure 1**. The slower the ball is thrown the larger the angle we have to throw it above a line between the centre of the holes. If there is a limit in the height the ball is allowed to be in between the holes, there is lower limit on the speed it can be thrown. In addition, depending on the size of the target, if the ball makes it through the second hole it still might miss the target as it can fall past the bottom. A SANS machine has exactly this problem where the two holes are the collimation and the target is the neutron detector. This places a limit on the largest object we can measure purely due to the effects of gravity. When we use the largest distances available on D11 (40.5 + 39 m), the longest SANS instrument in the world, we find that we cannot properly use neutrons traveling slower than 200 m/s which corresponds to a wavelength of about 20 Å or 2 nm.

In the past it has been found that these effects of gravity can be canceled using a prism which gives the neutrons a kick upwards allowing them to arrive at the centre of the detector but this only worked with beam sizes much smaller than we wish to use. We realised that a simple mirror near the second hole at the end of the collimation can do the same job as the prism but it will work with a much larger beam. Going back to the ball analogy: if there was a horizontal surface just before the second hole and below the centre line we don't need to aim the ball so high through the first hole to hit the surface as shown in **figure 2**.
The ball can then bounce off the surface and come out of the second hole rising not falling. Then it has a better chance of hitting the target. Neutrons bounce very well off well polished surfaces like glass and this is used in neutron guides all over the ILL to send neutron beams long distances rather like fiber optic cables that transmit light.

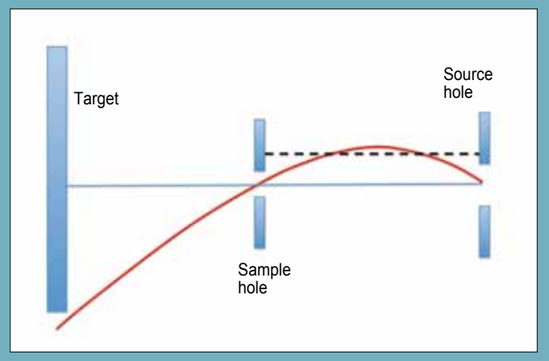

Figure 1: *Throwing a ball through two holes from right to left in order to strike a target.*

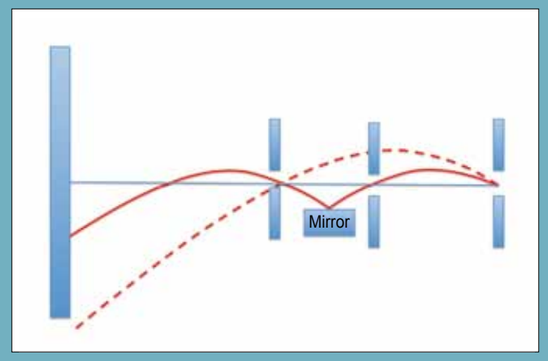

Figure 2: *By bouncing off a mirror we can reduce the maximum height between the holes and also hit the target/detector. The extra aperture ahead of the mirror was needed to block the original beam passing through the system.*

Before spending money on a special neutron mirror we realised that we could use the mirror on the bottom of one of these guides which already exists in the collimation section of D11. Normally when measuring the largest objects all these guide pieces are removed but we put one piece back and allowed the beam to fall naturally onto the bottom mirror and bounce up through the second hole. We found that this only happened for one special wavelength of 18.7 Å as shown in **figure 3**.
As the goal was to find longer wavelengths than 20 Å this was initially disappointing but we found that if we moved the second hole upwards by about 1cm we could get 23 Å to pass through at 1000 x the intensity before (this was because of the height limit in the collimation absorbing neutrons). Longer wavelengths than 23 Å were not possible without modifying the instrument. By reducing the size of the first hole to 1 cm and using three neutron lenses we now had a configuration where we could measure objects many times larger than previously possible. To test this we placed a grating in the beam which had a period of 4 microns, a length-scale not previously visible on D11 and we could clearly see peaks of neutron intensity associated directly with the repeating 4 micron structure (**figure 4**).

In conclusion we have made a significant improvement to the range of science that can be done on D11 by countering the effects of gravity. This resulted in a gain of 1000 x in intensity at 23 Å, took less than a day beamtime to accomplish at zero cost.

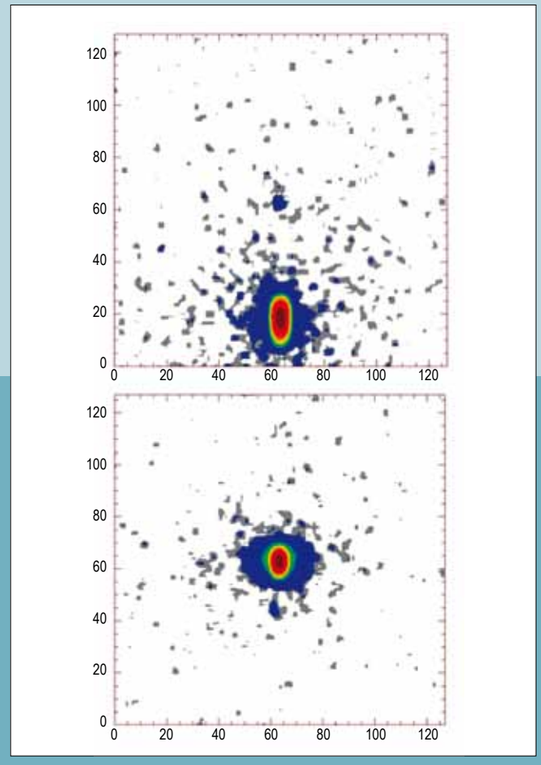

Figure 3: *The picture on the top shows 18.7 Å in the normal situation at the longest distances available on D11 and the picture on the bottom is with using the mirror. We can see that the beam is nearly in the centre of the detector and less spread vertically.*

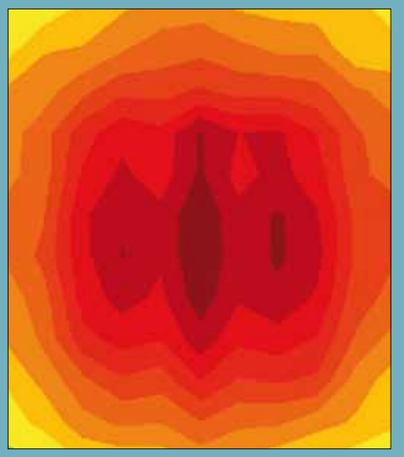

Figure 4: *Peaks on the detector either side of the main beam are scattering from a 4 micron repeating structure.*

AUTHORS
C.L. Bull, **M. Guthrie**, **K. Komatsu**, **H. Hamidov**, **C. Wilson**, **J.S. Loveday** and **R.J. Nelmes** (University of Edinburgh, UK)
M.T. Fernandez-Diaz and **J. Archer** (ILL)

REFERENCES
[1] R.J. Nelmes, Z. Tun and W.F. Kuhs, Ferroelectrics, 71 (1987) 125
[2] C.L. Bull, M. Guthrie, J. Archer, M.T. Fernandez-Diaz, J.S. Loveday, K. Komatsu, H. Hamidov and R.J. Nelmes, Journal of Applied Crystallography, 44 (2011) 831
[3] S. Klotz, G. Hamel and J. Frelat, High Pressure Research 24 (2004) 219
[4] Y. Moritomo, S. Koshihara and Y. Tokura, Journal of Chemical Physics, 93 (1990) 5429

High-pressure single crystal diffraction to 10 GPa and above

High pressure produces dramatic changes in matter, such as the numerous different crystal structures in ice to 2 GPa (20 000 atmospheres). Measuring the positions of atoms in high-pressure structures can provide fundamental insights into materials and their properties, including for practical applications like the storage of hydrogen in hydrogen hydrate. Single-crystal neutron diffraction is a powerful method for determining atomic positions in structures, and we present developments that extend the pressure range for such studies on D9 to 10 GPa, with the prospect of reaching 20 GPa in future.

High pressure can cause large changes in the crystal structure and properties of materials, which can provide both fundamental understanding and insight into practical applications. Many interesting and useful materials - ice for example - are held together by hydrogen bonds. There is widespread interest in the relationship between hydrogen bond strengths and the precise geometry of the bonds, ranging from theoretical physics and chemistry where the interest is in the behaviour of the proton as a quantum object, through planetary science where proton conducting ices may play a role in planetary magnetic fields, and onto biology where proton exchange reactions are important living processes. The application of pressure allows a hydrogen bond length to be altered cleanly and continuously within the same material. Neutron single-crystal diffraction is an ideal technique to explore such evolution because of its ability to resolve complex multi-site disorder and determine anisotropic atomic displacement parameters (ADPs) accurately. High-resolution studies of H-bonded systems were among the science-drivers behind the development of D9 which exploits ILL's hot source to provide a unique facility for high resolution crystallography [1].

Until recently, single-crystal neutron diffraction was limited to about 2 GPa because of the difficulty in compressing a sample of suitable volume (1-5 mm^3) to higher pressures, and the complications of rotating a large pressure cell and providing entry and exit windows for the neutron beam. The Paris-Edinburgh press is able to take suitable volumes of powder samples to pressures of up to over 25 GPa [2]. We have now adapted this type of press for single-crystal studies on D9 and have performed structural studies of the hydrogen bonded ferroelectric squaric acid to 10 GPa [3].

We devised a suitable gasket which provides a mount for the single crystal to maintain its orientation as the pressure is increased. This also holds a pressure-transmitting fluid around the crystal to provide hydrostatic conditions and prevent the crystal from being crushed on compression. We built a mount to place a 60 kg VX3 Paris-Edinburgh press [4] on D9 (**figure 1**) and developed procedures to place the sample (which cannot be viewed directly once inside the cell) accurately at the instrument centre. We also developed suitable collimation to reduce the parasitic scattering by the pressure-cell materials so as to optimise signal-to-background. This enhances the quality of the data and allows us to observe weak peaks. In particular, it makes it possible to exploit the unique power of D9 to collect data at wavelengths down to 0.33 Å, and thereby reduce the limitations on coverage of reciprocal space caused by the restricted apertures of the pressure-cell openings [3].

This approach has allowed us to collect data out to a resolution of $\sin(\theta)/\lambda = 1.5\,Å^{-1}$ and to refine these data using a full anisotropic model. **Figure 2** shows the pressure evolution of the ADP's of the H and O atoms in the hydrogen bonds, depicted as 63% probability surfaces. Squaric acid's structure consists of layered H-bonded molecules. At pressures below 3.5 GPa, the hydrogen bonds are two-site disordered and are presumed to fluctuate between asymmetric O-H...O and O...H-O configurations. While diffraction studies observe the time average O-H...H-O configuration, Raman studies sense the instantaneous O-H...O (or O...H-O) configurations. At 3.5 GPa, the Raman modes which correspond to the asymmetric H-bond configuration disappear and Raman senses a symmetric O..H..O configuration [2]. However, our diffraction data reveal that the hydrogen ADP almost certainly remains two-sited at 3.5 GPa and that it is still highly elongated even at 10 GPa, not the quasi-isotropic form expected for a well-centred single proton (**figure 2**). It thus appears that H-bond centring is a complex and gradual process.

This result demonstrates the capabilities of marrying modern high-pressure equipment with the unique capabilities of D9 and represents a major first step towards further developments. We have successfully tested methods to load low boiling point gases as pressure media, which will allow us to extend the pressure range further to 20 GPa and perhaps beyond. We have also devised a means to rotate the anvils of the cell while under load which increases the access to reciprocal space. Finally, we are developing *in situ* growth of samples loaded as liquids, which will increase the range of science open to single-crystal techniques; **figure 3** shows a crystal of ammonia hemihydrate (AHH) grown at pressure inside a diamond-anvil cell, from which a full neutron data set has been collected.

Figure 1: *VX3 Paris-Edinburgh press mounted on the omega table of the D9 instrument.*

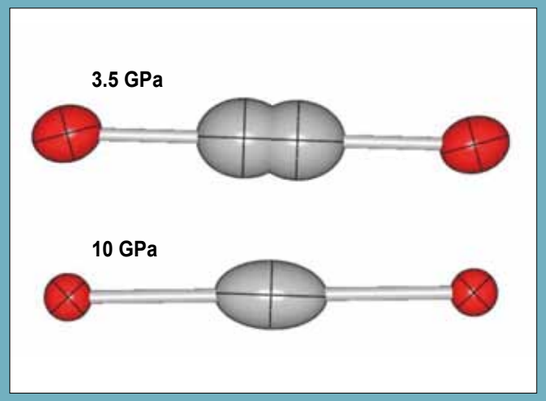

Figure 2: *Pressure evolution of hydrogen bond in squaric acid from 3.5 to 10 GPa. 63% probability surfaces are shown depicting the ADPs of the hydrogen (shown grey) and oxygen (shown red) atoms.*

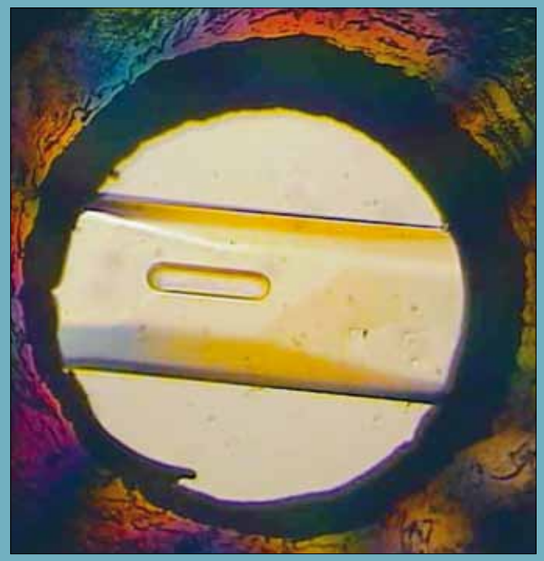

Figure 3:
A single crystal of AHH grown at high pressure, viewed through one of the diamond anvils of the pressure cells. The gasket hole has a diameter of 0.8 mm and a thickness of 0.3 mm.

AUTHORS
S.N. Ivanov, **K. Leung**, **F. Martin**, **F. Rosenau**, **M. Simson** and **O. Zimmer** (ILL)
F.M. Piegsa (ETH Zürich, Switzerland)

REFERENCES
[1] R. Golub, and J.M. Pendlebury, Phys. Lett. A 53 (1975) 133
[2] O. Zimmer, K. Baumann, M. Fertl, *et al.*, Phys. Rev. Lett. 99 (2007) 104801; O. Zimmer, P. Schmidt-Wellenburg, M. Fertl, *et al.*, Eur. Phys. J. C 67 (2010) 589
[3] A.I. Kilvington, R. Golub, W. Mampe, and P. Ageron, Phys. Lett. A 125 (1987) 416
[4] O. Zimmer, F.M. Piegsa, and S.N. Ivanov, Phys. Rev. Lett. 107 (2011) 134801

Ultracold neutrons from superfluid helium

Ultracold neutrons (UCNs) play an important role in addressing fundamental questions in particle physics. Due to counting statistical limitations, experiments often last one or sometimes even several reactor cycles, hence the need for a new generation of UCN sources. While the ILL's turbine UCN source PF2 has for the past 25 years been delivering the highest UCN fluxes in the world, a superior UCN density has recently been achieved based on the conversion of cold neutrons in superfluid helium-4.

Cold neutrons with a wavelength of 0.89 nm passing through a converter of superfluid helium may lose nearly all their energy in single scattering events and thus become ultracold. This produces elementary excitations ("phonons") with an energy of 1 meV (about 12 K) in the helium, which are cooled away by a refrigerator. At temperatures below 1 K, inelastic scattering of UCNs back to higher energies is strongly suppressed due to the Boltzmann factor. Since helium-4 has no nuclear absorption, and if it is contained in a vessel able to store UCNs for a long time, a high density of UCNs can build up prior to their extraction to an experiment.

This principle and its potential to generate unprecedented UCN densities have been known for at least 35 years [1]. Recent experiments in Munich [2] have shown it is possible to extract UCNs accumulated in the superfluid efficiently, using a cold UCN valve combined with a short section of vertical UCN guide (**figure 1**).

This avoids the need for the loss-prone windows through which UCNs had to pass in an earlier scheme using horizontal UCN extraction [3].

The method has since been further developed in the framework of the ESFRI project ILL 20/20 Upgrade. With the ultimate goal of making UCN production in superfluid helium amenable to users, ILL teams have designed and installed the new beam line H172. An intercalated graphite monochromator diverts the 0.89 nm component of the incident cold beam with an 80×80 mm^2 cross section into the secondary neutron guide H172A, at which an upgrade of the source prototype from Munich has been installed. First tests of this source, known as "SUN-1", were performed in a configuration typical for a user experiment [4], in this case simply a UCN detector at room temperature (**figure 2**). A converter with a volume of 5 litres cooled down to a temperature of 0.7 K by a helium-3 evaporation stage through a heat exchanger was exposed to the beam. **Figure 3** shows the UCN count rate as a function of time in a single UCN accumulation/extraction run. In demonstrating a superior UCN density of 55 per cm^3, these experiments constitute a milestone towards a "next generation" UCN source.

However, there is still plenty of room to improve both beam and source parameters. For instance, the UCN storage time constant, to which the saturated UCN density is proportional, was only in the order of one minute in the reported experiments. In order to perform the necessary R&D work, a new UCN source cryostat "SUN-2" has been developed in the last few years. Besides increased cooling power, it offers greater flexibility than SUN-1 for testing various types of converter vessels. A second beam position H172B is under construction where experiments with SUN-2 will be performed to bring UCN production in superfluid helium to maturity.

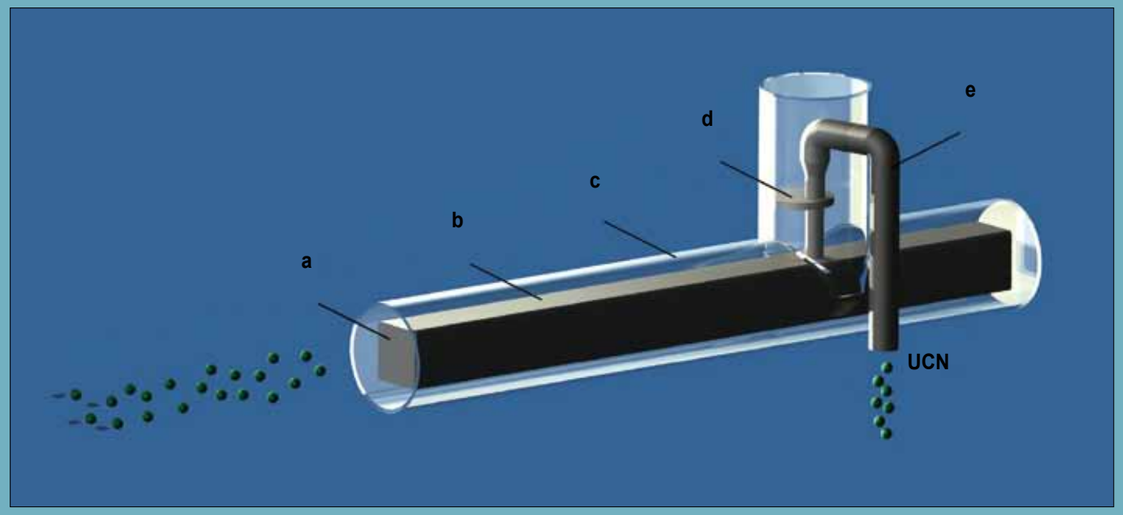

Figure 1: *Schematics of the apparatus [4].* ***a)*** *Beryllium entrance window for cold beam coming from left.* ***b)*** *UCN converter vessel made of BeO, filled with superfluid helium.* ***c)*** *Thermal shield (not shown are an outer shield and the vessel for the isolation vacuum).* ***d)*** *UCN valve.* ***e)*** *UCN extraction guide towards a detector at room temperature (not shown).*

Figure 2: *Set-up of the UCN source "SUN-1" at H172A. The cryostat containing the helium converter is situated inside a lead castle. Shown is the set-up with sideward UCN extraction as used in the experiments reported in [4]. The clean room in the background houses the gravitational spectrometer GRANIT under construction.*

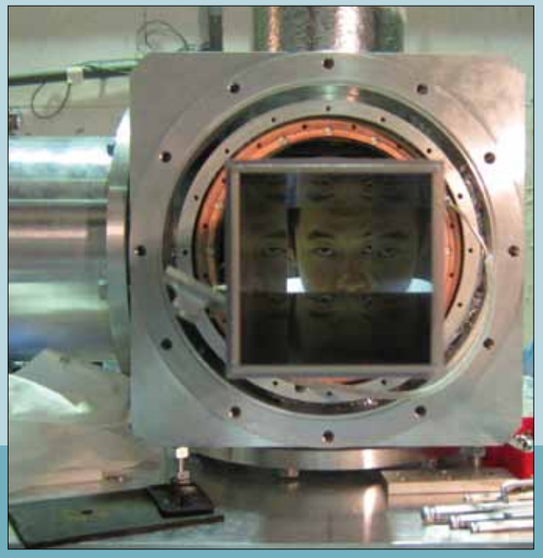

Figure 4: *Inspection of a converter vessel in SUN-2.*

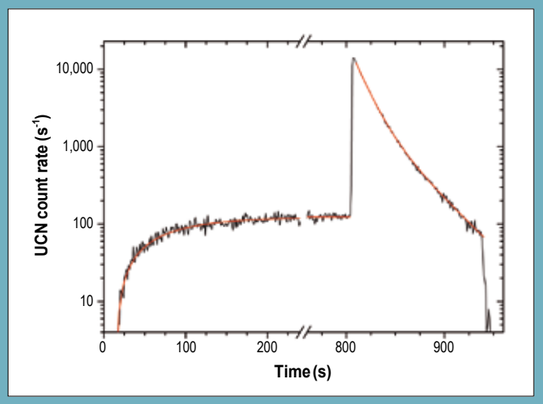

Figure 3: *UCN count rate as a function of time in a UCN accumulation/extraction experiment [4]. The UCN valve stayed closed during about 800 s of irradiation with the cold beam. Leakage of UCN through the closed UCN valve monitors the build-up of the UCN density in the converter. Then the beam was shut and the UCN valve opened. The peak on the right shows the extraction of 274 000 UCNs.*

EXPERIMENTAL AND USER PROGRAMME

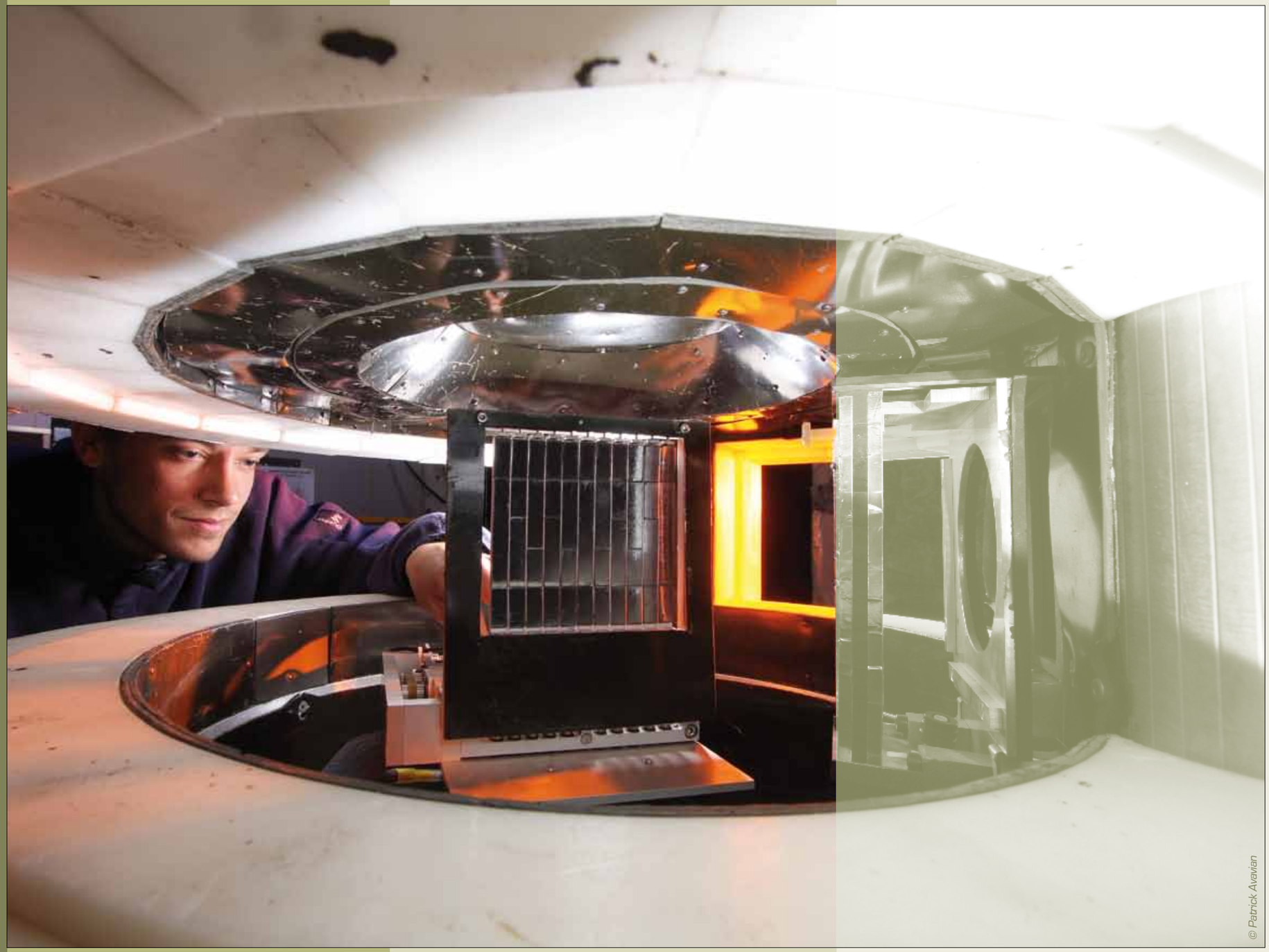

© Patrick Avavian

USER PROGRAMME
BEAMTIME STATISTICS
INSTRUMENT LIST

The ILL User Support team is dedicated to helping all visiting researchers to make the most of its facilities. If you are coming to the ILL to carry out experiments, the User Office is here to give you the organisational and administrative support you need to successfully perform your experiments.

Neutron beams and instrument facilities are free of charge for proposers of accepted experiments. Scientists affiliated to the Institute's member countries will also, in general, be assisted with necessary travel and daily subsistence for a limited period. The User Support Team makes all arrangements for accommodation and will process claims for expenses after you have completed your experiment.

If you would like more information about the Institute's facilities, application for beamtime, user support and experimental programme, please visit our web-site:

http://www.ill.eu/users

AUTHORS
G. Cicognani (ILL)

User programme

THE ILL VISITORS CLUB

All administrative tools for our scientific visitors are grouped together and directly accessible on the web, thanks to the Visitors Club. All information is presented in a user-friendly environment. After having logged in with your own personal identification[1], you will have direct access to all the available information which concerns you. Users with particular responsibilities have privileged access to other tools, according to their role. The ILL Visitors Club includes the electronic proposal and experimental reports submission procedures, and electronic peer review of proposals. Additional electronic services have also been put in place: acknowledgement of proposals, subcommittee results, invitation letters, user satisfaction forms and so on.

PROPOSAL SUBMISSION

There are different ways of submitting a proposal to the ILL:

- Standard submission - twice a year - via the Electronic Proposal System (EPS)
- Long-Term Proposals - once a year - via the Electronic Proposal System (EPS)
- EASY access system (EASY) throughout the year
- Director's Discretion Time (DDT) throughout the year
- Special access for proprietary research and industrial users

Submission of a standard research proposal

Applications for beamtime should be submitted electronically, via our Electronic Proposal Submission system (EPS), available on the Visitors Club web-site. Proposals can be submitted to the ILL twice a year, usually in February and in September. The web system is activated two months before each deadline. Submitted proposals are divided amongst the different colleges (***see box below***) according to their main subject area.

The ILL scientific life is organised into 10 colleges:

College 1	Applied Metallurgy, Instrumentation and Techniques
College 2	Theory
College 3	Nuclear and Particle Physics
College 4	Magnetic Excitations
College 5A	Crystallography
College 5B	Magnetic Structures
College 6	Structure and Dynamics of Liquids and Glasses
College 7	Spectroscopy in Solid State Physics and Chemistry
College 8	Structure and Dynamics of Biological Systems
College 9	Structure and Dynamics of Soft-condensed Matter

(1) If you are not yet registered in the Visitors Club and you wish to join it, you can register directly at http://club.ill.eu/cv/

Proposals are judged by a Peer Review Committee of the Subcommittees of the ILL Scientific Council. Subcommittee members are specialists in relevant areas of each College and they evaluate the proposals for scientific merit and recommend to the ILL Management the award of beamtime to the highest-priority proposals.
Before the meeting, the subcommittee receives a report on the technical feasibility and safety of a proposed experiment from the appropriate College at the ILL. Two proposal review rounds are held each year, approximately eight weeks after the deadline for submission of applications.

There are normally 4 reactor cycles a year, each of which lasts 50 days. Accepted proposals submitted by February will receive beamtime in the second half of the year and those submitted by September, in the first half of the following year. More detailed information on application for beamtime and deadlines is given on our website at
http://www.ill.eu/users/applying-for-beamtime/

Easy Access System

The Easy Access System (EASY) grants diffraction beamtime to scientists from ILL member countries, who need a rapid structural characterisation of samples and data analysis. Access is open all year long, and it does not go through the ILL standard proposal round and consequent peer review system.
The system offers one neutron day per cycle, on five instruments (D1A, D2B, D16, VIVALDI and OrientExpress) to perform very short experiments at room temperature. The users will not be invited to the ILL, but will send their samples to one of two designated ILL scientists, who will be responsible for the measurements and sample radiological control. The ILL will ship back the sample once the measurement is finished. You can apply for EASY beamtime on the Visitors Club. More information is available at ***http://club.ill.eu/cvDocs/EASY_Guidelines.pdf***

Long-Term Proposals

Users from ILL member countries can also apply for extended periods of beamtime, by submitting a Long-Term Proposal (LTP). Its purpose is to facilitate the development of instrumentation, techniques or software - which could be beneficial to the ILL community as a whole - through the award of beamtime over several cycles. The total amount of beamtime that may be allocated to LTPs on any particular instrument is capped at 10%, and beamtime is not awarded to LTPs to perform science beyond essential testing.
LTPs can be submitted once a year at the autumn proposal round using the specific LTP application form. The primary criterion for acceptance of a LTP is the excellence of the science that it will ultimately enable. The length of LTP projects is expected to be 3 years typically, with continuation approved at the end of each year, based on an annual report; a final report is also required at the end of the project. More details are given at
http://www.ill.eu/users/applying-for-beamtime/

Submission of a proposal to the Director's Discretion Time

This option allows a researcher to obtain beamtime quickly, without going through the peer-review procedure. DDT is normally used for 'hot' topics, new ideas, feasibility tests and to encourage new users. Applications for Director's Discretion Time can be submitted to the Head of the Science Division, Prof. Helmut Schober, at any time.

Access for proprietary research and industrial users

The ILL's mission is to provide neutrons for both public and industrial research. In November 2010 we appointed a business development officer who is charged with communicating more widely the services we can offer to the industry. He will also facilitate and coordinate centrally industrial R&D at the ILL, in particular access to the ILL's scientific expertise and instrument suite. He will work closely with the ILL "Industrial Liaison and Consultancy Group" (ILC) to assess the feasibility of the experiments and the quotation of the services.The ILC Group is composed of scientists with considerable experience and expertise in neutron techniques applied to industrial R&D; it ensures rapid access and total confidentiality for industrial companies, and provides specialised technical and scientific support. To apply for proprietary beamtime, please contact the Business Development Office at ***industry@ill.eu*** or by phone at +33(0)4 76 20 72 01 or consult the web site under ***http://www.ill.eu/industry/***

Experimental reports

Users are asked to complete an experimental report on the outcome of their experiments. The submission of an experimental report is compulsory for every user who is granted ILL beamtime. Failure to do so may lead to rejection in case of application for beamtime for a continuation proposal. All ILL experimental reports are archived electronically and searchable via the web server as PDF files (under ***http://club.ill.eu/cv/***). Experimental reports for experiments performed in 2011 are included in the CD-ROM of this year's Annual Report.

COLLABORATIVE RESEARCH GROUP INSTRUMENTS

The ILL provides a framework in which Collaborating Research Groups (CRGs) can build and manage instruments at the ILL to carry out their own research programmes. CRGs represent a particularly successful form of long-term international scientific collaboration. They are composed of scientists from one or two research disciplines, and often multinational, carrying out a joint research programme centred around a specific instrument. CRGs enjoy exclusive access to these instruments for at least half of the beamtime available. The CRGs provide their own scientific and technical support and cover the general operating costs of these instruments. If there is demand from the user community and the resources are available, the beamtime reserved for ILL can be made accessible to users via the subcommittees.
There are currently three different categories of CRG instruments:

- **CRG-A** in which the external group leases an instrument owned by the ILL. They have 50% of the beamtime at their disposal and for the remaining 50% they support ILL's scientific user programme.
- The **CRG-B** category owns their instrument and retains 70% of the available beamtime, supporting the ILL programme for the other 30%.
- Finally, **CRG-C** instruments are used full time for specific research programmes by the external group, which has exclusive use of the beam.

SUPPORT LABORATORIES

The opportunities we offer to our users extend beyond the privileges of access to the world's leading suite of neutron instruments. The ILL - in collaboration with the ESRF and other institutes - is actively responding to the needs of scientists unfamiliar with neutron techniques and in need of training and support facilities. New support facilities have been already set up on the ILL site. For more information see the chapter "More than simply neutrons", p.106.

User and beamtime statistics

THE ILL USER COMMUNITY

The ILL welcomed 1557 users in 2011, including 374 from France, 288 from Germany and 300 from the UK (**figure 1**). Many of our visitors were received more than once (for a total of 2570 user visits).

We value feedback from our users as an indicator of how well our facility is fulfilling their needs and to initiate actions when this is not the case (**see figure 2**).
The ***User Satisfaction Form*** is a means of finding out what our users think of the facility. Users who have just finished an experiment at the ILL are asked to complete the questionnaire on the Visitors Club and give us their views on different topics. User comments are made available to managers for their information and actions when appropriate.

INSTRUMENTS

The instrumental facilities at the ILL are shown in the schematic diagram on page 98. The list of instruments as of December 2011 is summarised on page 97. Besides the 28 ILL instruments, there are 9 CRG-instruments (*marked with an asterisk* *):

- Powder diffractometers: D1B*, D2B, D20, SALSA
- Liquids diffractometer: D4
- Polarised neutron diffractometers: D3, D23*
- Single-crystal diffractometers: D9, D10
- Large scale structures diffractometers: D19, LADI, VIVALDI
- Small-angle scattering diffractometers: D11, D22
- Low momentum-transfer diffractometer: D16
- Reflectometers: SuperADAM*, D17, FIGARO
- Diffuse scattering and polarisation analysis spectrometer: D7
- Three-axis spectrometers: IN1, IN8, IN12*, IN14, IN20, IN22*
- Time-of-flight spectrometers: BRISP*, IN4, IN5, IN6,
- Backscattering and spin-echo spectrometers: IN10, IN11, IN13*, IN15, IN16
- Nuclear physics instruments: PN1, PN3
- Fundamental physics instruments: PF1, PF2, S18*

LADI and IN15 have a special status, since they are joint ventures of the ILL with other laboratories: in the case of LADI with EMBL and for IN15 with FZ Jülich and HZB Berlin. Cryo-EDM is a CRG-C instrument and is not available as a 'user' instrument. Details of the instruments can be found on the web at ***http://www.ill.eu/instruments-support/instruments-groups/.***

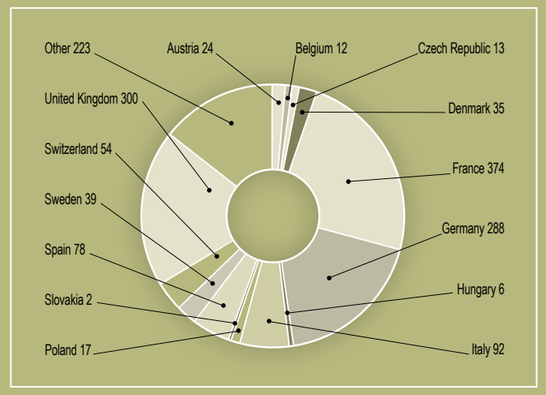

Figure 1: *National affiliation of ILL users in 2011.*

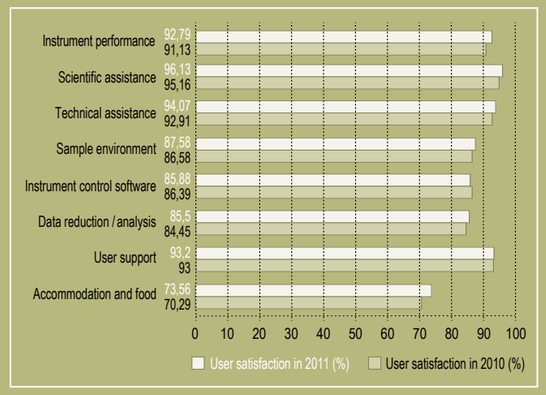

Figure 2: *User satisfaction survey results for 2011, compared with those obtained in 2010.*

BEAMTIME ALLOCATION AND UTILISATION FOR 2011

Overall, the Subcommittees of the Scientific Council (November 2010 and April 2011) examined 1370 proposals requesting 8945 days for 2011, out of which 767 proposals received beamtime, allocating 4082 days of beamtime on the different instruments. The distribution of accepted proposals amongst the different research areas and colleges is given in **figure 3**.

In 2011, the member countries of the ILL were: France, Germany, UK, Austria, Belgium, the Czech Republic, Denmark, Hungary, Italy, Poland, Slovakia, Spain, Sweden, Switzerland and India, which joined the ILL on 1 January as its 15th - and first non European - member.

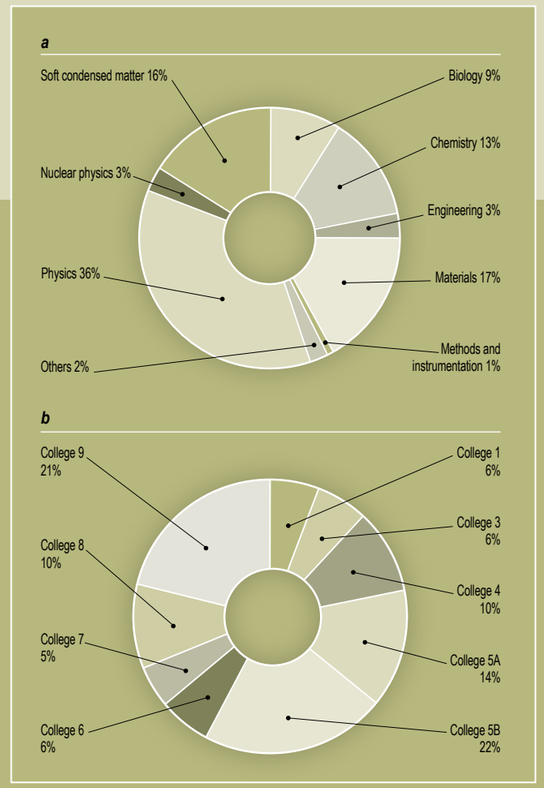

Figure 3: *Beamtime allocation in 2011: distribution amongst the different research areas* ***(a)*** *and colleges* ***(b)***.

Table 1 gives the beamtime distribution amongst the different member countries (request and allocation in 2011).

In calculating the statistics of beamtime per country, the attribution is based on the location of the laboratory of the proposers, not their individual nationality. For a proposal involving laboratories from more than one member country, the total number of days is divided amongst the collaborating countries, and weighted by the number of people for each country. Local contacts are not counted as proposers except when they are members of the research team.

The beamtime requested by and allocated to scientists from ILL, ESRF or EMBL is allocated to the member countries according to a weighting system based on the fractional membership of the country of the institute concerned. When a proposal involves collaboration with a non-member country, the allocated time is attributed entirely to the collaborating member country (or countries), and weighted by the number of people for each member country.
Proposals for which all proposers are from non-member countries therefore do not appear in this table.

Country	Requested days	Requested in %	Allocated days	Allocated in %
AT	155.12	1.79	98.56	2.45
BE	41.02	0.47	15.51	0.39
CH	541.60	6.25	198.74	4.94
CZ	136.54	1.58	54.71	1.36
DE	**2280.05**	**26.33**	**1016.27**	**25.26**
DK	102.80	1.19	66.21	1.65
ES	465.42	5.37	184.78	4.59
FR	**1928.20**	**22.26**	**943.32**	**23.45**
HU	31.94	0.37	10.03	0.25
IN	92.86	1.07	28.92	0.72
IT	627.77	7.25	263.95	6.56
PL	114.90	1.33	58.12	1.44
SE	209.72	2.42	82.33	2.05
SK	16.01	0.18	3.45	0.09
UK	**1900.20**	**21.94**	**996.88**	**24.78**
Total	*8660.45*	*100.00*	*4022.48*	*100.00*

Table 1: *Distribution amongst the Associate and Scientific-Member countries of beamtime requested and allocated in 2011 during the Subcommittees of the Scientific Council.*
Proposals from purely non-member countries do not appear in this table; this is why the total request and allocation looks different in ***Table 2*** *(page 97).*

A more complete view of beamtime use is given in **table 2**. Request and allocation of beamtime as well as the number of scheduled experiments refer to standard submissions to the subcommittee meetings. The effective number of days given to our users takes into account also Director's Discretion Time and CRG time for CRG instruments.

INSTRUMENT PERFORMANCE

Table 2 also gives a summary of instrument performance for 2011. For each cycle, a record is kept of any time lost from the total available beamtime and the reasons for the lost time are analysed for all the instruments. The table gives a global summary for the year.

Overall 5363 days were made available to our users in 2011 on ILL and CRG instruments, which represents 78.6% of the total days of operation. 324 days were used by ILL scientists to carry out their own scientific research. About 11% of the total beamtime available on the ILL instruments was allowed for tests, calibrations, scheduling flexibility, minor breakdowns recuperation and student training.
Beam days delivered for science in 2011 amount to 5687 (used for users and internal research).

A total of 840 experiments were scheduled. During 2011 the reactor operated for 4.0 cycles, representing 196 days of neutrons (**see § Reactor Operation, p.102**).

In 2011, 365 out of 6831 days were lost due to various malfunctions, which represent about 5% of the total available beamtime. The breakdown by reasons for beamtime losses is shown in **figure 4b**.

Detailed comments on the larger beamtime losses (above 25 days) are as follows:

- IN8 lost around 30 days because of its rebuilding after its beam-tube replacement.
- The H10 and IH4 beam-tubes work's delay prevented the testing of the PN1 target changer. Only one (manual) target change was possible during the first cycle and most experiments had to be cancelled.
- PN3 lost about three weeks because of several problems coming from its new digital acquisition system. Additional beamtime was lost due to the failure of one of the piezo-mechanisms of the GAMS-Axis.

In addition, the instruments IN12 and IN11 were only partially available in 2011, because of their dismantling and remounting, and LADI could offer very few days because of the heavy backlog due to the instrument closure in October 2010.
Please also note that, following the recommendation of the ILL instrument review committees, the instrument VIVALDI is now temporarily shut down and it was therefore only operational for the first two cycles in 2011.

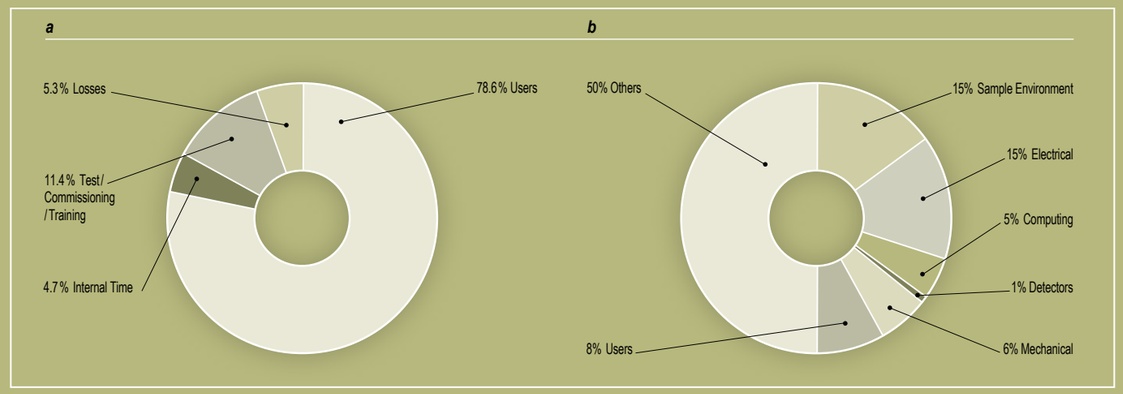

Figure 4: (a) *Use of ILL beamtime* ***(b)*** *Reasons for beamtime losses.*

REQUEST & ALLOCATION AND INSTRUMENT PERFORMANCE FOR 2011

Instrument	Days requested	Days allocated*	Number of scheduled experiments	Available days	Days used for users**	Days lost	Days for commissioning /test/training	Days for internal research
BRISP	**92**	**52**	**5**	**196**	**144.41**	**0.59**	**41**	**10**
D10	320	142	20	196	183	6	7	0
D11	267	130	65	196	159.92	1.79	34.29	0
D16	284	124	26	196	122	9.5	46.5	18
D17	307	137	44	196	161.33	4.17	17.5	13
D19	289	148	22	196	169	0.2	21.8	5
D1B	**105**	**49**	**23**	**196**	**132.06**	**1.94**	**58**	**4**
D20	294	129	61	196	164.05	6.75	7.2	18
D22	417	93	42	196	152.3	6.7	33	4
D23	**137**	**56**	**9**	**196**	**176**	**0**	**0**	**20**
D2B	324	132	64	196	178	1.5	7	9.5
D3	277	152	17	196	167	8.5	13.5	7
D4	169	76	20	132	113.85	6.9	11.25	0
D7	209	150	20	196	161.5	11.5	23	0
D9	332	137	22	196	161	10	25	0
FIGARO	322	140	52	196	161.51	3.98	21.51	9
IN1	83	32	7	64	37.5	0	25	1.5
IN10	74	115	14	196	122	9	35	30
IN11	98	14	2	50	0	50	0	0
IN12	**15**	**0**	**0**	**0**	**0**	**0**	**0**	**0**
IN13	**179**	**44**	**9**	**196**	**131.43**	**2.07**	**28**	**34.5**
IN14	464	144	26	196	167	7	13	9
IN15	366	78	13	196	142	6	35	13
IN16	265	132	26	196	166.84	5.14	21.02	3
IN20	326	135	19	196	158	14.75	11.25	12
IN22	**171**	**58**	**9**	**196**	**185**	**6**	**5**	**0**
IN4	171	105	25	196	172.34	2.66	11	10
IN5	274	132	33	196	157	12.25	19.75	7
IN6	226	121	31	196	178	0	14	4
IN8	284	108	16	196	127	37.5	28.5	3
LADI	135	61	6	11	0	0	11	0
PF1B	396	185	7	196	166	30	0	0
PF2 /set up	206	139	7	196	169.2	0	26.8	0
PN1	228	111	15	196	127	44	18	7
PN3 (GAMS 4 + 5)	250	155	6	302	135	40	75	52
S18	**105**	**78**	**5**	**196**	**178.35**	**12.65**	**5**	**0**
SALSA	226	136	28	196	164	3	14	15
SUPERADAM	**150**	**51**	**8**	**196**	**172**	**3**	**16**	**5**
VIVALDI	108	101	16	96	39	45	12	0
Total	*8945*	*4082*	*840*	*6831*	*5362.59*	*365.04*	*779.87*	*323.5*
Percentage of the total available beamtime					*78.6%*	*5.3%*	*11.4%*	*4.70%*

Table 2: *Beamtime request/allocation (via standard subcommittees and DDT together) by instrument and instrument performance. CRG instruments are in white.*

** 'days allocated' refers to only those days reviewed by the subcommittees (i.e., excluding CRG days and DDT).*

***'days used' refers to the total number of days delivered to users (i.e., including CRG days for CRGs and DDT).*
PF2 consists of different set-ups where several experiments are running simultaneously. The values given are averages for these positions.

Instrument list - December 2011

ILL INSTRUMENTS		
D2B	powder diffractometer	operational
D3	single-crystal diffractometer	operational
D4 (50% with IN1)	liquids diffractometer	operational
D7	diffuse-scattering spectrometer	operational
D9	single-crystal diffractometer	operational
D10	single-crystal diffractometer	operational
D11	small-angle scattering diffractometer	operational
D16	small momentum-transfer diffractometer	operational
D17	reflectometer	operational
D19	single-crystal diffractometer	operational
D20	powder diffractometer	operational
D22	small-angle scattering diffractometer	operational
FIGARO	horizontal reflectometer	operational
IN1 (50% with D4)	three-axis spectrometer	operational
IN4	time-of-flight spectrometer	operational
IN5	time-of-flight spectrometer	operational
IN6	time-of-flight spectrometer	operational
IN8	three-axis spectrometer	operational
IN10	backscattering spectrometer	operational
IN11	spin-echo spectrometer	operational
IN14	three-axis spectrometer	operational
IN16	backscattering spectrometer	operational
IN20	three-axis spectrometer	operational
PF1	neutron beam for fundamental physics	operational
PF2	ultracold neutron source for fundamental physics	operational
PN1	fission product mass-spectrometer	operational
PN3 - GAMS	gamma-ray spectrometer	operational
SALSA	strain analyser for engineering application	operational
VIVALDI	thermal neutron Laue diffractometer	on hold

CRG INSTRUMENTS		
SuperADAM	reflectometer	CRG-B operational
BRISP	Brillouin spectrometer	CRG-B operational
CRYO EDM	installation for the search for the neutron electric dipole moment	CRG-C operational
D1B	powder diffractometer	CRG-A operational
D23	single-crystal diffractometer	CRG-B operational
GRANIT	gravitation state measurement	CRG under construction
IN12	three-axis spectrometer	CRG-B operational
IN13	backscattering spectrometer	CRG-A operational
IN22	three-axis spectrometer	CRG-B operational
S18	interferometer	CRG-B operational

JOINTLY FUNDED INSTRUMENTS		
LADI (50%)	Laue diffractometer	operated with EMBL
IN15	spin-echo spectrometer	operated with FZ Jülich and HZB Berlin

TEST AND CHARACTERISATION BEAMS	
CT1, CT2	detector test facilities
CYCLOPS	Laue diffractometer
TOMOGRAPHY	neutrography
OrientExpress	Laue diffractometer
T3	neutron optics test facility
T13A, C	monochromator test facility
T17	cold neutron test facility

Instrument list - December 2011

ILL INSTRUMENTS		
D2B	powder diffractometer	operational
D3	single-crystal diffractometer	operational
D4 (50% with IN1)	liquids diffractometer	operational
D7	diffuse-scattering spectrometer	operational
D9	single-crystal diffractometer	operational
D10	single-crystal diffractometer	operational
D11	small-angle scattering diffractometer	operational
D16	small momentum-transfer diffractometer	operational
D17	reflectometer	operational
D19	single-crystal diffractometer	operational
D20	powder diffractometer	operational
D22	small-angle scattering diffractometer	operational
FIGARO	horizontal reflectometer	operational
IN1 (50% with D4)	three-axis spectrometer	operational
IN4	time-of-flight spectrometer	operational
IN5	time-of-flight spectrometer	operational
IN6	time-of-flight spectrometer	operational
IN8	three-axis spectrometer	operational
IN10	backscattering spectrometer	operational
IN11	spin-echo spectrometer	operational
IN14	three-axis spectrometer	operational
IN16	backscattering spectrometer	operational
IN20	three-axis spectrometer	operational
PF1	neutron beam for fundamental physics	operational
PF2	ultracold neutron source for fundamental physics	operational
PN1	fission product mass-spectrometer	operational
PN3 - GAMS	gamma-ray spectrometer	operational
SALSA	strain analyser for engineering application	operational
VIVALDI	thermal neutron Laue diffractometer	on hold

CRG INSTRUMENTS		
SuperADAM	reflectometer	CRG-B operational
BRISP	Brillouin spectrometer	CRG-B operational
CRYO EDM	installation for the search for the neutron electric dipole moment	CRG-C operational
D1B	powder diffractometer	CRG-A operational
D23	single-crystal diffractometer	CRG-B operational
GRANIT	gravitation state measurement	CRG under construction
IN12	three-axis spectrometer	CRG-B operational
IN13	backscattering spectrometer	CRG-A operational
IN22	three-axis spectrometer	CRG-B operational
S18	interferometer	CRG-B operational

JOINTLY FUNDED INSTRUMENTS		
LADI (50%)	Laue diffractometer	operated with EMBL
IN15	spin-echo spectrometer	operated with FZ Jülich and HZB Berlin

TEST AND CHARACTERISATION BEAMS	
CT1, CT2	detector test facilities
CYCLOPS	Laue diffractometer
TOMOGRAPHY	neutrography
OrientExpress	Laue diffractometer
T3	neutron optics test facility
T13A, C	monochromator test facility
T17	cold neutron test facility

Neutron guide hall / ILL22

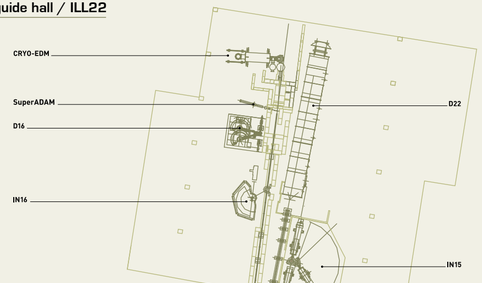

Reactor operational level (D)

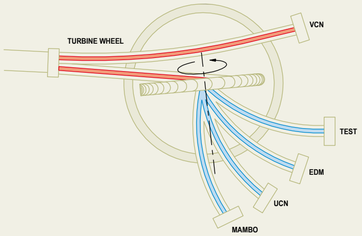

Reactor hall / Inclined guide H4

Neutron guide hall / ILL7 - Vercors side (WEST)

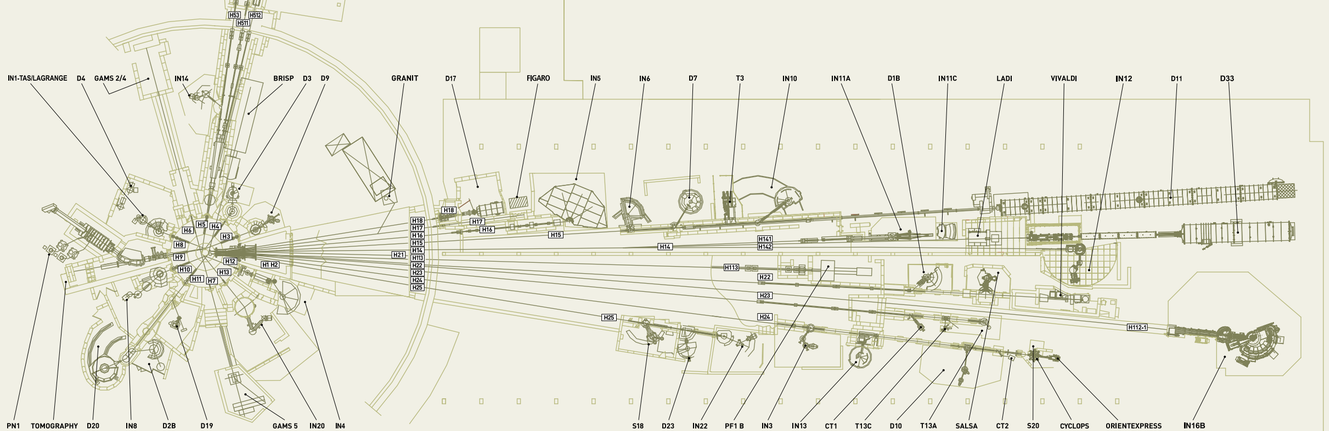

Reactor hall ILL5 / Experimental level (C)

Neutron guide hall / ILL7 - Chartreuse side (EAST)

REACTOR OPERATION

© Alexis Chezière

This ILL High Flux Reactor (HFR) produces the most intense neutron flux in the world: $1.5x10^{15}$ neutrons per second per cm^2, with a thermal power of 58.3 MW. The reactor operates 50-day cycles, with each cycle of operation followed by a shutdown period during which the fuel element is changed and a number of checks are carried out. Occasional longer shutdowns allow for equipment maintenance. There are normally 4 reactor cycles per year, supplying 200 days of neutron flux for scientific use.

Following the nuclear accident at Fukushima, in March 2011, the French nuclear safety authority (ASN) decided to launch additional safety assessments on all French nuclear bases (INBs), including the ILL. This additional safety review will have an impact on the Institute and will affect its budget over the next years.

The studies performed to analyse the behaviour of the ILL reactor under extreme conditions have been completely accepted

The studies performed by the reactor division teams analysed the behaviour of the ILL reactor under extreme conditions: the earthquake scenarios envisaged would have caused major damage to a town like Grenoble and would have led to the failure of all the dams on the river Drac, leaving the centre of town under 10 metres of water. On 15 September ILL submitted the results of its analyses to the IRSN (*Institut de Radioprotection et de Sûreté Nucléaire*) and the ASN. On 16 November the permanent group of experts for nuclear reactors replied with its conclusions: the ILL's proposals have been completely accepted.

We will now start putting the plans into operation. You probably know that a major seismic reinforcement programme (the so called REFIT programme) has already been carried out at the ILL, ending in 2007. The 2011 studies have prompted us to add the possibility of the loss of the 4 dams upstream on the river Drac; this implies reinforcement of elements traversing the reactor containment and the construction of a new emergency reactor control room for the crisis management teams from which all the emergency safety circuits can be controlled. The work is scheduled to be carried out over the next 3 years (between 2012 and 2014), with no major perturbation to the ILL user programme, and its total cost is estimated at 12 M€.

Hervé Guyon
Head of Reactor Division

AUTHORS
H. Guyon and **J. Tribolet** (ILL)

There were 4 cycles planned for 2011 and 196 days of scientific activity were provided overall. It was decided to interrupt the second cycle 4 days before its term, to avoid the risk of activating the argon that had found its way into one of the beamtubes (**Table 1**).

THE KEY REACTOR COMPONENTS PROGRAMME

In order to ensure reactor safety and reliability over the next years, the ILL continues to invest in the Key Reactor Components programme (KRC) - whose aim is to ensure that the most important parts within the reactor are regularly replaced and improved. The KRC programme will continue until the next ten-yearly safety review by the nuclear authorities in 2017.
The main operations currently planned under this programme are:

- replacement of the beamtubes,
- upgrade of the out-of-pile part of the horizontal cold source, including its instrumentation and control system,
- manufacture of the hafnium safety rods,
- renewal of the nuclear measuring channels,
- procurement of backup cells for the cold sources.

OPERATIONS CARRIED OUT DURING THE 2011 REACTOR SHUTDOWNS

- replacement of the H10 beamtube, and removal of the IH4 beamtube to allow the emergency core reflood system to be installed,
- despatch of 6 spent fuel elements to La Hague,
- replacement of the first primary pump and of the motor on the second primary pump,
- installation of the new H1/H2 pumping system,
- replacement of the H6 beamtube trolley (zircaloy and graphite) used for repositioning experiment samples,
- upgrade of the instrumentation and control system on the separate reactor circuit used for cooling the non-reactor cooling systems,
- irradiation of tungsten-186, for the production of a 188W/188Re source, for medical purposes (treatment of cardiovascular disorders),
- purge of the heavy water circuit and vacuum drying of the reactor block in order to be able to fill it with water from the pools, replace the V7 vertical irradiation canal remove the V3 plug and install the ultimate core reflood system, remove 2 safety rods, and replace for the first time the antiturbulence grid on the reactor block (modified in 1995).

REX FUKUSHIMA: THE ADDITIONAL SAFETY ASSESSMENT

The investigations carried out in 2011 and the discussions with the French nuclear safety authority's (ASN) expert groups successfully demonstrated that:

- the ILL has significant safety margins available with respect to the risk of a design-basis earthquake,
- the loss of a single safety function would never result in a major escalation of the danger (cliff-edge effect),
- the loss of both reactivity and the confinement would never result in a major escalation of the danger (cliff-edge effect),
- there are always at least two major barriers in place to prevent and mitigate the accidents to be feared,
- fusion under water would never result in a cliff-edge effect.

To comply with ASN requirements the ILL must ensure it is equipped with a "hard core" of safety provisions. This will involve completing its installation of the emergency core reflood system and seismic depressurisation circuit and installing a groundwater supply system, an emergency rod drop system, and a new emergency reactor control room.
These operations are scheduled to be complete by the end of 2014 for a total cost estimated at 12 M€.

WORK PLANNED FOR THE 2011/2012 WINTER SHUTDOWN

This involves both normal maintenance operations and the start of the work resulting from the additional safety assessment:

- servicing of the H11 secondary plug,
- vertical cold source instrumentation work,
- replacement of components on H9,
- maintenance work on the ventilation systems,
- replacement of adsorbents,
- cleaning of the exchangers,
- modifications to the H1/H2 guide exits,
- pump basin work,
- testing of a "cooling stop" pump,
- examination of the reactor block,
- radiological controls on the metal containment,
- electrical work,
- containment leak rate measurements,
- installation of the emergency core reflood system without automation,
- installation of a "tsunami" diesel generator,
- emergency water makeup system redundancies,
- upgrade to compliance of several elements, including the seismic gaseous effluents system, the supports for the seismic ventilation hoods, the seismic reinforcements on the steelwork protecting the vertical cold source, the seismic stabilisation measures for the instrumentation on level D and the flood reinforcements on the *cour à l'anglaise* passageway door.

RADIOACTIVE WASTE AND EFFLUENTS

The ILL's activities in 2011 generated waste and effluents respecting the regulatory limits applicable to our installation, as shown in the tables below.

Preparing the removal of the IH4 beamtube.

Cycle no.	Start of cycle	End of cycle	Number of days of operation	Number of days scheduled	Number of unscheduled shutdowns
161	19/04/2011	08/06/2011	50	50	0
162	20/06/2011	04/08/2011	46	50	0
163	29/08/2011	18/10/2011	50	50	0
164	02/11/2011	22/12/2011	50	50	0
Total			**196**	**200**	**0**

Table 1

Evacuation of radioactive waste	Quantity
Decay bin (60 l)*	0
5 m^3 pre-concreted crate (low and intermediate level waste)	0
5 m^3 crate (low and intermediate level waste)	0
200 l drums of "incinerable" waste (laboratory waste)	72
HDPE drums 120 l (laboratory waste)	14
30 l cylinders (liquid)	3

** Waste stocked in these decay bins is still quite active and requires several years of interim storage before meeting ANDRA's specifications for processing as intermediate-level waste.*

Gaseous effluents	Released in 2011 (TBq)
Tritium	14
Rare gas	1.2
Carbon-14	0.41
Iodine	0.0000023
Aerosols	0.00000021
Liquid effluents	**Released in 2011 (TBq)**
Tritium	0.12
Carbon-14	0.00027
Iodine	0.0000013
Other activation products	0.00013

40th anniversary of the ILL reactor's divergence

The ILL reactor went critical for the first time on 31 August 1971 (photos 1 to 4). On 31 August 2011, we celebrated 40 years of its operation. The ceremony provided an opportunity to bring together many former ILL's staff and especially those who had been at the ILL from the beginning of the adventure: the reactor design team, industrial engineers, members of the original shift teams, and so on.

In 40 years there have only been four Heads of the Reactor Division at the ILL, and they all met together for the first time during the event (photo 5).

We were also honoured to welcome Mr Robert Dautray, former High Commissioner for Atomic Energy and member of the *Académie des Sciences*, who was one of the founding fathers of the nuclear industry in France and participated in the design of the ILL's high-flux reactor.

The many stories and memories shared during the day gave us a chance to relive some of the enthusiasm felt by the pioneers of those early days, an enthusiasm still alive and well today.

40 years after, the ILL is still the world reference in neutron scattering science and techniques, and demand has never been higher (with a record number of more than 1400 proposals submitted in 2011).

A key factor in this success has been the continuous renewal or development of our instruments to ensure that they are world-leading. The latest upgrade project - the Millennium programme - has furnished the user community with 14 new or renovated instruments as well as supporting infrastructure. Funding and planning are in place to maintain the momentum of the programme to 2014, and we have started working with our scientists and users to develop a well-rounded case for the next-generation instruments and infrastructure to serve their science to 2025 and well beyond.

The ILL has still many successful years ahead!

Past and present Heads of Reactor together, from left: Franco Franzetti, Yves Droulers, Ekki Bauer, Richard Wagner, ILL former director general, Hervé Guyon et Jean-Paul Martin.

Jean-Paul Martin with Yves Droulers, Head of the reactor in 1971.

The start-up team.

31 August 1971, 19h29: Just before going critical.

The reactor went critical, hurray!

MORE THAN SIMPLY NEUTRONS

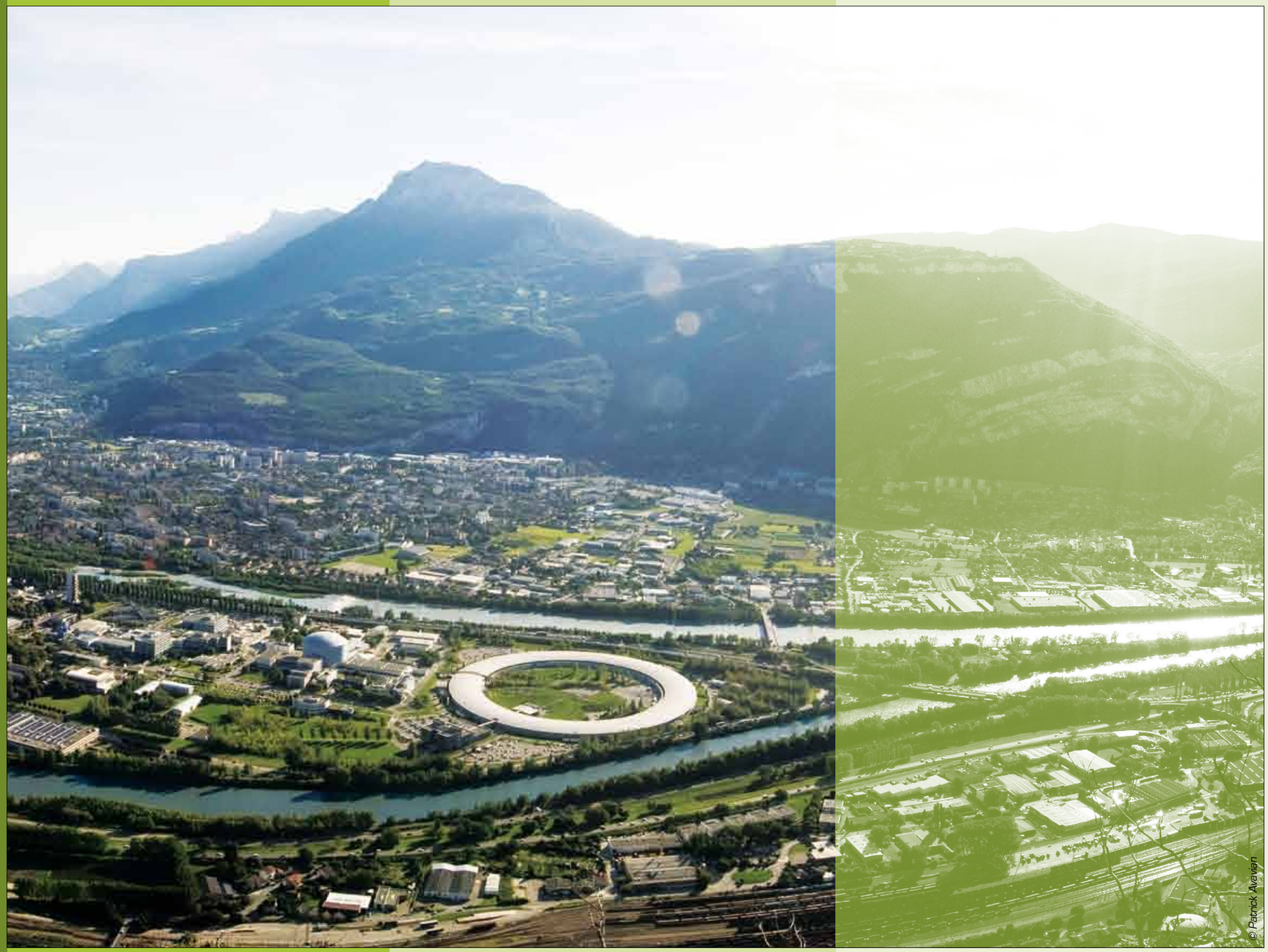

© Patrick Aavaian

SCIENTIFIC SUPPORT LABORATORIES
THE EPN-CAMPUS
GRENOBLE AND THE FUTURE

In order to maintain their ranking on the international scene, European research institutes must optimise their resources and develop synergies at every level.

The ILL is firmly committed not only to build high-performance instruments but also to offer the best scientific environment to the user community and it has established successful collaboration with neighbouring institutes over the years. After the successful Partnership for Structural Biology, we have now launched a Partnership for Soft Condensed Matter.
In parallel, the ILL and the ESRF have been working on plans to transform our joint site into a research campus – the **"European Photon and Neutron science campus", or EPN-campus for short** - with a truly international reputation, and launched an ambitious project to extend the facilities already offered by our international site. The new scientific and technological installations will be complemented with other more general improvements, such as a new Science Building, a new site entrance, a despatch and reception platform, a bigger restaurant and internal roadways.

The ILL is firmly committed not only to build high-performance instruments but also to offer the best scientific environment to the user community

In addition, the ILL has teamed up with the other institutes located on the Polygone Scientifique science park (where our Institute is located) for the GIANT partnership, a project which aims to develop our neighbourhood into a world-class science and technology park.

AUTHORS
G. Cicognani and F. Vauquois (ILL)

Scientific Support Laboratories

PARTNERSHIP FOR STRUCTURAL BIOLOGY

The Partnership for Structural Biology (PSB) contains a powerful set of technology platforms that are contributed by the various partner institutes (ILL, ESRF, EMBL, IBS, and the unit for host-pathogen interactions). These platforms include advanced capabilities that complement the powerful neutron scattering facilities available to ILL users: synchrotron X-rays, electron microscopy, NMR, high-throughput methods (soluble expression and crystallisation), and a range of biophysical techniques such as isothermal calorimetry and surface plasmon resonance. A joint SANS/SAXS platform has been developed and there is also an initiative to develop a joint X-ray/neutron low resolution crystallography capability. The aim of the PSB is to enhance the interdisciplinary capabilities of each of the facilities co-located on the site. Further details are provided on its website
http://www.psb-grenoble.eu/

DEUTERATION LABORATORY

Of particular interest to ILL's biology users is the ILL-EMBL Deuteration Laboratory. The aim of the platform is to provide a focus for European scientists wishing to make their own deuterated materials for neutron scattering or NMR experiments. D-Lab has had a decisive impact on biological neutron scattering and it plays a key role for the ILL user community, as the fact of having partially or totally deuterated molecules has now become essential to get beamtime. More information is given at ***http://www.ill.eu/sites/deuteration/***

MATERIALS SCIENCE SUPPORT LABORATORY

The joint ILL-ESRF Materials Science Support Laboratory provides a range of support to our users, from advice with experiment proposals to advanced sample metrology. In particular, the Laboratory works with users to optimise the experimental methodology before the start of an experiment. This takes the form of standardised specimen mounting, digitisation of samples, definition of measurement macros and liaising with the instrument responsible. It is recommended that users arrive at the ILL a day or two prior to the start of an experiment to enable these off-line preparations to be performed. More information may be found on the MSSL's website
http://www.ill.eu/sites/mssl/

PARTNERSHIP FOR SOFT CONDENSED MATTER

The Partnership for Soft Condensed Matter (PSCM) is now being set up, which will allow users to characterise samples before their experiments at both the ILL and ESRF and will facilitate the performance of complementary *in situ* measurements. By early 2013, the PSCM will be able to host 20 to 30 scientists and technicians working in the laboratories and office space of the new Science Building of the joint ESRF/ILL campus.
In these laboratories, scientists will prepare experiments with highly complex self-assembled and non-equilibrium soft matter systems which cannot be easily transported to Grenoble. Many materials related to nanotechnologies, life sciences, environment and renewable energy are, in fact, soft matter systems. Users wishing to use the facility in conjunction with neutrons or synchrotron radiation measurements should indicate this when submitting their request for beamtime.
Further details can be found at
http://www.ill.eu/instruments-support/labs-facilities/pscm/

C-LAB

The Computation-Lab is offering support to ILL users for atomistic simulations using classical and *ab initio* methods. Typical applications for simulations are structure, magnetism and phonons in crystals and liquid/glass structure and dynamics. As samples become more complex, simulations can provide key, complementary information that will help to interpret experimental data and understand how systems behave. Scientists and thesis students at the ILL benefit from the software, hardware and expertise of the C-Lab and users can benefit via their local contacts. In order to improve access to simulations for users, they are now able to request simulation support for their neutron scattering experiments on the official ILL proposal forms by ticking the appropriate box. For more information see ILL News N.47, June 2007
http://www.ill.eu/html/quick-links/publications/ill-news/

The EPN-Campus

CONSTRUCTION OF THE NEW IBS BUILDING

A new IBS building is rising on the joint EPN campus. The IBS (*Institut de Biologie Structurale*) studies the links between protein structure and function. It was created in 1992 and is now a three-way partnership involving the CEA, the CNRS and the Grenoble Joseph Fourier University.
The IBS has its own biological research themes, maintains a comprehensive series of experimental platforms and undertakes technical innovation.

The move will allow the IBS to expand physically and thereby to develop new research activities. It will also bring the IBS on the EPN Campus, closer to the other PSB institutes.
The concentration of such an outstanding range of expertise and facilities in life science will provide a unique environment for state-of-the-art integrated structural biology in Europe.
The construction work is scheduled to take 18 months and will result in a five floor building with 5 600 m^2 including 3 100 m^2 of usable laboratory and office space. The building will be ready in 2013.

The architect design for the new building of the IBS to be built on the EPN campus and a photo of its construction.

The EPN-Campus

Perspective (Chartreuse-side) of the ESRF EX2 upgrade programme.

Grenoble and the future

THE ESRF EX2 PROGRAMME

In 2010, it was ESRF's turn to launch its upgrade programme, called EX2. It will include major building extensions with 8 new, longer and more powerful beamlines, technology upgrades to the synchrotron, measurement instruments, and data processing systems.
The building programme comprises two new experimental halls with a total floor surface of 4500 m^2 to host the eight new beamlines, along with about 4000 m^2 for new laboratories and offices. Most of the latter will be located in a three-storey building adjacent to one of the new experimental halls. Finally, a new so-called satellite building for a very long beamline will be built some 300 m away from the new extensions.
On 29 November 2011, a ground-breaking ceremony marked the start of the civil construction works for several major building extensions of the ESRF.
The new buildings will be inaugurated in June 2013.

GRENOBLE AND THE FUTURE

The Grenoble Innovation for Advanced New Technologies partnership, or 'GIANT', is forging dynamic new links between higher education, research and industry, to foster technological breakthroughs for the future.

The city of Grenoble has been supporting the project with the construction of a new 250 hectare town quarter. 2011 saw the construction of several thousand new flats and the start of a new tramline.
There was also a major success for Giant in 2011: the "*Institut de Recherche Technologique NanoElectronique*" project (the IRT), being promoted by GIANT and its industrial partners, won the first place for funding from France's Grand Emprunt scheme. This means a further 260 M€ for the programme and support for thousands of jobs.

Technical and building programmes
The Clinatec building was opened in 2011 - a centre for biomedical research focusing on micro- and nanotechnological applications in the health field.

There were two other building operations that started in 2011:

- CNRS: the extension of the Institut Néel, with a new building for nanoscience experimentation
- NanoBio2, a project uniting the life sciences with nanotechnology for the development of tomorrow's healthcare applications.

Both buildings will be completed in 2013.

© Patrick Avavian

ILL workshops and schools in 2011

10-12 JANUARY
nDDB - Molecular dynamics in biology.

12-14 JANUARY
BILL 2011 - Structural and dynamical properties of lipid bilayers.
http://www.ill.eu/news-events/events/bill2011

24-29 JANUARY
FPSchool 2011 - 4th ILL Annual School on Neutron Diffraction Data Treatment using the FULLPROF SUITE Basic session.
http://www.ill.eu/news-events/past-events/2011/fpschool-2011/

30 JANUARY - 4 FEBRUARY
FPSchool for experts.

7-9 FEBRUARY
GIME GIANT workshop.
http://www.esrf.fr/events/conferences/usersmeeting2011/Energy-workshop

14-19 FEBRUARY
Modern Trends in Magnetism - Workshop dedicated to Igor Dzyaloshinskii on the occasion of his 80th birthday (ILL was one of the many organising institutes).
http://mid.workshop.online.fr/

18-22 SEPTEMBER
DyProSo XXXIII.
http://www.ill.eu/news-events/events/dyproso-xxxiii/home/

9-12 OCTOBER
EIROforum Teachers School 2011.
http://www.epn-campus.eu/eiro-teachers-school/home/

12-14 OCTOBER
ADD 2011 - Workshop on Analysis of Diffraction Data in Real *Space.*
http://www.ill.eu/news-events/past-events/2011/add2011/

19-23 OCTOBER
Neutrons in Biology 2011.
http://www.ill.eu/news-events/past-events/2011/nib2011/

26-28 OCTOBER
Topological Materials.
http://www.ill.eu/news-events/past-events/2011/topomat2011/

1-2 DECEMBER
EXILL 2011 - EXogam@ILL.

Short reports on the ILL workshops can be found on the ILL News for Reactor Users (June and December 2011 issues)
http://www.ill.eu/top-links/publications/ill-news/

ILL chronicle 2011

3 JANUARY
India joins the ILL as first non European Scientific Member.

16 FEBRUARY
Signature at ILL of an agreement for the creation of a technology platform within the GIANT collaboration.

27 FEBRUARY-30 MARCH
HERCULES, the Higher European Research Course for Users of Large Experimental Systems.

2 MARCH
PSB student day.

17 MARCH
Visit of M. le Préfet, M. Le Douaron.

8 APRIL
Visit of Prof. Luciano Maiani, president of Consiglio Nazionale delle Ricerche (CNR), our correspondent for the Italian partnership.

11 APRIL
Clip session of the ILL PhD students.

14 AVRIL
ILL seismic exercise.

26-29 APRIL
Meetings of the ILL Scientific Council and its Subcommittees.

2-4 MAY
HERCULES Specialised Courses: INDUSTRY Neutrons and Synchrotron X-rays for Industrial Applications

10-11 MAY
Meeting of the Subcommittee on Administrative Questions (SAQ).

9-10 JUNE
Meeting of the Steering Committee in Saclay (Paris).

31 AUGUST
Celebration of the 40 years of reactor operation since the reactor first diverged.

26 SEPTEMBER
ESS and ILL start joint R&D in neutron science.

1 OCTOBER
ILL's new management team.

26-27 OCTOBER
Meeting of the Subcommittee on Administrative Questions (SAQ).

15-18 NOVEMBER
Meetings of the ILL Scientific Council and its Subcommittees.

24 NOVEMBER
Visit of Catherine Cesarsky, High Commissioner for Atomic Energy, CEA Saclay.

30 NOVEMBER-1 DECEMBER
Meeting of the Steering Committee in Grenoble.

Visits and events

1 - On 8 April, ILL welcomed a delegation from Italy headed by Prof. Luciano Maiani (second on the left), President of the "Consiglio Nazionale delle Ricerche" (CNR), the entity that funds and coordinates a major part of the country's public research and which also represents the Italian interests in the ILL Council.

2 - From left to right: Stéphane Siebert (CEA Grenoble deputy director), Francesco Sette (ESRF director), Michel Spiro (CNRS scientific director) and Richard Wagner (ILL director from 2006 to 2011) signing on 16 February an agreement for the creation of a new technology platform for industry on the GIANT site.

3 - José Luis Martínez (left), Hervé Guyon and Bruno Desbrières (first and second on the right) guiding Monsieur the Prefet of Isère, Eric Le Douaron, on a tour of the ILL.

4 - Past and present Heads of Reactor together, during the 40th anniversary of the ILL reactor divergence celebration. From left: Franco Franzetti, Yves Droulers, Ekki Bauer, Richard Wagner (ILL former director general), Hervé Guyon and Jean-Paul Martin.

5 - The ILL directors welcoming Catherine Cesarsky, High Commissioner for Atomic Energy, CEA Saclay, on her visit on 24 November.


1


4


5


2


3

6 - Participants of HERCULES 2011, the Higher European research Course for Users of Large Experimental Systems.

7 - The ILL's new management team, from left to right: José Luis Martínez and Helmut Schober (Associate Directors) with Andrew Harrison (Director).

8 - Poster session of the PSB student day on 2 March.

9 - Catherine Chazette and Pierre Rivet during a seismic exercise on 14 April.

10 - Clip session of the ILL PhD students on 11 April.


6


7


8


9


10

Happy users

1 - Bérangère Raguenet (Université Montpellier, left) and Andrea Alejandra Piarristeguy (Université Montpellier, right) on D16 with Viviana Cristiglio (instrument responsible).

2 - Joe Zaccai (Senior ILL fellow) with a Japanese user team: from left to right, Masaaki Sugiyama (Kyoto University), Takashi Oda (Yokohama University) and Hirokazu Yagi (Nagoya City University).

3 - Indian users on SALSA: Kiranmayi Abburi Venkata (Bristol University), Santosh Kumar (Bhabha Atomic Research Centre) and Amrita Kundu (Open Univeristy, UK).

4 - Hartmut Lemmel (instrument responsible) on S18 with Debasis Sen and Jitendra Bahadur (Bhabha Atomic Research Centre) (from left to right).

5 - Tom Fennell (now PSI) with Ahmed Raihane, Christiane Alba-Simionesco (LLB, CEA SACLAY), Grégoire Sergeant Perthuis (ENS Paris) and Caroline Thibierge (LLB, CEA Saclay) (from left to right).

6 - From left to right: Gregoire Kessedjian and Florence Martin (LPSC Grenoble) on PN1 with Herbert Faust (instrument responsible).

7 - Gabriel Cuello (left) and Tapan Chatterji (right) setting up an experiment on D4 with a team from Helmholtz-Zentrum (Dresden-Rossendorf): Atsushi Ikeda-Ohno (left), Christoph Hennig (right) and Stephan Weiss (in the back).

8 - Lise Arleth (University of Copenhagen) (left) and her team during their experiment on D11, a fine illustration of the complementarity of neutron and X-rays scattering techniques. In the back, from left, Peter Lindner and Ralf Schweins (instrument responsibles).

9 - From left to right: Jacques Ollivier (instrument responsible) with Holger Euchner (University of Stuttgart), Tsutomu Ishimasa (University Hokkaido), Tsunetomo Yamada (Tokyo University) and Marc de Boissieu (in the front, INPG, Grenoble) during their experiment on the rejuvenated IN5.

10 - A happy user on FIGARO: Marianna Yanez Arteta (Lund University).

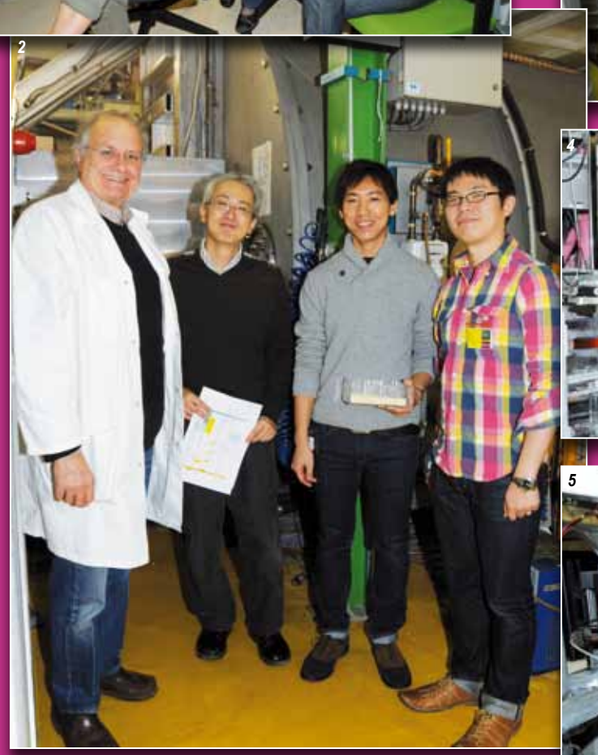

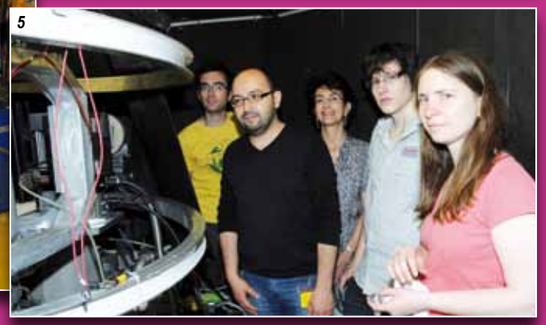

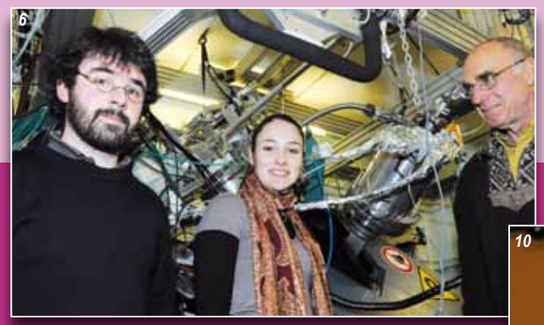

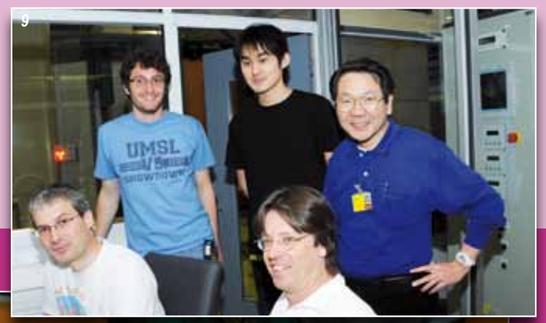

FACTS AND FIGURES
ORGANISATION CHART

2011 was a year of adaptation and construction at the ILL, and the Administration Division (DA) was busy on all fronts. One of its major missions in the year was to prepare the revision, signature and registration of the ILL statutes and the contract governing the Institute. The documents were reviewed and slightly adjusted with the input of a specially constituted working group of ILL Associate representatives; they now provide a solid administrative basis for ILL operations until at least 2030. In this context work was also progressing on the extension of the ILL's Intergovernmental Convention; it is expected that the 5th protocol to the Convention will be signed in 2012.

The ILL is continuing to build for the future

The ILL is continuing therefore to build for the future and it is not surprising that the DA's Building and Maintenance Service had to deal with an exceptional workload in 2011. Apart from its regular tasks of construction and maintenance the Service also finalised the studies for the new Science Building, the construction of a special heavy water unit, a backup control room, and extension of the experimental hall ILL22. Thanks to good collaboration with the Purchasing group and excellent levels of motivation, it was possible to place the main orders just before the end of the year, thus ensuring that construction can start early in 2012. The Service also provided technical assistance for the new site entrance project and the refurbishment of the site canteen, projects managed by the ESRF. These two projects and the construction of the Science Building have been made possible by the award of a grant from France's "Contrat Projets État-Région" (CPER).

On the financial front, in 2011 the Finance and Purchasing Service finalised its adoption of the International Financial Reporting Standards (IFRS), in response to requirements from one of our Associates. This should now allow for clearer consolidation of the ILL's accounts from 2012 onwards. The Service also started implementing the new interbank standards for the Single Euro Payments Area; this will facilitate financial transactions with our users, suppliers and employees. In addition to its routine budgetary and accounting activities, the Service was on the frontline in dealing with the 1% reduction in our 2011 budget; it was tasked with the preparation of budgetary scenarios incorporating known and potential financial constraints, as well as the unforeseen requirement for additional funding for the risk prevention programme introduced following the accident at Fukushima.

2011 also saw the appointment of a statutory auditor for the ILL, as required by the new statutes; the Finance and Purchasing Service launched a call for tenders and the selection process at the end of the year and the Associates approved the nomination of KPMG as ILL's statutory auditor for a six-year period. For the Purchasing group, 2011 involved the management of a very high number of international calls for tender, related essentially to the exceptionally busy building programme. The group also carried out a detailed investigation into the options for improving the balance of industrial return to our funders. They identified key areas of potential and will be targeting these in 2012.

Our third arm, the Human Resources Service, started the year with a successful conclusion to the negotiations with the trade unions on revisions to the ILL Collective agreement and conditions for retirement and early retirement. These negotiations were closely followed on by the annual salary negotiations, in the difficult budgetary context. The Service ran intense discussions between Management and the trade unions and - thanks to patience and dialogue on both sides - an agreement was obtained. Another major item on the human resources agenda was a review of the ILL's supplementary health insurance provisions. The Service, together with staff representatives, was able to identify and negotiate a new supplier providing comparable or better insurance coverage for staff at a lower cost.

The Human Resources Service was also active in 2011 on other fronts. It adapted its tools and procedures to new requirements from the Finance and Purchasing Service for the adoption of IFRS. It held discussions with the trade unions on a new "Job and skills management system" (the GPEC), including the elaboration of a staff development plan for 2011-2015. The new plan constitutes a response to the budgetary restrictions for this period; it provides for the reduction of up to 19 posts at ILL through the non-replacement of departing staff and introduces adjustments in the workforce to ensure minimum impact on science and our user services. The Service also, of course, continued its recruitment activity (30 new staff members), payroll management, staff training, and travel support for users and ILL staff.

The Administration Division's role is essentially to provide services for the other divisions of the Institute. In 2011 it assisted in the elaboration of a detailed proposal with financial projections on the potential for producing radioisotopes at ILL for nuclear medicine. With the Associates' recent approval, Management is now in the position to elaborate a focused and detailed business plan for an innovative project to be led by Dr Ulli Köster.

Martin Walter
Head of Administration (interim)

STAFF

- 474.5 people including 64 experimentalists in the scientific sector and 23 thesis students.
- 319.5 French, 43 German, 47.5 British, 42 scientific participating countries and 23.5 others.

Staff		%
French	318.5	67.12
German	43	9.06
British	47.5	10.01
Scientific Members	42	8.85
Others	23.5	4.95
Total	*474.5*	*100*

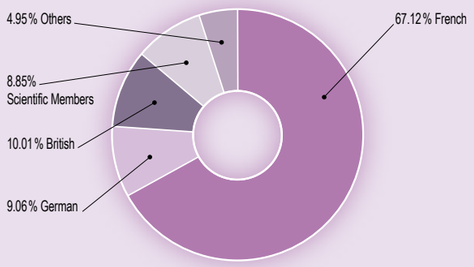

BUDGET 2011: 88.296 M€ (excluding taxes)

Income	M€	%
Income from Associates	57.610	65.25
Income from Scientific Members	19.359	21.93
Own income	3.530	4.00
Carry forward from 2010	4.574	5.18
Contribution from local autority	0.723	0.82
Cash flow	2.500	2,82
Total	*88.296*	*100*

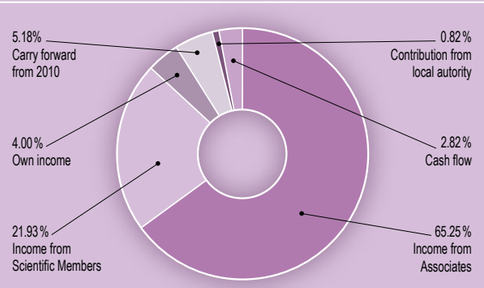

Expenditure	M€	%
Staff costs	43.150	48.87
Operating costs	15.913	18.02
Investment costs	16.211	18.36
Fuel cycle	13.022	14.75
Total	*88.296*	*100*

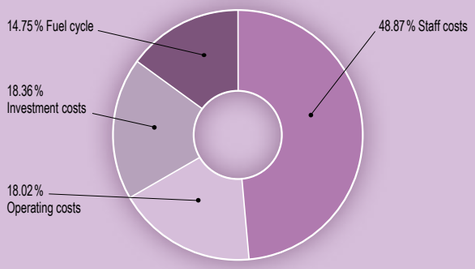

DISTRIBUTION OF ILL PURCHASES

Expenditure	M€	%
France (non-captive market)	12,25	66.40
Germany	3,21	17.40
United Kingdom	0,66	3.58
Scientific Members	0,76	4.12
Others	1,57	8.51
Total	*18.45*	*100*

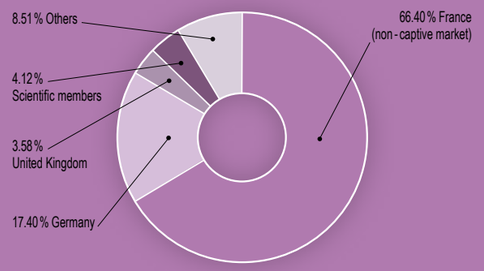

NAME

Institut Max von Laue - Paul Langevin (ILL)

FOUNDED

17 January 1967. International Convention between France, Germany and UK

ASSOCIATES

France
Commissariat à l'Energie Atomique et aux Energies Alternatives (CEA)
Centre National de la Recherche Scientifique (CNRS)

Germany
Forschungszentrum Jülich (FZJ)

United Kingdom
Science & Technology Facilities Council (STFC)

COUNTRIES WITH SCIENTIFIC MEMBERSHIP

Spain
Ministerio de Ciencia e Innovación (MICINN)

Switzerland
Staatssekretariat für Bildung und Forschung (SBF)

Italy
Consiglio Nazionale delle Ricerche (CNR)

CENI (Central European Neutron Initiative)
Consortium, composed of:
- Austria: Österreichische Akademie der Wissenschaften
- Czech Republic: Charles University of Prague
- Hungary: Research Institute for Solid State Physics and Optics / Budapest on behalf of the Hungarian Academy of Sciences (MTA)
- Slovak Republic: Comenius University Bratislava

BELPOLSWENI (the Belgian-Polish-Swedish Consortium)
- Belgium: Belgian Federal Science Policy Office (BELSPO)
- Sweden: Swedish Research Council (SRC)
- Poland: Polish Academy of Sciences

Denmark
Danish Agency for Science, Technology and Innovation
Interim scientific membership 01/07/2009 - 30/06/2011

India (from 1 January 2011)
Bhabha Atomic Research Centre (BARC)
Interim scientific membership 01/01/2011 - 31/12/2012

SUPERVISORY AND ADVISORY BODIES

- Steering Committee, meeting twice a year
- Subcommittee on Administrative Questions, meeting twice a year
- Audit Commission, meeting once a year
- Scientific Council with 9 Subcommittees, meeting twice a year

REACTOR

- 58 MW, running 4 cycles in 2011 (with cycles of 50 days)

EXPERIMENTAL PROGRAMME

- 840 experiments (allocated by subcommittees) on 28 ILL-funded and 9 CRG instruments
- 1557 visitors coming from 35 countries
- 1370 proposals submitted and 767 accepted

Organisation chart - january 2012

REVIEW PANELS (Chairs)

APPLIED METALLURGY, INSTRUMENTATION AND TECHNIQUES
J. Kohlbrecher (Paul Scherrer Institute, Switzerland)

NUCLEAR AND PARTICLE PHYSICS
W. Korten (CEA Saclay, France)

MAGNETIC EXCITATIONS
C. Rüegg (PSI, Switzerland)

CRYSTALLOGRAPHY
R. Walton (Warwick University, UK)

MAGNETISM
R. Kremer (MPI Stuttgart, Germany)

STRUCTURE AND DYNAMICS OF LIQUIDS AND GLASSES
D. Holland-Moritz (Institute of Materials Physics in Space, Cologne, Germany)

SPECTROSCOPY IN SOLID STATE PHYSICS AND CHEMISTRY
M. Dove (Cambridge University, UK)

STRUCTURE AND DYNAMICS OF BIOLOGICAL SYSTEMS
C. Cardin (Reading University, UK)

STRUCTURE AND DYNAMICS OF SOFT-CONDENSED MATTER
J. Cabral (London Imperial College, UK)

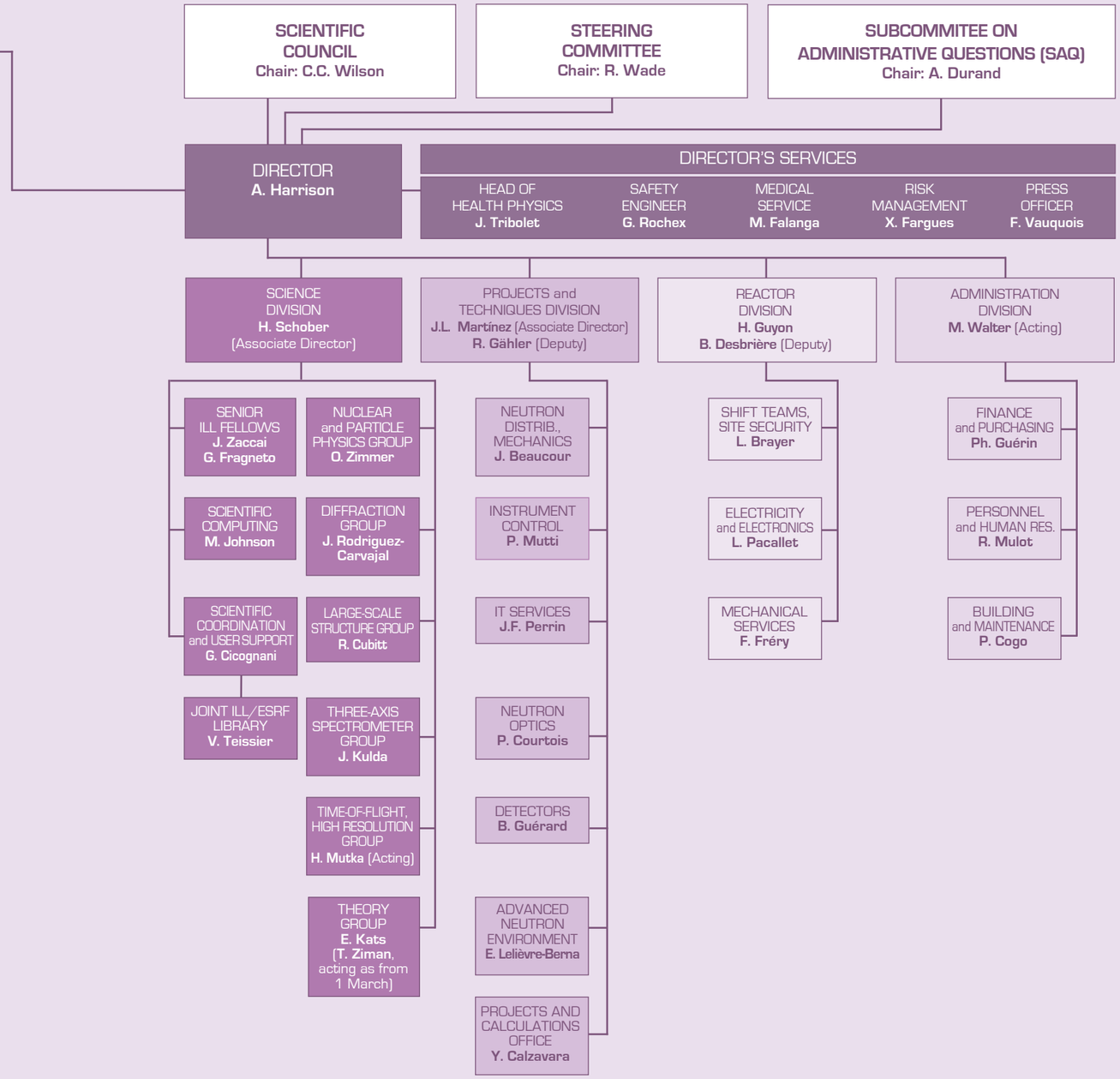

Publications in 2011

In 2011, the ILL received notice of 611 publications by ILL staff and users. They are listed in the CD-ROM of this year's Annual Report.

The distribution by subject is as follows:

Applied Physics, Instrumentation and Techniques	52
Biology	45
Crystallography	81
Liquids and Glasses	31
Magnetic Excitations	49
Magnetic Structures	88
Materials Science and Engineering	66
Nuclear and Particle Physics	54
Theory	18
Soft Matter	91
Spectroscopy in Solid State Physics and Chemistry	36

ILL PhD studentships

PhD students at ILL in 2011*	32
PhD theses completed in 2011	9

** receiving a grant from ILL*